

Alma Mater Studiorum – Università di Bologna

DOTTORATO DI RICERCA IN

Scienze ambientali: tutela e gestione delle risorse naturali

Ciclo XXVII

Settore Concorsuale di afferenza: 04/A2

Settore Scientifico disciplinare: GEO/02

TITOLO TESI

Geomorphological and statistical analysis on Ravenna dune fields changes, based on Terrestrial Laser Technology.

Presentata da: Dott. Stefano Fabbri

Coordinatore Dottorato

Relatore

Prof. Enrico Dinelli

Prof. Giovanni Gabbianelli

Esame finale anno 2015

1 INTRODUCTION

1.1 Generalities.

1.1.1 Research generalities and purposes.	1
1.1.2 Coastal sand dunes.	2
1.1.3 The dune/beach profile and the waves action.	4
1.1.4 Dune/beach system sand balance.	6

1.2 Dynamic Factors.

1.2.1 Wind flow.	9
1.2.2 Sand transport and moisture effect.	12
1.2.3 Vegetation.	14
1.2.4 Secondary factors.	16

1.3 Coastal Dune Development and Morphology.

1.3.1 Incipient and established foredunes.	17
1.3.2 Blowouts.	19
1.3.3 Dune micro-morphology.	22

2 AREA OF STUDY

2.1 Geological History.

2.2 Subsidence.

2.3 Emilia-Romagna Coastal Zone.

2.3.1 Local dune ridges evolution.	30
2.3.2 Coastal Geomorphology Map 2005.	30
2.3.3 The MICORE project.	32

2.4 Sites of Study.	
2.4.1 Bevano river estuary area.	34
2.4.2 Marina di Ravenna and Milano Marittima area.	37
2.5 The Reference System.	41

3 MATERIALS AND METHODS

3.1 Laser Scanning.	
3.1.1 Laser light theory.	42
3.1.2 Light behavior and laser scanning devices.	47
3.1.3 Laser scanning systematic errors.	51
3.1.4 The field methodology, theory and post-processing.	56
3.1.5 The laser scanning method application.	56
3.1.6 Post processing and data improvement application.	58
3.1.7 The applied validation methods.	60
3.2 The Morphological Analysis: Units, Sub-zones and their Variation.	
3.2.1 GIS environment processing: volumetric calculation, morphological analysis and DSAS application.	64
3.2.2 Morphological Sub-zones.	73
3.3 Potential Sediment Transport via Fryberger and Dean's Method.	
3.3.1 Theory.	75
3.3.2 Practice.	84

3.4	Meteo Data Analysis and Multivariate statistic (PCA).	
3.4.1	Meteorological data analysis.	87
3.4.2	Multivariate statistic and Principal Component Analysis (PCA).	90
3.5	Computational Fluid Dynamics (CFD).	95

4 RESULTS

4.1	Terrestrial Laser Scanner.	
4.1.1	Validation tests results.	99
4.1.2	Morphological units, Areas of Interest and morphological sub-zones.	104
4.1.3	Volumetric differences results.	111
4.1.4	Digital Shoreline Analysis System (DSAS).	113
4.2	Meteorological Data and Forcing Factors.	116
4.3	Grain Size and Drift Potential Results.	120
4.4	Principal Component Analysis (PCA).	122
4.5	Computational Fluid Dynamic Analysis.	126

5 DISCUSSION

5.1 Sand Grain Size Analysis.	128
5.2 Aeolian Data Analysis.	129
5.3 Terrestrial Laser Scanner Discussion.	
5.3.1 Validation tests.	134
5.3.2 Volumetric seasonal monitoring.	136
5.3.3 Morphological analysis: two examples of investigation.	141
5.3.4 The DSAS analysis.	148
5.4 Principal Component Analysis (PCA) Discussion.	154
5.5 Computational Fluid Dynamic (CFD) Discussion.	157

6 CONCLUSIONS

6.1 Terrestrial Laser Scanner.	
6.1.1 Validation tests conclusions.	160
6.1.2 Seasonal volume survey and morphological Sub-Zone analysis.	163
6.2 Meteorological Data and Multivariate Analysis.	
6.2.1 Aeolian data conclusions.	167
6.2.2 Principal Component Analysis (PCA).	169
6.3 Digital Shoreline Analysis System (DSAS) and computational Fluid Dynamic (CFD) conclusions.	170

References.	172
Appendix I: Morphological Units maps.	I
Appendix II: Morphological Sub-Zones.	XIX
Appendix III: PCA R script.	XXVI
Appendix IV: DSAS tables.	XXVII

1 INTRODUCTION

1.1 Generalities.

1.1.1 Research generalities and purposes.

Data collection for this study started in May 2012 and ended in May 2014 and it was entirely located in Ravenna coastal area. The focus was on sand dunes.

The principal purposes were substantially two: on one hand the author tried to investigate the Terrestrial Laser Scanner (TLS) possibilities as a tool applied to environmental monitoring. This powerful device indeed has been already used in this branch during last decades (i.e. Hodge R., 2010; Hoffmaister et al., 2012; Lague D., 2013), for many different environments (caves, rivers, dune fields, etc.) but its application is still lacking of a proper temporal and spatial scale. TLS has the possibility to reach an accuracy much higher than many other devices, in order of centimeters, thus it should be used.

First of all, in order to fill this gap, set of validation tests was put in place. This allowed to evaluate TSL data out of any doubts. Anyway this study is not be limited to test the specific device used, but try to propose a method to evaluate the reliability of any 3D monitoring tool (laser scanners, photogrammetry, multispectral images, etc.).

The next step was a seasonal monitoring campaign focusing on dunes volume oscillations. Then the analysis detail was increased, in both spatial and temporal scale, analyzing different dunes features, and reducing surveyed periods, all supported by the use of statistical tools.

It is important to highlight how difficult the sand dunes environment is to be studied. The next paragraph will explain how dynamical forces involved in this milieu are so strongly intertwined to make really hard their identification and definition, in terms of force and effects.

This introduces the second purpose which moved this research: the need of new features to survey and new tools to be available for environmental monitoring and management. In last years indeed many were the tries to find indexes or morphological

features which could help in this sense, with ambiguous results (i.e. Brunelli V., 2008; Montreuil A-L, 2013; Keijsers J., 2014)

This research tries to add some new ideas and proposals to reduce this problem, to have more realistic data able as much as possible to describe the real-world condition and the coastal dunes dynamic behavior.

1.1.2 Coastal sand dunes.

Any sand accumulation specifically due to the wind could be named “Dune”. Some authors think that the word itself “Dune” comes from Latin, “dunum”, and would mean “castle over a hill”, some others from the Irish “Dun”, “hill”. In any cases the dune is characterized by its different elevations features relative to the landscape.

According to Maun (2009) this kind of elements could be found in three particular environments, very different one from each other, but all equate by the presence of sand: river valleys, where floods can overflow river banks and deposit sand in the landscape, where later it is dried and shaped by winds; in desert environments, where the weathering of sandstone produces a large amount of sand which is subject to mass movement by wind; in sea coast regions, more frequently in temperate climate, less in tropical and sub-tropical. In this chapter only coastal sand dunes will be discussed, trying to describe all the complexity of their morphologies and their dynamics.

According to Martinèz et al. (2004), Coastal dunes are Aeolian landforms that develop in coastal zones where the general conditions guarantee an ample supply of loose, sand-sized sediment which must be available to be transported inland by the wind.

Three are the most important factors that dominate the dune evolution and morphology: the sea, the wind and the vegetation. The sea has a multiple role in this system: on one hand it is the first source of sand, on the other it is a factor that strongly influences morphology, in term of erosion due to storm waves which hit the dry beach. The wind is a chisel which erodes or deposits sand depending on its force and its interaction with morphological features of the topography. The dune vegetation is one of the most exemplifying cases of integrated biology: in this particular environment the biotic component, such as vegetation, is not only an ecological complement, but it is a

fundamental part of the structure itself of the dune, and of its dynamic. Vegetation effect starts with the consolidation of the soil, thanks to the roots action, and continues with forcing the deposition by cushion wind velocity. Moreover, vegetation has the effect to transform soil, enriching it with nutrient elements, thus there is a strong connection between the dune morphology and the phito-sociological successions which can colonize that environment. They basically evolve together.

The dune's importance is nowadays recognized by the whole scientific world for different reasons: first of all these morphological elements are the result of a complex sea-sand-wind-vegetation dynamic, and they reflect and monitor these dynamic forces, thus studying dune field behavior can be very helpful to understand this environment evolution. Moreover they are fundamental for the beach management, in terms of sediments store, protection from storm surges, as filter for rain water and barrier against salt water intrusion (Mollema P., 2008). From an ecological point of view, specifically in terms of biodiversity, sand dunes have a double absolute value: they are an ecosystem of transition, thus, as well as every other eco-tone, their extension is limited by their own characteristics, so for the living species linked to these environment (in this case, most of all migratory species) they become vital; furthermore sun, sand, salt, wind and surge make this an extreme environment, which selects species with extreme adaptations, thus rare.

Considering dunes from both an ecological and a physical/morphological point of view, these elements represent a buffer zone, what is called an "eco-tone", a transitional ecosystem between land and sea environments: coastal sand dunes could be interpreted as the most stable part of the beach and the most unstable part of the land. This is one of those ecosystem which allowed to evolve in a (as much as possible) natural way, would rewards the humankind with not only cultural/landscape contents but also with strictly economics values (just thinking about the protection from storm surge could make an idea of it).



Figure 1.1: Coorong barriere island, South Australia, 2014.

1.1.3 The dune/beach profile and the waves action

Genesis and evolution of sandy beaches are related to the geological conformation of the neighbor areas, the sandy sediment supply and the littoral drift acted by tidal waves and currents. Sediment source could be a near river estuary, the erosion of contiguous beaches or underwater bars in front of the beach. In any cases waves and flows are protagonists of the “wet” part of the beach system, while wind (and vegetation) is the dominant force of the dry (sub-aerial) part.

According to the Short and Woodroffe’s schematic diagram (2009) shown in figure 1.1, describing this environment profile, the most important elements are:

- The near shore zone: the area from the spot where waves starts to interact with the sea bottom, to the waves’ first break.
- The surf zone: defined by breaking waves and delimited, landward, by the intertidal area (“swash zone”).
- The subaerial beach, which lies between the swash limit and the low tide line..

The landward limit of the sub-aerial beach is represented by the coastal sand dune.

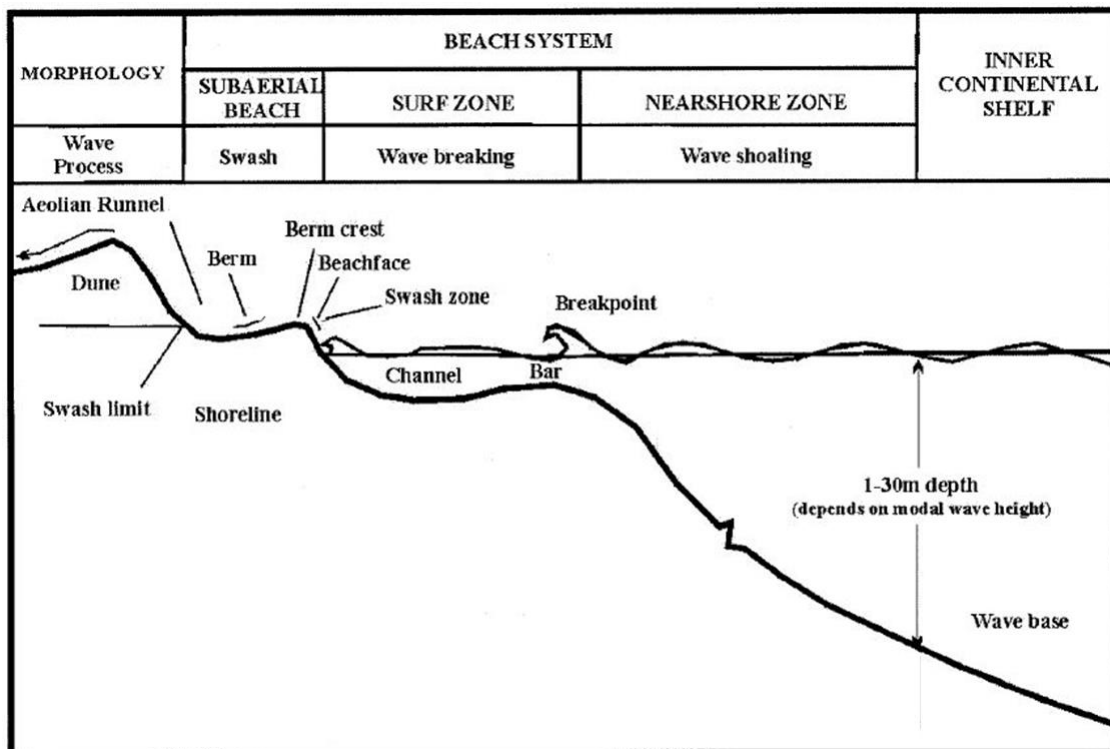


Figure 1.2: the beach profile model (modified from Short & Woodroffe 2009).

Waves are generated by the wind which, blowing on the sea water table, transmit a part of its energy to water particles and induce a movement; the latter is mostly vertical in depth water, while approaching the shore tends to transform itself in a horizontal movement depending on the slope and orientation of the sea bottom and its depth.

Tidal waves are the gears of the sand conveyor belt which works between the foreshore and the backshore, because they can use their kinetic energy to climb the aerial beach and bring a sediment loan.

According to Pranzini (2004), the beach, under the waves actions, responds assuming a morphology which let the best dissipation of energy, depending on the grain size and the sea conditions. This dynamic classifies beaches in three different types:

- Reflective beaches: coarse sediment and low energy waves, which are almost completely reflected to the sea. The typical morphology is narrow and steep (without dunes).
- Dissipative beaches: high energy waves and fine sediment. Much of the incoming energy is dissipated and the landscape is typically flat and wide, in the sub aerial zone, while it is characterized by bars in the near shore zone.
- Intermediate: between the two extremes above.

It is assumed how this dynamic makes the beach profile reflecting the sea “climate” (Hesp, 2012). This mechanism in effect, can fluctuate during different seasons depending on many meteorological factors. In any cases, the morphological relationship between the sea conditions and the beach aspect is so strong that many authors treat about a winter and a summer profile (Seymour J., 2005). These are the two extremes of a theoretical model, which has some lacks, but it resulted to be very realistic, especially at some latitudes (such as Mediterranean sea).

During winter, storms wave energy should be high, so that they can take in charge a huge part of the beach sand and bring it back to the sea: the so called “storm profile” includes narrow subaerial beaches with landscape dominated by strong slopes. During summer the situation is the opposite, and wake tidal waves are more prone to deposit the sand they transport rather than eroding some other from the beach: this makes the beach landscape more smooth and it is called “swell profile”.

Obviously once the sand get into the aerial/sub-aerial system it is pretty easy for it to become part of the dune body (entering in the wind cycle). According to Hesp (2002) the seasonal dominance of wave over wind process can alter the predominant behavior of a dune: during storm periods (with significant sedimentation and change) the wind deposition was found to be minimal (Arens, 1996).

1.1.4 Dune/beach system sand balance

Every beach system is crossed by a sediment flux which links it to the adjacent coastal sectors and to the frontal near shore. This sediment balance is determined by three principal elements:

- Sediment input: the most part of sediment entering into this system is carried by the river network and is strongly influenced by its condition and all those human activities that influence its transport capacity.
- Along shore movement: this is due to littoral currents and to the oblique waves fronts; usually the volume of sand is moved from a sector to the contiguous one, thus in natural condition, the sediment total balance is not influenced by this dynamic. It becomes a problem when human infrastructures for the coastal defense modify the system lateral continuity.
- Sediment output: in last decades many researches have highlighted how the sea level rise, making simultaneously rise the sea bottom too, is the main natural cause of sediment output (much more than waves' action). Anyway the human impact is the responsible of the most damages.

The strong connection between the dune and the beach was highlighted by Psuty (1988), who proposed a model that links the overall sediment balance affecting both systems. According to this author sediment circulation could extends from the offshore bar, through the dry beach and onto the dune, where vegetation trap it and each component of this system episodically can release or store sand as answer to the general pattern oscillations.

In this sense both the beach and the dunes are forms of sediment accumulation and they respond with morphological answers to the short and long term sediment balance:

the beaches can widen and narrow, while the dune can react varying the height and the relative width. Beach and dune can be considered as two separate components of the same system.

The model in figure 1.3 describes the possibilities from a very high sediment input to a very low one. In a positive sediment balance (the upper half of the diagram), dune dimension is inversely related to the rate of beach accretion (Psuty, 2004).

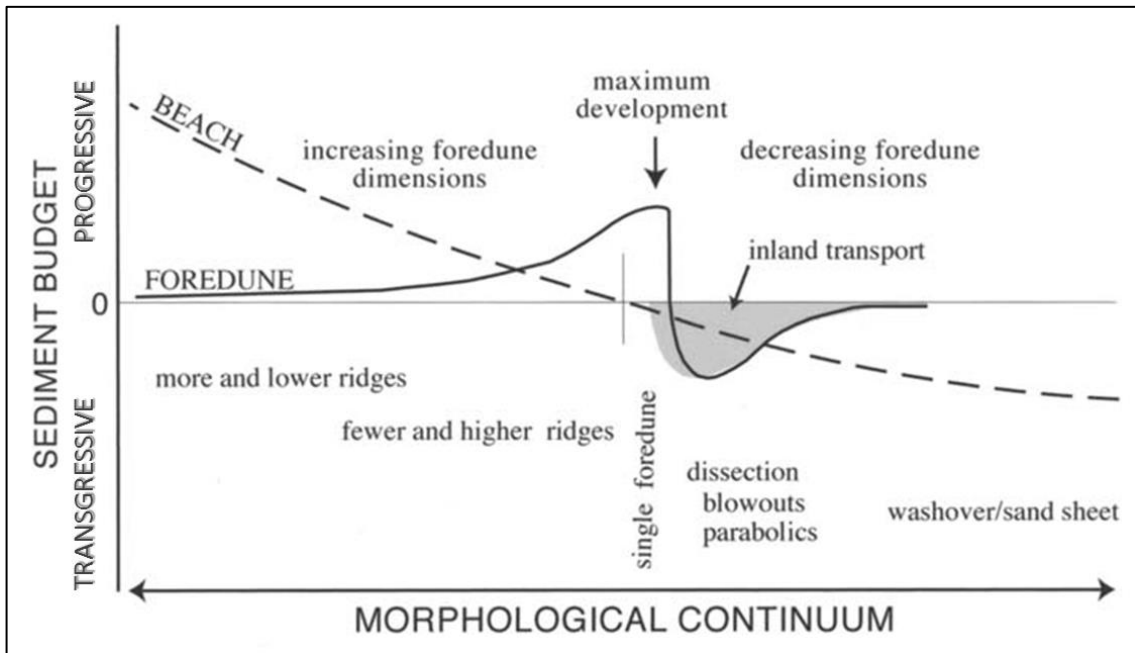


Figure 1.3: Morphological dune/beach continuum (modified from Psuty, 2004)

This is the basic concept of the model: high rates of shoreline progradation are enemies of the dune development, because of the lack of time for sand transfer into the land; as this mechanism slows there is an increase in dune dimensions. In the second part of the diagram, the transgressive portion, the supply of the beach suggests an opposite behavior of the system in these conditions: at some point the loss of sand is more than the accumulation by the dune, thus wash-over and sand sheet (thus outputs) will dominate this side of the continuum. Although this model is nowadays worldwide accepted, the author himself recognize a problematic component, when the balance is stable or minor negative, because numerous evidence demonstrate the possibility of well-developed dunes on eroding coasts (Psuty, 2004).

Always according to Psuty (1989), a first dune classification can be done basing on sediment balance:

- Primary Dune: it represents the most seaward part of dune (the “foredune”) and it is very active in exchanging sediment with other components of the profile. Its presence indicates a positive sediment budget, but at different time scales, it could be in negative or neutral balance too. It is the most dynamic part of the profile and it usually has a ridge form.
- Secondary Dune:
 - Active: it is the evolution of the primary dune, created by its modification and the transfer of sand inland. Its morphology is much more complex than primary dunes because of the active migration of sand, which is highlighted by deflation hollows and parabolic morphologies. It usually assumes a transgressive ridge form.
 - Stable: these forms usually have been stranded by the system, due to the beach progradation, and then they become stable thanks to the vegetation during their passage inland (as active-transgressive form). They are linear and represent a paleo-feature that retains the morphology of the dune but is not being maintained by dune formational processes (Psuty, 2004)
- Sand sheet/Washover: areas with no primary dune or any dune form, where the inland transfer of sand is very active. They can be found, for example, in correspondence of a pre-existing wash over or very strong on shore winds impede the formation of retention structures.

1.2 Dynamic Factors

1.2.1 Wind flow

In the sub-aerial beach system, wind force represents the engine that pushes sand inland, thus it can be considered the fundamental mechanism that leads to the dune morphological development. According to Hesp (2004), this component, in terms of sand transport, is controlled by several key factors: the magnitude and frequency of transporting winds; the influence of incident wind direction; beach fetch effect and sediment supply; vegetation type and density; moisture content. This ascertained theory introduces the two scales of influence on dunes development, by wind: at high detail, the wind climate, at small detail, the ground wind behavior.

The wind climate of a region influences drastically Aeolian landforms, for what concerns their existence, evolution and morphology. It describes not only which winds are most frequent (regnant), which reach most high velocities (dominant), but also the angle of incidence with which prevalent winds blows on shores, thus on dune ridges.

Onshore winds are those that come from the sea to the land, offshore winds are those which blow in the opposite direction and, at last, along shores winds, which blow almost parallel to the longitudinal axes of the dune ridge. Obviously in coastal science, these terms are referred to the shoreline, but in this study treating about shoreline foredunes ridges, they can be referred to the dune as well.

It is pretty intuitive understanding how onshore winds are more effective than any other: first of all they blow in the “right” direction (from sea to land), thus they can take in charge sand from the beach and transport it to the land and the dune; moreover they usually reach highest speeds because of the fetch effect related to blowing on a clean surface (the sea) without obstacles. Not every onshore direction has the same effect: winds approaching the dune with an angle of 15-60° are usually deflected, while winds approaching with an angle higher than 60° are deflected parallel to the dune: angles low to moderate of wind approaching are responsible for localized accretions, especially on the upwind slopes, on crests and blowouts (Hesp P., 2004). This is one of the most important processes increasing topographic variability.

Offshore winds have an opposite behavior blowing from land they do not find bare sand on their path, fact that decreases their transport potential; furthermore it is much easier for offshore winds to be slowed down by obstacles, such as urban buildings or natural features. Anyway they are considered to be important because of their contribute in increasing topographic variability.

Alongshore winds place themselves between these two “extremes”, they are much more effective than offshore winds, but much less than onshore ones, anyway their role in beach/dune dynamic is still hard to investigate and understand.

For what concerns near-surface airflow, it is important to consider that wind vertical profile in ideal conditions, is logarithmic (Hsu, 1988): this means that wind velocity tends to increase with elevation and that the profile changes in relation of the topography, and so it is for dunes (figure 1.4) environment.

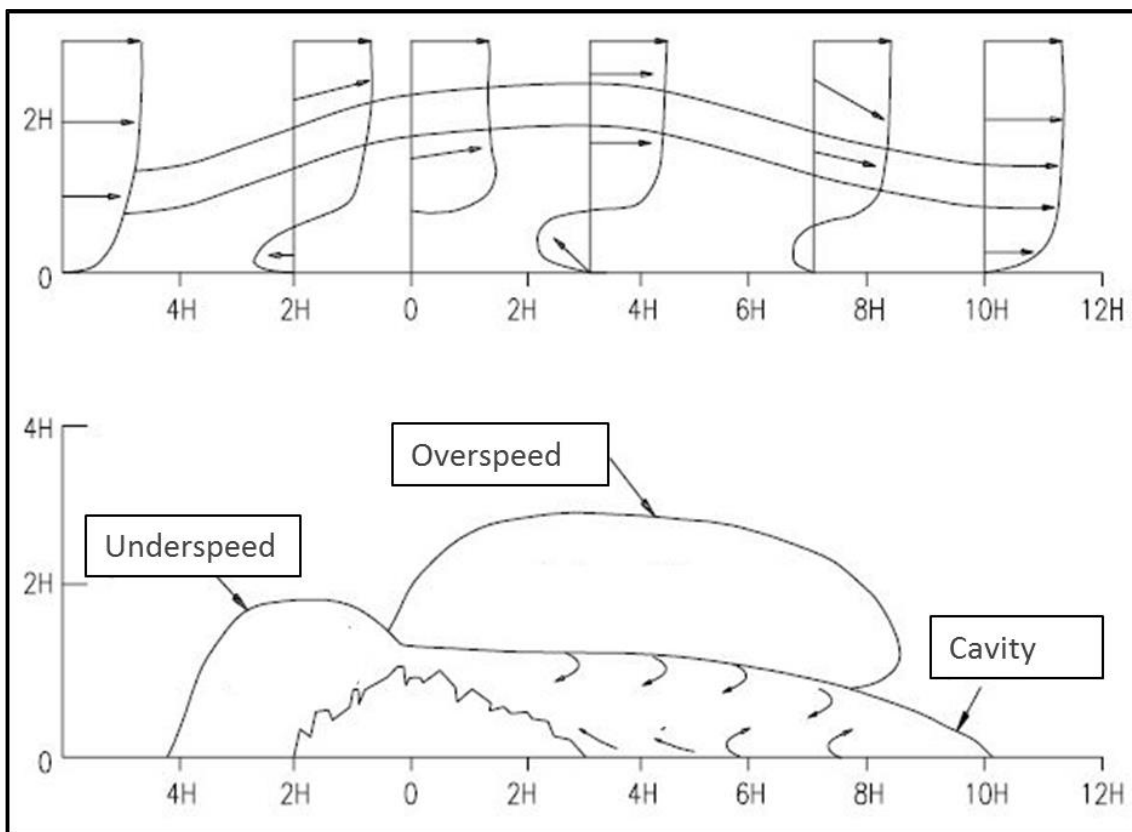


Figure 1.4: Wind logarithmic profile on dune (modified from Hsu, 1988)

In this work Hsu proposed a general model for onshore airflow. According to this model going from sea to land, first there is an area of underspeed onto the seaward

side of the dune; the crest part and the upper landward slope are two areas of acceleration of the flow; the lower landward slope which is another area of deceleration.

Many other authors modified this model to make it fit with the real-world behavior, especially for what concerns foredunes: Arens (1995) has found that wind flow is topographically accelerated over foredunes, especially up stoss slopes, and over crests; Hsu (1977) has understand how flow compression and acceleration in foredunes of virtually any height.; Hesp et al.(2005), highlighted that the principal sand deposition on a foredune varies markedly depending on approaching wind speed, vegetation cover and topography variations.

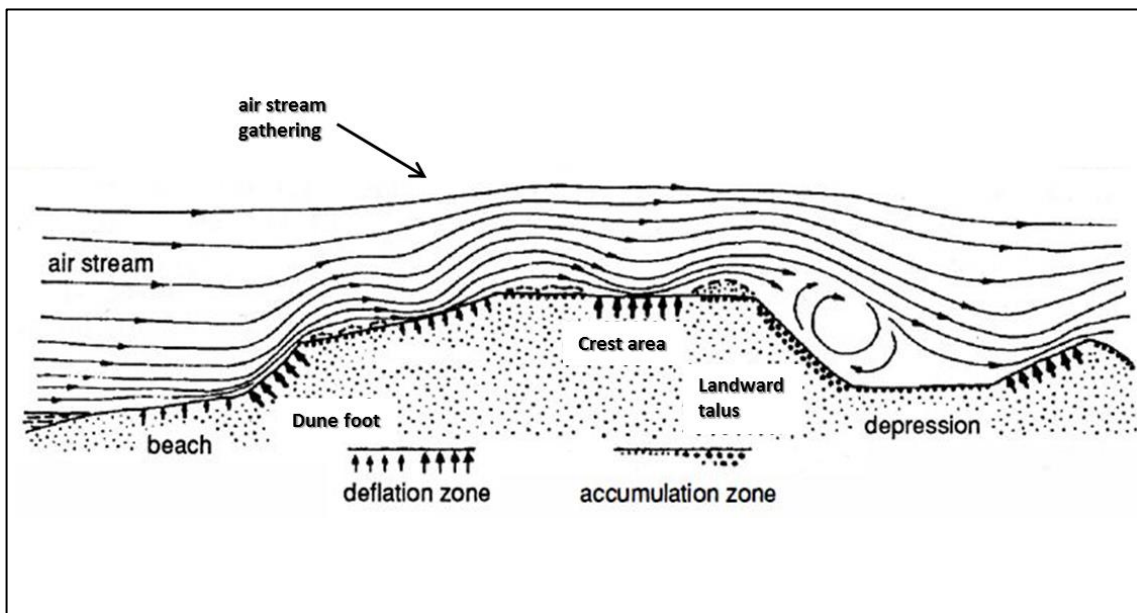


Figure 1.5: wind behavior on different morphological zones (modified by Barrere, 1992).

The basic principle which govern this pattern is a simple mechanism picked from the fluid dynamic, more specifically the “Bernoulli’s Effect”, which claims that for a fluid flowing in a confined system, the product of the speed for the area of the system section must be constant in every moment. This means that if the section decreases, the speed must increase: that is exactly what happens when wind bump into the dune (figure 1.5), and that is fundamentally why it accelerates on the foredune scarp and on the crest.

Another aspect to consider is that wind velocity moving on a sand surface is decreased by friction. The wind velocity profile shows how the speed decreases with height and it reach the zero at a height which is not zero. This height is called “surface

roughness constant”, abbreviated to “k” by Bagnold (1960) and z_0 by Olson (1958). K constant decrease when wind velocity increases (Deacon 1949) and vegetation obviously has a strong influence on its dynamic. The logarithmic relationship between speed and height, at last, can be expressed by the Prandtl von Karman equation (1935):

$$\frac{U_z}{U_*} = \frac{1}{K} \ln \left[\frac{z}{z_0} \right] \quad \text{Equation 1.1}$$

Where:

- U_z : wind velocity at height of z
- U_* is the shear velocity (it is going to be explained in next paragraph)
- K = von Karman’s constant (0.4)

1.2.2 Sand transport and moisture effect.

Before explaining the role of vegetation, it is helpful to understand how the sand is moved within the system. It is intuitive how sand mobility is strictly linked to its moisture content, because water increases sand weight and cohesion.

In any cases usually the material deposited by waves is dried by sun and wind, thus it can be transported (by wind). The basic mechanism is substantially dominated by wind speed in relationship with sand grain size. In any cases, once started the physical movement of sand grains, it can involve substantially three processes:

- Suspension: wind carries up those grains whose size is thin enough be suspended particles into the air, as dust (Bagnolt 1960).
- Saltation: this mechanism seems to be the major force that moves sand in coastal sand dunes environment (Maun, 2009). To move sand grains, the wind has to hit them with a properly force or “Shear Velocity” (U_*): this force must exceed a “critical shear velocity”, which is related to the root of grain diameter. The shear velocity is logarithmic proportional to the slope of the wind velocity profile. Once a grain is moved it tends to be moved forward until it reaches the same speed as wind, but contemporarily it loses height because of the gravity. According to

Bagnold (1960) this mechanism makes the sand trajectory elongated and curved, falling down with an angle of 10-16°. This fall causes a chain reaction inducing many other grains to be ejected with the opportunity of starting another saltation events. The greater is wind velocity, the greater is the height reached by the sand, the greater is the force of falling grains, thus of the chain reaction too.

$$U_* = \sqrt{\frac{\tau}{\rho_a}} \quad \text{Equation 1.2}$$

Where:

- U_* : Shear stress velocity
 - ρ_a : Air density
 - τ : boundary shear stress
-
- Surface creep: grains which are too large to be moved by bare wind force can be pushed by other falling particles, if the energy in game is high enough. It has been proved that an high-speed grain of average dimension can move a particle six time its diameter (Maun, 2009).

The moisture content of sand influences the sand capacity of movement across the beach primarily increasing the threshold shear velocity and, consequently decreasing the sand transport rate. This is acted thanks to the capillary force which draws sand particles together, and it is a direct function of moisture content of the soil. Thus, when wind flow exerts a shear drag on the moist sand, it will have to apply an additional force to beat the coalescence force too.

Hotta (1994) expressed a mathematical expression to quantify the moisture influence and showing it linear correlation:

$$U_{*tw} = U_{*t} + 7.5 w$$

Where:

- w : moisture percentage contained in the upper 5 cm of sand.

Always according to this author the model works only for sand whose grain size goes from 0.2 mm to 0.8 mm, and a moisture percentage until 8%. Surface moisture content on a natural beach is dynamic and it varies drastically in time and in space.

1.2.3 Vegetation

It is known that vegetation is a fundamental part of the dune structure and has a vital role in its evolution. Their double action on the environment, soil consolidation and wind speed slowing down are two basilar mechanisms of dune development, especially for what concerns first states of dune life.

Vegetation can colonize a dune area by discrete seedling germination on the back shore, by colonization from parent source areas or by laterally continuous germination (for example on the neckline). In any cases, plant usually colonizing these environments follow a phyto-sociological succession which starts with pioneer species.

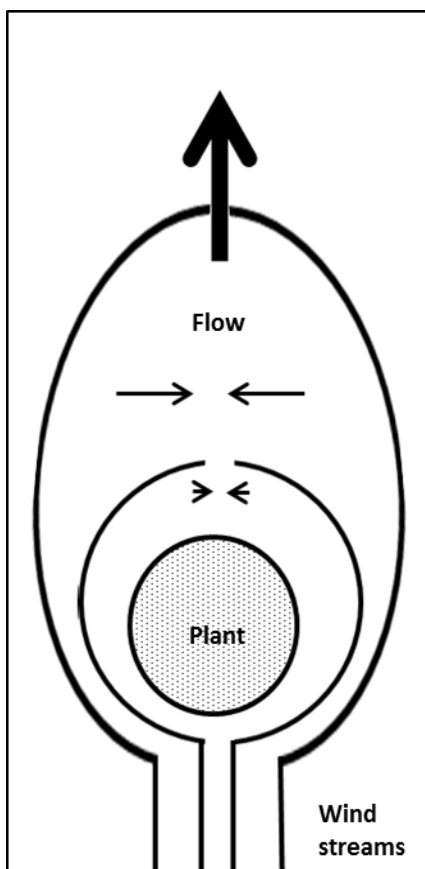


Figure 1.6: Wind flow bumping into a Plant.

These organisms allow the germination to many other vegetal form, from grass to trees, starting the modification of the soil: the ground consolidation made by roots and its nutrient enrichment.

For what concerns interactions between vegetation and wind, four are the most important vegetation feature: form, height, density and distribution (Hesp P., 2012). Those are linked to the shadow effect the plants have on wind flow (figure). This mechanism represents the born of a new dune, starting from a form called “Nebka”, which is also known as “shadow dune”. From this point to the most complex morphology, the vegetation leads the development behavior, influencing the wind flow logarithmic profile, depending on its density. This influence is particular on the near-surface velocity, reducing the bed shear stress. According to Hesp

(1989) plant density is the most influencing factor: once sand pass the leading edge of a

plant canopy, deposition occurs. The higher is plant density, the more often this happens; moreover the degree on near-surface flow penetration decreases, drag increase and the rate of downwind deceleration increases (Hesp, 1983). A high density vegetated dune traps most of incoming sand: this is the process which allows the dune to grown vertically in places.

Plant height has a similar effect on wind flow and a similar proportional correlation, and thus which species are present become a very important factor. At last, plant distribution influences wind flow and deposition, because vegetation tends to germinate in a random fashion.

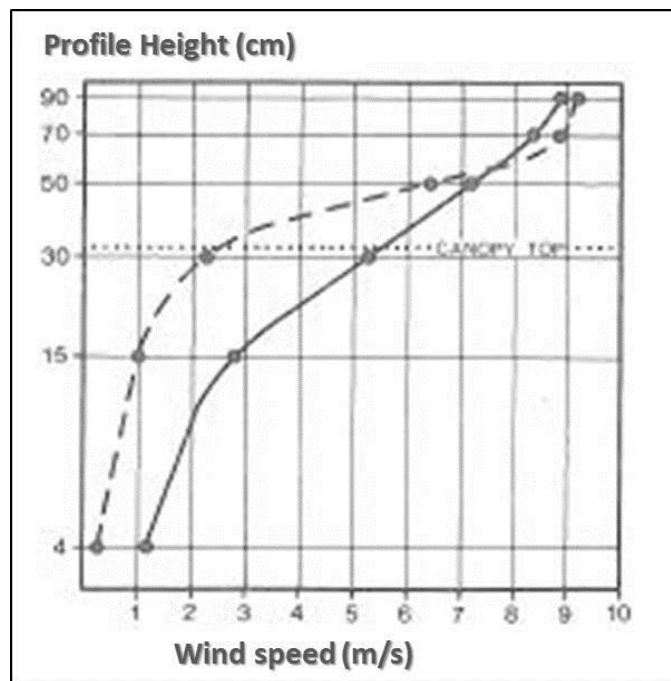


Figure 1.7: Wind logarithmic profile in tunnel (solid line) and in presence of vegetation (dotted line) (modified from Olson J., 1958)

What makes this system unique is the positive feedback between all these variables: for example, where plant density is high, sand deposition will be strong and this will encourage the growth of more plants, which are going to increase the shadow effect and related deposition.

There are a lot of mathematic equations in literature, which try to model the vegetation effect on airflow, but these will not considered in this study because this fall outside its purposes. The author will limit to highlight how the vegetation component principally affects the Z in wind logarithmic profile (equation 1, Chapter 3).

1.2.4 Secondary factors.

Beyond the principal factors, there are many others which locally influence dune evolution. According to Hesp (2012) five are the natural secondary factors, for the most part related to the sea conditions and the waves' action:

1. The frequency of swash inundation, which has the effect of killing all the vegetal species which do not tolerate regular wetting or inundation by saline water. This can have a strong influence on the long term dune morphology (Hesp, 2002).
2. Storm wave erosion: beyond the obvious same effect of the factor 1, this has a direct impact on the dune in term of erosion, to various degrees.
3. Overwash incidence, which have the same effects of both swash and storm waves.
4. Rates of progradation or retrogradation (of the beach): this especially affect the dune width and its height; the latter is in a positive curvilinear relationship with the progradation (Hesp 1989).
5. Wind direction and fetch effect, which influence the sediment transport budget.

1.3 Coastal Dunes Development and Morphology.

In literature there are innumerable definitions of “coastal sand dunes”. An interesting and complete one, in the author’s opinion, was enunciated by the Virginia Marine Resources Commission in the Coastal Primary Sand Dune Protection Act, in 1980: coastal sand dunes can be defined as a mound of unconsolidated sandy soil which is contiguous to mean high water, whose landward and lateral limits are marked by a strong change in grade and upon any part of which is growing a minimal number of species associated with dune environments. In 1986 Hesp described four types of coastal dunes: foredunes, blowouts, parabolic dunes and transgressive dunes. In order of the purposes of this study only the first two types are going to be treated.



Figure 1.8: Foredune ridge at Coorong National Park, South Australia.

1.3.1 Incipient and established foredunes

According to Maun (2009), three are the essential requirements that have to be satisfied to have coastal dune formation: a wind regime dominated by on-shore winds, a continuous sand supply and obstacles to reduce wind velocity and to induce deposition.

Beyond these general settings, the evolution of a dune starts from the shadow dune state: if a sand hill is able to overtake this passage, then it can become a “Foredune”. Hesp (2002) defines this element as “shore-parallel dune ridges formed on the top of the backshore by aeolian sand deposition within vegetation”. From an evolutionary point of view, foredunes are classified in two types: incipient and established.

Incipient foredune, also called “Embryo dune”, represents the natural development of Nebka, and typically can be found in three different morphologies: ramps, which can be created by germination of seeds on a seaward sloping backshore, by rhizomatous plants growing seaward from landward or by the colonization at the base of a dune scarp which gradually accretes; terraces are formed by a rapid plant growth on a rapidly accreting beach, or when the seaward plant growth equal the accretion rate; ridge forms are typical of beaches where accretion rate is rapid (relative to plant growth) or where plant density and height are both high.

The natural evolution of an incipient foredune is to become an established foredune: this process starts as embryo dunes are enough vegetated to be “stabilized” and soil development begins. Carter and Wilson (1990) found that the transition between the two stages last from 5 to 8 years, however this time depend on many variables. Established foredune are distinguished by the growth of intermediate/woody plants and by their greater morphological complexity (which includes height, width, volume and geographical position).

In any cases their morphological development depends on several factors as sand supply, degree of vegetation cover, plant species present, thus climate a bio-geographical region, aeolian sand accretion/erosion trend, wind and sea forces, storms and over-wash processes and the extend of human impact and use (Hesp P., 2002).

In a long time scale, the evolution of the system considers a series of dune ridges, where the first is still active, as well as the embryo dune in front of it, while the subsequent ridges represent later stages in evolution of the whole sand dune system. The possibility of development of these forms is connected to the general features of the beach-surf zone: dissipative beaches allow the dune to become larger (maximum potential sediment supply), while reflective beaches produce smaller foredunes.

Hesp (1999) described how a foredune can evolve: according to his theory the foredune state can represent the stable state on which a dune pass most of its life, but it

can be also interpreted as an intermediate passage in an evolutionary sequences which foresees Aeolian erosion, vegetation reduction and waves impacts.

This sequence includes five stages from a morphological continuum form, to an almost complete erosion. Intrinsic features of the dune/beach system can make the dune jump some stages, for example in correspondence of catastrophic events (huge storms), but it is expected also the possibility to stop erosion and (with some limitations) to proceed back on the sequence.

1.3.2 Blowouts

Most authors define a blowout as a trough (narrow and deep), saucer (semicircular but shallow and wide) or cup (semicircular and deep) shaped depression formed by wind erosion on a pre-existing sand deposit (Hesp, 1996). Usually blowouts present some morphological characteristic elements: lateral erosion walls, deflation basin and a depositional lobe, landward (figure 1.9).

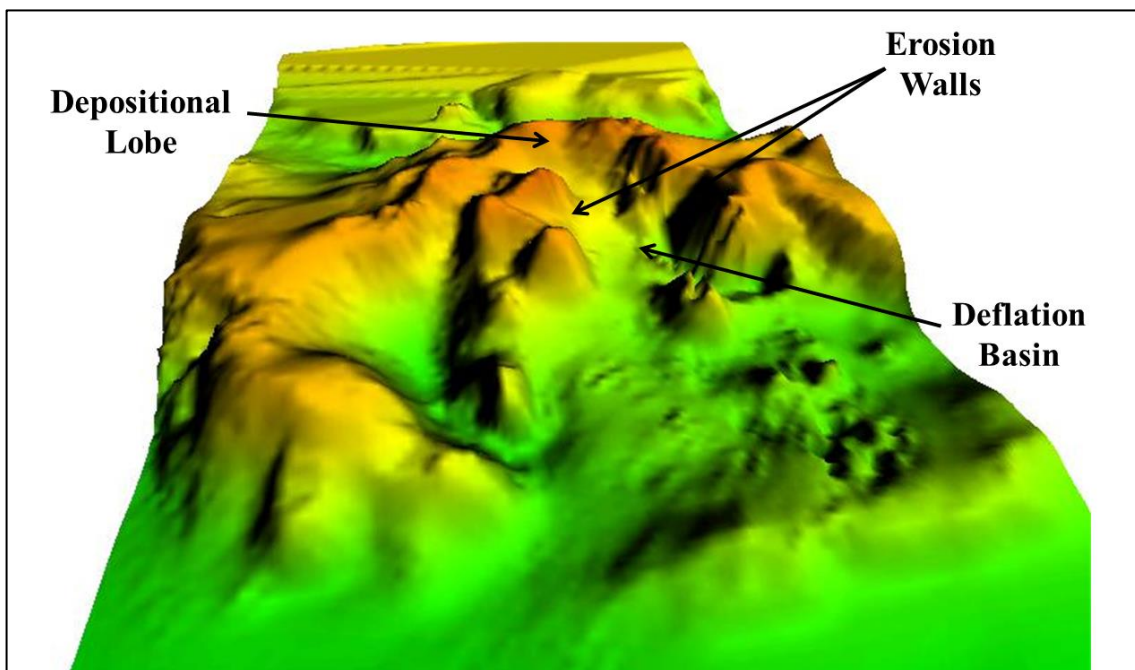


Figure 1.9: Blow out morphology: laser scanner 3D reproduction (Marina di Ravenna); it can be seen the deflation basin, the erosion walls and the depositional lobe.

This erosional element can be born in every type of dune, at any latitude, usually in low vegetated areas. There are several causes, natural and anthropic, which can start

the blowout creation: animal grazing or digging nests, wave erosion and slumping, vegetation removal in different areas, topographic acceleration of wind flow over the crest, sand inundation and human impact (for example pedestrians).

In any cases just a little scar in the dune body is enough to develop a huge erosional form. This is due to the intrinsic characteristic of the force that creates blowouts: the wind flow. Remembering what wrote before about the Bernoulli's effect, it became easy to understand what happens here: blowing in a section with a lower width the wind flow is accelerated and increases its erosional power. This is a part of the dangerousness of blowout: the mechanism that generates them is "self-powered", thus the more the wind digs, the less wide become the section, the faster the flow blows. In 1996 Hesp and Hyde proved that wind speeds in blowout can be significantly greater than remotely sensed wind speed.



Figure 1.10: View of a wide saucer blowout in Coorong National Park, South Australia.

Starting from this basilar process, many authors in past years tried to study the interesting flow dynamic of wind blowing into blowouts. In 1981 Hails and Bannet found that the wind flow within the blowout is separated in many different flow streams directly influenced by the angle between the approaching wind flow and the blowout

entrance: the more they are normal to the blowout the higher speed is reached. Beyond the separation mood of the flow, it was often observed as morphological effect, the presence of a nebka at the entrance area (Carter et al., 1990).

In any cases the erosion/deposition process occurs in a complex manner related the varying wind speeds and directions: the flow separates as it enters the blowout and then, depending on several factors, it forms different turbulent flow (for example an helical flow or a reverse rotor flow). Usually the most common effects of this topographically accelerated flow accompanied by turbulent jets, is deepening the deflation basin and enlarge the erosion area; Carter (1990) described the roller vortices transporting sand out of lateral walls forming rim dunes, and through the middle axis creating a depositional lobe parabolic shaped or radial (depending on the initial type of blowout). Mid-axis flows are usually the highest for speed: on a transverse plan the wind profile is Gaussian decreasing outwards. Moreover when it exits landward it is subject to a strong deceleration and a flow expansion causing the depositional lobe creation.

In most cases blowouts grown in length upwind against the prevailing wind (Jungerius et al, 1989). According to Hesp (2002) blowout width is proportional to the depositional lobe length, in a ration of around 1:2: as a blowout become wider it becomes longer as well.

Blowouts evolution is related to several factors such as aeolian climate, beach/dune erosion pattern, high energy events, and many others (Hesp, 2002). In many cases they tend to become a parabolic dunes, but in some cases it is possible for them to stop the erosional trend thanks to an occasional re-vegetation.

1.3.3 Dune micro-morphology

Considering all the dynamics in action in this environment, it is easily understandable how the dune morphology became really complex. In this study the author tried to describe specific behavior of particular morphological units, which are going to be described in this paragraph. Taking inspiration from the 1992 model published by Barrère (figure 1.11), the author identifies some morphological features which could be representative of the dune dynamic behavior.

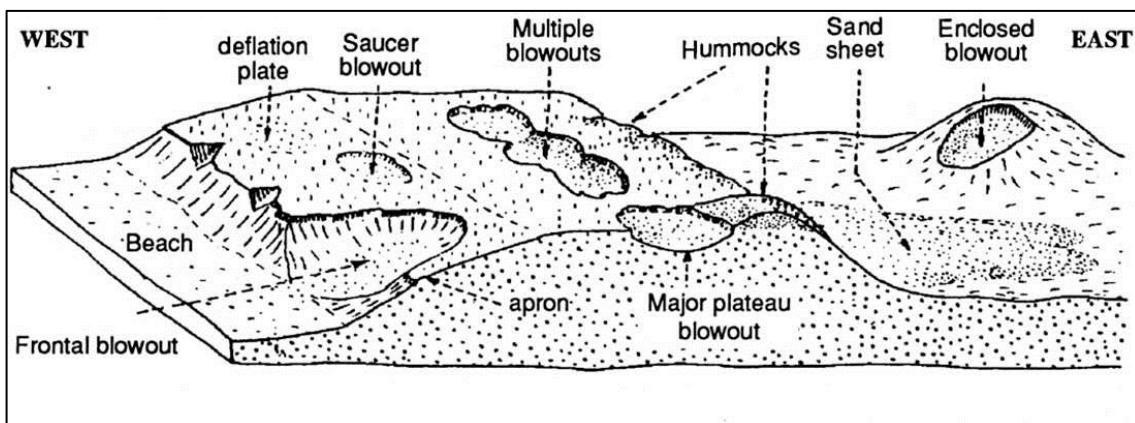


Figure 1.11: Dune morphology scheme (modified from Barrère P., 1992)

The dune foot is the most forward part of the dune and it can be interpreted as the line of contact between the dune system and the beach system. What characterizes this element is the drastic change of slope crossing it. As seaward limit of dune, it can be representative of progradation/retrogradation by the whole system.

The crest is represented by the dune highest elevations; in analogy with the dune foot line, the crest line joins the highest elevation points, but it is expected that it is much more conservative than dune foot (Psuty, 2009).

Moving landward, the next morphological element is the landward “foot”, which is called “talus” and is consistently smoother, such that an upper and a lower limits are identifiable.

Passed this feature usually begins a depression limited landward by the vegetated dune line, after which habitat raises and became the vegetated dune (“fixed dune”).

All these features are distinct morphological elements and individuates particular sections of the dune body which have a different dynamic behavior and a different response to the vary forces acting in this environment (wind, sea and vegetation).

2. AREA OF STUDY

This study was developed sampling data from three particular areas in Ravenna territory, located on the North Adriatic coast between Venice and Ancona (about a hundred kilometers from both). The Ravenna area is raised a few kilometers South of the Po river delta, the most important river of Italy. The three areas are located onto the coastal zone and they cover almost the whole coastal Ravenna belt from the most North site, Marina di Ravenna, to the most South, Milano Marittima, passing through the Bevano river natural area. In figure 2.1 the national/regional area can be consulted.



Figure 2.1: area of study location within the State and Regional territory.

2.1 Geological History.

From a geological point of view, the zone including the three site of study is the most South-East part of a wider macro-region represented by a flood plain created by the Po river, called “Padan flood plain” (“Pianura Padana”), which took place starting from the Oligocene/Miocene, when the Apennines mountain range emerged.

After this the geologic evolutionary event, the system was dominated by dynamics linked to the sea level oscillations and consequential complex depositional conditions. During the Last Glacial Maximum (70.000 – 18.000 years ago), the sea level was lower than actual of about 120 meters: the North Adriatic zone was a wide flood plain whose shoreline was located approximatively in the Ancona area (Correggiani, 1996), and the zones between Ancona and Pescara were characterized by wet lands and lagoon environments (figure 2.1).

At the end of the Wurm glacial period, the general climate started to heal, getting warmer, and it brought a decreasing of glaciers and, consequentially, a sea level rise. 5.500 year ago, the climate Optimum was reached and the sea level went into a high standing phase, characterized by a strong shoreline backing to the lowest areas of the Padan Flood Plain, about 20 km inland relative to its actual position. Amorosi (2005) observed within high-stand deposit the lateral contiguity of peat sediments (4000 years ago), which indicates a marsh/wetland environment.

In last 2400 years has prograded for 11 km, on an 80 km of coastal band (Cremonini, 2007). Figure 2.2 proves this situation: fossil traces of paleo dune fields are clearly seeable, disposed on arcs, in the inland. From the most ancient and most inland dune field, dated XII-XI sec. B.C., moving to the actual shoreline, it is possible to individuate the VII sec. B.C. formation, and those developed between the V and II sec. A.C., VI and X sec. A.C (Bondesan et al., 1995). 3000 years BP the climate conditions turned colder and wetter, thus the Padan flood plain was passed through by a hydrographic network much denser. Between 2500 and 1500 years ago the climate turned warmer but the general hydrographic condition stand stable. It was a heavy rainy period thus many river channel overflowed towards more depressed areas, creating a huge zone of lakes which slowly turned into wet lands.

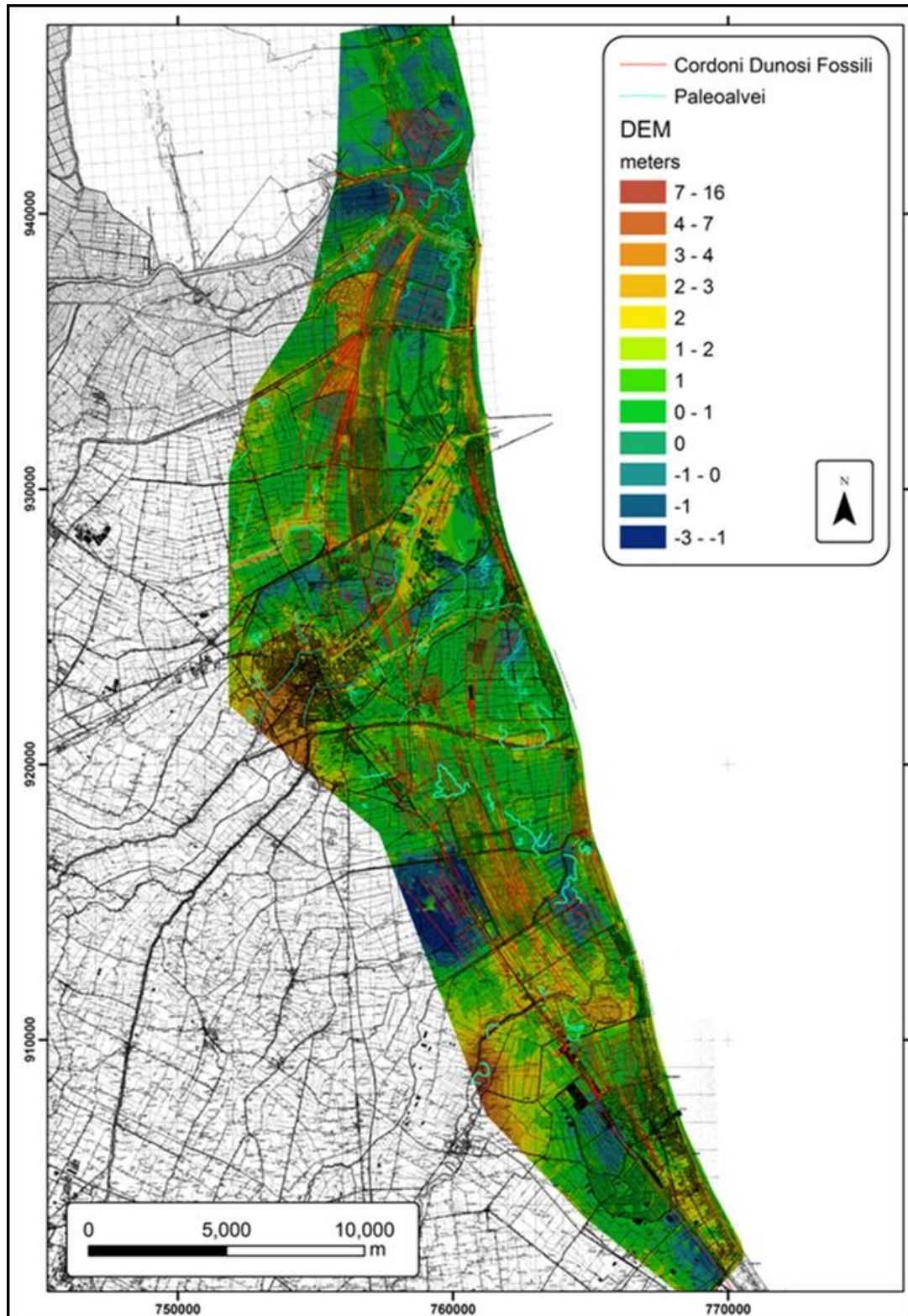


Figure 2.2: Digital Elevation Model of Ravenna territory: paleo dunes and paleo river channels are figured in red (Regione Emilia-Romagna Cartography, 1999)

Starting from 1500 years B.P., climate general conditions got worse, reaching its climax during the period between VI and VIII sec. A.C., which is called “Little Ice

Age”. In this period river estuaries became stable and stopped their pro-gradation. The current configuration of the system is the result of these natural processes and what humans did basically in last 400 years, especially for what concerns hydrographic basins regulation. The latter strongly influenced the river regime and its loan of sediment distribution. Many authors have discovered how estuaries geometries are under a constructive trend until 5 centuries ago, then they turn in a “destructive” one, and the forms are dominated by wave erosion and littoral drift. Nowadays thank to the strong decrease of sediment contribution by rivers (due to the human civilization), that domain of the sea on this zone is consolidated: dunes and beaches systems along the Ravenna coastline, are subjected to an erosional trend. In figure 2.3 a schematic draw of the Padan Flood Plain evolution can be consulted.

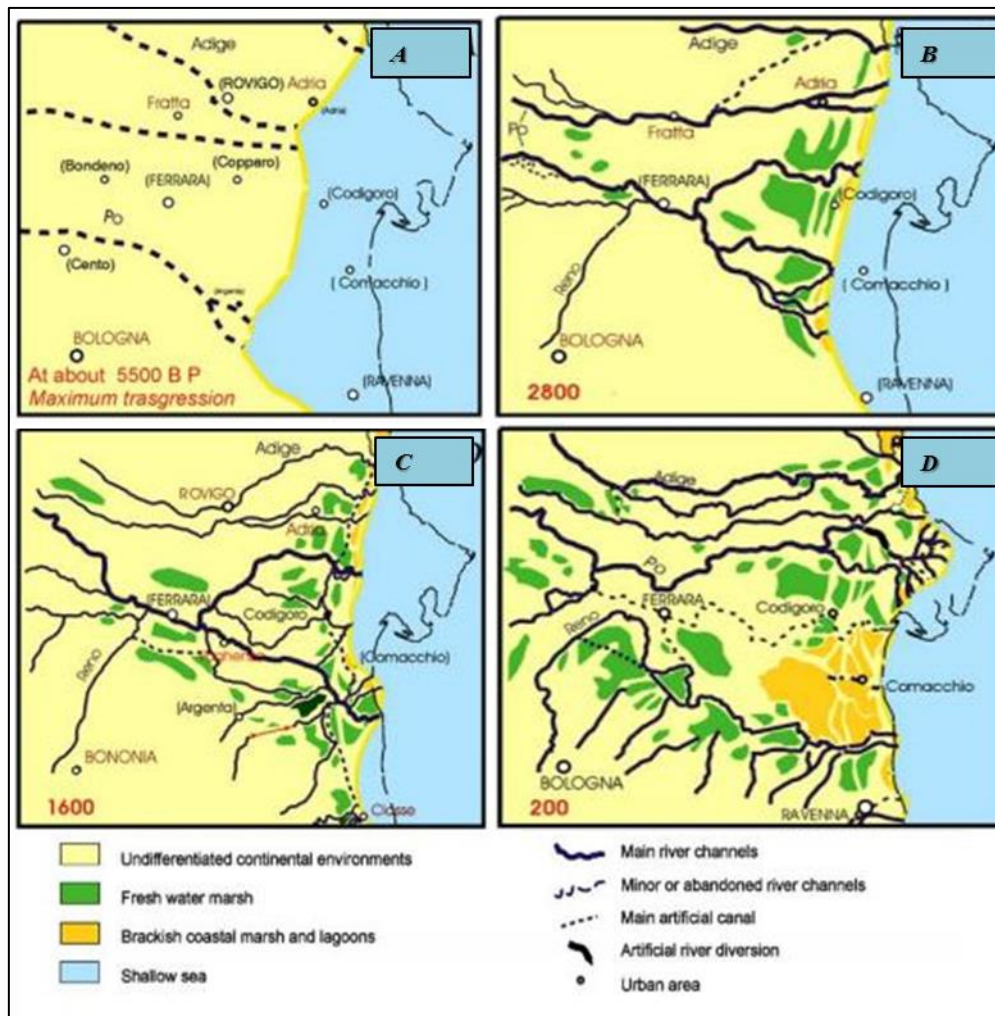


Figure 2.3: recent regional evolution of the shoreline. From the Maximum Transgression (5500 years BP) to 200 years ago. (modified from Stefani & Vincenzi, 2005).

2.2 Subsidence.

It has been calculated that the average subsidence speed in the Ravenna area, for the whole Quaternary, varies from 1.8 to 3 mm/year (Bertoni et al., 1988). This intense phenomenon is due both to deep tectonic causes and the differential compaction of the Pliocene-Quaternary sediments.

Unfortunately this averaged calculation is destined to a marked increase if the period taken in consideration is limited to the last 40 years, when the industrialization of the area started. In this period anthropic activities became forceful, especially those related to the fluid extraction from the subsoil (water and hydrocarbons) for the industry need; simultaneously the hard management of numerous rivers which cross the Padan flood plain caused a reduction of sediment which before used to fill the coastal area. From 1972 to 1977 the average speed value was about 40/60 mm per year, with a highest value of 110 mm/year.

In the 1981 the Regional Agency for the Environment Protection (ARPA) staged a subsidence monitoring network which recorded a considerable quantity of data about its trend: during the 80's the subsidence started to decrease and nowadays the rate varies from about 3 to 8 mm/year. During this period the potable water network was connected to the macro-area network, thus the extraction of water from the subsoil was almost stopped.

This situation is very dangerous for a coastal area as Ravenna, in terms of risk of inundation. This risk is amplified by two problems: on one side, the eustasy for which the sea level has raised about 1 mm/year in the last century; on the other side some coastal areas, corresponding to gas wells for methane extraction, are sinking with a 10 mm/year rate.

In spite of this, Carbognin (1984) have discovered that even if gas wells effects have a strong influence on the risk dynamic because of their position, they do not induce the most critical situation on the local territory, which instead is located in correspondence to the industrial zone and where the extraction of water still continues (causing the depressurization of the aquifer). The water extraction in effect causes a decrease of the interstitial pressure, which makes heavier the load on sediment; this

2. Area of Study

causes an elastic deformation of the soil and usually an additional compaction of sediments.

In conclusion the subsidence is the main problem that the Ravenna territory faced in last 50 years. Many areas both inland and on the seaside are under the sea level, and the whole territory is under unstable condition.

The geological Survey Office of Ravenna City asserts in a recent study that in a period of 15 years, from 1996 to 2011, the cumulative subsidence have reached a maximum of about 20 to 22 cm, in the coastal Lido di Dante area. Data relative to other zone can be consulted in map 2.4, below.

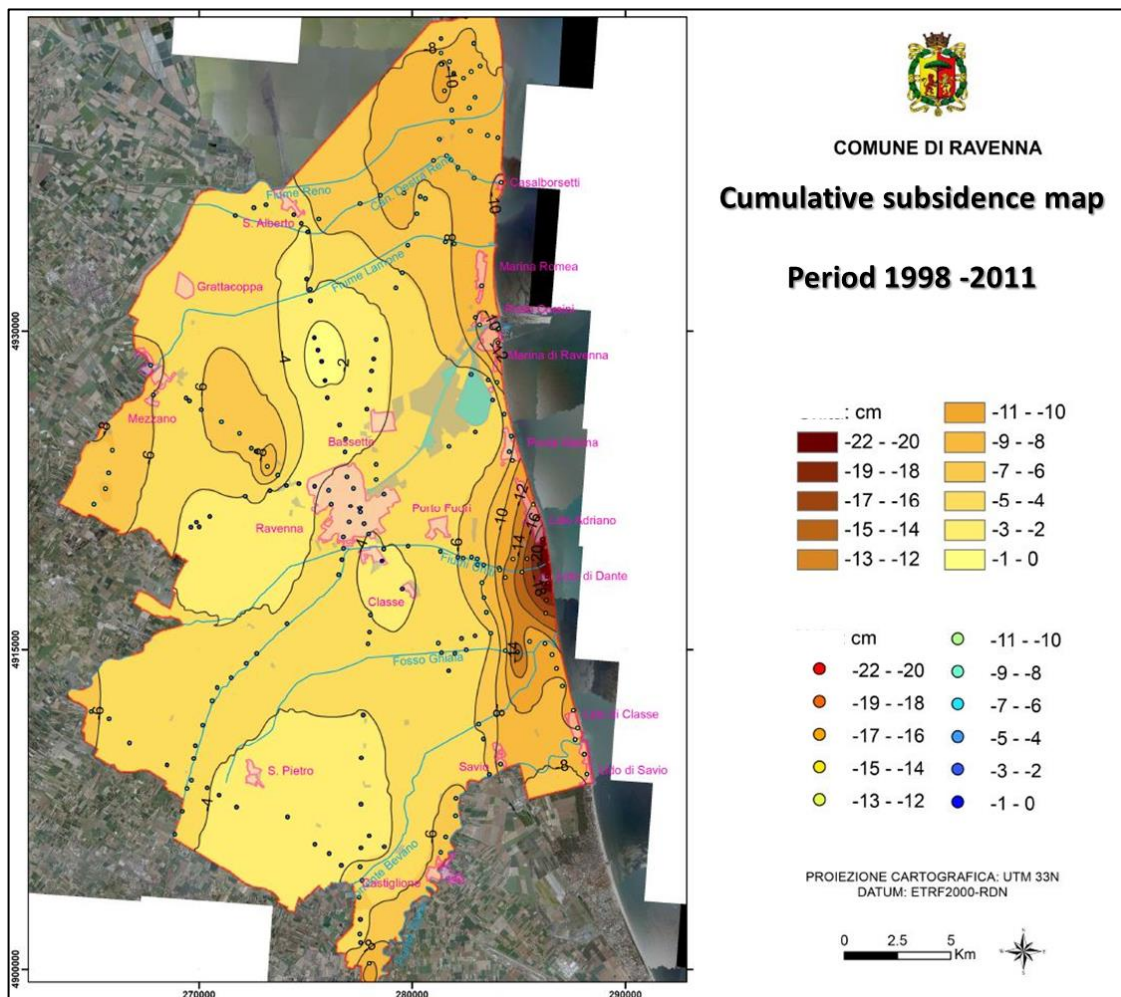


Figure 2.4: Cumulative subsidence map for the period 1998-2011. Ravenna area.(Servizio Geologico – Comune di Ravenna, 2006)

2.3 Emilia-Romagna Coastal Zone.

The Emilia-Romagna coast goes from the estuary of the Goro's Po river at North, to the Cattolica town, South, for an extension of about 150 km. The most part of this landscape is occupied by low and sandy dissipative beaches, sometimes protected by offshore breakwaters (Armaroli et al., 2011). The North part is crossed by the Po river and many other rivers coming from the Apennines as Savio river, Lamone river, Fiumi Uniti river and Reno river; moreover in this area a lagoon system created by the estuary of the Volano's Po river (abandoned) and the Goro's Po mouth (Calabrese et al., 2010).

This hydrologic network makes the area very dynamic from a morphological point of view, thanks to the activation/deactivation trend of these numerous river estuaries; it has been already explained how, in last five centuries, following the Po river's delta progradation, the shoreline has shown forward movement of more than 20 km in the neighborhood, while in other sectors the average value didn't exceed 5 km.

According to the National Group for Coastal Research (2006) the general wind climate of this area are concentrate in the I, II and IV Quadrant, with particular peaks for what concerns energy, from ESE and SSE ("Scirocco"), from NNE and E ("Bora") and from NO (Maestrale). According to Lamberti and Zanuttigh in this North Adriatic area the wind intensity is stronger if linked to a short fetch effect, such as Bora wind which reach highest speeds, while with wider fetch effect the speed peaks are lower (Scirocco wind).

This obviously influences the sea climate too: storms are frequently produced by Bora, especially coming from ENE, and Scirocco from South-East. In general the wave climate is mild with low energy waves, and a significant height lower than 1 meter for the 65% of cases, usually coming from Est (Gambolati et al., 1998).

According to Ciavola and Grottoli (2012) the sediment transport environment is domain of the littoral drift, basically moving from South to North. The tide regime is defined micro-tidal, with daily and nocturnal components range which goes from 30 to 70 cm.

2.3.1 Local dune ridges evolution

During the XIX century the whole Ravenna coastline was bordered by linear dunes, which could reach a length of some kilometers and a width of about 100 meters. Locally the medium height was oscillating from 3 to 5 meters.

At the end of that century, the human impact on this environment became stronger and stronger was the deviation from the natural behavior. A wide area was covered with Pine forests in order to protect inland agriculture from the salty aerosol. These actions had the effect of stabilizing paleo-dunes, while at the middle of the last century, any other dune left out of the forest area were flattened to build tourist infrastructures.

Starting from the 50's the Italian tourist economy had a boom, and thus the need of infrastructures raised. This was more true in the south part of the regional coast (the Rimini area), while some more dune residual were left in the North area, even though the sand taking for construction industry was already a threat. Between the 50's and the 80's the surface occupied by dunes was halved in the whole region, leaving some considerable residuals only in the Ferrara and Ravenna area.

Fabbri (2001) verified that the Ravenna's dune field in 1982 was extended for 38.2 km, while in 2001 they were decreased to 11.2 km, of which just 9.2 km in a good state of conservation. From this study emerged that 12.3 km disappeared because of the shoreline regression; 9.5 km were lost for the edification industry; 7 km were in a bad state of conservation because of the effects of the tourist buildings construction on the beach. On an area of 19 km² only the 3% was occupied by active dunes (in 2001), while the 97% is stable, vegetated or under a Pyne Forest (thus, more than stable). Unfortunately many parts of these active dunes are in bad dune/beach equilibrium, so they basically should be defined "unstable", beyond the "active" definition.

2.3.2 Coastal Geomorphology Map 2005

In 2005 the Regional Agency for the Environmental Protection (ARPA) released the Coastal Geomorphology Map (CGC2005), based on airborne photo-interpretation, LIDAR data, bathymetrical data and a terrestrial survey campaign. The technical staff who worked on it focused the study on six principal topics: dunes, subaerial beach,

defensive infrastructures, surf zone, river estuaries, lagoon and wet lands. In this paragraph only the first three arguments will be treated.

The dunes were surveyed and subdivided in three classes relative to their “maturity degree”, substantially in terms of vegetation cover: active, stable and partially stable. Beyond this index the CGC2005 can give many information about the dune ridge, on regional scale, such as its width, its continuity and elevations.

The Emilia-Romagna coastal belt is occupied for the 48% of its extension by coastal dunes, much more concentrated in the Po river area, on the Ferrara and Ravenna territories, than the Rimini area. In absolute terms in 2005 the length of the coastal area bordered by linear dunes decreased to 37 km along the Region; in the Ravenna specific area the extension was limited to 23 km.

Most part of coastal dunes are short dimensioned, with an average height of 2/3 meters, stable or partially stable, while a very little percentage rests active. The width is obviously limited fundamentally by the strong urbanization and human impact and it oscillates between 0 and 200 meters.

The beaches (aerial backshore) general state is not encouraging too; on the whole territory the 25% is occupied by touristic infrastructures, especially in the South part of the region (Rimini area). The beach width can reach a maximum of 300 meters, but its average value is about 70 meters. The two parts are very different one from each other: the south part presents a lateral continuity much more accentuated than the North one where the width has intense variations, up to disappear in correspondence of some segments.

The generic erosional pattern and the strong alongshore drift towards North are proved by the shoreline trend and the many erosional features seeable on the dune/beach ridge. Going further towards the sea, the beach has a gentle slope and the fore shore is characterized by the presence of 2 to 3 bars, typical of a dissipative system; usually these bars systems, oriented alongshore or oblique, are developed up to 100 meters from the shoreline.

2.3.3 *The MICORE project.*

In 2011 the ARPA Agency and the University of Ferrara published a detailed work focused on the sea and storms impacts, primarily trying to extend the data set in terms of time as much as possible, then monitoring specific sites and testing new methodological tools studied to measure storms, their energy and their impact.

A very interesting part of this study is focused on storms and their impact, which MICORE project faced on two fronts with two relative data sets: on one side it proceeded to an identification analysis of high energy events from 1992 to 2010, using data from the different buoys which operated in that period and area (Ancona, Venezia and Ferrara); on the other side, the project included a reconstruction of all storm events, in term of impact, from 1946 to 2010.

The “storm catalogue” (1992-2010) has identified 225 high energy events for that period and it has described each storm in terms of waves height, period and direction (for buoys that didn't record the direction, the wind direction was assumed as substitute). Moreover applying the same methodology proposed by Armaroli et al. (2007) for local study, the total energy was calculated correlating the waves' height to the storms last.

For each event, the sea level was recorded too, considering a temporal window going from the 24 hours before the event to the following 24. The impact was calculated in terms of dune/beach erosion, sea ingression, canals flood, infrastructures and touristic building damages.

An interesting characterization of the storms pattern resulted from the analysis of the number of storms per year linked to the carried energy: histogram in figure 2.x shows these results. The Energy datum represents the storm's impact force. It is clear how there are some years with many low energy events, which didn't emanated much energy, while during some other years the number of storms was lower, but with a strong energy, and this made the impact raise.

Ferreira in 2005, proved the increasing damages due to the occurrence of two events in a relative short time. For last years the 2000 was a poor year both for number and energy of events, while the 2002 and 2005 are the two years during which the most damages were registered. 2004, 2009 and 2010 registered many low energy events, but concomitant occurrence of the storm surge conditions aggravated their impact. In

conclusion of about 50 events surveyed (4 multiple) 26 have an intensive impact on the coast area.

December, November, May and April seem to be the months more affected by these events, which usually are accompanied by I and II quadrant wind and a sea level exceeding 0,8 meters. In the Ravenna area storms are concentrated in November, December and January, with storm surge condition and II quadrant winds (Perini et al., 2010).

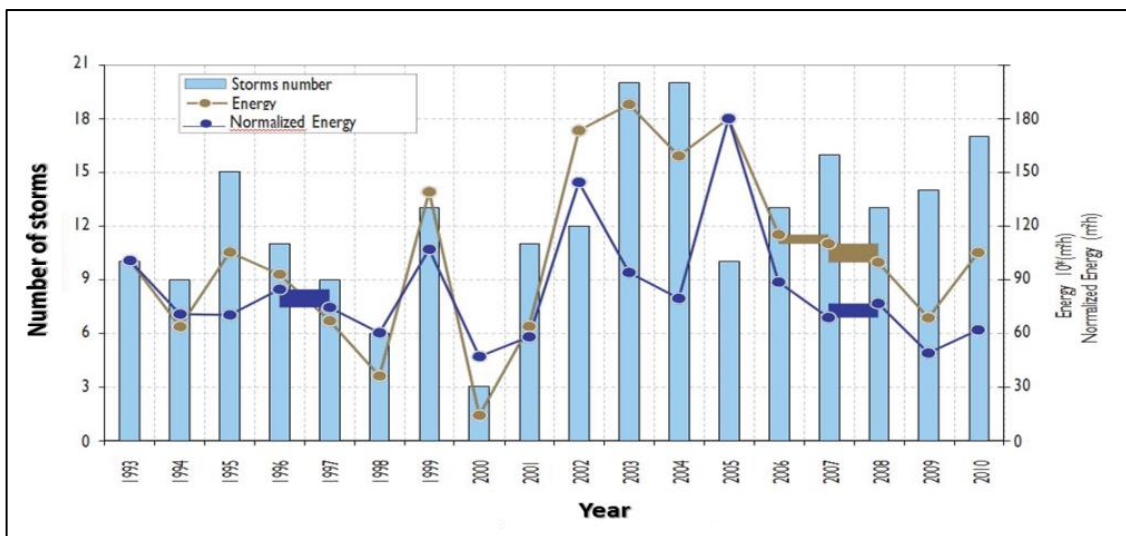


Figure 2.5: histograms represent number of storms per year; the green line the total energy and the blue line the normalized energy (Modified from Perini L. et al., 2011)

The impact catalogue (1946-2010) is the result of a much more complicated data collecting, but, in spite of the lack of data, some interesting data appeared. Even if the storms number increase from the 90's is not directly ascribable to a real increment, because of the lack of data, the analysis on the maximum sea level gave interesting results. Canestrelli et al. (2011) described how the number of storm surge events per year increased from 50's to 70's, stayed stable from 70's to 90's and then boosted in last ten years.

2.4 Sites of Research.

2.4.1 Bevano river estuary area.

The Bevano river estuary has a high environmental value and it is inserted within the Biogenetic State Natural Reserve (“Duna Costiera ravennate e foce torrente Bevano”), under the forestry police shelter (Gabbianelli, 2009). This reserve is included in the wider “Regional Po river delta park” and it is classified as a Special Protection Zone (ZPS), managed by the European Community.

This particular area is part of the Ramsar Convention for wetlands and migratory species thanks also to the presence of *Charadrius alexandrinus*, a migratory bird which use to keep its eggs on the dune seaward stoss. This allows the administrators even to completely forbid parts of the beach to tourists walking, for some periods during the year.

Until the 2006 this was the only natural river mouth left in Italy, but, due to hydraulic and environmental problems (the mouth was keeping migrating to North, damaging the dunes), the management chose for a strong action on it.

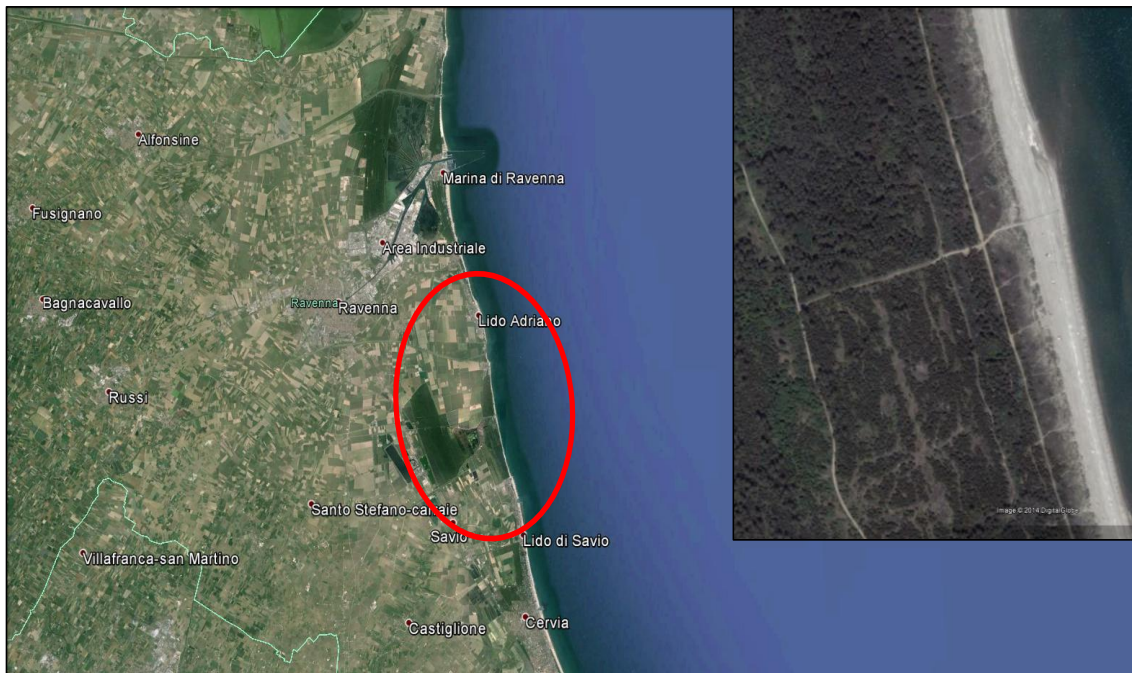


Figure 2.6: The Bevano river natural area.

This site is the only, in the Ravenna zone, where the dunes are continuous for about 5 km, undamaged and natural looking. Backward to this dune ridge there are two artificial state-owned Pine forests (“Ramazzotti” and “Savio”), planted in 1881, which have by now replaced the typical and natural back-dune vegetation (bushes). Another effect is the complete stabilization of the paleo dune field inland, for about 500 meters width (Perini et al., 2009).

The author focused his study on a sector of the dune ridge, South of the river mouth, which is about 3 km long, from the estuary to Lido di Classe. The about 200 meters long section studied in this work is about 800 meters, South of the estuary (figure 2.6). The beach width, measured on five transects in GIS environment, oscillates from about 32 to about 44 meters, for an average approximated value of 36 meters.

From a morphological point of view this dune field is composed by a linear dune, which could be called a linear foredune ridge, because of the constrained development that the local environment imposes to this element (figure 2.7). The narrow beach and the wide Pine forest, in effect limits the dune system development on both seaside and landside (the distance between the beach and the Pine forest never overtakes 80 meters).

Wind and sea action is clearly visible in the frontal part of the dune, which present a very sloped shape and it is sprinkled with many erosional forms due to these factors. The result is a narrow dune ridge with an almost vertical Hummocky looking frontal part (foot) (figure 2.8).



Figure2.7: The Bevano dune ridge (frontal view).

The dune “body” (crest and landside) is almost completely vegetated, with grass, shrub and arboreal species. In the central zone of the area of study is split in two by a path for tourists’ access to the beach, bordered by wooden fences, made to allow tourists to go to the beach without stepping on the dune. Unfortunately, for the dynamic explained in the previous chapter about blowout/wind interaction, this element has become a zone of particular and strong erosion.

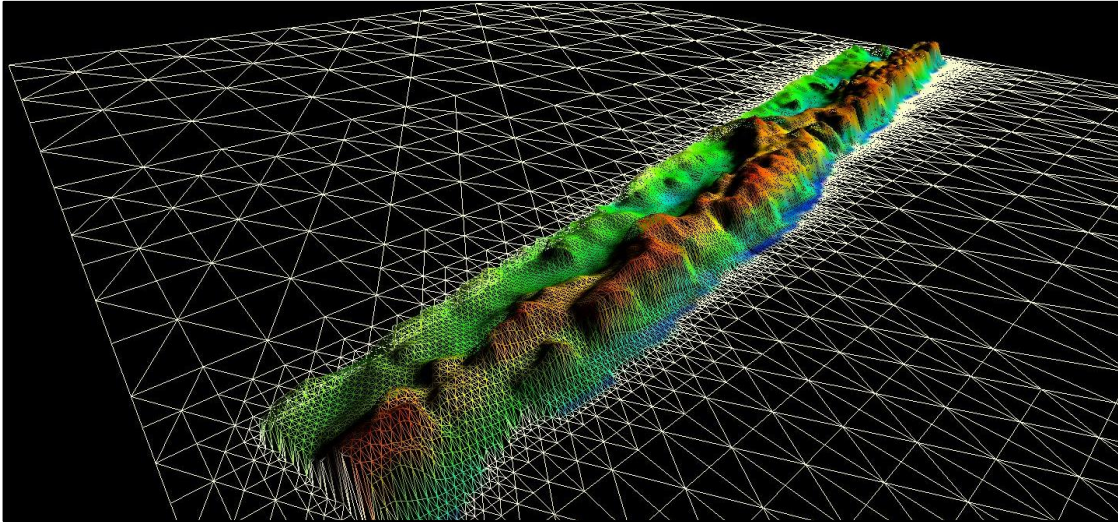


Figure 2.8: Bevano dune ridge Digital Elevation Model

2.4.2 Marina di Ravenna and Milano Marittima area..

Both Milano Marittima and Marina di Ravenna are renowned Italian seaside towns and very crowded during summer periods. The Marina di Ravenna dune (figure 2.9) is called “Giacobazzi”, taking inspiration from an old important building in town; it represent the widest residual of the much more continuous dune ridge of about 50 years ago.

The beach in front of the dune is much wider than in the Bevano area; as before, it was measured by 5 transects in GIS environment, resulted oscillating between about 61 meters and 73 meters, for an average of 68 meters. As the Bevano area, even Marina di Ravenna coastal landside is bordered by a Pine forest, but the dune, which is much more fragmented, reaches higher average elevations, exceeding in some spots the 6.5 meters.

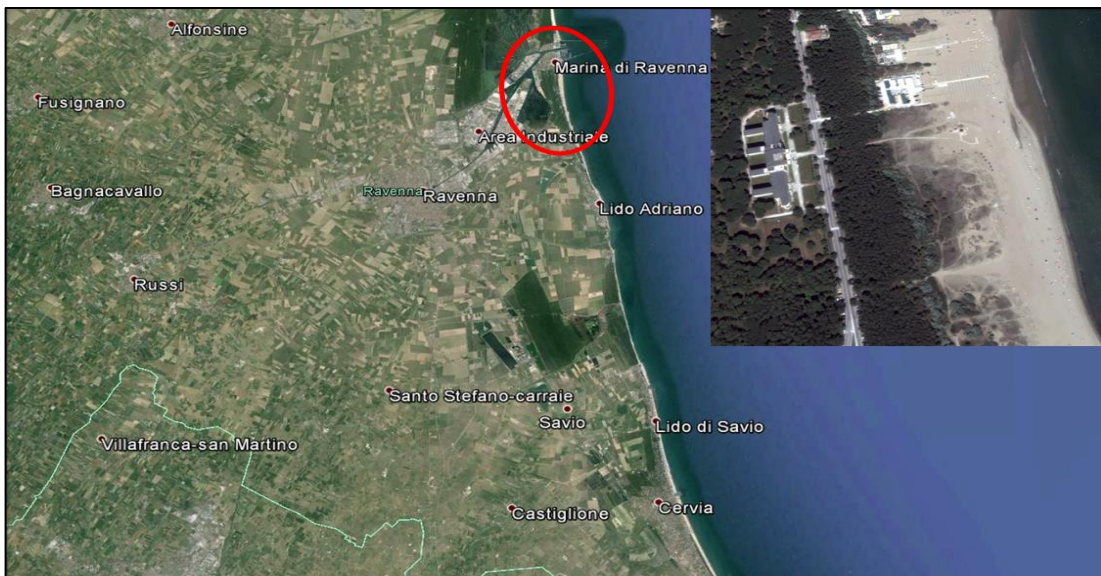


Figure 2.9: Marina di Ravenna location.

The morphology of this dune, as well as the Milano Marittima one is constrained by the hard management of the beach: on the two lateral sides of both dunes there are two paths for tourists, which are kept clean thanks to the use of caterpillars. This practice gives to dune a “barchanoidal” shape which finds no explanation in natural dynamics.

Moreover, as it is going to be better explained in further chapters, during winter period the local administration builds sand walls (called “winter dunes”) to protect

economic activities on the beach, with strong morphological effects. The summer periods behavior is subject to human influence as well, due again to the caterpillars use to “organize” the beach before the tourist period to the consequent crowding.



Figure 2.10: Marina di Ravenna dune (photographed from the crest)

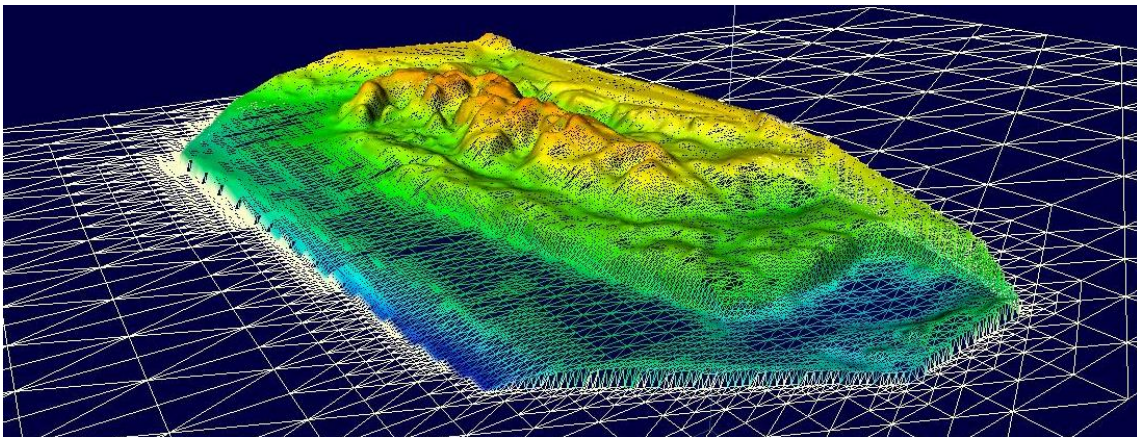


Figure 2.11: Marina di Ravenna dune Digital Elevation Model.

Milano Marittima is the most urbanized and most tourist site of those studied. The human impact on the dune/beach system is even stronger than in Marina di Ravenna. The beach in front the dune have an average width of about 56 meters, but the situation of this area is worsened by the presence of small building for tourists, straight on the beach. As Marina di Ravenna, even this dune has a particular name “Varese”, linked to the old abandoned building on the dune’s backyard.

2. Area of Study

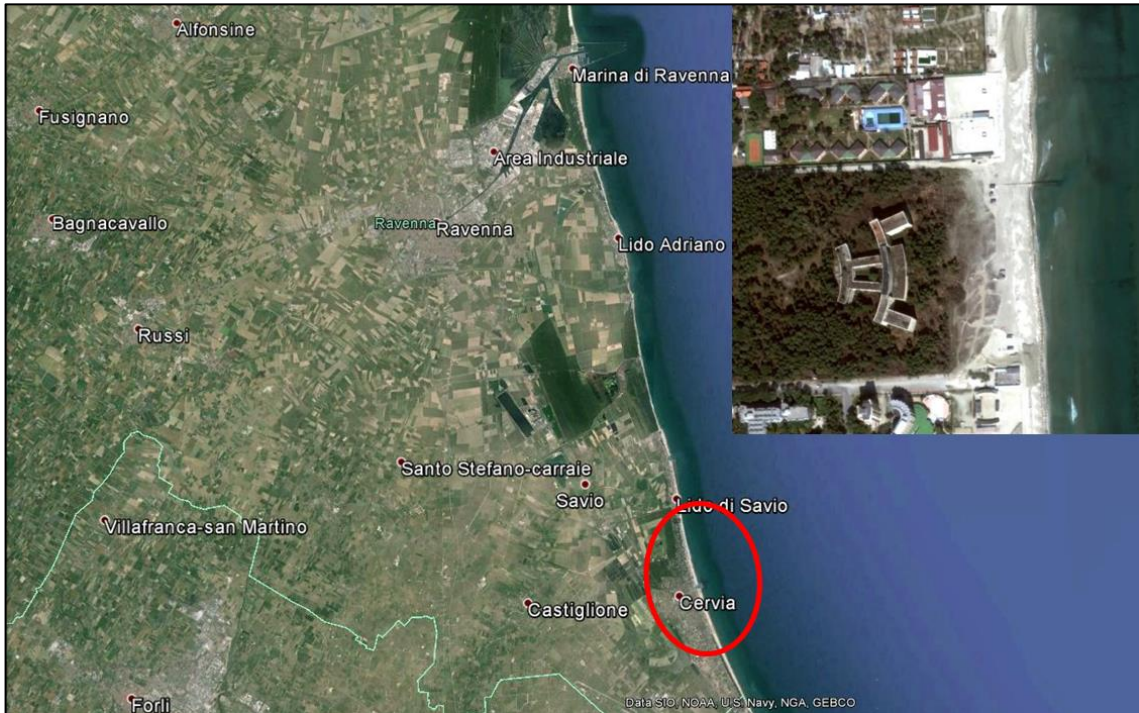


Figure 2.12: Milano Marittima location.

Even in this case there is a Pine forest on the backyard, limited only to the dune area, but it is about 500 meters far from the sea. Anyway, in spite of all those constrictions, the dune is still active and still exchanging “energy” with wind and sea. Examining figures 2.13 and 2.14, it can be clearly seen how both dunes are vegetated, most of all with grass species.



Figure 2.13: Milano Marittima dune. In the picture is seeable the laser scanner working and caterpillars footprint on the sand.

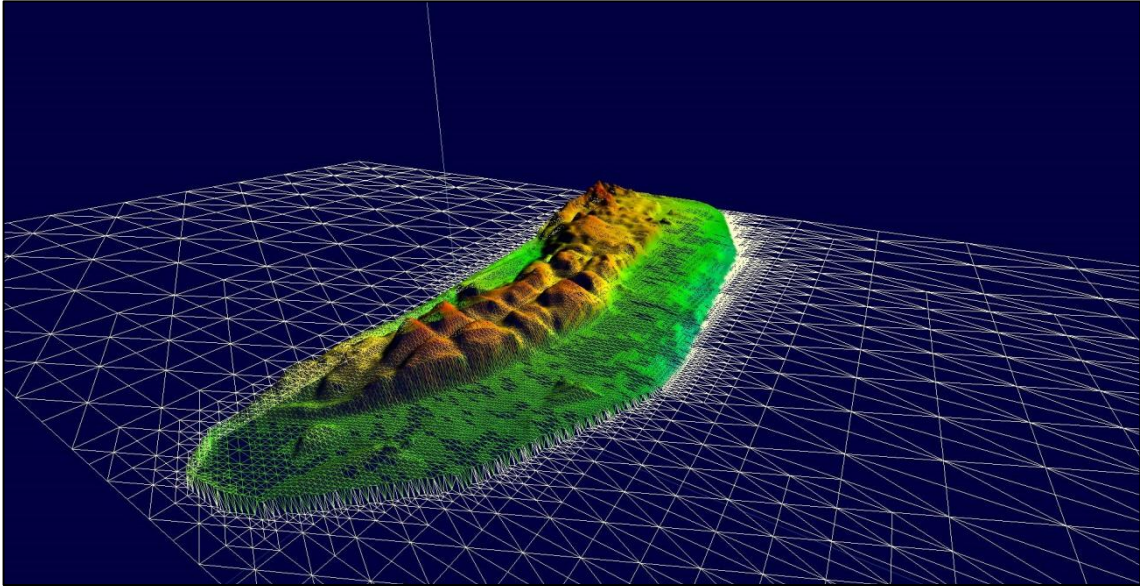


Figure 2.14: Milano Marittima dune Digital Elevation Model.

2.5 The Reference System.

Every geographical data presented in this study is referred to the ETFR2000 System (Europea Terrestrial Reference Frame). This system adopted in 2008, based on the U.T.M. cartographic system (Universal Transverse Mercator) has born from the necessity of having a geodetic reference with appropriate characteristics to be suitable for any geodetic GPS survey, worldwide comparable, especially if requires a particular accuracy (such as Real Time Kinematic activities, which are going to be discussed in next chapter). This is done compensating the error due to the earth masses influence on to the satellites' signal (the same done by the global dynamic system WGS84).

Moreover this local system was studied to include corrections relative to crustal movements: the Euro-Asiatic Plaque, in effect, is moving towards North-East, with a velocity exceeding 2 cm per year, thus in the global reference system the point's coordinates change in time. This reference system is basically updated in relation of these movements.

The whole system is supported by the Dynamic National Net (RDN), which is composed by a huge number (100) of ground control stations uniformly distributed on the national territory, which continuously receive data from satellites and communicate to the computer main center of the Army Geographical Institute (IGM), which manages the whole net. Before of ETFR2000, in Italy the ETRS89 (European Terrestrial Reference System 1989) was used. It simply represented the same system, but with the coordinates updated at that date (1989). It was the European version of the world wide famous WGS84 (World Geodetic System 1984).

The study area presented in this work is geo-referenced, according to the Datum ETFR2000, in the Zone 33, Northern Hemisphere.

3 MATERIALS AND METHODS

3.1 Laser Scanning.

3.1.1 *Laser Light Theory.*

Light has been employed as a measurement tool of the environment since last century: aerial orthogonal photos as well as multispectral satellite images are just two examples of methodologies, which during last fifty years have been universally used.

Every kind of measurement made on an object by a sensor placed at a defined distance, is considered part of the geo-physic branch called “Remote Sensing”. What associate all these techniques is that whatever is the sensor, it uses electromagnetic radiations (and their interaction with environmental surfaces), to get information from the environment around. Two are the categories in which remote sensing techniques can be divided: active and passive. While the last decade was dominated by the cheaper, but less accurate, passive methods, in last years, active techniques, which include active emission of radiation, have breakthrough (Van Genechten et al., 2008).

“Laser Scanning” is an active method of surveying environment, based on the characteristics of laser light optics: its aim is to reproduce the environment in a very accurate and tridimensional way, giving, as result, what is called “Digital Elevation Model” (DEM), otherwise a 3D reproduction of the real-world topography.

The huge variety of applications of this technique includes cartography, architecture, territorial planning, urban management, survey and control of engineering construction activity, monitoring of environmental dynamic changes, and so on.

The general advantage of laser scanning is the possibly to acquire a huge numbers of points with high accuracy in a relatively short period of time. “It is similar to taking a photograph with depth information” is a good way to describe this practice (Van Genechten et al., 2008).

The theoretical principle of laser scanning is founded on the basilar electromagnetic and optical characteristics of light: a laser is a device that can generate and amplify light operating to give to laser light some very special properties, which

distinguishes it from light from other origins (Paschotta, 2007). The word “laser” itself, in effect, stands for “Light Amplification by Stimulated Emission of Radiation”.

As known light is the electromagnetic radiation that allows the environment to be seen, and it is composed by both electromagnetic waves, which can be classified by their wavelength (figure 3.1), and small particles called “photons”. Wavelength is inversely proportional to frequency, thus, to related energy too.

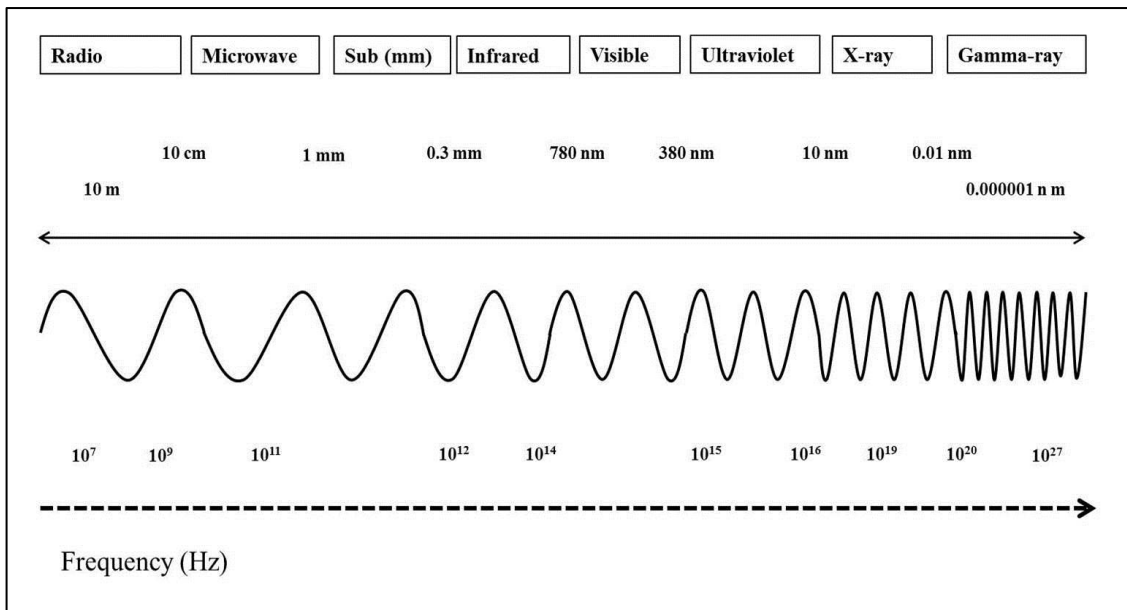


Figure 3.1: scheme of the electromagnetic spectrum.

In general, the easiest way to amplify light is to shine light on an excited atom, whose electrons are in a higher energy state. Moreover when a photon hits an excited atom causes a generation of a second photon, with the same energy, which is going to stimulate another emission causing a cascading effect (Angelopoulou et al, 1999); this procedure will emit energy in form of light.

What is really important for laser scanning technique is light propagation behavior, which is influenced by several properties: refraction, reflection, absorption, scattering and polarization. Different materials show different combinations of those propagation effects, therefore analyzing the propagation of (laser) light can give information about properties of the surface.

As source, a laser is the very opposite of an incandescent light bulb, which emits a wide spectrum of wavelength with a large angle. A typical laser light must have the form of a light beam and be emitted in a narrow spectral bandwidth; then, laser light

have to be linearly polarized, so it propagates dominantly in a well-defined direction, with moderate (as much as possible) beam divergence; last, it must have an high degree of both spatial and temporal coherence, which allow the beam to propagate over long distances. Over all these properties, what makes laser light highly suited to measurement of objects is the waves' velocity of propagation in a determined medium, which is finite and constant, thus measurable.

Laser light can be emitted in the Ultra Violet (from 100nm to 400nm), Visible (from 400nm to 700nm) or Infrared (from 700nm to 0.3mm).

The most essential optic phenomena, in laser scanning, are refraction and reflectance. The first is related to the part of light beam which, when it hits a surface, propagates through the material, bending it. It is linked to the light velocity and as a material property, can be defined by an "index of refraction", n :

$$n = \text{light velocity in vacuum} / \text{light velocity in material}$$

Reflectance, instead, is related to the part of beam which is redirected away from the surface. Ingensand (2003) suggests that "reflectance may be defined as the ratio between reflected and incident laser power", and it is influenced by some parameters of the laser light beam:

- Wavelength;
- Incidence angle;

and of the object:

- Electromagnetic characteristics;
- Surface color;
- Surface roughness;
- Temperature of the surface;
- Moisture of the surface;

This means that when a beam of a defined wavelength is shined to a surface, the reflectance depends only from material properties and, as refraction, it can be described by a simple index, called "R":

$$R = I_r/I_i \quad \text{Equation 3.1}$$

Where:

I_r = intensity of reflected radiation.

I_i = intensity of incidence radiation.

The relationship between the reflected laser intensity and surface reflectance is commonly described by the geometric optics Lambertian reflectance model (figure 3.2); basing on this model, object surface can react in different ways. The two opposite extreme behavior are: the perfect specular reflection (mirrors, metals, etc.) and the perfect diffuse (Lambertian) reflection, where the reflected direction is absolutely independent from the incidence angle (figure 3.2).

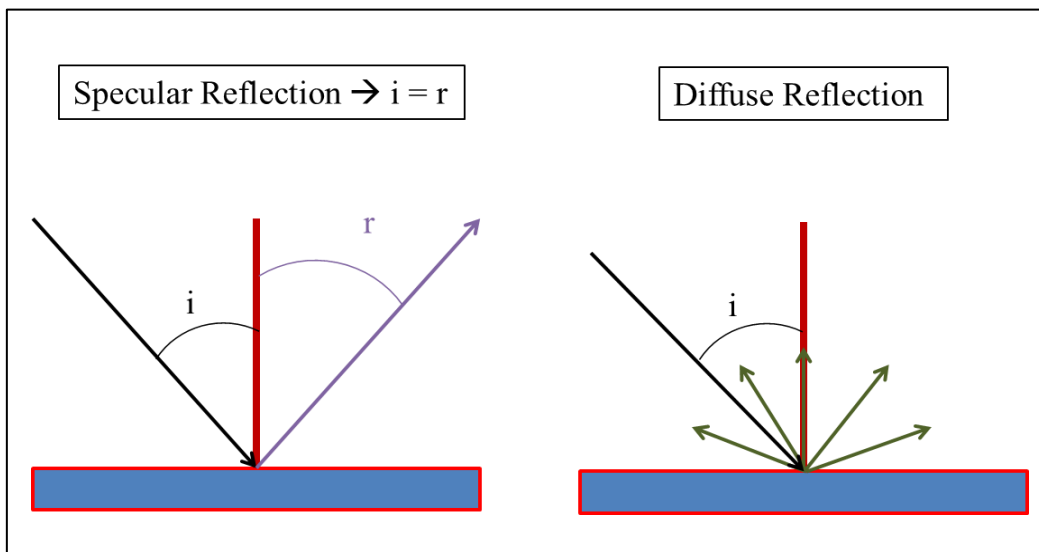


Figure 3.2: specular/diffuse reflection scheme; i is the incidence angle value, while r is the reflection angle value.

Different materials obviously have different R index, thus they reflect the same light in different ways: the geometrical behavior of the reflected component of light is governed by the Rayleigh criterion, which describes the roughness of a surface related to the wavelength of incidence light:

$$\Delta h \geq \frac{\lambda}{8 \cdot \cos \theta} \quad \text{Equation 3.2}$$

Where:

Δh = average height of superficial asperities of the surface

λ = incidence beam wavelength.

θ = incidence beam angle.

Thus the concept of surface roughness is strongly influenced by the incidence beam wavelength and its angle. In table 3.1, as example, the behaviors of different materials, in term of reflectance percentage, are shown; the reflectance values are calculated for a laser light with an almost 900nm wavelength. Last three materials have a particular optic behavior, called “almost-reflective” or “retro-reflective”, and they are usually used to build up scan targets.

Material	reflectance
White paper	More than 100%
Dry wood	94%
Snow	80-90%
Limestone, Clay	More than 75%
Broad-leaved Tree	About 60%
Conifer Tree	About 30%
Sands	About 50%
Smooth Concrete	24%
Pebbled Asphalt	17%
Lava	8%
Black Neoprene	5%
Black Rubber	2%
Reflective Leaf (3M2000X)	1250%
White Opaque Plastic	110%
Black Opaque Plastic	17%

Table 3.1: Reflectance percentage of some natural/synthetic material.

3.1.2 Light behavior and laser scanning devices

As mentioned above, a laser scanner is a device able to amplify light energy, thanks to stimulation. This stimulation must be applied on those atoms, of the “laser material”, in high energy state: “population inversion” is that process, which alters the energy distribution of atoms in a material. This is usually made by laser devices, using the light or the electrons.

The second step to produce laser light is the “light amplification” itself: this happens thanks to the cascading effect already described, and its magnitude is linked to the distance the light travel through the laser material (Angelopoulou et al., 1999); this is why usually the laser material is shaped as an elongated stick. Moreover very often is possible to extend the distance the light travel, by using mirrors at the extremities (Figure 3.3).

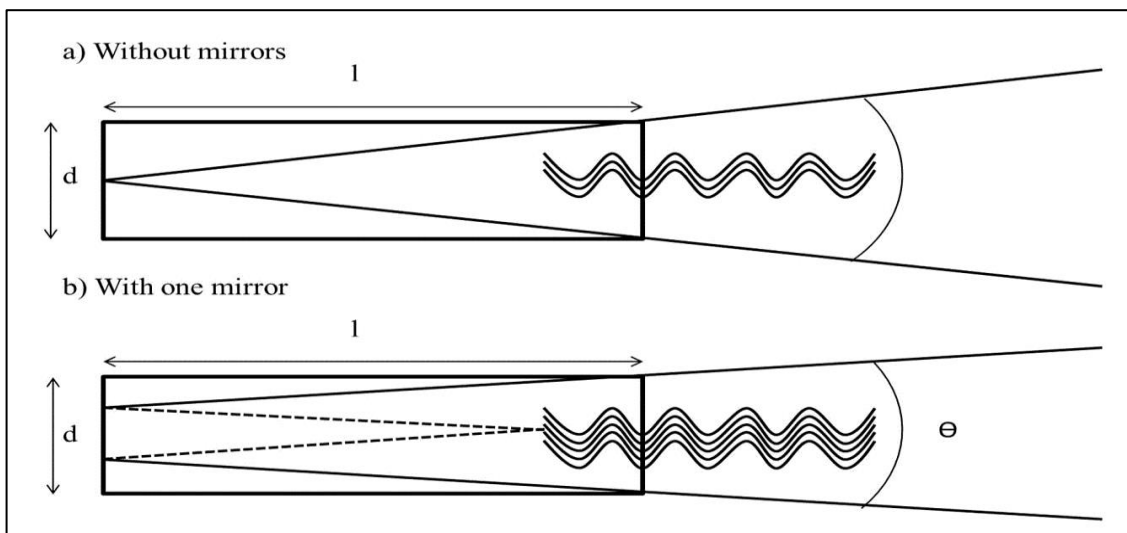


Figure 3.3: Stimulated emission in a laser stick, without (a) and with one mirror (b). (Modified from Angelopoulou 1999)

This procedure is also fundamental to produce a narrow laser beam, and its diameter is depending on the travelled length by the light: the angle of emission Θ is determined by the ratio:

$$\Theta = \sin^{-1} \left[\frac{d \cdot n}{2 \cdot l} \right] \quad \text{Equation 3.3}$$

Where:

d = laser material stick diameter

l = laser material stick length

The presence of a mirror would duplicate the effect of the length ($4 * l$), reducing the angle of emission. Unfortunately, as the beam move out of the laser cavity, it spreads out, starting its divergence. It is important to remember that the angle of divergence is proportional to the wavelength, which depends on laser material composition and on the optic of the laser cavity.

Current laser scanner technology can be divided into many categories, depending on which is the criterion. Active material used (gas, solid or semiconductor) or biological risks annexed, are just two examples. According to the purpose of this study the author will focuses on the class of devices related to the topographic surveying, which are instruments used to measure the environment. In order to measure linear distances terrestrial laser scanners can proceed in two ways: triangulation based or the time based.

- Triangulation based measurement: trigonometry is the basis for this kind of devices. It measures the distance creating a triangle (“triangulation”) between the laser emitter, the camera and the target. The emitter releases the laser beam under a constant angle: knowing by default the distance and the angle between camera and laser emitter, the device can recreate a measurable triangle by determining the angle between the camera and the laser reflection bean, looking at the location of the laser beam in the camera’s field of view. Hence, knowing just 3 elements, such as the distance between emitter and camera (triangle base), the constant angle of emission (the first base angle) and the angle of return of the reflected bean to the camera (the second base angle), it is pretty easy to rebuilt the whole triangle and measure it with accuracy (Euclid’s theorem). The laser projection, obviously, changes in the camera field of view (hence the object position) depending on the distance (figure 3.1). Triangulation devices are limited in their technological development, because the measurement accuracy depends strictly on the base width (for obvious geometrical reasons): they usually have not a long distance range and are not too much handy, because of their dimensions.

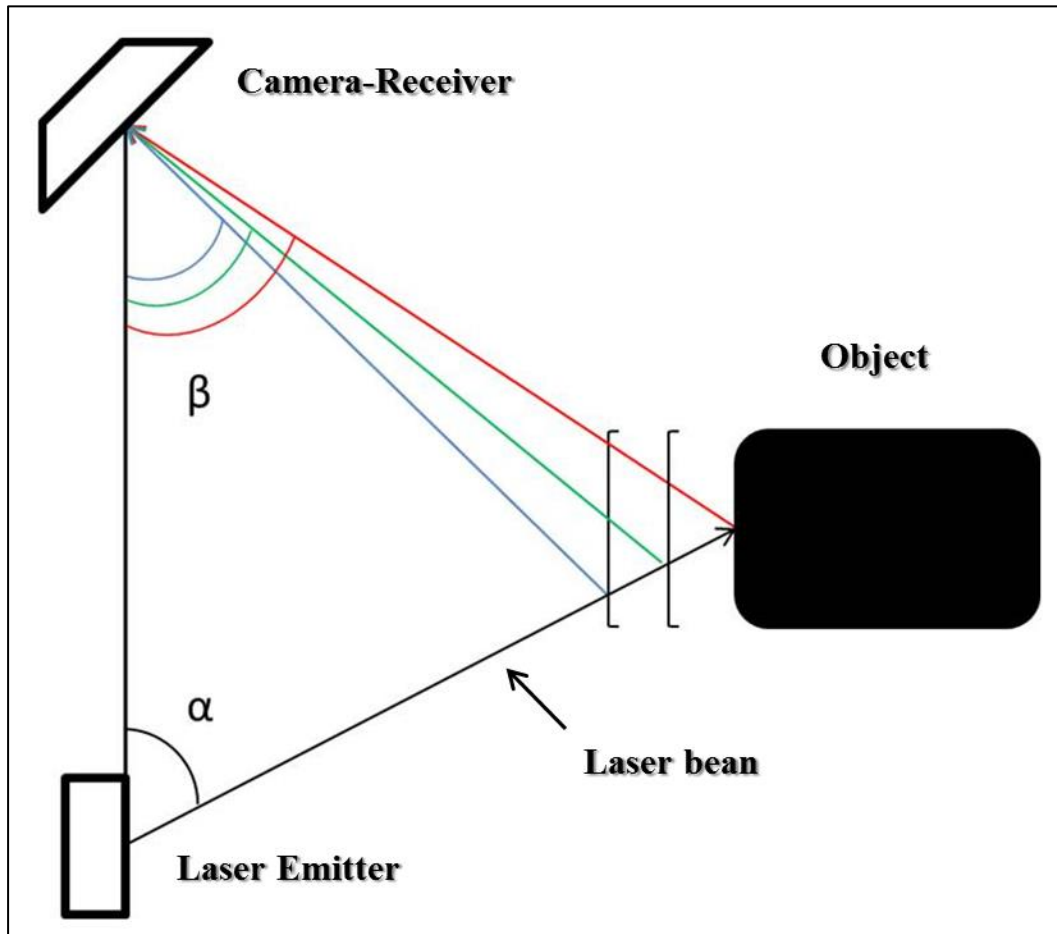


Figure 3.4: Triangulation scheme. α is the emission known angle, β is the reflected beam angle caught by the camera (Modified from Van Genechten et al, 2008)

- Time based measurement: there are two time-based scanning principle, both based on the measurement of the Time Of Flight (TOF), thanks to the fact that light waves travel with a finite and constant velocity, in a certain medium (in vacuum, $c = 299'792'458$ m/s).
 - Pulse-based laser scanners, instead of using a continuous laser beam, it uses a laser pulse, reaching superior power peaks, thus reaching longer distances, but keeping the required SNR (Signal to Noise Ratio) needed to maintain the reliability of measures at long ranges. These tools scan the entire environment one point at the time by changing the range finder's direction, using a deflection unit (usually a mirror) and calculating the TOF thanks to a high precision clock (Van Genechten et al., 2008). They can measure up to 50000 points every second. This number is limited by the condition that the device

is not able to emit a beam until the previous beam has returned and received.

- Phase-based laser scanners can modulate the power of the laser beam emitted, which is usually in the infrared field. They are very similar to pulse based, but utilize a constant beam of laser energy and, instead of using a clock to measure the TOF, there is a circuit (phase discriminator) which measures the phase difference between the sent and received waveforms. Obviously, this property gives to these devices a better accuracy in measuring “time”, thus in measuring the points distance (between 2 and 4 millimeters), than pulse based scanners. Phase-based scanners are also faster and can acquire data at a rate up to a million points per second. However their range is limited to around 80 meters.

3.1.3 Laser scanning systematic errors

In the very last year laser scanning is one of the most developed techniques, especially improved in the environmental monitoring field. This happened because of two factors: first of all the decreasing cost simultaneous to the increasing power and manageability of these devices; second for the many operating benefits of these systems: they do not require ambient lighting, they provide high density measurements, they are fast and the procedure is deeply automated, they are useable on featureless surfaces, they give very accurate results and so on.

On the other hand, even these devices can be affected by systematic errors due to four main causes: instrumental, object-related, environmental and methodological.

- 1) Instrumental: this source of error is strictly linked to the intrinsic characteristic of the instrument itself. First of all, beam divergence can have a strong effect on the point cloud resolution, as well as on the positional uncertainty: because of the divergence, the beam width tends to “enlarge” itself running out from the source to the target, hitting an area large likewise, which will project a reflected beam even more large; since it is assumed that the laser reflection has a Gaussian shape, there is a proportional error linked both to the angular location of the measured point and to the range: obviously the longer is going to be the range, the larger is going to be the positional uncertainty. Another important problem is due to the behavior of the beam when it hits a corner (mixed edge effect), because it can be split in two beams which will give two different impulses to the receiver, increasing the noise effect. Angular measures can be affected by a huge error, because the most part of scanners uses a rotating mirror to guide the laser signal, so any error in the positioning of the mirrors influences the accuracy of the angular measurement device: a small angle difference can cause a considerable coordinate error when the distance of the object/target from the laser scanner increases.
- 2) Object-related: the first and foremost source of object-related errors is the reflectance of the object surface. Since TLS is a reflector surveying technique, this implies that the results of the range measurements strongly depend on the reflectance, which affects the SNR to a great extent (Thiel et

al., 2004). Anyway, surfaces of different reflectance will introduce offsets into the measured ranges: surfaces with high reflectance (bright) give more reliable and precise range measurements than those with low reflectance (dark), due to the fact that a larger portion of the laser energy is not reflected back to the sensor (Reshetyuk Y., 2006).

- 3) Environmental condition: Temperature can affect laser scanner measurement in two ways: first of all, directly, increasing the device the internal temperature, having a mechanical effect due to the heat dilatation of important parts of the tool. Whatever could be the distorted part this can cause consequentially distortion in the scan process. The indirect effect, instead, it is due to the temperature of scanned surface, because it can be itself a radiation source, increasing the noise effect.

Atmospheric variations in composition, such as absorption gasses increasing or decreasing, is obviously the most direct way in which this element affects laser measurements. Moreover laser light moves into the air medium, so its velocity is strictly dependent on the air density, which is influenced the most by atmospheric temperature, pressure and humidity. This can involves several types of distortion especially on the returning signal, and thus on the measurements. The sun can be a source of errors not only because of its influence on the surface temperature, but also because it is itself a source of radiations which can interfere with the laser light band. There also is an atmospheric effect connected to the adverse weather condition: haze, fog and rain not allow the TLS to work properly, while the snowy environment can be only scanned by exceptional scanners, because the most part of these tools don't work with a temperature down to -10°C .

- 4) "Distortion from motion" is the name of a set of errors connected to the environmental disturbances which can affect directly the TLS while it is operating: for example, in this study a very common problem during surveys was to keep targets in their position, because the strong wind (typical of coast environment) could move them during the TOF, giving a distorted measure. This was not the only distortion from motion error: when the TLS was relocated to a second scan position, in order to get a complete scan of the dune, the researchers had to rotate targets on their vertical axis to face the

emitter. This operation, without preventative measures, can generate large measurement errors. Different nature errors, instead, are generated by device movements (i.e. tripod oscillation) during TOF. At the moment common terrestrial laser scanners have an integrated dual axis compensator to compensate this kind of errors.

- 5) Methodological errors: this group includes the errors emerging from the chosen survey methodology for example such error sources as the density of laser spots or the range to scans (Staiger, 2005); usually, a very common methodological distortion is connected to the geo-referencing procedure, direct and indirect:
- Errors in direct geo-referencing are due to the precision of the GPS instrument mounted on the laser device.
 - Errors in indirect geo-referencing are due to the precision of the measurement of the targets (sphere or chessboard) center position.

3.1.4 *The field methodology, theory and post-processing.*

The field methodology for terrestrial laser scanning (figure 3.5) asks for a preliminary analysis on the environment to survey, projecting on the map the distribution of scan points and targets. This is linked to the fact that laser scanners are line-of-sight instruments (even though they usually can scan a full 360°); this is more than true on a dune field, where the distances to cover are usually high and the morphology presents many shadowing features. Thus in environmental monitoring multiple are often required, and then is expected to merge data. This introduces probably the most important protagonist of laser scanning field methodology: the target.



Figure 3.5: terrestrial laser scanner in action during a survey.

It is the physical object to place in the scene, which it is seen by the laser device; usually it could be of two types, square chessboard or sphere, and in both cases, they are used to get references (coordinates) and possibly merge all scans in that operation called “registration”.

Relative to the well positioning of targets, the laser scanner software is programmed to automatically (as much as possible) recognize them: since these artificial targets are made from highly reflective material, their reflectance value is much higher than its surroundings. If the environment gives the possibility, it is possible

to bypass the use of target, by acquiring geometrical points highly distinguishable, called “points-of-detail”. The latter are not so used in natural environmental monitoring, because not so applicable: this is due to the fact that it is not so easy to find a one (or more) precise points, with unequivocal position, easily identifiable from different points of view.

Obviously an external device must be used to get target references, and its features affect the precision of the measure and, then, the precision of the whole survey. Once the targets are positioned it is important for them to stand still during the scanning procedure, which in a natural environment it is not so obvious.

There are several techniques to merge scans, each useful depending on what is the final aim. In any case, each scan position is defined in a scanner coordinate system: to align different scans it is necessary to know the exact position and orientation of these scanner coordinate systems according to a local/global coordinate system. This process, called “Registration and Geo-Referencing”, can be indirect or direct:

- Indirect. There are two types of indirect registration: the “Target-to-Target” registration, is a pre-processing technique, which considers at least three target (natural or artificial) correspondence between two scans and it is usually used in pretty accessible environments; the “Cloud-to-Cloud” registration, instead, is a half manual, half automatic, technique to align scans, in post-processing, based on point cloud overlapping. It consists in selecting, manually, three or more (9 is the maximum) corresponding points in two point clouds; then the software, using the automatic algorithm called Interactive Closest Point (ICP), iteratively checks the distance between all the points of the cloud and estimates the transformation to align both sets.
- Direct. Direct registration means that the position and the orientation of the scanner are directly computed; this can be done, by placing the scanner over a known point, or by mounting a GPS receiver to the scanner.

3.1.5 The laser scanning method application



Figure 3.6: target center reference acquisition.

A FARO Laser Scanner Focus 3D was used in this study. This device uses Phase Shift technology to measure distances, which makes it a very accurate tool; its maximum theoretical range is more than 100 meters, but the real one depends on the environmental conditions, especially ambient light, which can act as a source of noise (FARO white papers, 2013); as every common phase based scan, it emits a laser light in the short infrared field (905 nm) with a laser power of 20 mW and the measurement speed can reach almost one million point per second. What makes this tool so proper to environmental monitoring are the multiple sensors, in addition: a dual axis compensator, which level each scan with an

accuracy of 0.015° and a range of $\pm 5^\circ$; height sensor, which detects the height relative to a fixed point via an electronic barometer; an electronic compass, which gives to scans an orientation (FARO white papers, 2013).

In this study, since the availability of high precision tools, a particular, but very useful methodology was applied, a sort of a direct-“Target-To-Target” registration: since the three dune field to survey are about 200 meters long, from 20 to 30 scans were required for every survey, with a range of about 40 meters and a spatial resolution of 6 mm (reflection points were spaced of 6 mm).

The scan “points of view” have been chosen in a part on the map, before to go on the field, in another part directly on the field regarding particular morphology and vegetation condition. The targets used were 50 cm^2 chess-board square, mounted on 1.5 meters poles (made of wood).

An important part of this methodology, involves an highly accurate GPS (Global Positioning System) device: a Leica Viva GS14 GPS (Global Positioning System) device link to the Global Navigation Satellite System (GNSS), which can receive and elaborate data from up to 60 satellites simultaneously on two frequencies; its precision

is improved by RTK-technology: Real Time Kinematic is a differential GNSS technique used to enhance the precision of position data derived from satellite-based positioning systems; it is based on the use of carrier measurements and the transmission of corrections from the base station, of well-known position, to the rover, to provide real-time corrections, providing up to millimeter-level accuracy. This device has been used to get references of the targets' center, so a 0.25 m offset correction was applied.

Since the dune field morphology (transversal dune field), the surveys were executed by sets of three scans per frame (a "strip" of land): one scan on the beach, one on the crest area and one on the backfield; thus for any set, six targets were placed (two by two, far about 40 meters along the beach direction) in the same places, beach, crest and backland, before starting a scan set. After completing a frame stripe, the scanner can be moved alongshore on the dune field to process another frame taking care of drawing the survey scheme.

A useful property of FARO Focus 3D is the preview showed after every scan on the device's touchscreen, which give the opportunity of realize possible scan errors on the field. Since in this method it is not necessary for the scans to have at least three targets in common, the only precaution taken has been the visibility of targets, thus their orientation relative to the scanner position or the presence of shadowing vegetation.

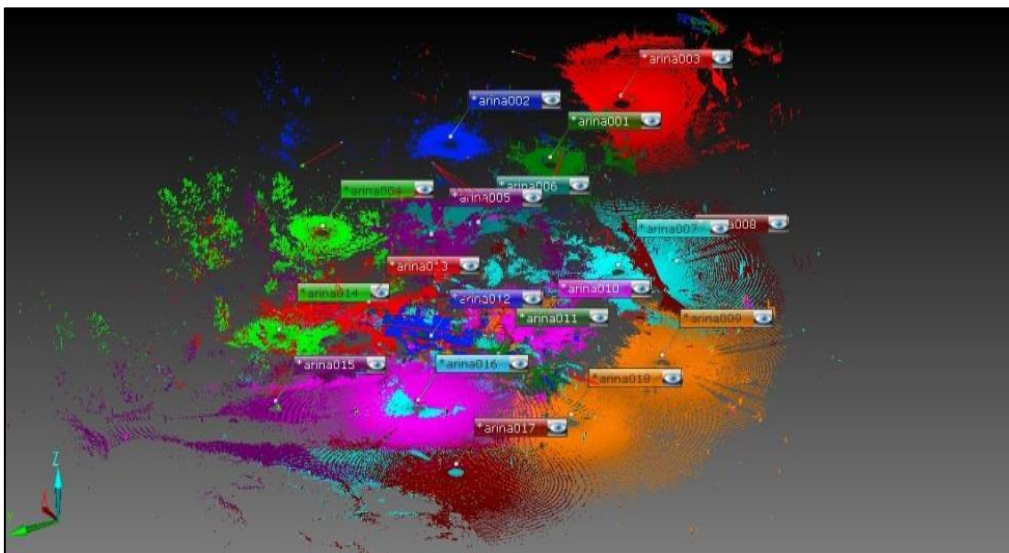


Figure 3.7: example of multiple scan survey scheme (Marina di Ravenna dune).

3.1.6 Post processing and data improvement application

Once accomplished the survey, the revealed data is brought in laboratory to be post-processed. Several softwares were used for the different phases. First of all “SCENE 3D”, the laser scanner software specifically designed for the FARO Focus^{3D}, processes and manages scanned data with a dual purpose: on one hand it can be used to

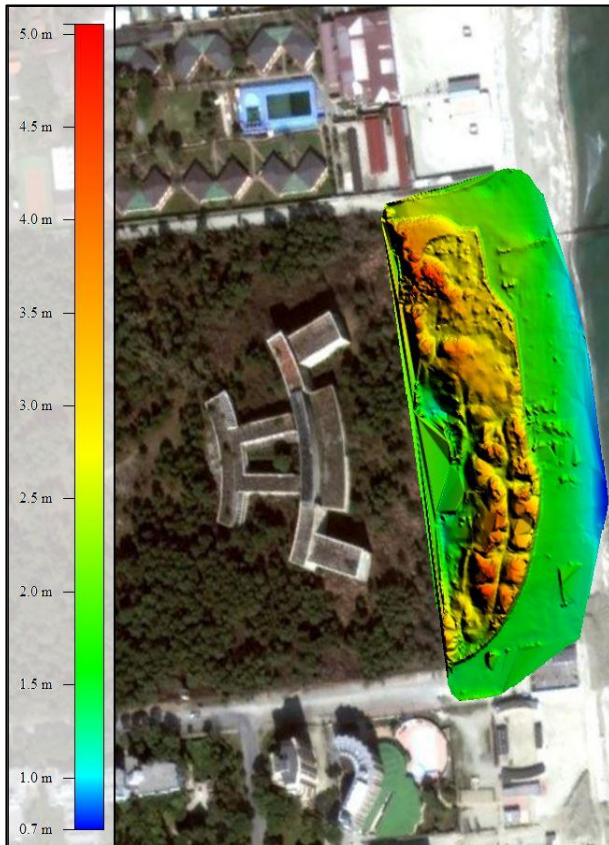


Figure 3.8: Milano Marittima D.E.M. 3D projected by Global Mapper.

filter dark scan points and stray scan points, as well as filtering points under a specific reflectance threshold, all made to reduce noise; on the other hand, this software is fundamental to recognize targets (automatically or manually), and to identify them according to the scheme drawn during the field survey, thus operate the “Registration and Geo-Referencing” process. Every scan was treated individually, registered in the geodetic UTM (Transverse Mercator) coordinate system, ETRF2000 datum, and the exported in .xyz format, which is an unordered text format containing xyz coordinates.

The further step involves “Geomagic Studio 2012” software, a complete toolbox for transforming 3D scanned data into highly accurate surface. Importing all .xyz files, their references make possible a perfect positioning of scans, without the need of an additional alignment.

After manually removing points clearly belonging to vegetation or people, this software was used first of all to reduce the number of points in an “object” by creating an evenly spaced set of points; this was done by spacing points by 0.1 mm. Then, the disconnected components and outliers (points that have little or no other points in their direct surrounding) filtering is applied: this operation is helped by a specific tool which compensates for scanner errors by moving points to statistically correct position.

Other automatic algorithms help to reduce noise moving points slightly, or fitting planes to points in the point cloud (shading). At this point it was possible to convert the cloud point to a mesh. After elaborating every scan singularly, they could be merged just as they are, because of their millimetric positioning in the WGS84 datum system.

The exported format was an ASCII file (American Standard Code for Information Interchange): this is a text array, in which every row store 3 values representing latitude, longitude and elevation data, of every point.

To project the obtained surface, the Digital Elevation Model, in the UTM system, another software must be used, “Global Mapper 15.1”, which can import ascii files, project them in a 3D view (figure 3.6), and export them in another ascii format, Arc Ascii Grid, after choosing the grid dimension: the result it is going to be another array, where every value represent the elevation (or non-elevation data), while the first five lines are different, since they store information about the number of columns and rows in the array, longitude and latitude coordinates of the last left corner, the cell size and the no data value. The grid dimension is the fundamental basic for further volume and area calculation.

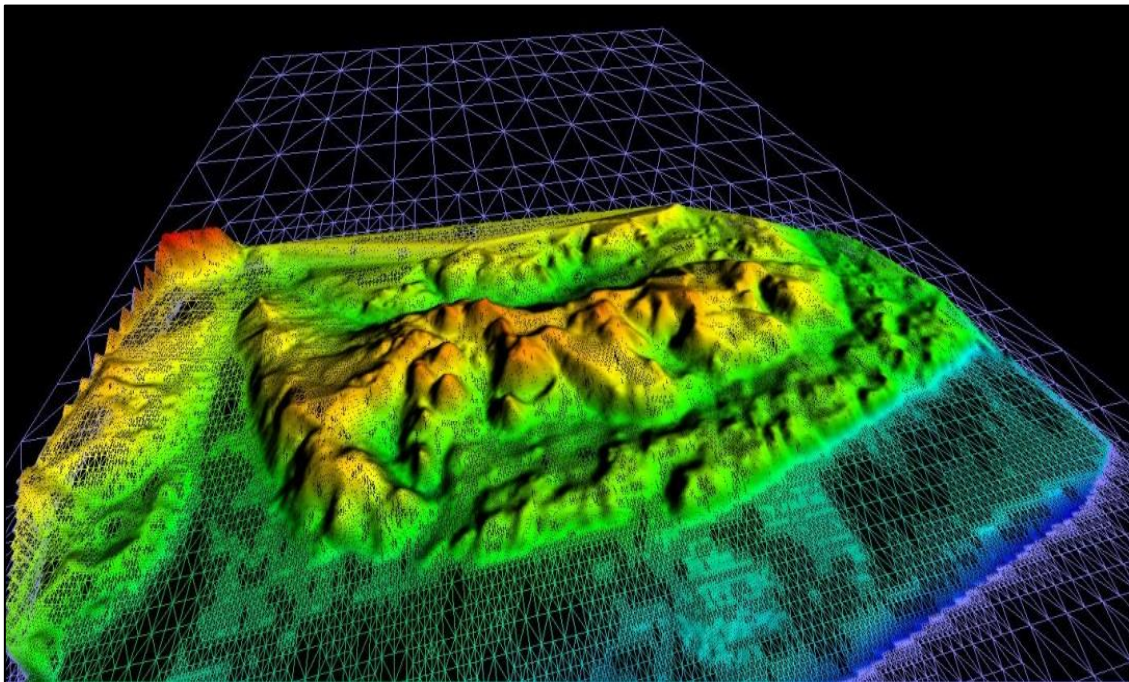


Figure 3.9: Digital Elevation Model (Marina di Ravenna) in 3D view (Global Mapper).

3.1.7 The applied validation methods

A specific set of tests was made to validate both the laser scanner proposed methodology, and resulting DEMs reliability. On 27 May 2013, in a Marina di Ravenna dune field, the “Giacobazzi” dune, a Networked Real Time Kinematic (NRTK) survey was carried out using the Virtual Reference Station (VRS), together with data acquisition by TLS and Unmanned Aerial Vehicle (UAV).

The NRTK survey, performed by a dual frequency GRS1 (Topcon), had a threefold point collection purpose (figure 3.8): the field was staged with eighteen 3D Ground Control Points (GCP), consisting of parallelepipeds (30 x 40 x 30) with a 20 cm wide chessboard printed on the upper side, 126 Validation Points (VP) at surface ground level along five transects evenly distributed across the dune extent, and 19 Vertical Targets (VT) designed to georeference and merge the TLS acquisition (Mancini, 2013).

Horizontal coordinates were referenced to UTM Zone 33 N (ETRF00), while the vertical values were referred also to the mean sea level using the geoid model ITALGEO2005 provided by the Italian Geographic Military Institute (IGMI).

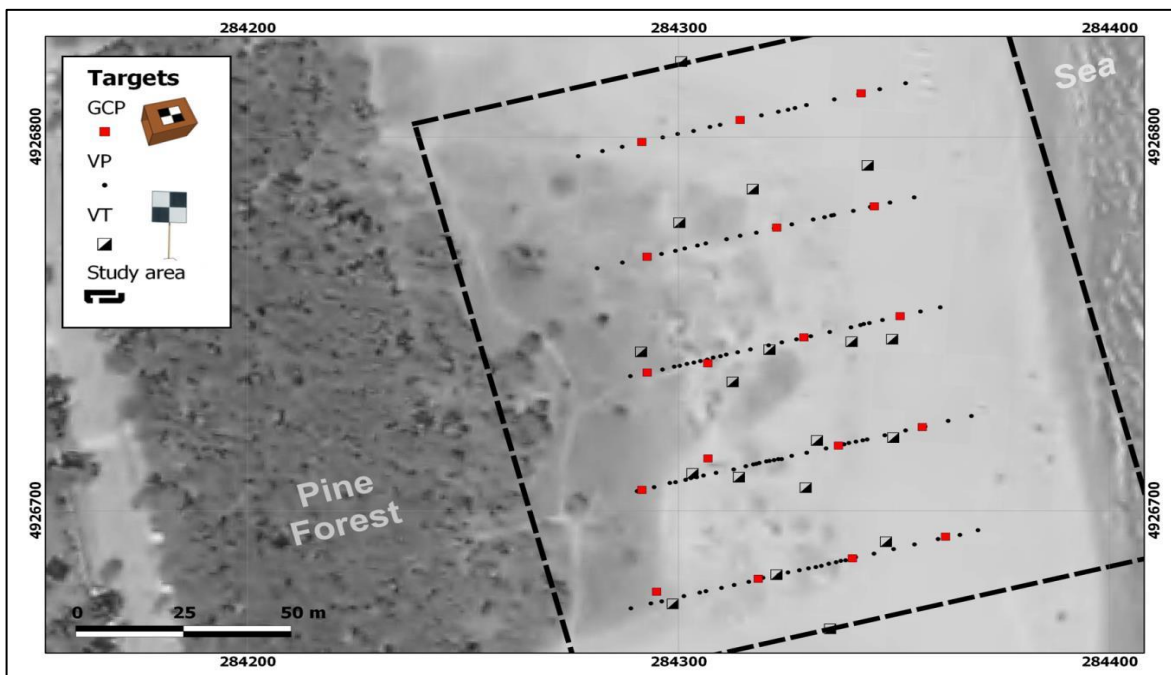


Figure 3.10: Aerial photo of the testing field. GPC= Ground Control Points; VP = Validation Points; VT = Vertical Targets.

The UAV system used was a VTOL (Vertical Take Off Landing) hexacopter designed and manufactured by SAL Engineering, equipped with a calibrated Canon EOS model 550D digital camera (figure 3.9). A remote pilot controlled the most part of

the survey, the take-off, the landing and the flight on survey lines, which are based on waypoints decided before on aerial photos.

Due to wind conditions (during the survey an average speed of 5.14 m/s was recorded, with gusts of up to 9.6 m/s), so corrections were calculated to compensate for horizontal and vertical deviations. The flight time was of 7 minutes at an average speed of 4 m/s and the final aerial dataset resulted in more than 800 images of which 550 were selected following successive data processing (Mancini, 2013).



Figure 3.11: the UAV hexacopter (reference length in figure: 1 m).

Obviously the UAV data post processing, is completely different from the TLS one: the Structure for Motion (SfM) Algorithm implemented by Agisoft PhotoScan, a stand-alone software made to performs photogrammetric processing of digital images and generates 3D spatial data (www.agisoft.com), was used. SfM approach refers to image-to-image registration methods for surface restitution (in term of Digital Surface Model), with an high level of automation and a great ease of use.

SfM strategy is to reconstruct 3D scene geometry and camera motion from a set of images of a static scene by matching features on multiple images (Tomasi C., 1992).

The reconstruction of ground surface and objects by Photoscan is a three- step process:

1. Alignment of acquired images: the software detects feature points and reconstructs their movement along the sequence of images.
2. From the aligned dataset to the pixel-based dense stereo reconstruction : a fine topographic details could be meshed to the original images.
3. Texturing.

The point cloud obtained from the 550 pictures, then, was shaped and framed in the

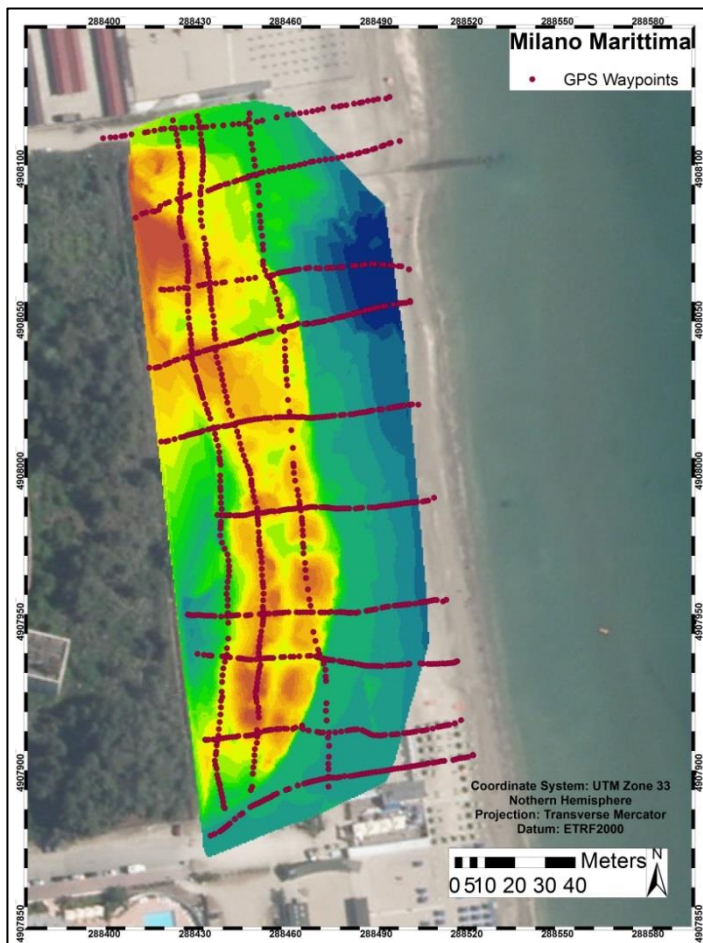


Figure 3.12: GPS transects upon the Milano Marittima DEM

UTM coordinates system: the bundle adjustment procedure was chosen over the similarity seven-parameter transformation, since it was known to produce more accurate results, despite possibly higher time consumption, this depending on the number of images acquisitions (Mancini F., 2013).

Two other tests were performed during this research, to ensure that the laser data were fitting the real topographical surface, both comparing TLS DEMs to GPS-RTK sets of marked points, one

in Milano Marittima (906 ground control points, figure 3.12), while the other on the dune field located in Marina di Ravenna (472 ground control points; figure 3.13), several kilometers south. In both case transects were performed to be representative, as much as possible, of the topography, and the comparison was made in term of statistic linear regression.

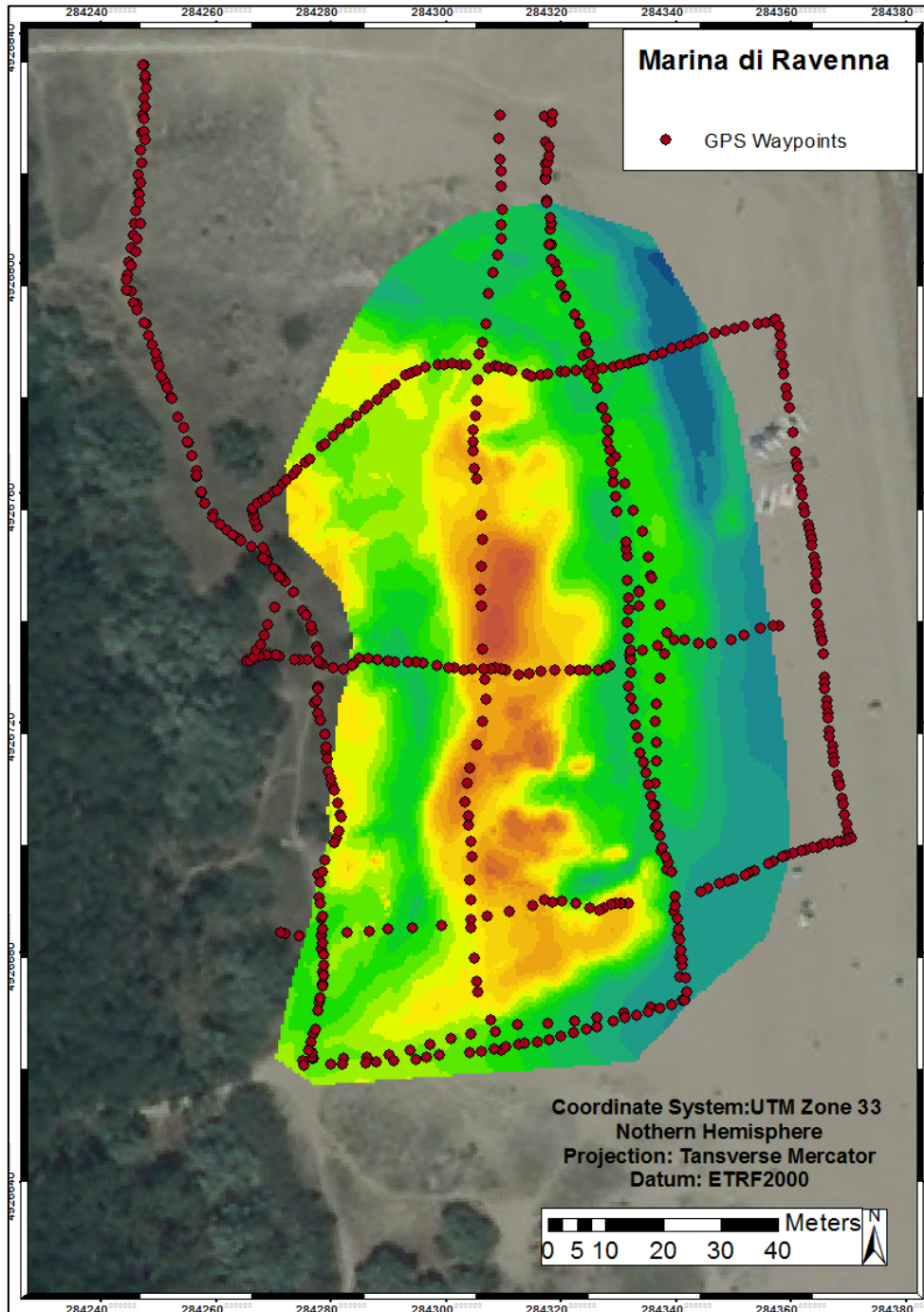


Figure 3.13: Marina di Ravenna gps control points transect.

3.2 The Morphological Analysis: Units, Sub-zones and their Variation.

3.2.1 GIS environment processing: volumetric calculation, morphological analysis and DSAS application.

Data detected by TLS were finally analyzed and elaborated, in GIS environment, with the aim on one hand to evaluate volume changes, on the other hand to identify the basic elements of the dune morphology. The latter was made starting from the Barrère schematic diagram (1992) shown in figure 3.14, modified.

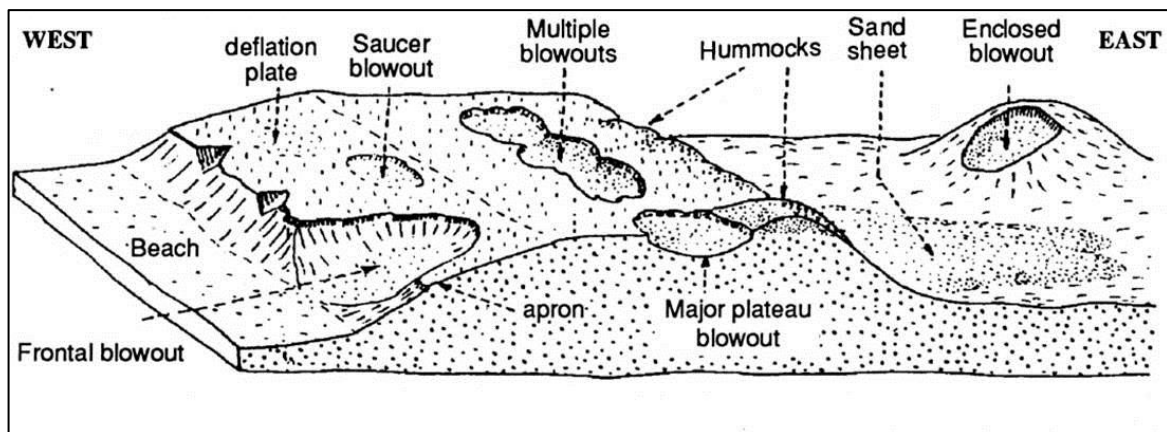


Figure 3.14: Morphological units diagram (modified from Barrere, 1994)

Whatever was the aim, the first step of this method starts from the ASCII gridded file exported by Global Mapper: the grid size chosen was $0,25 \text{ m}^2$; this is going to be the geometrical basis for any further calculation. Once imported in ArcGIS Platform (ESRITM), these ASCII DEMs were converted to the raster form. The first elaborated layout was based on elevations, divided in 20 equal intervals, identified by a different color (figure 3.14); two types of elevation contours were calculated for any DEMs, one with a $0,25 \text{ m}$ interval, one with $0,06 \text{ m}$ interval. Then the slope of the leaning surfaces was calculated by another feature of the 3D analyst tool and plotted, with its relative 2° interval contours (figure 3.15).

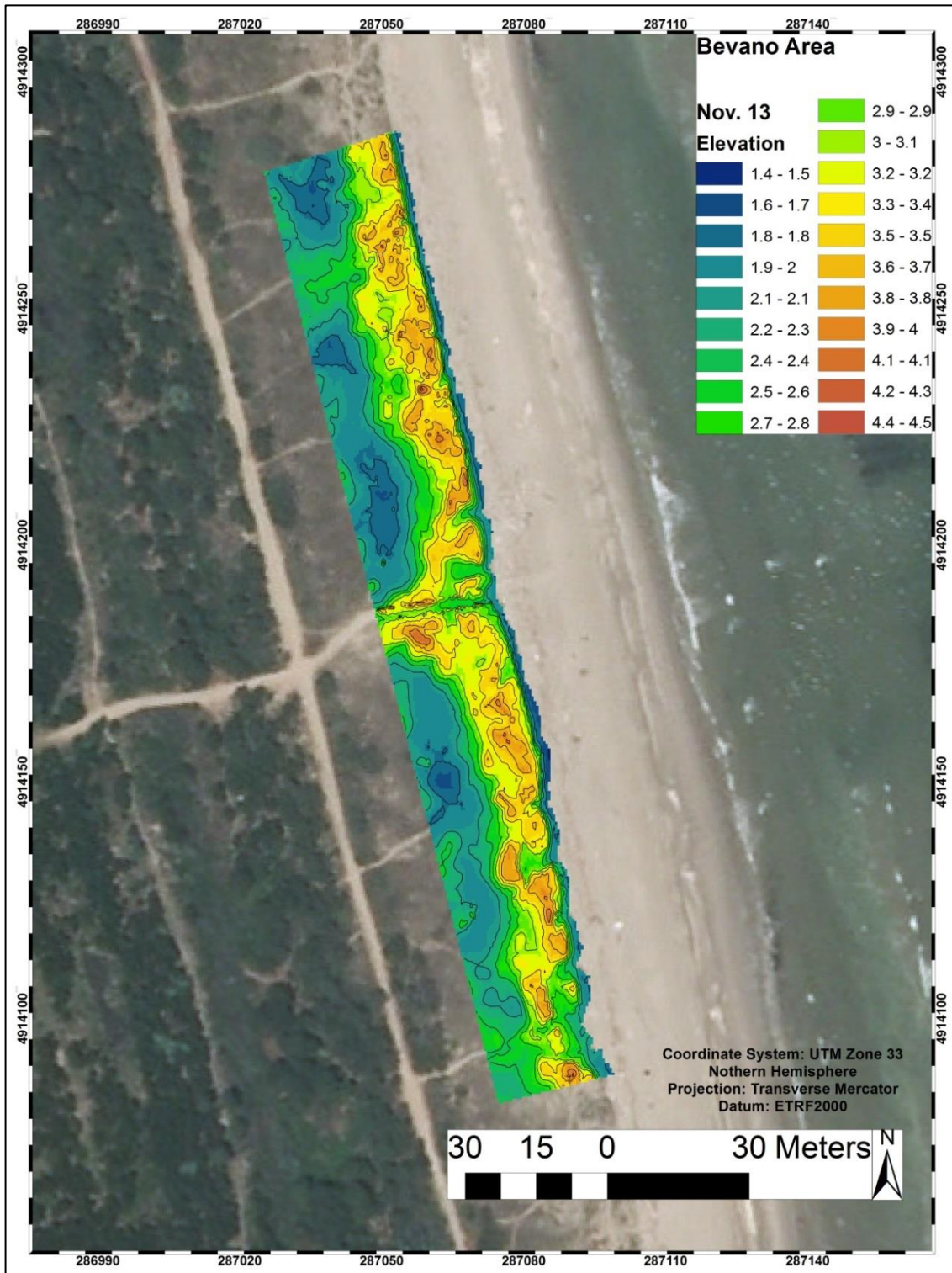


Figure 3.15: elevation DEM, Bevano dune field.

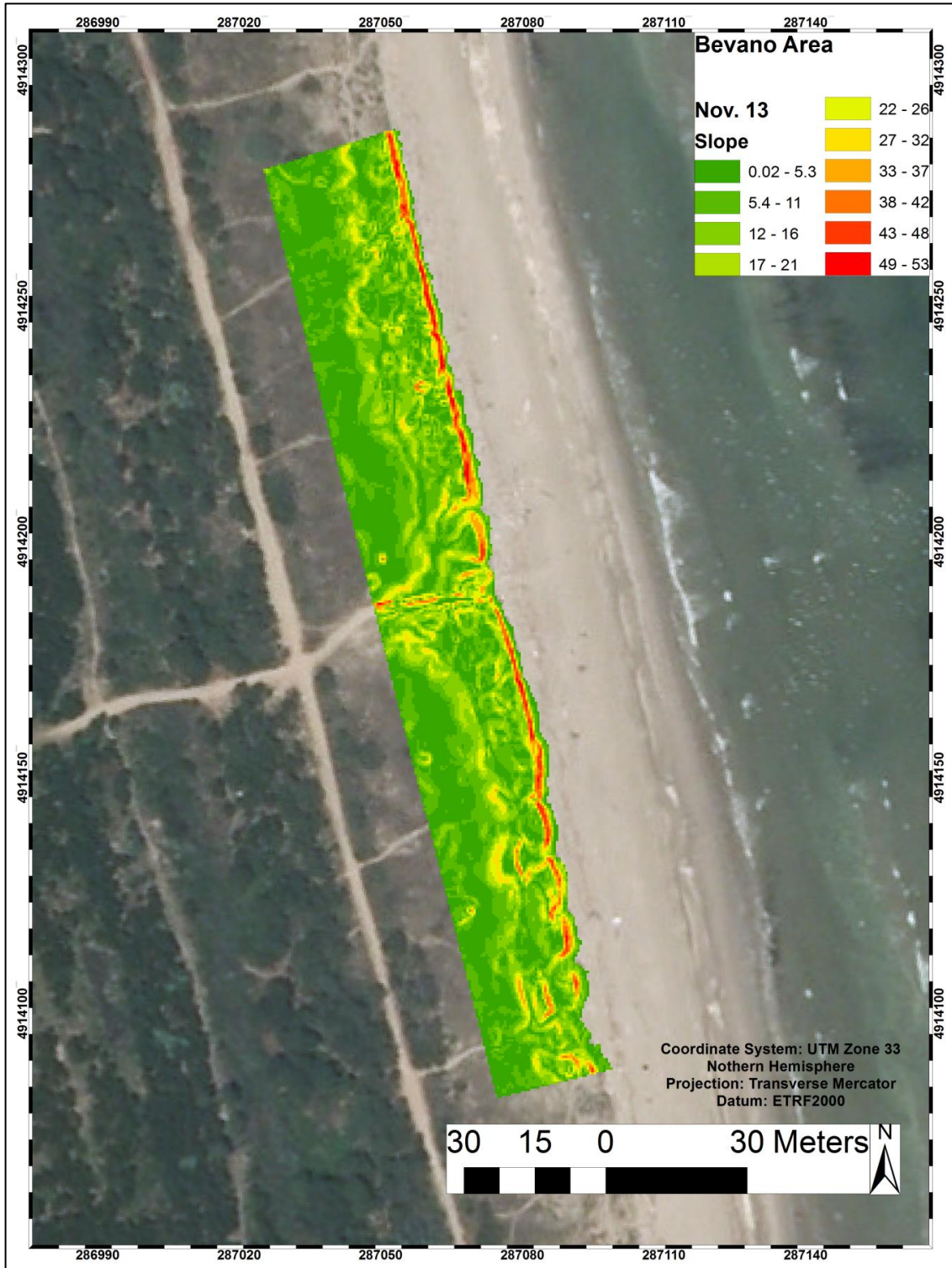


Figure 3.16: the Slope DEM, Bevano dune field.

This double dataset (slope and elevations) was the base to approach the identification of the basic morphological units, across the dune complex:

- the dune foot line;
- the upper and lower talus (landward slope) lines;
- the crest area and the crest line;
- the vegetated dune line (landward limit to the dune backward depression);
- the erosion forms (made both by sea and wind);

The dune foot line is a fundamental unit of the dune morphology, because it is the most seaward part of the dune, representing the buffer between the dune system and the beach system; from a morphological point of view, it is marked by a highly accentuated change of slope, in a very short distance (figure 3.16). Since this, overlapping a contour set relative to the elevations to an slope DEM, is a reliable method to identify the dune foot line (Mitasova et al. 2005).

The procedure used in this study takes inspiration from the already applied methodology by the Italian Environmental Department, ISPRA (Istituto Superiore per la Protezione Ambientale), on airborne LIDAR data (ISPRA, 2010). There is a strong difference between ISPRA works and this one: ISPRA, using airborne LIDAR data, had to work at a small scale, so that the only recognizable features were the dune foot line and the dune landward limit.

Since TLS data are much more detailed (it can scan one point every 6 mm), the same methodology, with a supposed higher accuracy, has been used to draw other morphological lines, such as those of the talus and the vegetated dune line, regarding obviously the smoother surface slope (figure 3.17).

The dune foot line was drawn overlapping the elevation contours to the slope layer, which previously has been elaborated, data subdivided in ten equal classes with a proper color tone (to make more easy the founding).

The same basic process allowed to identify the vegetated dune line represents the landward limit of the fore dune system, after which, a brush/wooden vegetation, typical of a much more stabilized environment, can grow (a Pine forest in some cases). The landward Talus too was drawn using this technique and identifying both the upper and the lower limits.

The dune crest is commonly determined as the highest spots of a dune system, so it is usually described as the line built by the highest points founded starting from seaward; in this study, it was chosen first to identify a crest “area”, instead of a line, because of the intense fragmentation of the crest, that makes really hard to draw a crest continuous line, especially for what concerns Milano Marittima dune.

In spite of this for the Bevano and Marina di Ravenna area the author had to possibility to draw an almost continuous crest line, considered significant based on the highest elevations in the crest areas.

This feature could be very important according to Psuty (2009), because the crest could show a different behavior from other morphological features, it is supposed to be much more stable, and it should shift (thus indicate) in response to sediment budget and under extreme events when waves have the possibility to reach it (Psuty, 2004); always according to this author there usually the crest back movements are linked to the wave action, but there are even conditions that can cause deposition of sand on the crest line seaward margin, such as to produce a displacement; in any cases its position in the dune-beach profile is much more conservative than shoreline.

Blowout area drawing was more difficult, because while the upper limit was determined by the contours relative to the crest area trend, the lower limits was difficult to set because of the hardness to understand where, in the foot slope, erosion starts. The choice made was taking as “starting line” the first contour line evidently changing the trend relative to other contour lines, index of incipient erosion, starting from the seaward.

It is very important to specify that for statistical purposes of this study it has been considered “Blowout” any deflation morphological element.

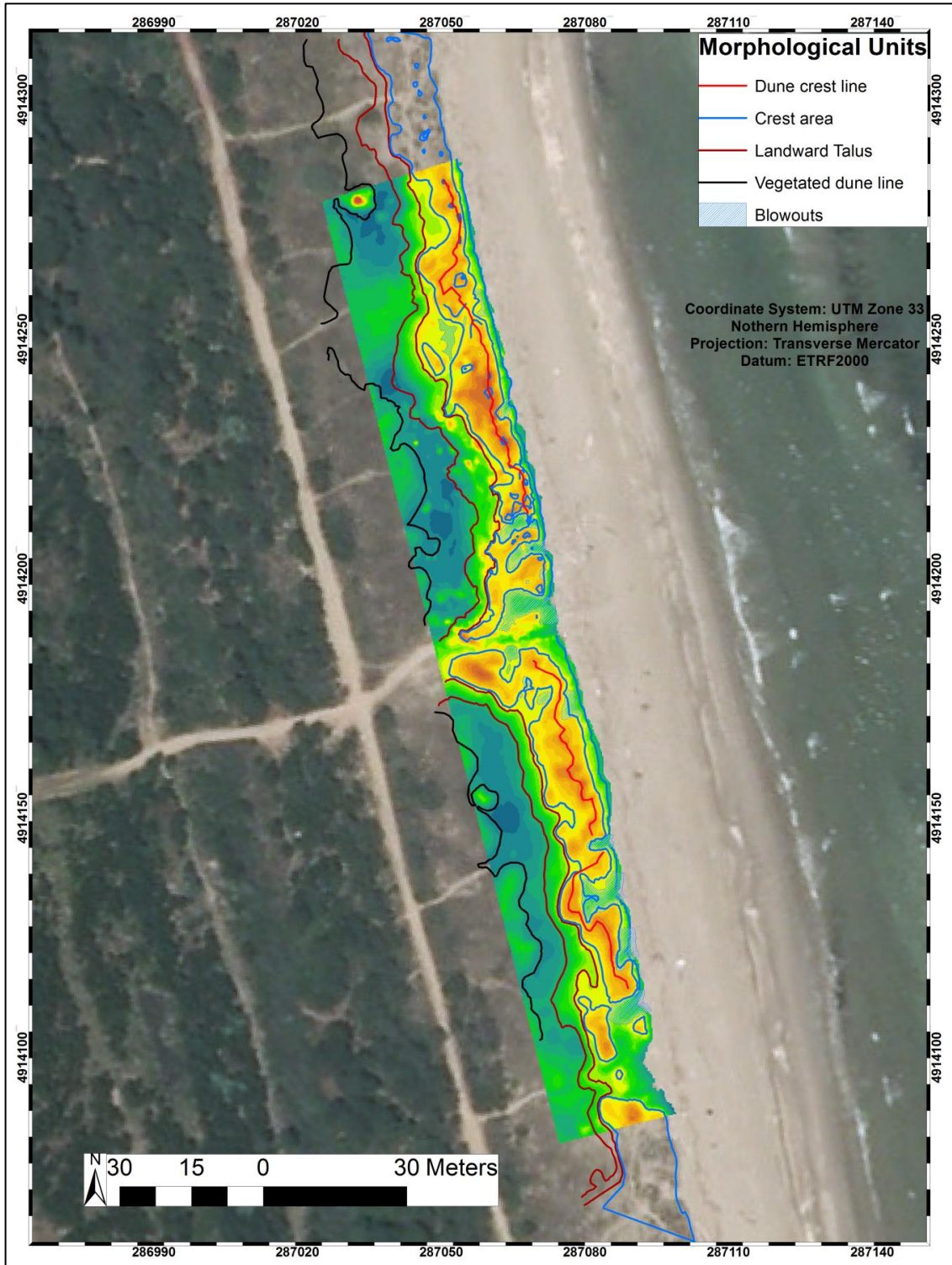


Figure 3.17: Morphological elements in the Bevano River dune field (October 2012).

An immediate application of the Dune Foot line, is founded in the Area Of Interest determination (A.O.I.), which is a common area between every survey, for a determined site. This is the portion of surface where every calculation is made, as well as every comparison (figure 3.18). While on the landward side it was possible to ground the determination on the widest and best overlapping between DEMs, on the seaward side it was not so easy, for several reasons. Especially in volume calculations, in effect, including in the A.O.I. even a small portion of the beach causes strong variations in sand volume amount.

Since this, it was decided to draw all the dune foot lines (relative to the same dune field) together in the same layer and draw a line which, starting from north, retrace meter after meter, the most external dune foot line.

In this way it was obtained an Area of Interest strictly (as much as possible) belonging to the dune system.

Identifying the dune foot line gave the opportunity to monitor another interesting morphological process: the

dune foot line movement during the surveyed period. This was done using a particular tool, programmed by the USGS (United State Geological Survey): the Digital Shoreline Analysis System (Thieler et al., 2009).

This software is an application that works within the already mentioned ESRI ArcGIS software. Even if it is born, and usually used, to compute rate-of-change statistics for a time series of shoreline vector data (Himmelstoss, 2009), in this study it was applied in a first approach to investigate the dune foot line movements.

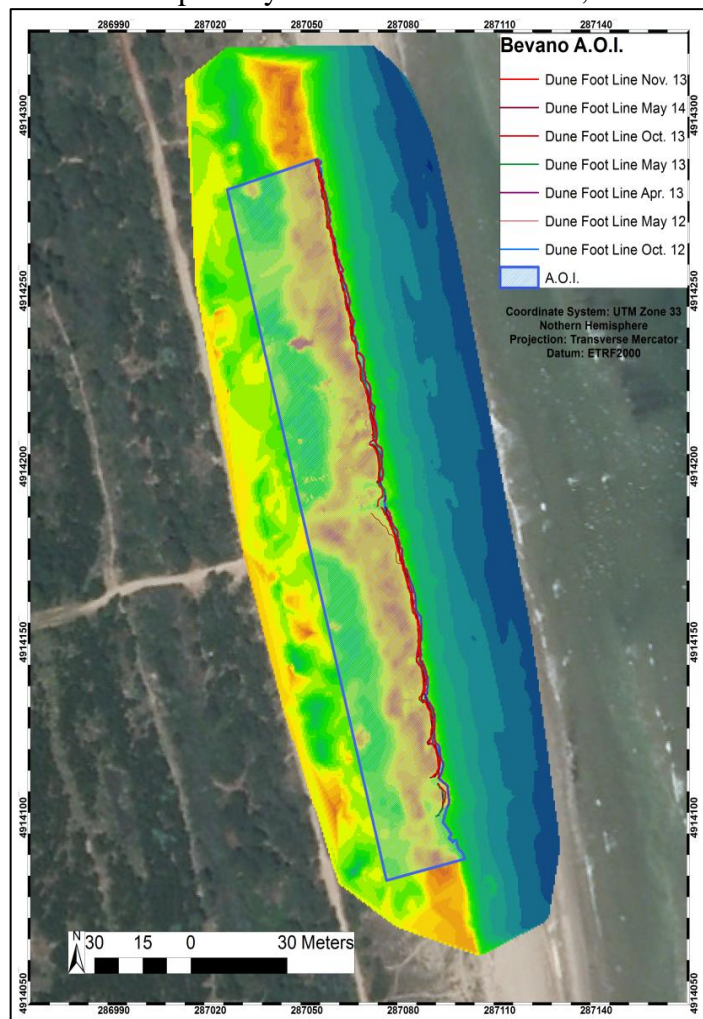


Figure 3.18: determined AOI. Bevano area.



Figure 3.19: DSAS analysis example. Transect intersections points are drawn for both foot and crest lines.

The author applied the DSAS analysis to all three sites of interest, to test this brand new methodology, but application to the Bevano river area (figure 3.18) gave most interesting results, primarily because this area is included in a completely natural environment; secondly the availability of seven different DEMs made this data set more

“well-fitting”. In this prove the author chose to evaluate both the dune foot line and the crest line movement. This was done for Marina di Ravenna and the Bevano area, but not for the Milano Marittima site, where the author tested only the dune foot line.

This application was done taking inspiration from the work by Psuty (2009) who claims the need of monitoring alternative features in the beach profile, not only the shoreline. The Author tried to use these two features (foot and crest line) on one hand to purpose a new methodology for the dune beach profile analysis, on the other hand to verify the Psuty hypothesis of the more conservative behavior of the crest line in relation to other features (such as the dune foot line). Data resulted from this test will be shown in next chapter.

The DSAS tool makes available several ways to calculate movements, depending on what is the aim: the choice made in this research focused on the Net Shoreline Movement (NSM), the End Point Rate (EPR) and the Linear Regression value (LRR). The first one it is just a measure of a distance, not a rate, and the algorithm just calculate the movement between the oldest and the youngest vector line. The second one, as written in its name, it is a rate, thus it calculate the distance traveled by the vector line, and it divides it by the time passed between the oldest and the youngest survey: the result is the movement rate per period.

To have a more sharpen measure the author chose to include an index called “Linear Regression”, which indicates always a rate, but is more accurate because it calculates the statistical linear regression between the shoreline position data (y) respect to the time (x), for every measures. The LRR index in conclusion is represented by the angular coefficient of the resulted line (referred to the mathematical linear equation), thus by its slope, and describes the rate.

3.2.2 Morphological Sub-zones

Once determined all morphological elements, for every dune area and for every survey, it is pretty easy to divide dunes in 3 different portions, called by the author “morphological sub-zone”, representing 3 different dynamic areas (figure 3.19); starting from the sea to landward:

1. White dune: from the dune foot line to the upper limit of the landward talus. It represents the most seaward area of the dune, and probably the most active part, because of its relationship with the sea and the wind force: it is the zone where the most part of erosion forms is founded.
2. Grey dune: from the talus’ upper limit to its lower. It represents the landward slope, very important, in a morphological point of view, because it is an area characterized by gravity collapses and consequent sand remobilization.
3. Black dune: from the talus’ lower limit to the vegetated dune line; it represents the upper limit of the landward dune grass vegetated depression, where the dune should be more stable.

It is important to specify that, because of the aim of this study, the sub-zones were expressly identified using only morphological characters, without taking any account of vegetation characteristics, although it is known that this is a fundamental element influencing the dune morphological behavior.

For every survey, the 3 morphological sub-zones were determined, and their area was calculated, with the basic aim of identifying potential seasonal or annual trend. The area calculation was done using some appropriate tools of ArcGIS: first of all starting from the original DEM and the sub-zones polygons, the subzone corresponding raster can be extracted from the original DEM. Then applying a new tool of the 3D Analyst, called “Surface Volume” calculates the extracted zone area geometrically (2D) and topographically (3D). Every surface calculated in this study was done using this method and calculating areas in a topographic way.

Moreover this methodology is supposed to represent a smart way to highlight some particular situation or data, not in line with others, giving the opportunity to investigate causes and effect in a very detailed scale.



Figure 3.20: example of morphological sub-zones identification (Bevano river area, May 2014)

3.3 Potential Sediment Transport via Fryberger and Dean's Method.

3.3.1 Theory.

In an environment as a dune field, which is a classical aeolian landform, the wind energy is the force that controls the general morphology. It explicates its control through the expression of its energy, which can be described by the wind regime, translatable in amount of wind energy and its directional variability (Walker et al, 2004). Because of its importance, during last decades many attempts have been made to try to assess the so called "Sand Drift", the process of sand movement across the desert as a result of surface wind (Fryberger, 1979), in a more accurate statistical way (Bagnold, 1941; Hsu, 1973; Lettau, 1978; are just some examples).

One of these models was developed by Fryberger and Dean (1979) as part of the "Study of Global Sand Seas" by the U.S. Geological Survey and the U.S. National Aeronautics and Space Administration (McKee, 1979) and has become widely used for estimating sediment transport potential in aeolian environments.

This method gives an accessible way to determinate aeolian sediment drift potential, using standardized wind data and giving not only the opportunity of having a quantitative reference of the sand drifting, but also to compare data and graphs from different places and environment.

Basically the method follows two fundamental principles: (1) when considering the role of wind regimes in geomorphology, only those winds exceeding the threshold velocity for sand transport are important; (2) stronger winds are more effective in transporting sand than weaker winds (Bullard, 1997).

As logical consequence, the first step of any calculation is the threshold velocity for sand transport determination, based on the sand grain size (diameter):

$$V_t = 5.75 (V * t) \log(Z \div Z') + (V' t) \quad \text{Equation 3.4}$$

Where:

V_t = threshold velocity at 10m height (= V_{10})

V^*_t = threshold velocity at the bed (equation 2)

Z = height (10 m is the pattern)

Z^0 = roughness of the grain surface (10 * grain diameter (mm) according to Belly, (1964))

(V^*_t) = shear stress velocity, given by Zingg (1950) as $894 * \text{grain diameter (mm)}$ and the result is in cm/s.

The threshold velocity is standardized at 10 meters height (on the ground) as a convention, but it is a common occurrence the mounting of an anemometer at a height other than the standard 10 m specified by the World Meteorological Organization (Fryberger and Dean, 1979).

The threshold velocity it is obviously subordinate to the threshold velocity at the bed: if sensors are mounted lower than the standard 10 m, calculated drift potential will be slightly less than the true drift potential (based on elaborations at 10m height). This is because wind velocities, for many reasons, are lower near ground.

$$V^*_t = A \sqrt{((\delta s - \delta a) \div \delta a * g d)} \quad \text{Equation 3.5}$$

Where:

V^*_t = threshold velocity at the bed

$A = 0.1$ according to Bagnold 1941

δs = sand grain density (2650 Kg/m³ for quartz)

δa = air density (1,22 Kg/m³)

d = grain size (in meters)

g = gravity acceleration (9.81 m/s²)

Commonly, wind data are just converted to standard 10 meters, by using a simple conversion formula, based on the simplified wind logarithmic law:

$$U_z = (U_*/k) \ln[(Z - Z_d)/Z_0] \quad \text{Equation 3.6}$$

Where:

U_* = the friction velocity

- k = von Karman’s constant (0.40);
- z0 = the surface roughness length;
- Z_d = the zero-plane displacement height

Thus the conversion is easily achieved applying last equations to two heights, as suggested by the World Meteorological Organization in the “Guide to Meteorological Instruments and Method of Observation” (2008):

$$U_1/U_{ref} = \ln(Z_1/Z_0)/(\ln(Z_{ref}/Z_0)) \quad \text{Equation 3.7}$$

Where:

- U₁ = measured velocity
- U_{ref} = wind speed at the chosen reference height
- Z_{ref} = the chosen reference height
- Z₁ = the height of the site anemometer
- Z₀ = the roughness length of the urban climate zone (UCZ).

The roughness length is linked to roughness effects: the World Meteorological Organization (2008) suggests that the “upstream roughness effects as well as the effects of surface obstacles can be corrected by extrapolating the wind speed logarithmic profile to a height of 60 m with the station specific effective roughness length Z_{0u} and by interpolating back to 10m with the roughness length Z₀ necessary for the application. The roughness length Z_{0u} should be representative of a 2 km fetch upwind of the wind station; the value usually depends on wind direction”.

Class	Short terrain description	z ₀ (m)
1	Open sea, fetch at least 5 km	0.000 2
2	Mud flats, snow; no vegetation, no obstacles	0.005
3	Open flat terrain; grass, few isolated obstacles	0.03
4	Low crops; occasional large obstacles, x/H > 20	0.10
5	High crops; scattered obstacles, 15 < x/H < 20	0.25
6	Parkland, bushes; numerous obstacles, x/H ≈ 10	0.5
7	Regular large obstacle coverage (suburb, forest)	1.0
8	City centre with high- and low-rise buildings	≥2

Table 3.2: Terrain classification in terms of aerodynamic roughness length Z₀ (Davempport (1960) adapted by Wieringa (1980b).

As an approximation, the roughness length is approximately one-tenth of the height of the surface roughness elements. In table 3.2 terrain classification from

Davenport (1960) adapted by Wieringa (1980b) in terms of aerodynamic roughness length Z_0 .

Once threshold velocity has been determined, wind classes and weighting factors have to be calculated. Weighting factors are numbers which represent the relative rates at which winds of differing average velocities can move sand. It is important to notice that, even though the DP is expressed in dimensionless vector units (V.U.), the method for calculating weighting factors is dependent upon the specific units of wind velocity (knots or m/s), because the midpoint of each velocity category is used as the starting point for each calculation (Bullard, 1997).

$$Wf = [V^2 (V - V_t)] \div 100 \quad \text{Equation 3.8}$$

Where:

V = midpoint (statistical average) between speed classes

V_t = threshold velocity at 10m height (=V₁₀)

Weighting factor calculation				
	Mid point			Wf
Speed class	(V)	(V) ²	V-V _t	V²(V-V_t)/100
0.5 - 3.0	1.75	3.06	1.75	0.05
3.0 - 5.6	4.3	18.49	4.30	0.80
5.6 - 7.1	6.3	39.69	6.30	2.50
7.1 - 8.7	7.9	62.41	7.90	4.93
8.7 - 11.3	10	100.00	10.00	10.00
11.3 - 14.3	12.8	163.84	12.80	20.97
14.3 - 17.4	15.85	251.22	15.85	39.82
17.4 - 21.0	19.2	368.64	19.20	70.78
21.0 - 25.0	23	529.00	23.00	121.67

Table 3.3: Weighting factors calculation. In the first column the classes used for this research are reported.

In this study, following Miot da Silva 2010, wind speed classes from the original Fryberger's work (1979) were slightly modified for several reasons (Table 3.3): first of all, the different wind environment and the more precise data now available.

Moreover wind classes were determined in regard of the calculated threshold (approximate 7.1 m/s) and another class below was added, from 5.6 to 7.1, to not omit data which could be important, since many authors before this study considered 5.6 m/s

the real threshold wind speed for this region (Bezzi, 2009). This class was applied only to the description of the Aeolian climate (thus, the creation of wind roses) and it was not included in DP calculation. One of the reasons is that several authors have already admitted that it is an underestimated value (Caruso, 2006).

Specific wind data are treated as frequency table, where every record is relative to a specific wind speed class and a particular sector of provenience. Table 1.4 shows the percentage of wind occurrence which in the summary represents the length of time during which that wind blew.

The direction classes used were 16 equal 22.5° sectors, as proposed by Pearce and Walker (2005) as more appropriate to conform to the original method, and to minimize the influence of systematic frequency and magnitude biases (Miot da Silva, 2010).

WIND DATA FREQUENCY (%) TABLE										
Dir	Angle	Speed		3.6 - 4.6	4.6 - 7.1	7.1 - 8.7	8.7 - 11.1	11.1 - 15.0	15.0 - 21.0	TOTAL %
		0 - 2.1	2.1 - 3.6							
N	0	0.53	0.33	0.26	0.24	0.03	0.01	0.20	0.01	1.61
NNE	22.5	0.65	0.77	0.50	0.59	0.19	0.39	0.37	0.14	3.60
NE	45	0.81	0.99	0.46	0.60	0.11	0.40	0.44	0.21	4.01
ENE	67.5	0.93	1.22	0.76	0.98	0.16	0.21	0.15	0.03	4.43
E	90	1.46	3.18	2.13	1.91	0.18	0.18	0.05	0.00	9.08
ESE	112.5	1.40	2.99	2.54	3.69	0.50	0.38	0.00	0.00	11.51
SE	135	1.32	2.32	2.28	3.17	0.31	0.13	0.00	0.00	9.52
SSE	157.5	1.15	1.96	1.65	2.29	0.40	0.11	0.03	0.00	7.59
S	180	1.93	1.22	0.74	1.03	0.18	0.14	0.04	0.00	5.29
SWS	202.5	2.75	0.94	0.28	0.45	0.04	0.00	0.01	0.00	4.47
SW	225	1.93	1.04	0.66	1.59	0.72	0.13	0.00	0.00	6.07
WSW	247.5	2.89	1.96	1.37	1.19	0.20	0.06	0.00	0.00	7.65
W	270	3.45	4.81	2.52	1.13	0.01	0.01	0.01	0.00	11.94
WNW	292.5	1.80	2.17	1.42	0.76	0.02	0.00	0.00	0.00	6.17
NW	315	1.25	1.01	0.32	0.18	0.02	0.01	0.01	0.00	2.78
NNW	337.5	0.68	0.48	0.25	0.29	0.03	0.01	0.01	0.01	1.75
Calms										2.52
TOTAL (%)		24.92	27.38	18.15	20.07	3.10	2.15	1.31	0.40	99.99

Table 3.4: Example of Wind data Frequency table.

Taking only the real effective winds, those that exceed the threshold velocity and multiplying every record for the corresponding weighting factor will give as result, partial and total Sand Drift Potential.

DP'S CALCULATIONS									
	7.1-8.7	wf	8.7-11.1	wf	11.1-15.0	wf	15.0-21.0	wf	DP's
		0.473815		2.704289		10.06351		17.68319	
N	0	0	0	0	0	0	0	0	0
NNE	0	0	0.01419	0.038374	0.05677	0.571305	0.08515	1.505724	2.1154
NE	0.08515	0.040345	0.09935	0.268671	0.11354	1.142611	0.02838	0.501849	1.95348
ENE	0.04258	0.020175	0	0	0	0	0	0	0.02018
E	0.32643	0.154667	0	0	0	0	0	0	0.15467
ESE	1.77406	0.840575	0.78058	2.110914	0.04258	0.428504	0	0	3.37999
SE	1.56117	0.739705	0.96509	2.609882	0.85155	8.569581	0	0	11.9192
SSE	0.34062	0.161391	0.26966	0.729238	0.01419	0.142801	0	0	1.03343
S	0.14192	0.067244	0.01419	0.038374	0	0	0	0	0.10562
SWS	0.11354	0.053797	0.05677	0.153522	0	0	0	0	0.20732
SW	0.26966	0.127769	0.01419	0.038374	0.01419	0.142801	0	0	0.30894
WSW	0.1845	0.087419	0.02838	0.076748	0	0	0	0	0.16417
W	0.02838	0.013447	0.01419	0.038374	0	0	0	0	0.05182
WNW	0.05677	0.026898	0.08515	0.23027	0	0	0	0	0.25717
NW	0	0	0.01419	0.038374	0	0	0	0	0.03837
NNW	0.01419	0.006723	0.07096	0.191896	0	0	0	0	0.19862
TOTAL	4.93897	2.340156	2.42689	6.563011	1.09282	10.9976	0.11353	2.007573	21.9083

Table 3.5: Example of DP calculation table

This value represents the theoretical amount of sand drifted in the time period during which those winds blew and are very useful especially for comparing different locations in relation to their climate.

A sand rose is a circular histogram which represents potential sand drift from the 16 direction of the compass and every arm is proportional in length to the potential sand drift from a given direction as computed in vector units (Fryberger and Dean, 1979): it is the graphical expression of both the amount of potential sand drift and its directional variability.

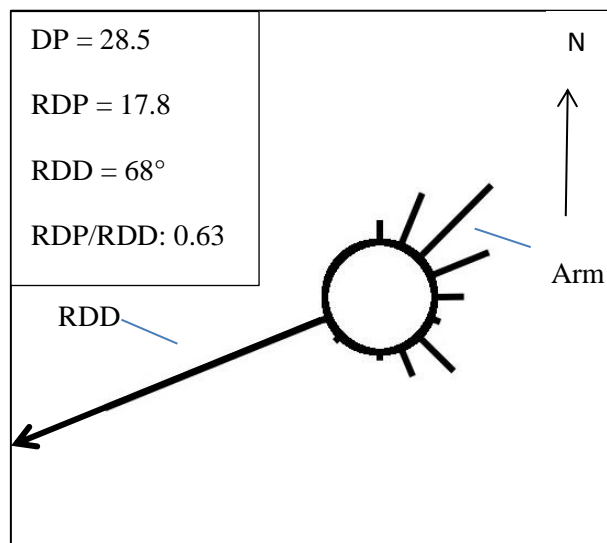


Figure 3.21: example of Sand rose graph, relative to year 2012 in the study area.

Vector unit totals from different directions is vectorially resolved to a single vector resultant: the vector representing the total DP will have a Resultant Drift Direction (RDD), resolved by trigonometrical calculation, which expresses in degrees the direction in which sand would tend to drift under the influence of winds from the different directions:

$$RDD = (tg^{-1})\left(\frac{x}{y}\right) \quad \text{Equation 3.9}$$

Where:

X = the total of partial DP multiplied for the cosine of angle related to every quadrant.

Y = the total of partial DP multiplied for the sine of angle related to every quadrant.

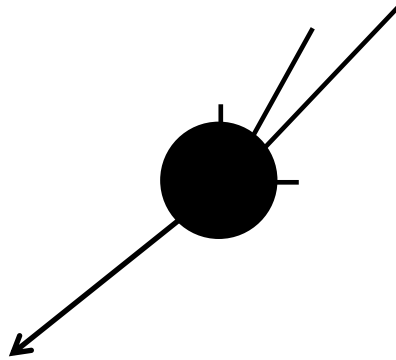
The resultant vector's magnitude, the Resultant Drift Potential, is calculated using the Pythagorean theorem and represent in vector units the net sand transport potential when winds from various direction interact:

$$RDP = \sqrt{x^2 + y^2} \quad \text{Equation 3.10}$$

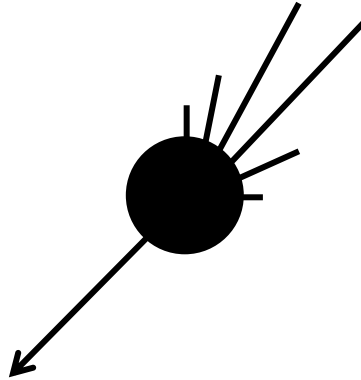
The ratio RDP/DP is called "Directional Variability Index", goes from 0 to 1, and describe the long term pattern of the wind: higher RDP/DP values reflect unimodal winds, while lower values indicate complex wind regime.

Fryberger developed a classification scheme to link different wind regimes to various dune landscapes; the following are the 5 commonly occurring relationship of modes on sand roses:

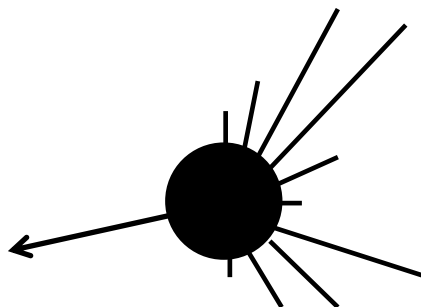
- I. Narrow Unimodal: 90% or more of the DP falls within a 45° arc of the compass.



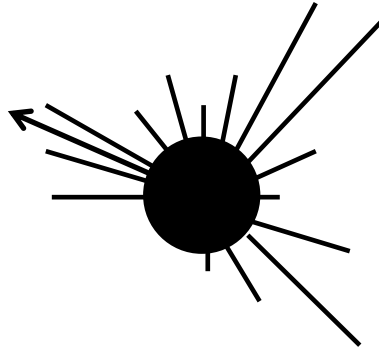
- II. Wide Unimodal: similar to the previous, a single peak, but with a wider directional distribution.



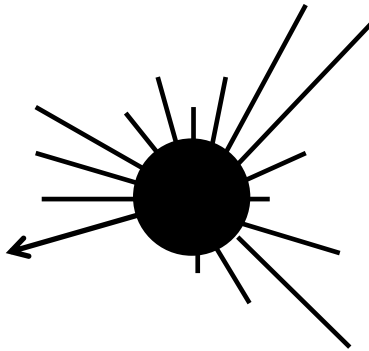
- III. Acute Bimodal: two peaks, with the longest sand rose arms which form an acute angle.



- IV. Obtuse Bimodal: as before two peaks, but with the longest sand rose arms which form an obtuse angle.



- V. Complex: any distribution with more than 2 peaks or modes.



The ratio Directional Variability Index in this case, is very high in the first case, next to 1, and decreases in the following examples until the last which is very near to 0.

3.3.2 Practice.

In this study, Drift Potential calculations were made both for annual period (to describe the sand drift climate) and for every time period between two surveys.

Whatever was the aim, wind data were extracted in m/s from the National Tide-gauge Network database (Rete Mareografica Nazionale - RMN), composed by 36 measuring stations, uniformly distributed on the national territory, mainly located in port structures. This network, established in 2008 by the Environment National Department, ISPRA (Istituto Superiore per la Protezione e la Ricerca Ambientale) replaces the system of pre-



Figure 3.22: Porto corsini Meteorological station.

existent tracking Tide-gauge Network in full. All the stations are equipped with a local system of data management and memorization and a device to transmit them to the central site in Rome.

All data are real time available for the public. For the purpose of this study data from the Ravenna Porto Corsini station (Lat. $44^{\circ} 29' 31.47''$; Long. $12^{\circ} 16' 58.57''$), were used. This station measures every 10 minutes wind direction in degree and speed, in m/s. The direction is measured thanks to a transducer made up by a counterbalanced vane coupled to an optical encoder disk, equipped with a series of infrared emitter–receiver LEDs (Light Emitting Diode) which detect the disk position, allowing to calculate the wind direction, with an angular resolution of $\pm 2^{\circ}$ degrees (Accuracy: $\pm 0,5\%$) (www.mareografico.it).

The wind speed transducer is constituted by a “3-cup Robinson” assembly coupled to an optical encoder disk, where a series of infrared emitter–receiver LEDs detects the encoder disk movement calculating the wind speed (Resolution: 0,1 m/s; Sensitivity: 0,25 m/s; Accuracy: $\pm 0,5$ m/s ($0 \div 20$ m/s); ± 1 m/s (>20 m/s)). No significant lack of data was registered for the studied periods, so no other station data was needed to be used.

Since the plan where sensors are mounted is 10 m upon sea level, no correction factor had to be applied to those data

A useful free software was used to compute wind data, WRPLOT View™ (1998-2011 Lakes Environmental Software), which provides visual wind rose plots, frequency analysis, and plots for several meteorological data formats. The operator is allowed to import data from excel (.xls format) and export in .csv format. To draw the sand roses, GIMP (GNU Image Manipulation Program), an open-source software, was used drawing on a millimeter based graph template.

Since Drift potential calculation starts from the grain size of the local sand, a parallel campaign to sampling sand in every area surveyed was conducted. In each site 20 samples were collected using a small drill, 10 between 0 and 20 cm depth, 10 between 20 and 50 cm. the sampling position was decided by the author in order to make the samples representative of the dune-beach system. Sampling position can be seen in further chapters.

The grain size determination was made, once in laboratory, thanks to the traditional sift technique, using six sieves with different Mesh number: 40, 50, 60, 70, 80 and 100. Every sample was sifted and every fraction was weighted, to have the cumulative graph. An example of grain size analysis is reported in figure 3.23, with frequency classes and cumulative curve graphic.

3.4 Meteo Data Analysis and Multivariate statistic (PCA).

3.4.1 Meteorological data analysis.

A substantial part of this research is based on the meteorological data analysis, trying to understand the link with dune morphological changes, and in particular which are most influential factors and on what mostly depend volumetric and areal changes in the dune field.

To try to describe the influence that wind and sea forces have on this environment, a group of indicator factors, called “Forcing Factors”, was chosen, in part taking inspiration from other authors’ previous works, in part trying to set new ones.

For what concern the wind dynamic, data were extracted from the National Tidegauge Network database (Rete Mareografica Nazionale - RMN), taking those from station Ravenna Porto Corsini, which is a few kilometers north the three study sites. Those data were elaborated not only to determining the Drift Potential for every period between two surveys, but also to describe the DP regime, in term of yearly calculation. Moreover, those data were used to describe the seasonal and yearly aeolian climate, to understand for example which winds are dominant or regnant, or which season is the on-shore winded and which is the off-shore one.

As aeolian Forcing Factors, five statistical indicators were chosen: the Drift Potential value and the Directional Variability Index, as indicated by Walker (2004); the relative percentage of on-shore along-shore and off-shore winds, as indicated by Montreuil (2013).

Assuming that the dunes orientation of the three study sites about goes from 165° to 170° South, and 345° to 350° North, the wind subdivision was operated as follow, considering an arc of 70° for the alongshore winds and a 145° arc for other two:

- Onshore Winds → from 5° to 150°.
- Offshore Winds → from 185° to 330°.
- Alongshore winds → from 0° to 5°, 150° to 185° and from 330° to 360.

The author as many other in past, considered for alongshore winds a degree width of 15° in both front and back direction; try to avoid deviation of data from the natural behavior, as much as possible, the author considered the 5° width of dune fields as part of the alongshore domain: this is the reason for this quadrant subdivision.

The elaboration was applied only the effective wind, thus only to those values which exceed the threshold drift velocity. For each class the percentage on the total effective wind records was extracted and reported in statistical analysis.

For what concern the sea forces, the Regional Agency for the Environment Protection of Emilia Romagna (ARPA-ER) databased was consulted, thanks to the DEXTER system which is a software that allows the operator to visualize and questioning every meteorological station on the Regional area. In this specific case the data coming from Cesenatico buoy (44.2155°N 12.4766°E) were elaborated, focusing on the high energy events, such as storms.

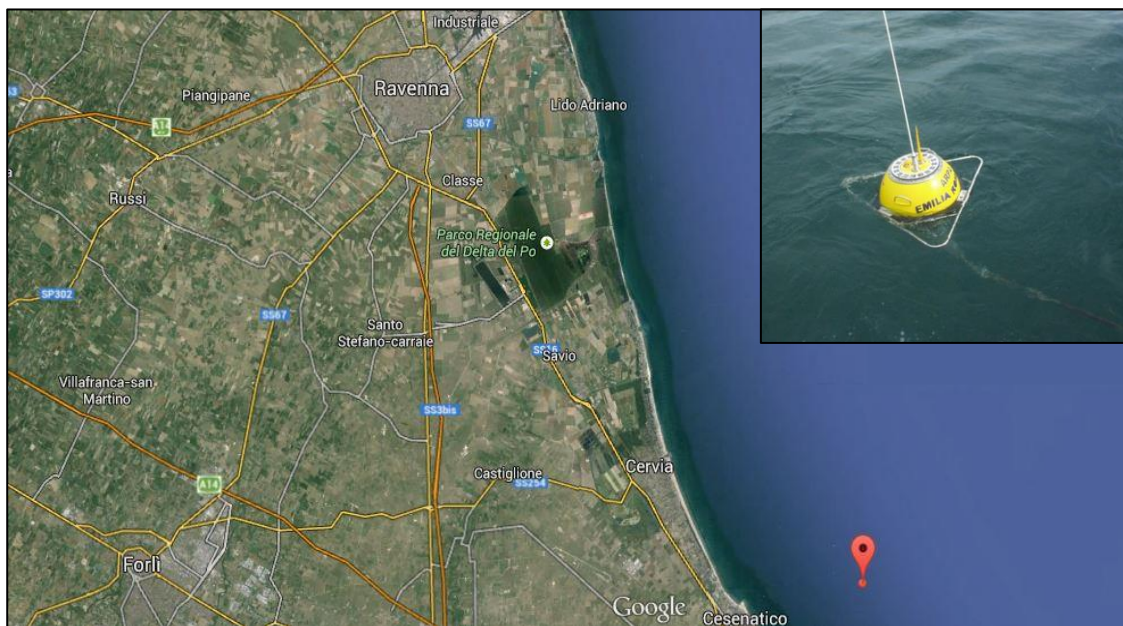


Figure 3.24: Cesenatico survey buoy geographical position.

It is important to remember that was considered “storm” any event when wave high was more than 1.5 meters for at least six hours, as indicated by ARPA-ER (2011).

Moreover two storm events were considered separated by a period of at least three hours, when waves height was below 1.5 meters. In this way, for every period between two surveys was extracted the maximum water level (Keijsers, 2014) and the

maximum waves height (Montreuil, 2013), both in meters; as proposal by the author, the total number of storm's hours and the average waves height (m) were calculated.

The average daily rain (mm), based on data from Ravenna-Le Bassette, was another proposal by the author. For the period from the 3rd February 2014 to the 23rd June 2014, the buoy unfortunately stopped recording and transmitting data, so these were integrated with data from the Ancona and Venezia buoy (belonging to the National Tidegauge Network).

All the forcing factors are listed in the table below, with the abbreviation used and the measurement unit.

Forcing Factor	Abr.	m.u.
Drift Potential	DP	u.v.
Directinal variability index	DVI	--
Water Level	Wl	m
Maximum Waves Height	Sm	m
Average Waves Height	Sa	m
Total number of storms' hours	T	h
Effective onshore winds percentage	Won	%
Effective alongshore winds percentage	Wa	%
Effective offshore winds percentage	Woff	%
Daily average rainy	P	mm

Table 3.6: Forcing Factors list, with abbreviations used to plot results and measurement units.

3.4.2 Multivariate statistic and Principal Component Analysis (PCA).

The determination of one variable in huge data set of samples or of many variables in just one sample is the application field of univariate statistical analysis; when, instead, both variables and samples are many, multivariate statistical analysis is one of the most useful methods.

Variables involved in a multivariate problem, usually, have different natures, and thus they are always expressed in different measurement units. Most part of multivariate techniques considers a pre-treatment of data to minimize the effect of different measurements units and try to give to every variable a comparable relative weigh.

Multivariate statistic has two major approaches to the treatment of data:

- Statistical technique applied to a data set, in which all variables are independent. These methodologies, for example, include the Correlation Analysis, the Cluster Analysis and the Principal Component Analysis (PCA);
- Statistical technique applied to a data set, in which independent and dependent variables are present. The most applied techniques of this group are the multivariate linear regression, the Principal Component Regression (PCR) and the Partial Least Regression (PLS).

In this text will be debated only the Principal Component Analysis (PCA), because it is a useful statistical technique for finding patterns in data of high dimension, with very variegate variables (and measurement units), expressing them in such a way to highlight their similarities and differences. It has been applied in many fields such as medicine, astronomy or agronomy, and it has been described as a powerful and robust technique to identify dominant patterns of change in meteorology and coastal sciences (Houser et al., 2008).

In general, it is a factor methodology, because it permits the reduction of variables' number thanks to the construction of new synthetic variables, called Principal Components (PCs), based on a factorial linear combination between starting variables. The new Principal Components are axis relative to the maximum variance direction, in a decreasing order: what makes this technique so reliable is that this transformation is driven by original data.

The extractions of PCs can be made using either original multivariate datasets or using the covariance or the correlation matrix if necessary: the correlation matrix is commonly used when different variables in the data set are measured using different units or if different variables have different variances. Using the correlation matrix is equivalent to standardizing the variables to zero mean and unit standard deviation. The amount of the variation explained by each PC is called “Eigenvalue”, while “Eigenvectors” provide the weights to correlate PCs.

From a mathematical point of view, the first step of a PCA, as announced, is to subtract the mean calculated across each dimension. Starting from a data set matrix where columns represent samples while variables are in rows, the aim is to produce a data set, whose mean, thus every partial sum, is zero. Table 3.7 is a simplified example of this.

The second step involves the covariance matrix calculation. To understand covariance it is necessary to be familiar with standard deviation and variance concepts: given a data set, they both measure the amount and the dispersion from the average, but they operate only on one dimension, so that for example it could be calculated only the standard deviation for each dimension of the data set independently of the other dimensions (Smith L., 2002).

Value	Value sub	Value	Value sub	Value	Value sub
2.3	-2.26	20.6	2.48	11.9	-17.62
7.9	3.34	10.2	-7.92	59.6	30.08
1.1	-3.46	25.7	7.58	33.6	4.08
8.9	4.34	14.2	-3.92	27.1	-2.42
2.6	-1.96	19.9	1.78	15.4	-14.12
Avg=4.56	Sum=0	Avg=18.12	Sum=0	Avg=29.52	Sum=0

Table 3.7: example of a mean subtraction data set with.

Mathematically, Standard Deviation is defined as “the average distance from the mean of the data set to a point” and it is calculated computing the squares of the distances from each data point to the mean: is a measure of how numbers are spread out.

Variance is the average of the squared differences from the mean and express how far each number in the set is from the mean. Diverging from this two dimensions,

covariance is a useful tool to have a similar measure of how much the dimensions vary from the mean, but with respect to each other. Mathematically it is very similar to the variance, whose formula is:

$$var(x) = \left(\frac{\sum_{i=1}^n (x_i - x_a)(x_i - x_a)}{n-1} \right) \quad \text{Equation 3.11}$$

Where:

- x_i = a value from the dataset.
- x_a = the average value of the variable.
- n = number of values for that variable.

The covariance formula, which instead is always measured between 2 dimensions, is:

$$cov(X, Y) = \left(\frac{\sum_{i=1}^n (X_i - X_a)(Y_i - Y_a)}{n-1} \right) \quad \text{Equation 3.12}$$

For an n -dimensional data set, it is possible to calculate $\frac{n!}{(n-2)!*2}$ different covariance values. In general, what is important is the sign of resulting value: a positive value indicates that the two variables are in positive correlation, and as the first increases or decreases the same does the second one; a negative value means instead that if the first one increases the second one decreases and vice versa; a zero value indicates no correlation between the two dimensions. Covariance matrix is an algebraic tool to get all covariance values calculated between all the variables in the data set. For mathematical reason this is going to be a square matrix.

The third step calls for eigenvectors and eigenvalues calculation. In general eigenvectors are the product of the multiplication of a two-dimensional vector for a square transformation matrix that, when multiplied reflects vectors in the line $x = y$. Thus the eigenvector is the reflection of the original one, transformed by a special square matrix; “special” means that the resultant vector must be a multiple integer of the original. Every square $n * n$ matrix has n eigenvectors; hence to have a unique solution

a condition must be placed: the eigenvector must have an unitary norm. This means that the sum of its square elements must be 1.

A fundamental property of eigenvectors is that they are perpendicular to each other; this is important because it means that it is possible to express the data in terms of these perpendicular eigenvectors (Smith, 2002). Those vectors are then lined up following a variance decreasing order. The eigenvalue is strictly connected to the eigenvector, because it represents the scale factor multiplying the original vector.

The final step of PCA consists in multiply the matrix with the eigenvectors in the columns transposed in rows (ordered by significance), for the mean-adjusted data transposed, with data items in each column and each row holding a separate dimension.

The aim of this procedure is to “translate” original data solely in terms of eigenvectors. This is very useful in statistic cases described above (large amount of variables very different each from each other), because it is possible to plot the resulting matrix in many ways, usually easy to be read.

In this study the author chose to adopt the “bi-plot”, a graphic which plots both the scores as points, and eigenvectors as arrows. All the PCA procedure and plotting was computed using “R”, a free software environment for statistical computing and graphics, co-operating with Rstudio, a set of integrated tools designed to make easier the computation.

Bi-plot is composed by an image of the principal plane, where the horizontal and vertical axes are the first and the second Principal Components (in order of variance).

For what concerns scores, their particular position in the principal plane is very important, because it gives information about how samples influenced a vector variance, depending on proximity (Borcard, 2011).

For what concerns vectors, remembering what wrote about their orthogonal properties, they all take origin from a common point in the graph plane. What is really important is the orientation of every vector relative to each other: when two arrows are parallel, that means that those two variables are strongly connected; if they go in the same direction this correlation is positive, if they go in two opposite directions they are in negative correlation. If two vectors are not so parallel, but they orientation is under a right angle, they still are in positive correlation, but in a lower way than before.

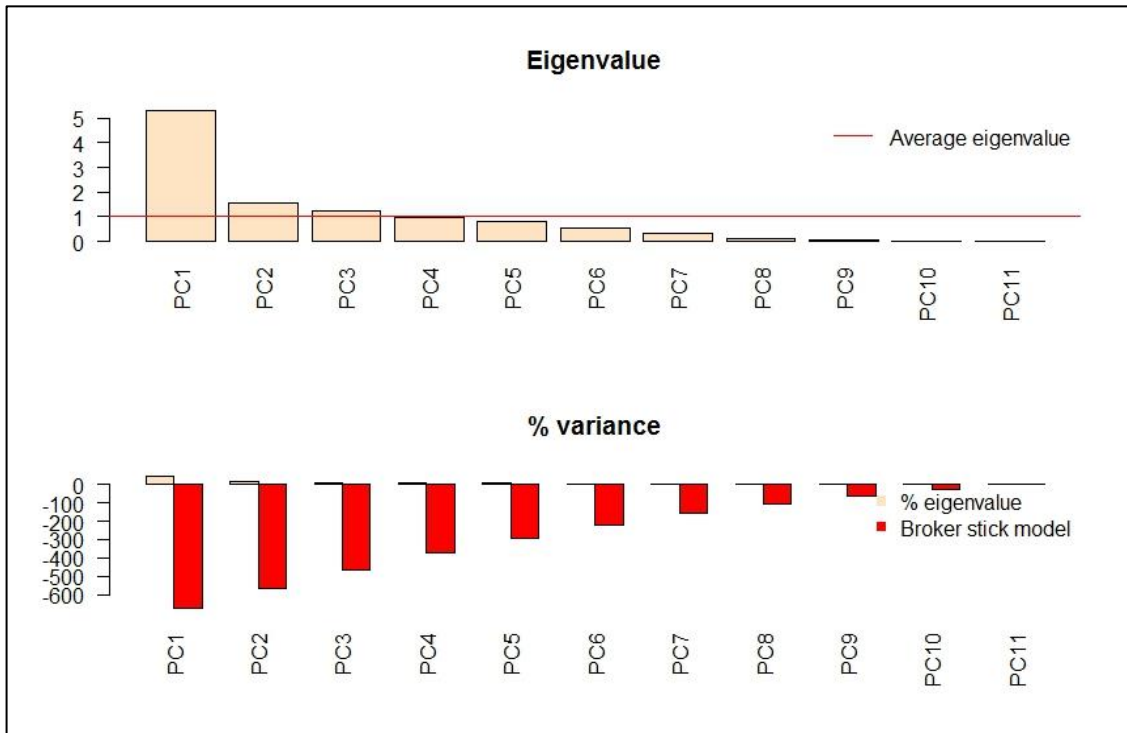


Figure 3.25: example of eigenvalues ordered by variance.

The more this angle approaches the right angle, the more there is no correlation between the two variables represented.

In this study this powerful statistical technique was used to find pattern in data sampled. More specifically the author tried to find correlations between the already described meteorological “Forcing Factors” and morphological changes of surveyed dune fields: seasonal volumetric variation, spatial (area) changes of the morphological sub-zone and blowouts areas oscillations.

3.5 Computational Fluid Dynamics (CFD).

The Fluid Dynamic is the science which studies the fluid (gas or liquid) behavior. Until the 1970's this science included only the theoretical study, before taking two paths: the classic fluid dynamic and the numerical one. According to Capozzi (2013), the first one uses analytical approach to formulate models, the second one faces fluid dynamic problems from a strictly mathematical (numerical) point of view. This is called "Computational Fluid Dynamics" (CFD).

This technique, thanks to numerical elaboration and mathematical models, simulates the fluid behavior and its temporal evolution in complex physical problems. This is done working on the four fundamental parameters (of Fluid Dynamic): speed, pressure, temperature and density. What makes this method highly suitable for this application is its High Performance Computing (HPC): it allows, in a relative simple and fast way, the computation of initial conditions, the environmental parameters and the system answers. This technique is related to the computer cluster technology which links together different computing work stations, with the result to have a very high calculation speed. Probably CFD will replace wind tunnels, in a few decades.

According to Veersteeg et al. (1995), the CFD works with codes, which include numerical algorithm to face fluid dynamic problems: the codes structure must be set up in three main elements: pre-processor, solver and post-processor.

The pre-processor is an element which includes the input of a flow problem. This is computed and transformed on a CFD program, in order to define:

- Computational domain: definition of the area of interest.
- Grid of cells: domain subdivision based on a grid.
- Definition of the physical problem to solve.
- Fluid properties.
- Cells boundary conditions.

It is very important to highlight that the grid definition is strictly connected with accuracy of the model and the value used in the process is the one resulting from the cells' "nodes", the central point of each cell.

The solver represents the numerical solution technique include four different possibilities, which have the basic aim of approximating the unknown variables, substitute these approximations into the governing flow equations (discretization) and the solution of the resulting equations. Assuming that the four techniques differ for the way of variables approximation, they are:

- The "Finite difference method" approximates using the means of point samples at the node points
- The "Finite Element Method" uses piecewise functions to evaluate local variations of the variables
- Spectral Methods use means of truncated Fourier series
- The "Finite Element Method" is the most used nowadays and it integrates the differential equations into the fluid flow over all control volumes of solution domain. This is what distinguishes this technique from others.

The post-processor step is represented fundamentally by a wide range of tools with outstanding graphic capabilities, which enable better data visualization, such as color postscript output or 2D/3D surface plots.

Remembering what the author wrote in Chapter 1 for what concerns wind flow and its complex interaction with topography, it is intuitive to understand how CFD is highly suitable for this kind of study, because of its complete spatial coverage of the wind (Jackson D. et al., 2011). Moreover thanks to the intense development of the 3D technology in last decades CFD models have reach a very high level of accuracy and its results are more and more suited to describe the real-world dynamics. It has been largely applied in environmental monitoring, especially where the interest was the interaction between flow and non-uniform topography, such as hydrology and geomorphology (Bates et al., 1998).

Thanks to a profitable collaboration with the Flinders University of South Australia, in this study the CFD powerful technique has been tested to evaluate the wind flow behavior during a high energy event, in a natural dune environment. The starting and ending conditions consisted in two DEMs representing a sector of the Bevano foredune ridge, surveyed in October the 18th and November the 17th, 2013. The DEMs were constructed starting from TLS data.

The second survey was done “ad hoc” to evaluate the environmental modifications after a stormy period. A few days before the survey, a moderate storm happened in this area, November the 11th. In this occasion wave height exceeded even the 3 meters (from North-East) and the high energy conditions lasted until the 12th afternoon. On The 15th November another event happened, but with lower energy. The wave rose of the whole period surveyed can be consulted in figure 3.25; the diagram has been constructed on the Cesenatico buoy data (Regional network).

The anemometry data, recorded by the Porto Corsini meteorological station (National Tide-gauge Network-RMN) every ten minutes, indicate that wind speed peaked at 20 m/s, from North East (Bora), and that for a huge part of storms periods the wind speed was above the threshold velocity and from NE. The wind rose can be seen in figure 3.26.

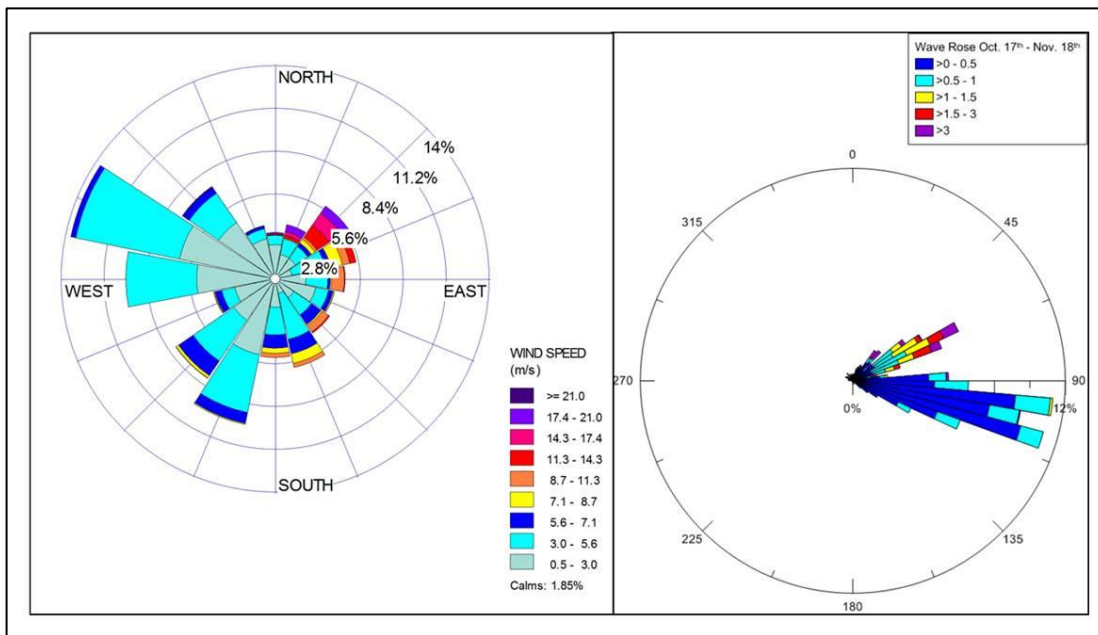


Figure 3.26: Meteorological climate of the surveyed period. a) Wind rose; b) Wave rose.

Flow simulation were conducted with the open-source CFD modeling software OpenFOAM, applying the two-equation Re-normalized Group (RNG) k—Epsilon turbulent model. The RNG (Yakhot V. et al., 1992) is based on Reynolds-Averaged Navier-Stokes (RANS) equations, which average the motion fluid over time (Smyth T. et al., 2012). The solver applied was PIMPLE, a large time-step transient solver for incompressible flow; the Computational System was Colossus high performance computer facility (Flinders University).

Boundary conditions involved the logarithmic wind profile at inlets based on the already described nearby meteorological data during average conditions between the two scans. Uniform surface roughness height of 0.0015 m throughout computational area was assumed. The whole computational area (115 m * 180 m * 40 m) was gridded to a cell size of 0.15 square meters at the surface: this resulted in 2,088,233 cells. Probes, which represent the point where data was interrogated at, were located at 0.2 meters above the DEMs surface.

4 RESULTS

4.1 Terrestrial Laser Scanner.

4.1.1 Validation tests results.

The post processing procedure applied on UAV data generated a digital terrain surface (figure 4.1), which is the result of the elaboration of 550 selected images, through the feature-matching procedure implemented by “Structure From Motion” (SfM) algorithm (Mancini F., 2013). The resulted point cloud was composed by 831,153 points, covering a geometrical surface of 27500 m².

Taking inspiration from the similar TLS field methodology, the UAV procedure was modeled in order to register this model (as the TLS one) in the UTM reference system: this was done by using a set of 10 Ground Control Points, distributed around the study area. The principal aim was to have absolute references to perform an evaluation in term of surface comparison and linear regression’s root mean square (RMS) values.

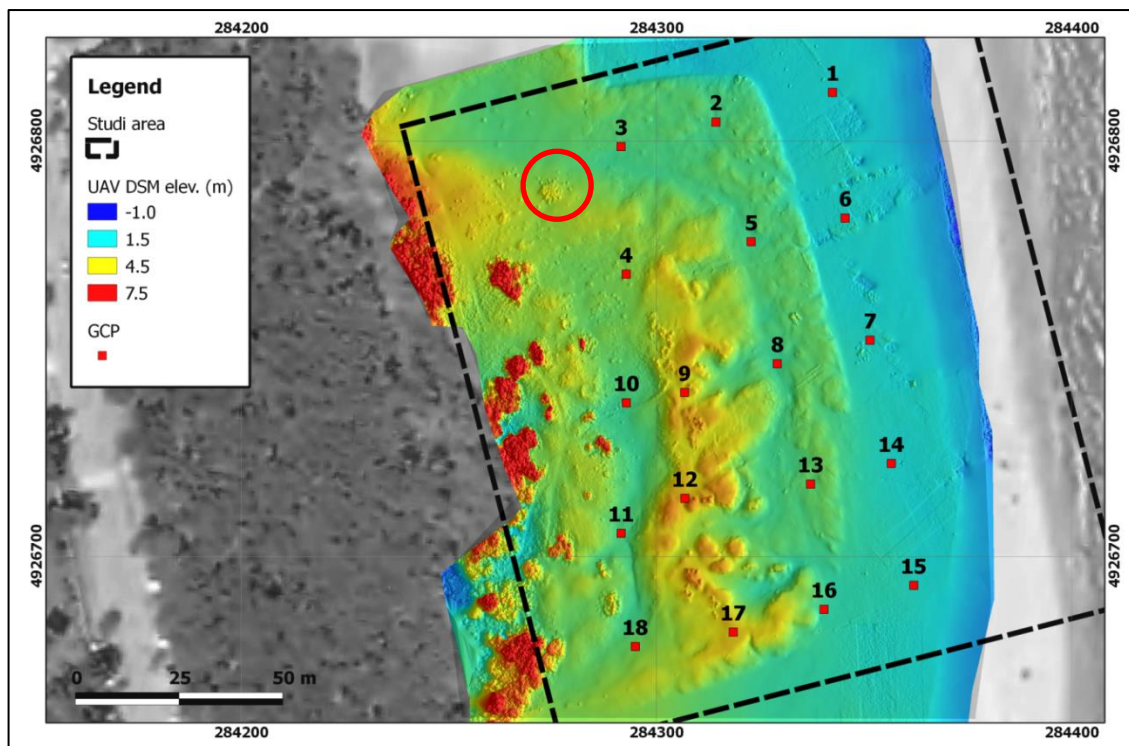


Figure 4.1: projected Digital Surface Model (DSM) obtained by UAV data. In the red circle there is an example of vegetation feature.

The registration procedure, right after the SfM approach, involves a bundle adjustment to project the DSM (Digital Surface Model) data in its UTM precise position. The whole transformation resulted in table 4.1: 0.008 m in the East direction; 0.007 m in the North one; 0.077 in the vertical direction (which is usually the most important and most prolific source of errors); 0.078 within the 3D component (Mancini F., 2013).

GCP	UTM coord. (m)			Individual residuals after the transformation (m)			
	East	North	Elev.	East	North	Elev.	3D
1	284342.420	4926811.730	1.900	0.005	0.000	-0.023	0.024
3	284291.510	4926798.710	2.720	0.022	0.016	0.160	0.162
4	284292.740	4926768.000	3.760	0.001	0.002	-0.004	0.005
5	284322.820	4926775.800	2.770	-0.005	0.009	-0.081	0.082
7	284351.450	4926752.100	2.020	0.001	0.007	-0.010	0.012
10	284292.760	4926737.020	2.890	-0.007	0.000	-0.153	0.153
13	284337.150	4926717.480	3.130	-0.004	0.000	-0.020	0.020
14	284356.590	4926722.440	1.970	0.001	-0.001	0.005	0.005
15	284361.990	4926693.110	2.020	0.000	0.002	0.058	0.058
18	284294.940	4926678.390	3.500	-0.004	-0.006	-0.008	0.011
		Total error		0.008	0.007	0.077	0.078

Table 4.1: residual of adjustment transformation on the selected GCPs, used to register the DSM.

As shown in table 4.1, planimetric error is almost negligible, because less than 1 cm, while vertical accuracy is lower, due to the offset of two GCP (3 and 10), which strongly influenced that measure. The result is that the vertical error has an order of magnitude more than planimetric errors (centimeters instead of millimeters). To avoid vegetation feature strong influence, patches with height over 7.5 m were not included in

the validation process (figure 4.1). Vegetation under 20 cm was not removed from the DSM.

The TLS survey procedure was already discussed in the previous chapter. A total of 18 scans were necessary to complete the DEM, which counted 115 million points in its cloud. Every single scan, as indicated by the procedure, was referenced independently by every other in the UTM system. The area to compare was exported and gridded, with 4 cm resolution.

The first comparison was made between the two digital models and the GNSS validation points, independently, taking elevation as comparison value. This was done assuming that the GNSS references are the most precise data over all and indicate the most next to real-world positions. Both comparisons gave positive results (figure 4.2).

The average elevation difference between UAV and GNSS data was -0.01 m, with a root mean square (RMS) of 0.11 m: this happened because of the presence of significant differences on few validation points, which are represented in the frequency graph by the tails. Probably the vegetation has its role in this deviation too. Anyway it is important to notice that the linear regression value (R^2), with its 0.9915 value, is absolutely next to 1 (the completely positive correlation).

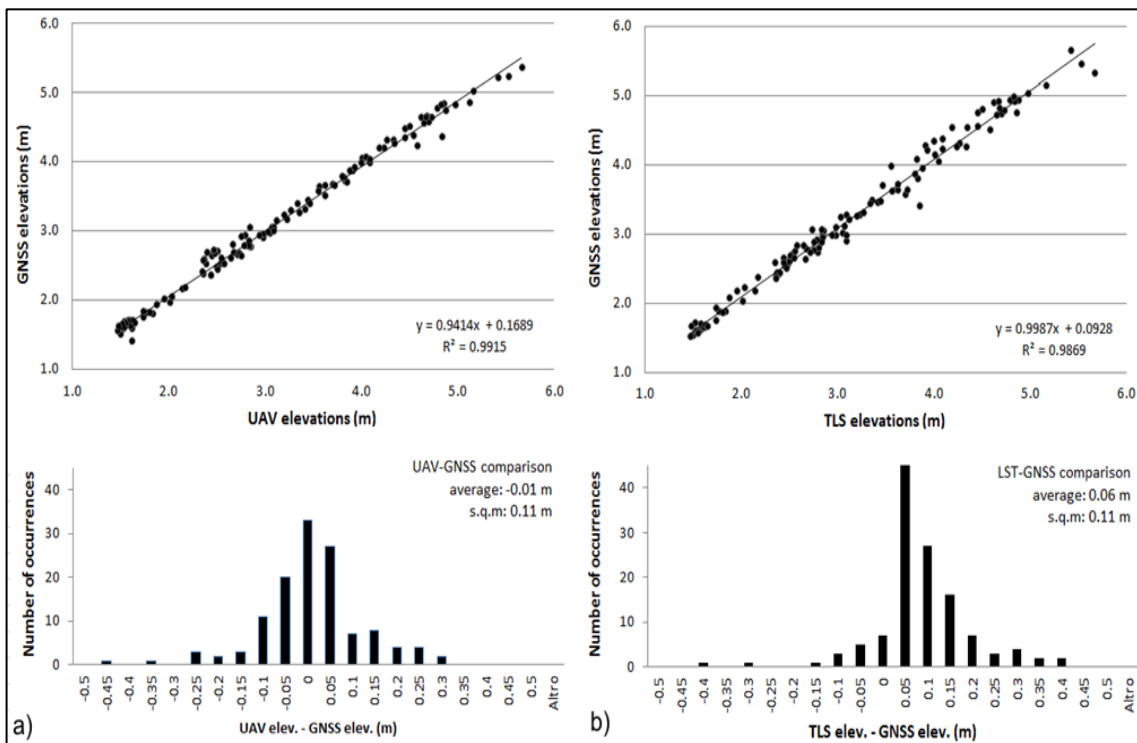


Figure 4.2: comparison between elevation values of virtual GNSS points, with digital surfaces elaborated. A) UAV Vs GNSS; b) TLS Vs GNSS

In figure 4.2 b), the TLS-GNSS comparison results are reported. Linear regression shown a strong positive correlation as before ($R^2 = 0.9869$), but there is a stronger average distance (0.06 m) and a different frequency distribution of elevation differences (positive tail). The source of this deviation and the comparison between the two devices will be discussed in next chapter, in term of spatial errors distribution map.

Anyway it is important to specify that the digital models computed by each device have a different point density (TLS cloud is much more dense), depending on the image textural properties (for UAV) and the TLS settings (Figure 4.3).

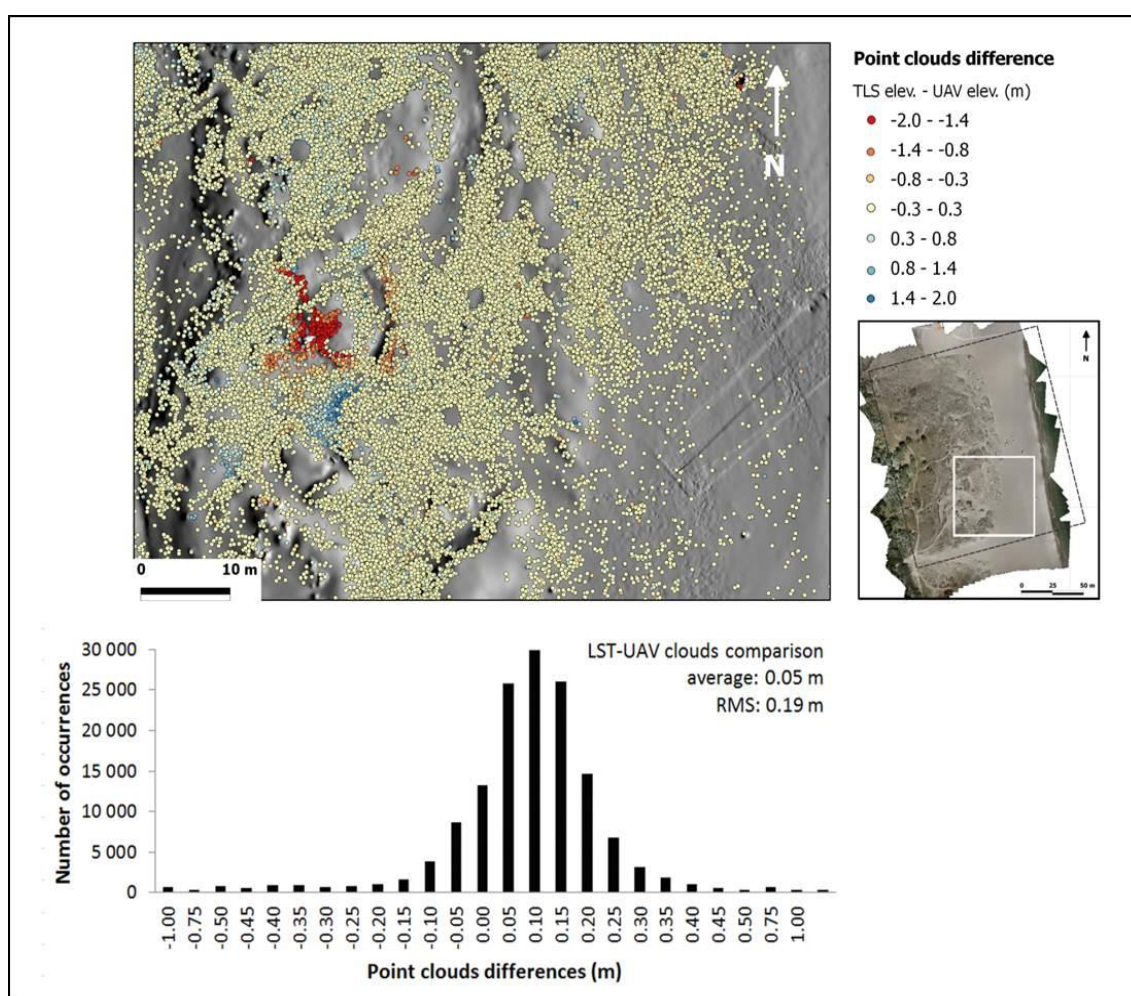


Figure 4.3: Points clouds comparison obtained by subtracting the UAV elevations from closest TLS elevations. Differences are represented by a color-coded solution over the shaded UAV DSM and frequency histogram of differences reported (statistic parameters referred to the whole dataset).

In order to guarantee the reliability of laser scanner data, two more test were execute, using only TLS and GPS-GNSS devices, on Milano Marittima and Marina di Ravenna dune fields. These surveys were made a few months later and took advantage

of two sets of very dense GPS transects: the Milano Marittima one has 906 points, while the Marina di Ravenna 476 (during the UAV comparison test, the GNSS points, GCP, were 18). Results are shown in term of linear regression in figure 4.4. For both cases linear regression indicates a strong positive correlation, very close to unity. The very next to zero standard error value (which is the average standard deviation), indicated the absolute reliability of test executed.

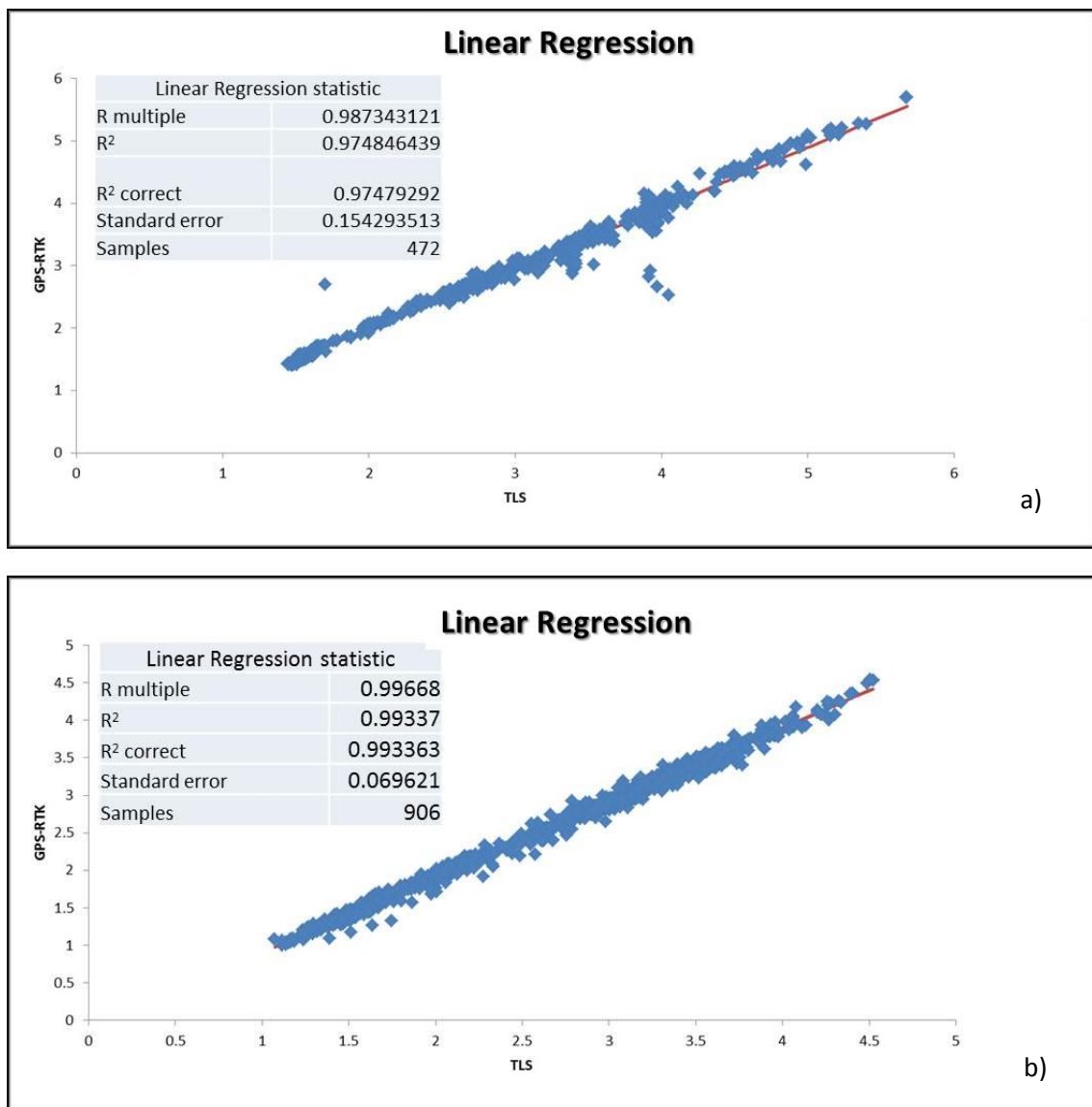


Figure 4.4: GNSS validation of TLS data: linear regression results. A)Marina di Ravenna test; b) Milano Marittima test.

4.1.2 Morphological units, Areas of Interest and morphological sub-zones.

The sample campaign conducted for this study included 17 surveys, of which 15 were programmed in relation to the supposed summer and winter habitus of the dune: during 2012 and 2013, for each of the three areas of interest, two “seasonal” surveys per year were made, one in the period of the end of May/begin of June (depending on weather and beach management condition), the other at the end of October. In 2014 only the spring one was made. During 2013 other two surveys were made “ad hoc”, on the Bevano river area, one at the beginning of April, the second in November, two days right after a strong storm (the strongest of the three years research period). In table 4.2 the survey campaign calendar is reported.

Survey Area	Date
Milano Marittima I	30/05/2012
Bevano I	06/06/2012
Marina di Ravenna I	11/06/2012
Marina di Ravenna II	01/10/2012
Milano Marittima II	23/10/2012
Bevano II	25/10/2012
Bevano III	09/04/2013
Marina di Ravenna III	27/05/2013
Bevano IV	29/05/2013
Milano Marittima III	29/05/2013
Marina di Ravenna IV	03/10/2013
Bevano V	17/10/2013
Milano Marittima IV	18/10/2013
Bevano VI	18/11/2013
Milano Marittima V	10/06/2014
Bevano VII	19/06/2014
Marina di Ravenna V	30/06/2014

Table 4.2: TLS campaign calendar

4. Results

For each DEM obtained five different morphological units were identified: dune foot line, crest area, landward talus, vegetated dune line and blowouts. The relative layer for every single survey can be consulted in Appendix I.

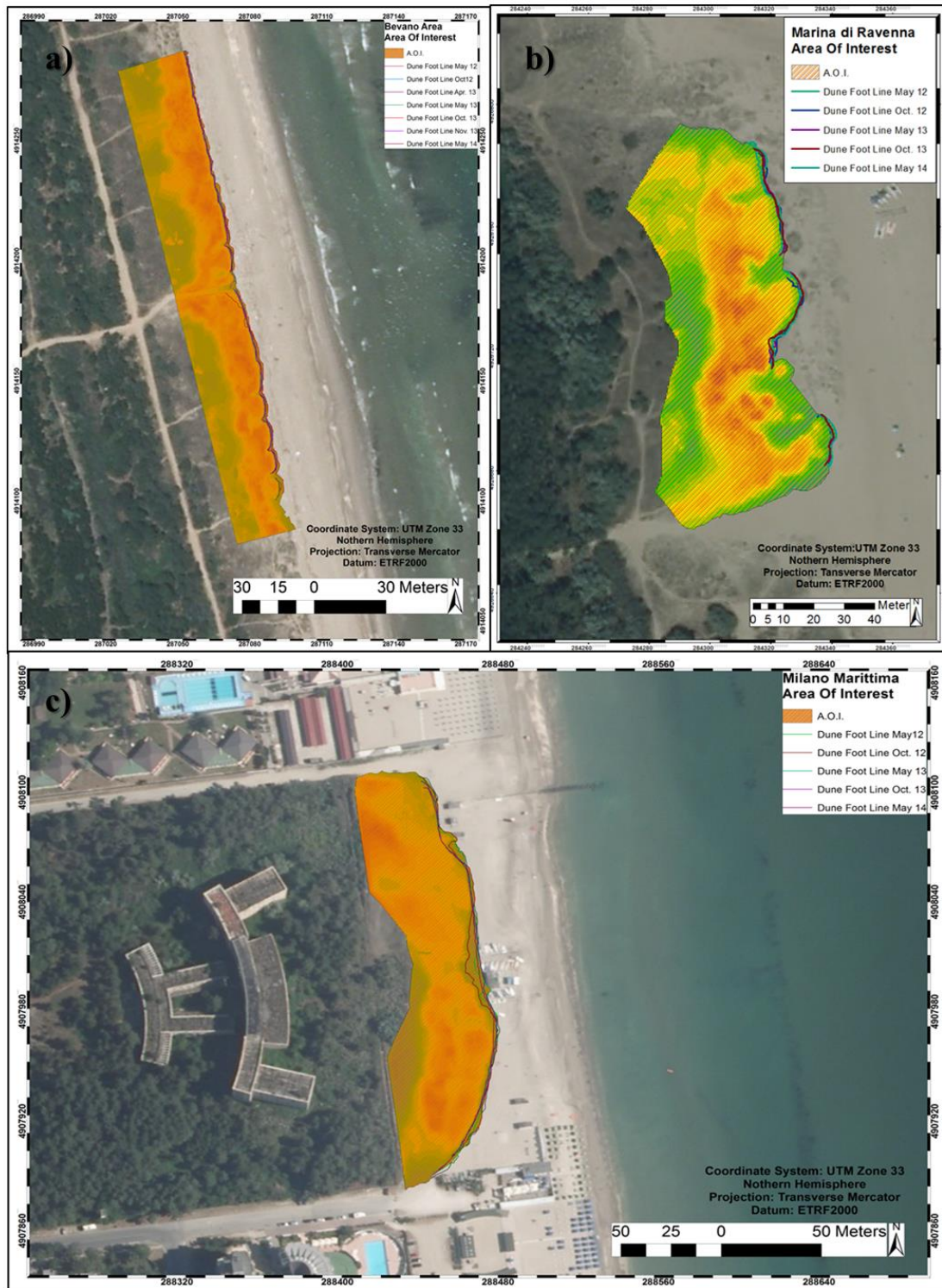


Figure 4.5: the three Areas of Interest. a) Bevano river area; b) Marina di Ravenna; c) Milano Marittima.

As explained in previous chapter, the most direct application of the dune foot line feature is to help the area of interest seaward limit determination. This was done in order to extract an Area Of Interest (A.O.I.) which was, as much as possible, strictly belonging to the dune itself, trying to leave the beach out.

The three different areas are shown in figure 4.6: the Bevano river dune field Area of Interest has a perimeter of 480 m with a surface 5696 m² wide; the Marina di Ravenna A.O.I has a 367 m long perimeter with an extension of 5422 m²; at last Milano Marittima area of interest has a perimeter 541 m long and is 8366 m² wide.

Every calculation was made using the Surface Volume ArcGIS tool, in order to calculate the surface areas not only in a geometrical way, but also, and much more important, in a topographic way (Area 3D).

Area	Dataset	Plane_Height	Area_2D	Area_3D	Volume
Bevano A.O.I.	May '12	1.36	5696	5986	7916
	Oct. '12	1.41	5696	5939	7524
	Apr. '13	1.51	5696	5981	6348
	May '13	1.52	5696	5932	6322
	Oct. '13	1.53	5696	5930	6363
	Nov. '13	1.24	5696	5948	7662
	May '14	1.58	5696	6056	6326
Marina di Ravenna A.O.I.	May '12	1.88	5423	5631	10426
	Oct. '12	1.86	5423	5614	10113
	May '13	2.2	5423	5589	8579
	Oct. '13	2.09	5423	5611	9232
	May '14	2.23	5423	5778	8823
Milano Marittima A.O.I.	May '12	0.98	8366	8527	16211
	Oct. '12	1.16	8366	8707	14378
	May '13	1.3	8366	8545	14347
	Oct. '13	1.2	8366	8538	14638
	May '14	1.26	8366	8553	14236

Table 4.3: Areas of Interest statistic table. Dataset is the date of the relative survey; plane height corresponds to the plane elevation from which the comparison started; Area 2D is the geometric area; Area 3D is the topographic area; Volume reports the volume calculated starting from the plane height.

Once identified, the dune foot line and other features were applied to the determination of the three morphological sub-zones within each DEM.

The so called “White Dune” starts from the dune foot line and ends, landward, on the upper limit of the landward talus. The “Grey Dune” corresponds to the landward scarp, from the upper to the lower talus’ limit. The “Black Dune” includes the backward dune depression and it ends at the vegetated dune line. This nomenclature takes

inspiration from a preexisting one based on vegetation environment, but this one takes into account only the morphological characteristics.

For each sub-zone the topographic extension was calculated in a GIS environment, in order not only to evaluate spatial changes in an absolute way (as well as in a statistic-wise) but also to understand possible seasonal trends and special circumstances.

The Bevano area has been split in two parts (then summed), with the purpose to leave the tourists path influence out. Results are shown in tables 4.4, 4.5 and 4.6.

Area	Dataset	Plane_Height	Area_2D	Area_3D	Volume	H min	H max
Bevano WD	May '12	1.39	2765	2955	5000	1.39	4.46
	Oct. '12	1.64	2562	2708	4113	1.64	4.34
	Apr. '13	1.55	2420	2633	4083	1.55	4.26
	May '13	1.60	2405	2564	3861	1.60	4.28
	Oct. '13	1.54	2518	2680	3978	1.54	4.17
	Nov. '13	1.60	2332	2515	3744	1.60	4.32
	May '14	1.87	2168	2364	3093	1.87	4.72
Marina di Ravenna WD	May '12	1.88	2788	2928	6212	1.89	6.08
	Oct. '12	1.90	2929	3047	6236	1.90	6.36
	May '13	2.29	2804	2928	5014	2.29	5.80
	Oct. '13	2.14	2829	2967	5474	2.14	6.15
	May '14	2.27	2811	3044	5353	2.27	6.62
Milano Marittima WD	May '12	1.42	7331	7464	12380	1.42	4.66
	Oct. '12	1.51	7367	7465	11867	1.51	4.61
	May '13	1.49	7209	7371	12686	1.49	5.20
	Oct. '13	1.56	7162	7321	11614	1.56	5.16
	May '14	1.49	7269	7449	12313	1.49	5.05

Table 4.4: White dunes statistic table. Topographic area is reported in the Area_3D column.

As it can be seen, for the Milano Marittima area, it was not possible to determinate the vegetated dune foot line, and thus the black dune limit. This was due to the physical obstacles (high fences and dense vegetation) on the field, which obstructed the operator passage and limited the laser light travel.

This dune in effect, unfortunately stands in front of a huge neglected building, erected during the last century and now waiting for the demolition, thus hardly fenced-in because of its dangerousness. So even though, the black dune extension has been determined for every Bevano and Marina di Ravenna DEMs, it wasn't possible to use it in PCA, due to the lack of Milano Marittima data. However it was useful in indicating special occurrences, as it will be seen and discussed in the next chapters.

After identifying the relative subzones or polygons, these areas were used to extract portions of the original raster DEM, on which making calculations. Once again the 3D analyst tool “Surface Volume” was used, which calculates the projected area (2D), surface area (3D), and volume of a surface relative to a given base height, or reference plane. Every measure is taken in the same measurement unit of the projected environment used (ETFR2000) and m, m² and m³ were used.

Area	Dataset	Plane_Height	Area_2D	Area_3D	Volume	H min	H max
Bevano GD	may '12	1.89	752	802	571	1.89	4.00
	oct '12	1.76	673	706	595	1.76	3.89
	apr '13	1.98	544	568	365	1.98	3.56
	may '13	1.82	736	761	574	1.82	3.91
	oct '13	2.06	588	609	367	2.06	3.26
	nov '13	2.07	612	636	344	2.07	3.63
	may '14	2.03	573	612	489	2.03	3.62
Marina di Ravenna GD	may '12	2.88	673	701	774	2.88	5.71
	oct '12	2.67	626	646	679	2.67	4.77
	may '13	2.98	699	720	682	2.98	4.97
	oct '13	2.68	742	763	890	2.68	4.57
	may '14	3.10	652	684	535	3.10	5.01
Milano Marittima GD	may '12	1.66	931	957	786	1.66	3.41
	oct '12	1.55	877	893	858	1.56	3.41
	may '13	1.97	748	761	563	1.97	3.48
	oct '13	1.83	790	804	556	1.83	3.30
	may '14	1.89	691	705	452	1.89	3.14

Table 4.5: Grey dune statistic table.

Area	Dataset	Plane_Height	Area_2D	Area_3D	Volume	H min	H max
Bevano BD	May '12	1.69	1428	1446	562	1.69	3.34
	Oct. '12	1.69	1368	1386	534	1.69	4.34
	May '13	1.67	1328	1333	505	1.67	2.62
	Oct. '13	1.67	1955	1974	765	1.67	2.74
	May '14	1.59	2101	2163	1133	1.59	3.44
Marina di Ravenna BD	May '12	2.49	905	914	546	2.49	4.37
	Oct. '12	2.37	868	873	589	2.37	3.75
	May '13	2.53	876	881	542	2.53	3.76
	Oct. '13	2.49	830	836	533	2.49	3.94
	May '14	2.43	777	815	662	2.43	4.94

Table 4.6: Black dune statistic table.

The Plane Height column reports (measured in meters) the elevation of the plan from which the calculation starts, included the volume one, thus it is related with minimum elevation recorded.

This is one of the reasons why tables report the maximum and minimum elevation (in meters) recorded for each sub-zones: this element can give information on the survey reliability, because the data have to be aligned one to each other; moreover they are important for giving information on potential special cases.

For what concerns Bevano area, on the two “special” surveys, those execute in

Area	Δ area WD (m ²)	Δ area GD (m ²)
Bev I	247	-95
Bev II	75	-138
BevIII	-69	193
Bev IV	115	-153
Bev V	-164	27
Bev VI	-152	-24
MdR I	119	-55
MdR II	-119	74
MdR III	39	43
MdR IV	77	-79
MM I	1	-64
MM II	-94	-132
MM III	-50	43
MM IV	128	-99

Table 4.7: Morphological sub-zones spatial

April and November 2013, only the white and grey dune extension was calculated. This was done because the author considered those data useful for the statistical analysis, unfortunately limited by the Milano Marittima situation, and not for the seasonal monitoring. For the purpose of applying these calculations to the Principal Component Analysis, it was needed to find the spatial variations of those sub-zones, subtracting one area from the following. Those results are listed in table 4.7.

Another important feature, considered by the author was the blowout total area. This was calculated by ArcGIS software, which provides the appropriate tools.

Dataset	Plane_Height	Reference	Z_Factor	Area_2D	Area_3D	Volume
Bev_may_12	2.1	ABOVE	1	215	229	159
Bev_oct_12	2.05	ABOVE	1	249	265	191
Bev_apr_13	1.79	ABOVE	1	179	192	191
Bev_may_13	2.09	ABOVE	1	166	174	134
Bev_oct_13	2.06	ABOVE	1	135	142	113
Bev_nov_13	1.87	ABOVE	1	179	188	166
Bev_may_14	1.97	ABOVE	1	179	189	157
MdR_may_12	2.23	ABOVE	1	601	633	835
MdR_oct_12	2.12	ABOVE	1	580	613	756
MdR_may_13	2.34	ABOVE	1	699	736	899
MdR_oct_13	2.28	ABOVE	1	605	641	746
MdR_may_14	2.35	ABOVE	1	611	650	725
MiMa_may_12	2.38	ABOVE	1	389	391	155
MiMa_oct_12	2.19	ABOVE	1	298	301	181
MiMa_may_13	2.55	ABOVE	1	280	281	73
MiMa_oct_13	2.16	ABOVE	1	287	289	155
MiMa_may_14	2.18	ABOVE	1	233	234	122

Table 4.8: blowout total area, summary: Area 2D reports the geometrically calculations results; “Area 3D” is the topographic result.

After identifying blowouts areas and drawing it as a polygon, the original topographic data are filtered extracting from the original DEM the surfaces corresponding to the polygons.

Table 4.8 is the original version of the Surface Volume table. It is reported to

Area	Δ area BO (m ²)
Bev I	36
Bev II	-73
Bev III	-18
Bev IV	-31
Bev V	46
Bev VI	1
MdR I	-20
MdR II	123
MdR III	-95
MdR IV	9
MM I	90
MM II	-18
MM III	7
MM IV	-55

show two more features of this tool: “Reference”, which is linked to the plane height and it indicates substantially where the reference plane is located in relation to the calculation: in this case the plane is located below the DEM and the calculation process involves the “above” surface. “Z Factor” is a conversion index to apply, if the projection and the calculation units of measure are different for any reasons; in this case the Z factor is obviously equal to 1. As before, even in this case, relative areas were subtracted each from the subsequent, in order to evaluate changes and use relative data in the PCA. In table 4.9 blowouts surface changes are shown in m².

Table 4.9: Blowouts areas

4.1.3 Volumetric differences results.

After determining the area of interest for each site, the operator had to extract it from each whole digital model. In order to identify seasonal trends, obviously only “seasonal” DEMs were compared in their volume: that means four comparisons per area.

The operation has been made in GIS environment using a 3D analyst tool called “Cut and Fill”. The choice of this tool, this time, is due to the fact that the reference plane is automatically calculated, while in the “Surface Volume” tool it should be selected manually.

It is important to remember that this operator consider to subtracting the youngest DEM to the oldest. That means that results should be read in reverse: a positive value indicates that the older DEM was bigger than the younger, thus erosion happened; subsequently a negative value indicates accumulation.

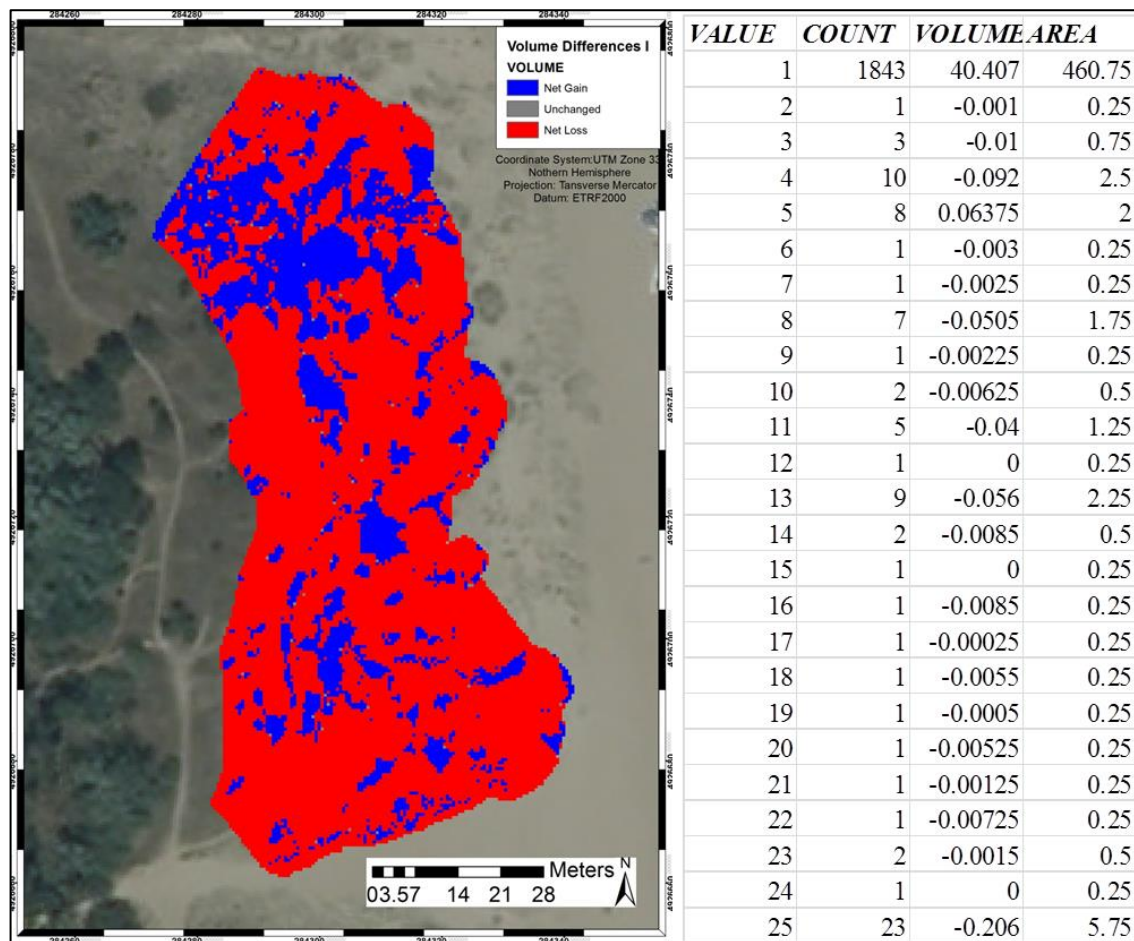


Figure 4.6: “Cut and Fill” example (Marina di Ravenna). Erosion area are colored in red, while deposition in blue. The seaward front of the dune is delimited by the dune feet. On the right the relative table, used to calculate.

A useful property of the cut and fill tool is incidental to the plotting (figure 4.6): using the grid as geometrical base the new layer will show which cells have been eroded (usually in red), and in which deposition happened (usually in blue). This could be helpful to identify possible seasonal or annual trends.

Each volumetric comparison map is going to be shown in the next chapter. For what concern the results, every cut and fill layer owns a data table, where the cells are banded together for volume value. The statistic tool calculator applied to the volume column gives a prospectus of the major statistics (figure 4.7).

In table 4.10 only results relative to the seasonal survey are reported. There are two more surveys, execute “ad hoc”, made both in the Bevano river area, both made in 2013: the first in April, while the second in November, two days after a severe storm. These results will be shown in further paragraph, when forcing factors will be discussed.

Site - Period	Min	Max	Mean	Sum
Bevano I	-266	161	0.15	133
Bevano II	-118	761	1.05	384
Bevano III	-235	104	-0.15	-29
Bevano IV	-469	111	-0.45	-194
Milano Marittima I	-460	702	0.47	258
Milano Marittima II	-1418	120	-3.00	-1164
Milano Marittima III	-169	592	1.33	564
Milano Marittima IV	-254	171	-0.15	-103
Marina di Ravenna I	-126	1308	2.18	458
Marina di Ravenna II	-1054	124	-1.50	-349
Marina di Ravenna III	-158	267	-0.17	-60
Marina di Ravenna IV	-605	107	-0.68	-349

Table 4.10: Volume calculation values; the sing “-“ means accumulation; the sign “+“ means erosion.

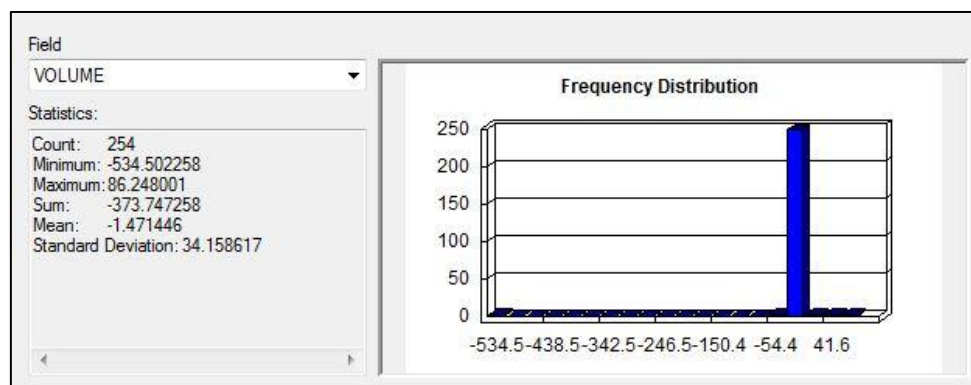


Figure 4.7: Major stats prospect, relative to a comparison on Marina di Ravenna dune field.

4.1.4 Digital Shoreline Analysis System (DSAS).

DSAS analysis tool expects for an arbitrarily determined baseline. Assuming that each dune foot line vector represents a specific position in time, the DSAS algorithm uses transects cast from the baseline to the intersection in order to measure the movement. It is important for the baseline to lay entirely on the same side of the dune foot.

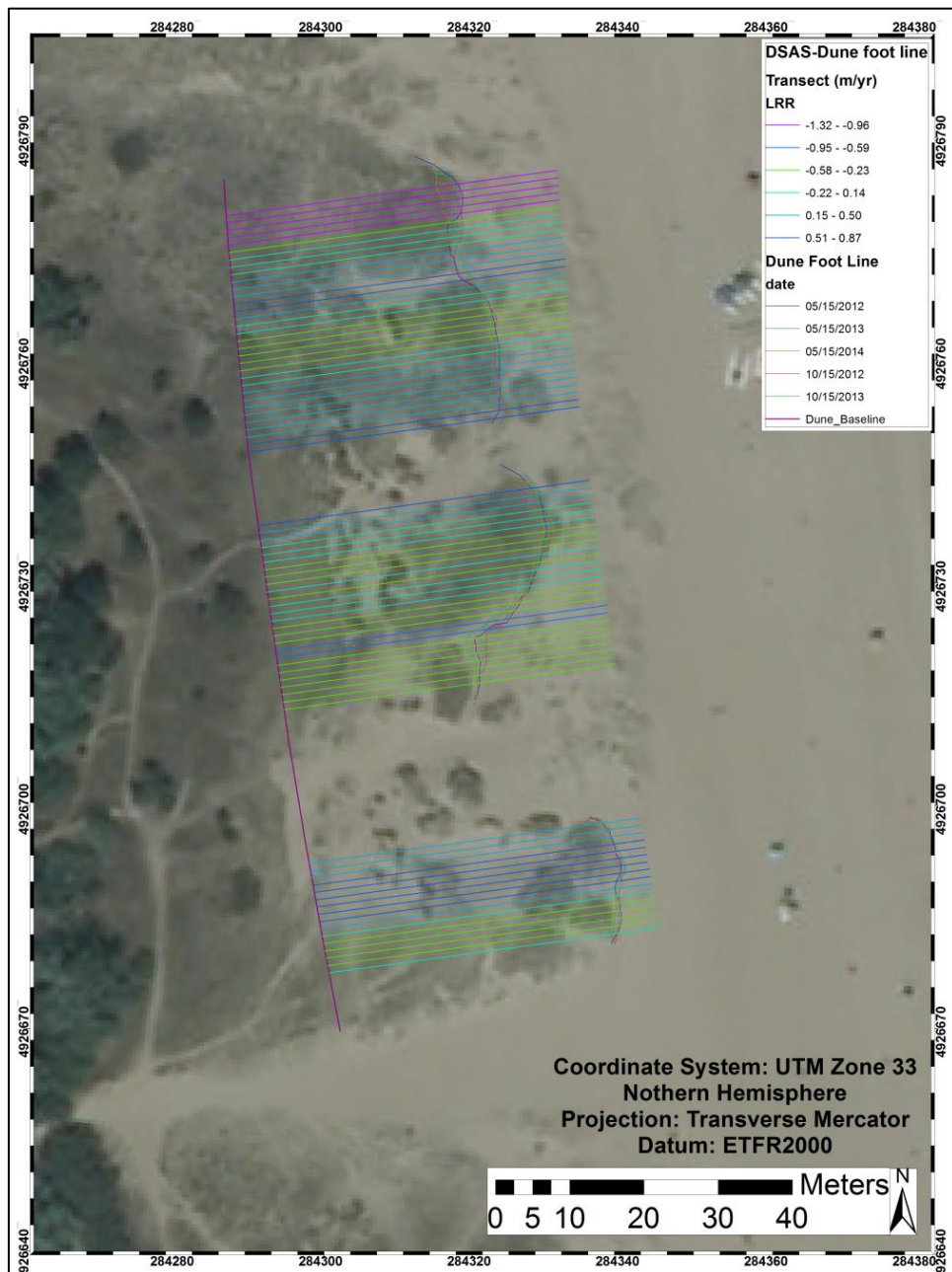


Figure 4.8: DSAS example of dune foot analysis draw on the Marina di Ravenna area.

Transects will be perpendicular to it, thus it should be approximately parallel to other vectors. In this work, the author decided transects position basing it, where possible, on the correspondence between crest and foot lines. They resulted spaced for 1 meter. In figure 4.8 a resulting map is shown (Marina di Ravenna dune foot line movements).

Once again the two sites in urbanized areas revealed to be more problematic: due to the touristic management of the beach, those dune fields have an artificial barchanoidal shape, which is maintained by human activities through bulldozers used to keep the side paths clean. This strong deviation from the natural morphological behavior, forced the author to make a decision about the shape and position of the baseline. The choice made was to use only the frontal part of the foot lines for both side, the one which contemplates the shoreline direction of DSAS vectors, and it can be consulted in figure 4.7. For the Milano Marittima area, unfortunately, it wasn't possible to draw the crest line, because of the too intense fragmentation.

An example of numerical results DSAS table is shown in table 4.11. To plot results only LRR values were taken in regard and parted in six classes, identified by a different color, from blue tones, for the most positive values, which indicate a forward movement, to red tones, for most negative, which indicates a back movement. Green tones indicate almost stable behavior.

OBJECT ID	TransOrder	ProcTime	StartX	StartY	EndX	EndY
1	1	10/17/2014 22:59	284274.81	4926671.5	284322.71	4926657.2
2	2	10/17/2014 22:59	284279.6	4926673	284327.85	4926659.9
3	3	10/17/2014 22:59	284284.39	4926674.4	284332.94	4926662.5
4	4	10/17/2014 22:59	284289.18	4926675.9	284337.97	4926665
5	5	10/17/2014 22:59	284293.96	4926677.3	284343.09	4926668
6	6	10/17/2014 22:59	284298.75	4926678.7	284348.24	4926671.6
7	7	10/17/2014 22:59	284303.54	4926680.2	284353.3	4926675.3
8	8	10/17/2014 22:59	284308.33	4926681.6	284358.26	4926678.9
9	9	10/17/2014 22:59	284313.12	4926683	284363.12	4926682.6

Azimuth	SHAPE_Leng	TransectId	ECI	EPR	NSM	LRR
106.66	49.99999901	1	0.20	2.12	3.00	-0.08
105.18	50.00000016	2	0.14	-0.70	-1.39	-0.17
103.83	49.99999744	3	0.14	-0.40	-0.79	0.03
102.58	50	4	0.14	-0.12	-0.24	-0.11
100.73	50.00000003	5	0.14	0.05	0.10	-0.03
98.2	50.00000124	6	0.14	-3.13	-6.25	-0.18
95.62	50.00000026	7	0.14	-2.20	-4.40	-0.27
93.06	49.99999903	8	0.14	-0.40	-0.79	-0.02
90.51	50.00000067	9	0.14	-0.05	-0.09	0.16

Table 4.11: Example of DSAS result table.

For what concerns the results table 4.6, “Trans Order” is the transect order along the baseline, automatically assigned by DSAS; “Proctime” reports the date when data were processed; “StartX”, “StartY”, “EndX” and “EndY” indicate the coordinates of the beginning and the end of the transect; “Azimuth” is the angle of the transect measured clockwise from North (in degree). The ECI column reports the “confidence of end point rate”, which is a measure of uncertainty related to the EPR calculation. Mathematically it is the square root of the two positions used summation in the end point calculation divided by the number of years between the two shorelines (Himmerlstoss, 2009).

Last three columns, EPR, NSM and LRR contain the principal results. These were used as average to identify particular patterns or situation (table 4.12).

Even though, these results are pretty difficult to be interpreted, especially those belonging to Marina di Ravenna and Milano Marittima, they gave interesting sparks, which are going to be discussed in the next chapter. Results tables relative to the two other sites can be consulted in Appendix IV.

SITE		Foot Line	Crest Line
Bevano	<u>EPR</u>	-0.16 m/yr	0.01 m/yr
	<u>NSM</u>	-0.29 m	0.02 m
	<u>LRR</u>	-0.11 m/yr	-0.09 m/yr
Marina di Ravenna	<u>EPR</u>	-0.06 m/yr	-0.32 m/yr
	<u>NSM</u>	-0.13 m	-0.62 m
	<u>LRR</u>	-0.09 m/yr	-0.31 m/yr
Milano Marittima	<u>EPR:</u>	-0.60 m/yr	
	<u>NSM:</u>	-1.20 m	
	<u>LRR:</u>	-0.41 m/yr	

Table 4.12: DSAS averaged results relative to dune foot lines and dune crest lines movement.

4.2 Meteorological Data and Forcing Factors.

Forcing Factors are indexes specifically elaborated with the aim to evaluate the environmental influence on dunes morphological changes. They are all coming out from meteorological data, relative to wind, sea and rain.

For what concerns wind data, their first application was the definition of the aeolian climate, based on seasonal and yearly records. Thanks to WRPLOT software (Chapter 3) it was easy to transform numerical data in wind roses, straight readable. This kind of graph has the useful property of plotting all together velocity in m/s, frequency in percentage and compass source, in term of quadrants.

According to author's decision the wind speed is subdivided in nine classes (plus calms), indicated by a different color; the frequency is represented by the size of slices, anyway a reference percentage (on the whole data) is highlighted on the diagram, to have an absolute "landmark". Wind roses can help to understand the wind general condition during a year (total percentages, maximum and minimum, calms, averages, frequency of onshore, offshore or alongshore winds) and to identify seasonal trends, especially in terms of "regnant" and "dominant winds" (figure 4.9).

In this particular research the word "season" means a period of 6 months, about from May to October, for what concern (wind) "summer", from November to April, for what concern (wind) "winter".

"Regnant winds" describe those winds which are more frequent than any other and they usually are not too strong. In this case they are pretty much offshore and they blow especially during winters. "Dominant winds" are much less frequent but much stronger, and they blow during the whole year; they are almost always onshore, with two preferential directions (from SE, which is called "Scirocco", and from NE, called "Bora").

Obviously when determinate an aeolian climate relative to a dune field study, it is very important to understand which winds are onshore, which one is offshore and which one is alongshore, because their efficacy changes a lot. This is due to two fundamental reasons: first of all the angle of incidence of the wind on the dune; the other reason is linked to the macro-region geography, and on which kind of terrain the wind blows before to meet the dune.

4. Results

This concept is the fundamental part of the other elaboration of wind data, when on-shore, off-shore and along-shore winds were extracted, considering only the effective winds, those which exceed the threshold velocity. Results are reported in table 4.13.

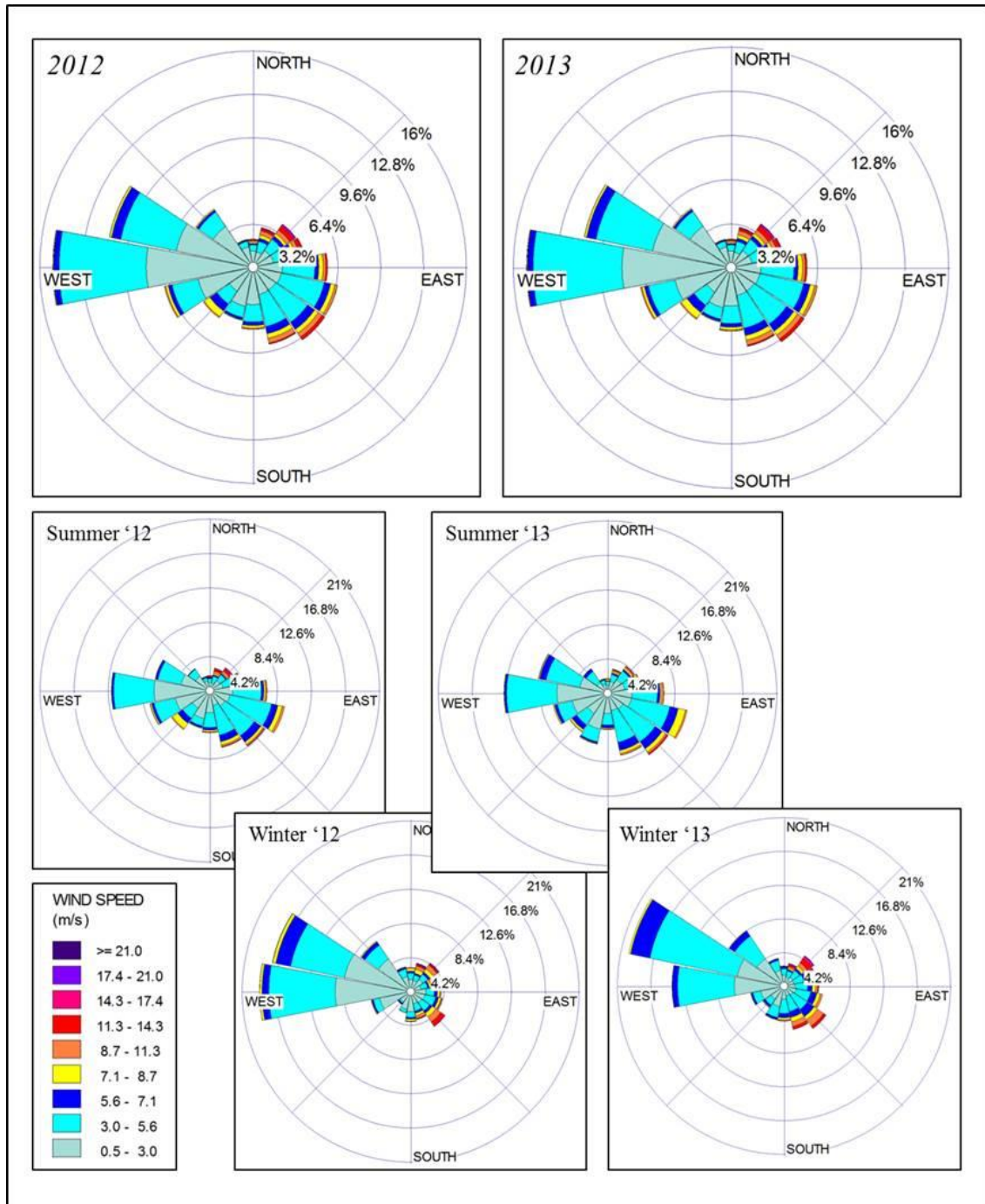


Figure 4.9: wind rose graphs, relative to aeolian yearly and seasonal climate.

In this table, for each survey period, both calculations made on the total of records and only on the effective ones are reported. The absolute number of records consulted is reported too. For the statistical purpose only the partial ones were used.

	Records					Percentage					
	TOT	EFF	A	ON	OFF	Tot A	Tot ON	Tot OFF	Eff A	Eff ON	Eff OFF
BEV	19986	1410	224	852	334	1.12	4.26	1.67	15.89	60.43	23.69
	23684	2201	323	1598	280	1.36	6.75	1.18	14.68	72.60	12.72
	7047	628	39	516	73	0.55	7.32	1.04	6.21	82.17	11.62
	20027	981	155	709	117	0.77	3.54	0.58	15.80	72.27	11.93
	4262	403	56	328	19	1.31	7.70	0.45	13.90	81.39	4.71
	34639	3406	527	2625	254	1.52	7.58	0.73	15.47	77.07	7.46
MM	20639	1427	224	869	334	1.09	4.21	1.62	15.70	60.90	23.41
	30100	2864	372	2139	353	1.24	7.11	1.17	12.99	74.69	12.33
	21900	1051	171	722	158	0.78	3.30	0.72	16.27	68.70	15.03
	33496	3150	520	2380	250	1.55	7.11	0.75	16.51	75.56	7.94
MDR	15891	1149	166	773	210	1.04	4.86	1.32	14.45	67.28	18.28
	33123	3005	430	2216	359	1.30	6.69	1.08	14.31	73.74	11.95
	18300	667	78	467	122	0.43	2.55	0.67	11.69	70.01	18.29
	38398	3856	631	2933	292	1.64	7.64	0.76	16.36	76.06	7.57

Table 4.13: wind data analysis in term of quadrant of provenience. TOT: percentage calculated on the total amount; EFF: percentage calculated on effective winds only; A: alongshore; ON: onshore; OFF: offshore.

Periods	Wl (m)	S _{max} (m)	S _{avr} (m)	T (h)
6th June 2012				
1	0.74	2.93	2.05	69.7
22-Jul		2.93	2.15	29.7
13-Sep		2.81	1.94	40
25th Oct. 2012				
2	1.16	3.68	1.92	204
01-Nov		2.43	2.02	17
11-Nov		2.04	1.70	19
08-Dec		3.23	2.49	23
17-Jan		2.31	1.94	15
24-Jan		2.42	1.86	28.5
03-Feb		3.68	2.42	13.5
11-Feb		2.05	1.57	16
21-Feb		2.05	1.76	17
14-Mar		2.26	1.86	16
18-Mar		1.76	1.61	12.5
24-Mar		2.55	1.94	26.5
9th Apr 2013				
3	0.82	2.12	1.71	14
16-May		2.12	1.71	14
29th May 2013				

Table 4.14: elaboration of sea force data, for the Bevano dune field.

Sea force data were taken from the regional monitoring network. As wrote in the chapter before, those data were for a large part elaborated to analyze high energy events. In table 4.14 is reported an example of this elaboration for the Bevano area: in green are highlighted surveys dates, which are the begin and the end of each period; in white cells, between a period and the other, high energy events are isolated to be elaborated; in blue rows there are surveys relative numbers and the final indexes results. In table 4.15, all the missing Forcing Factors (without drift

potential indexes) are shown in their original form and measurement unit. Maximum water level and average rainfall were not elaborated, and they are reported straight from regional monitoring network.

Period	S_{avr} (m)	T(h)	S_{max}(m)	Liv(m)	P(mm)	Wa(%)	Won(%)	Woff(%)
Bev I	2.05	69.7	2.93	0.74	0.957	15.89	60.43	23.69
Bev II	1.92	204	3.68	1.16	2.682	14.68	72.60	12.72
Bev III	1.71	14	2.12	0.82	1.102	6.21	82.17	11.62
Bev IV	1.71	20.5	2.3	-0.72	0.867	15.80	72.27	11.93
Bev V	2.55	46	10.69	0.84	3.077	13.90	81.39	4.71
Bev VI	2.09	430	3.88	0.92	1.691	15.47	77.07	7.46
Mima I	2.05	69.7	1.93	0.74	0.931	15.70	60.90	23.41
Mima II	1.9	218	3.68	1.16	2.306	12.99	74.69	12.33
MiMa III	1.71	20.5	2.3	0.74	1.645	16.27	68.70	15.03
MiMa IV	2.05	418.5	3.88	0.92	1.815	16.51	75.56	7.94
MdR I	2.05	69.7	2.93	0.69	1.066	14.45	67.28	18.28
MdR II	1.815	218	3.68	0.53	2.152	14.31	73.74	11.95
MdR III	1.64	11	1.95	0.62	0.846	11.69	70.01	18.29
MdR IV	2.09	430	3.88	1.49	2.077	16.36	76.06	7.57

Table 4.15: Forcing Factors table.

4.3 Grain Size and Drift Potential Results.

Due to their strong connection, none of the Drift Potential calculations can be done without having data about the grain size of the sand. Even through in laboratory all 60 samples were analyzed, only those belonging to the first 20 cm of depth were used to determinate grain size. This was because other samples were considered not so representative of the aeolian environment investigated.

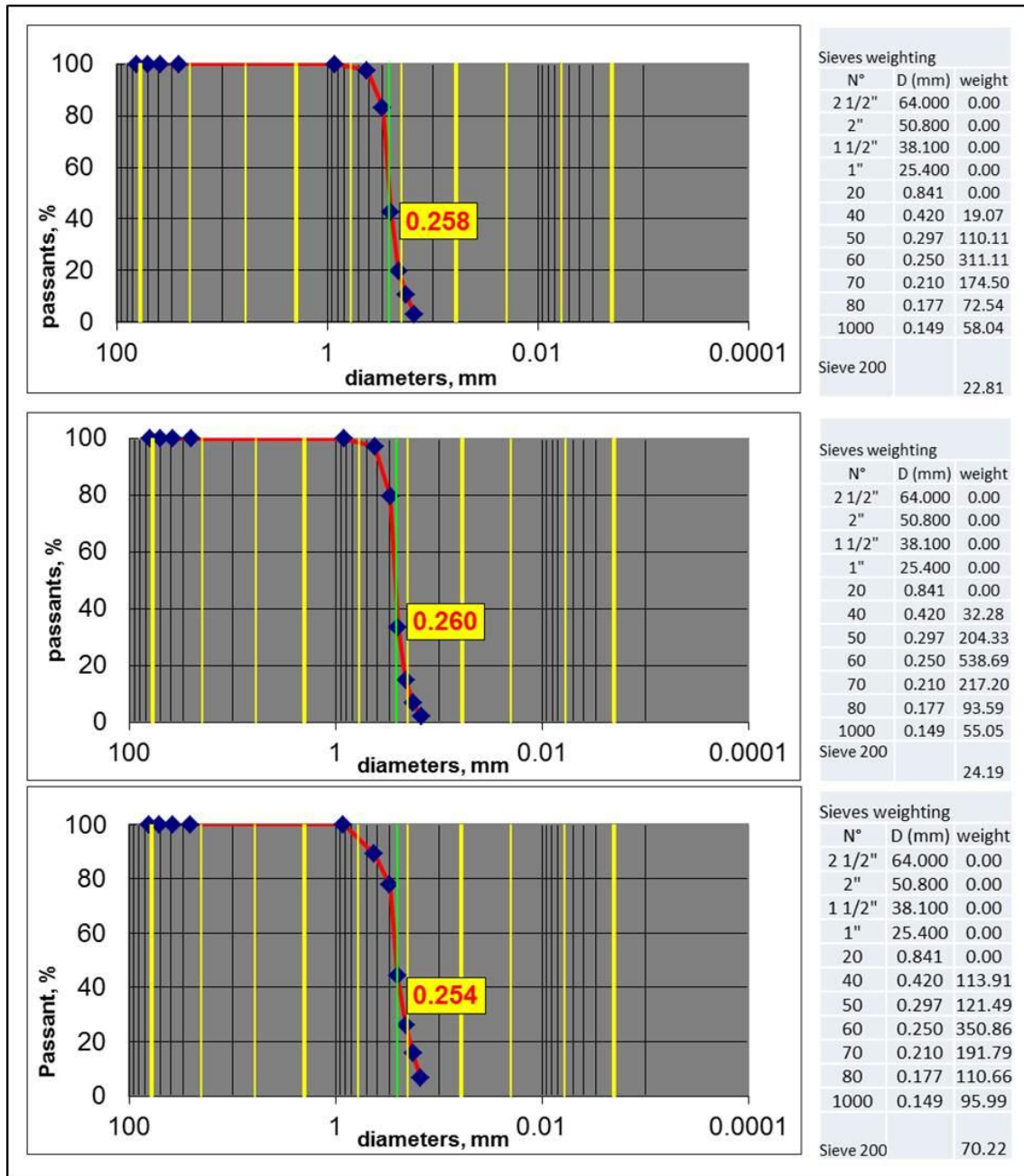


Figure 4.10: Cumulative curve graph for: a) Bevano; b) Marina di Ravenna; c) Milano Marittima.

For every sample a cumulative curve graph and a class frequency histogram were elaborated, to see possible differences (thus, trends) between samples. The final step involved averaging the data for each site and to calculate the three “final” grain sizes. In figure 4.10 cumulative curve graph are reported, with their sieves-weighting table.

No trends appeared between samples on the same site, but in general it is pretty easy to see how there is a soft gradient in these data, from the most North site, Marina di Ravenna, where there are the largest grains, to the most South one, Milano Marittima, which have the thinnest sand. Anyway, as wrote in the chapter before, the little difference in the three diameters slightly effects the threshold velocity. This influence can be easily seen in table 4.16.

Site	Grain Size (mm)	Threshold Velocity (m/s)
Bevano	0.258	7.140803470
Milano Marittima	0.254	7.076492987
Marina di Ravenna	0.260	7.172849309

Table 4.16: grain size and threshold wind velocity results.

The analysis first part was focused on understanding the Drift Potential annual climate. Thus 2012 and 2013 data were elaborated to highlight yearly and seasonal trends. The threshold wind velocity this time was calculated on an average of the grain size, resulted from every site analysis. This means that the DP calculation begun from a grain size of 0.257 mm and its relative threshold wind velocity equal to 7.124753 m/s.

At this time scale, following the Pearce and Walker work (2005), the potential sand transport could be estimated be by the Lettau and Lettau (1978) equation:

$$Q \propto V^2(V - V_t) * t$$

Where $V^2 (V-V_t)$ is the already seen equation to calculate the weighting factors and Q is the annual rate of potential sediment drift, in vector units. The index “t” represents the frequency of transporting winds in each direction and it is expressed as percentage of the total period analysis.

The resulting Sand Roses will be shown, with relative values (Drift Potential, Resultant Drift Potential, Resultant Drift Direction and Directional Variability index) in next chapter to facilitate the discussion.

The next step focused on determining DP for every survey period, making it available for the multivariate analysis. Obviously for each site a different grain size was applied, thus a different threshold: this slightly effected the weighting factors, which a bit different for each site. In table 4.17 these results are reported, together with RDD, RDP, Directional Variability Index (RDP/DP) and cosin/sin sign.

Site-Period	DP	RDP	RDD	RDP/DP	Cosin - Sin
Bev I	27.48	18.21	46°	0.66	++
Bev II	44.18	25.76	71°	0.58	++
Bev III	22.65	15.01	-65°	0.66	-+
Bev IV	8.83	4.82	62°	0.55	++
Bev V	101.80	90.70	41°	0.89	++
Bev VI	45.68	30.16	71°	0.66	++
MdR I	32.01	23.69	42°	0.74	++
MdR II	37.35	21.42	79°	0.57	++
MdR III	6.42	4.14	37°	0.64	++
MdR IV	43.09	28.14	73°	0.65	++
MiMa I	27.12	17.79	46°	0.66	++
MiMa II	41.18	23.68	78°	0.57	++
MiMa III	8.81	4.43	63°	0.50	++
MiMa IV	45.92	29.80	72°	0.65	++

Table 4.17: Drift Potential result.

4.4 Principal Component Analysis (PCA).

The entire PCA procedure, as well as its results, was executed using the open-source software “R”, with the helpful “RStudio” interface. The relative script can be entirely examined in Appendix III. The analysis involved three procedures of PCA, comparing three different types of morphological changes with the same, and already discussed, Forcing Factors.

In the first test the volume differences (V) extracted by the “Cut and Fill” tool, and the 3D surface topographic changes (A), of each area of interest (“Surface Volume” results), were compared. In the second test Sub-zones morphological changes, in term of 3D spatial differences, were analyzed, while in the last try, it was the blowouts area to be examined. In tables 4.18, 4.19 and 4.20 are shown the data table relative to these three executions.

	A	V	DP	Sa	T	Sm	R/D	Woff	Won	Wa	P	WI
1	46.66	126.73	27.48	2.05	69.50	2.93	0.66	23.69	60.43	15.89	0.96	0.74
2	42.50	580.13	44.18	1.92	204.00	3.68	0.58	12.72	72.60	14.68	2.68	1.16
3	54.14	78.60	22.65	1.71	14.00	2.12	0.66	11.62	82.17	6.21	1.10	0.82
4	105.17	48.12	8.83	1.71	20.50	2.30	0.55	11.93	72.27	15.80	0.87	-0.72
5	17.68	369.32	101.80	2.55	46.00	3.57	0.89	4.71	81.39	13.90	3.08	0.84
6	108.04	645.32	45.68	2.09	168.00	3.88	0.66	7.46	77.07	15.47	1.69	0.92
7	179.78	257.86	27.12	2.05	69.70	1.93	0.66	23.41	60.90	15.70	0.93	0.74
8	161.86	1164.10	41.18	1.90	218.00	3.68	0.57	12.33	74.69	12.99	2.31	1.16
9	6.89	564.46	8.81	1.71	20.50	2.30	0.50	15.03	68.70	16.27	1.65	0.74
10	14.64	102.57	45.92	2.05	158.00	3.88	0.65	7.94	75.56	16.51	1.82	0.92
11	17.27	458.08	32.01	2.05	69.50	2.93	0.74	18.28	67.28	14.45	1.07	0.69
12	24.97	348.57	37.35	1.81	218.00	3.68	0.57	11.95	73.74	14.31	2.15	0.53
13	22.19	60.18	6.42	1.67	20.50	1.95	0.64	18.29	70.01	11.69	0.85	0.62
14	167.02	348.97	43.09	2.09	158.00	3.88	0.65	7.57	76.06	16.36	2.08	1.49

Table 4.18: Volume (V) and 3D area changes (A). the first six rows are relative to Bevano results, including the April and the November surveys.

	WD	GD	DP	Sa	T	Sm	R/D	Woff	Won	Wa	WI	P
1	246.94	95.15	27.48	2.05	69.50	2.93	0.66	23.69	60.43	15.89	0.74	0.96
2	74.92	138.34	44.18	1.92	204.00	3.68	0.58	12.72	72.60	14.68	1.16	2.68
3	69.13	192.98	22.65	1.71	14.00	2.12	0.66	11.62	82.17	6.21	0.82	1.10
4	115.46	152.63	8.83	1.71	20.50	2.30	0.55	11.93	72.27	15.80	-0.72	0.87
5	164.49	27.48	101.80	2.55	46.00	3.57	0.89	4.71	81.39	13.90	0.84	3.08
6	151.70	24.43	45.68	2.09	168.00	3.88	0.66	7.46	77.07	15.47	0.92	1.69
7	119.00	55.00	27.12	2.05	69.70	1.93	0.66	23.41	60.90	15.70	0.74	0.93
8	119.25	73.95	41.18	1.90	218.00	3.68	0.57	12.33	74.69	12.99	1.16	2.31
9	39.01	42.95	8.81	1.71	20.50	2.30	0.50	15.03	68.70	16.27	0.74	1.65
10	77.44	78.70	45.92	2.05	158.00	3.88	0.65	7.94	75.56	16.51	0.92	1.82
11	1.42	63.59	32.01	2.05	69.50	2.93	0.74	18.28	67.28	14.45	0.69	1.07
12	94.43	132.50	37.35	1.81	218.00	3.68	0.57	11.95	73.74	14.31	0.53	2.15
13	49.73	43.20	6.42	1.67	20.50	1.95	0.64	18.29	70.01	11.69	0.62	0.85
14	127.69	99.10	43.09	2.09	158.00	3.88	0.65	7.57	76.06	16.36	1.49	2.08

Table 4.19: Spatial changes in morphological Sub-zones (WD: white dune; GD: grey dune;).

4. Results

	BO	DP	Sa	T	Sm	R/D	Woff	Won	Wa	P	WI
1	35.81	27.48	2.05	69.50	2.93	0.66	23.69	60.43	15.89	0.96	0.74
2	73.46	44.18	1.92	204.00	3.68	0.58	12.72	72.60	14.68	2.68	1.16
3	17.99	22.65	1.71	14.00	2.12	0.66	11.62	82.17	6.21	1.10	0.82
4	31.18	8.83	1.71	20.50	2.30	0.55	11.93	72.27	15.80	0.87	-0.72
5	45.77	101.80	2.55	46.00	3.57	0.89	4.71	81.39	13.90	3.08	0.84
6	1.10	45.68	2.09	168.00	3.88	0.66	7.46	77.07	15.47	1.69	0.92
7	19.73	27.12	2.05	69.70	1.93	0.66	23.41	60.90	15.70	0.93	0.74
8	123.13	41.18	1.90	218.00	3.68	0.57	12.33	74.69	12.99	2.31	1.16
9	95.49	8.81	1.71	20.50	2.30	0.50	15.03	68.70	16.27	1.65	0.74
10	9.45	45.92	2.05	158.00	3.88	0.65	7.94	75.56	16.51	1.82	0.92
11	90.17	32.01	2.05	69.50	2.93	0.74	18.28	67.28	14.45	1.07	0.69
12	18.00	37.35	1.81	218.00	3.68	0.57	11.95	73.74	14.31	2.15	0.53
13	7.25	6.42	1.67	7.00	1.95	0.64	18.29	70.01	11.69	0.85	0.62
14	54.97	43.09	2.09	158.00	3.88	0.65	7.57	76.06	16.36	2.08	1.49

Table 4.20: Spatial changes in Blowouts areas.

In order to evaluate the variability of these morphological features, and trying to have a data set, as much as possible, homogeneous, the author chose to use in this analysis, not the true value, but the Absolute Value, without sign. This is a fundamental concept, because it means that it is not the erosion or deposition process to be evaluated, but only its general variability. Every other data used, were elaborated in its integer form, without any manipulation.

DP	Sa	T	Sm	R.D	Woff
Min. : 9.01	Min. : 1.670	Min. : 14.00	Min. : 1.930	Min. : 0.1000	Min. : 4.2
1st Qu.: 26.14	1st Qu.: 1.735	1st Qu.: 26.88	1st Qu.: 2.300	1st Qu.: 0.1900	1st Qu.: 6.875
Median : 39.44	Median : 1.985	Median : 69.60	Median : 3.250	Median : 0.4000	Median : 9.4
Mean : 42.06	Mean : 1.954	Mean : 103.87	Mean : 3.051	Mean : 0.4186	Mean : 9.671
3rd Qu.: 60.62	3rd Qu.: 2.050	3rd Qu.: 165.50	3rd Qu.: 3.680	3rd Qu.: 0.6200	3rd Qu.: 11
Max. : 67.87	Max. : 2.550	Max. : 218.00	Max. : 3.880	Max. : 0.8600	Max. : 16.4
wa	wl	WD	GD	A	Won
Min. : 9.30	Min. : -0.7200	Min. : 1.42	Min. : 24.43	Min. : 2.099	Min. : 30.10
1st Qu.: 11.38	1st Qu.: 0.7025	1st Qu.: 70.58	1st Qu.: 46.15	1st Qu.: 17.370	1st Qu.: 40.00
Median : 14.90	Median : 0.7800	Median : 104.94	Median : 76.33	Median : 33.735	Median : 55.15
Mean : 14.48	Mean : 0.7607	Mean : 103.61	Mean : 87.14	Mean : 61.467	Mean : 53.47
3rd Qu.: 16.73	3rd Qu.: 0.9200	3rd Qu.: 125.58	3rd Qu.: 124.15	3rd Qu.: 93.263	3rd Qu.: 69.05
Max. : 19.50	Max. : 1.4900	Max. : 246.94	Max. : 192.98	Max. : 179.781	Max. : 78.70
v					
Min. : 26.96					
1st Qu.: 105.42					
Median : 348.77					
Mean : 368.65					
3rd Qu.: 537.86					
Max. : 1164.10					

Table 4.21: PCA initial data organization.

The final results of Principal Component Analysis process, in term of vector graphs, will be shown and discussed in the next chapter. In this paragraph, instead, the statistic base from which PCA started, can be examined below (table 4.21). This table

shows for each data set, the mean and the median, the maximum and the minimum value, the first and the third quarter mean.

Last it will be shown the Eigenvectors relative values, the so called “Eigen value”, with two more rows after: one which explains the proportion of variance explained, one which reports the cumulative proportion.

Importance of components (Blowouts ANALYSIS):											
	PC1	PC2	PC3	PC4	PC5	PC6	PC7	PC8	PC9	PC10	PC11
Eigenvalue	5.2054	1.6348	1.4702	0.87882	0.732	0.46363	0.29059	0.21845	0.05888	0.0409	0.006312
Proportion Explained	0.4732	0.1486	0.1336	0.07989	0.06655	0.04215	0.02642	0.01986	0.00535	0.00372	0.00057
Cumulative Proportion	0.4732	0.6218	0.7555	0.83538	0.90193	0.94408	0.9705	0.99036	0.99571	0.99943	1
Importance of components (Volumes Analysis):											
	PC1	PC2	PC3	PC4	PC5	PC6	PC7	PC8	PC9	PC10	PC11
Eigenvalue	5.593	1.8309	1.4948	0.7811	0.7572	0.65423	0.39206	0.26915	0.15072	0.04008	0.03517
Proportion Explained	0.4661	0.1526	0.1246	0.06509	0.0631	0.05452	0.03267	0.02243	0.01256	0.00334	0.00293
Cumulative Proportion	0.4661	0.6187	0.7432	0.80832	0.8714	0.92594	0.95861	0.98104	0.9936	0.99694	0.99987
Importance of components (Sub-Zones Analysis):											
	PC1	PC2	PC3	PC4	PC5	PC6	PC7	PC8	PC9	PC10	PC11
Eigenvalue	4.5371	1.798	1.618	1.1422	0.72984	0.62165	0.30853	0.12464	0.0831	0.02864	0.008811
Proportion Explained	0.4125	0.1635	0.147	0.1038	0.06635	0.05651	0.02805	0.01133	0.00755	0.0026	0.0008
Cumulative Proportion	0.4125	0.5759	0.723	0.8268	0.89315	0.94966	0.97771	0.98904	0.9966	0.9992	1

Table 4.22: Eigenvalues tables.

4.5 Computational Fluid Dynamic Analysis.

Assuming that the meteorological forces that acted during the examined period caused morphological modifications on the dune ridge, the differences between the two DEMs, were calculated in terms of difference of height between the two surfaces (also in order to measure the erosion/deposition pattern during this period). The average height difference resulted about 0.16 meters, while the whole range of values oscillates between -1.7 and 1.7.

In any cases from the volume evaluations (the “cut and fill” application), a strong modification of this dune ridge appeared, with a value of about 340 m^3 of difference between the two areas of interest. The specific height differences, calculated cell for cell, can be consulted in part a) of figure 4.23.

The b) part of this figure instead, represents the projections of the wind velocity at the ground (20 cm), recorded in meters per seconds. It is interesting to notice how the highest speeds are recorded on the crest, especially on the highest ones. Proceeding landward, the wind flow crosses an area of general speed decreasing, in correspondence of the back dune depression (the Black Dune). Then both the both the wind velocity and the DEM elevations return to increase.

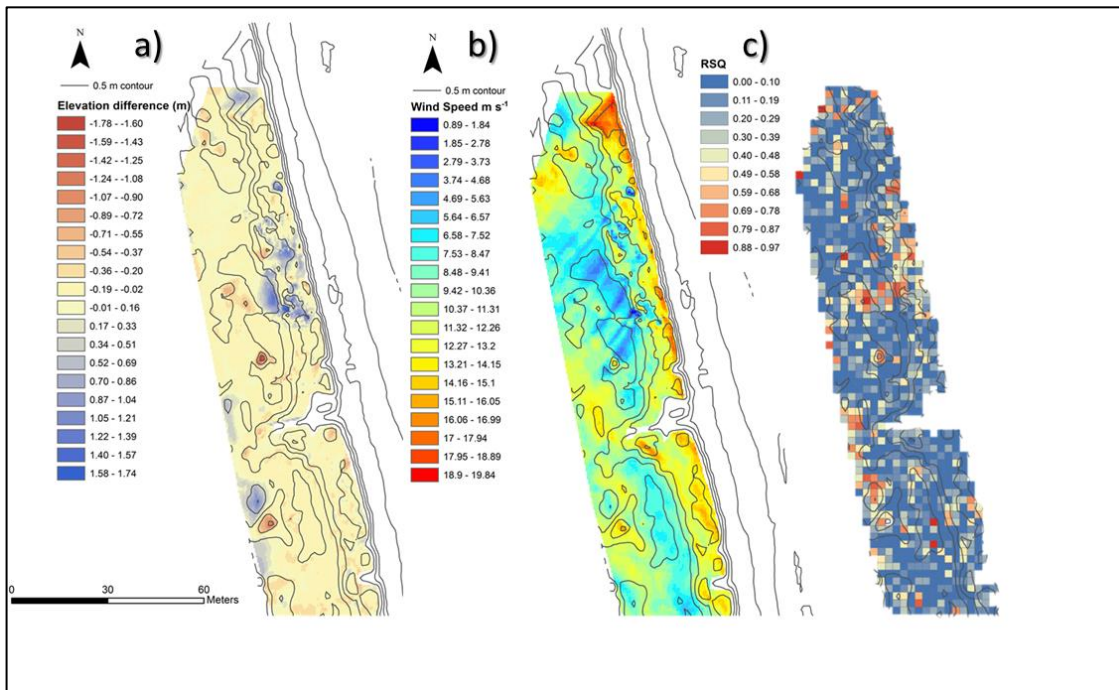


Figure 4.11: a) Height differences plot; b) Wind speed projection plot; c) Linear regression plot.

The last section of figure 4.11 includes the linear regression plot, where values plotted are those coming from the linear regression calculation between height differences and wind speed, relative to each cell. This elaboration gave most interesting results, identifying some areas where a strong positive correlation was found, and other where no correlation was found at all. Into the graph, positive relations correspond to red tones, while no correlations to blue tones.

The table 4.18 shows a part of the data elaboration from which results were obtained. “X” and “Y” values represent the cells’ node coordinates. Due to the coordinate system limitations in CFD the x values need to have 280000 added to their value and the y values 4900000. The “DELTA H” values are the height differences. “U”, “V” and “W” column represent respectively along wind speed (U), V is across wind speed (both used to calculate wind direction), while “W” represent the vertical component of wind speed.

X	Y	DELTA H	U	V	W	Speed
7029.341	14299.686	-0.3284667	-7.86764	-7.42972	-0.777974	10.85
7029.769	14299.686	-0.3305235	-7.79065	-7.24825	-0.866691	10.68
7030.197	14299.686	-0.3264118	-8.09997	-7.73512	-0.689548	11.22
7030.625	14299.686	-0.3165192	-8.1337	-7.63997	-0.814055	11.19
7031.053	14299.686	-0.3044637	-8.02451	-7.48236	-0.950063	11.01
7031.481	14299.686	-0.2918581	-8.06613	-7.48109	-0.964695	11.04
7031.909	14299.686	-0.2726535	-8.36033	-7.95388	-0.650815	11.56
7032.337	14299.686	-0.2304995	-8.40501	-7.95888	-0.736766	11.60
7032.765	14299.686	-0.2082853	-8.42713	-7.87439	-0.875028	11.57
7033.193	14299.686	-0.193176	-8.25488	-7.69183	-0.971135	11.32
7033.621	14299.686	-0.1772033	-8.30841	-7.67414	-0.987895	11.35
7034.049	14299.686	-0.1582863	-8.29769	-7.60743	-1.00706	11.30
7034.477	14299.686	-0.1368438	-8.3424	-7.56183	-1.10181	11.31

Table 4.23: Statistical data elaboration by CFD.

5 DISCUSSION

5.1 Sand Grain Size Analysis.

The sand grain size analysis was primarily done to calculate, with the maximum accuracy possible, wind velocity threshold to activate sand drift. Anyway trying to make the survey representative of the environment and in order to individuate any pattern in sand distribution, the sample points were diffuse onto the dune-beach system (figure 5.1); in spite of this no interesting spatial differences or trends were founded within each site samples, while a slight gradient from North to South appeared: in Marina di Ravenna the average sand size is 0.260 mm, in Bevano area it was 0.258 mm, and in the most south place, Milano Marittima, it resulted 0.256 mm.

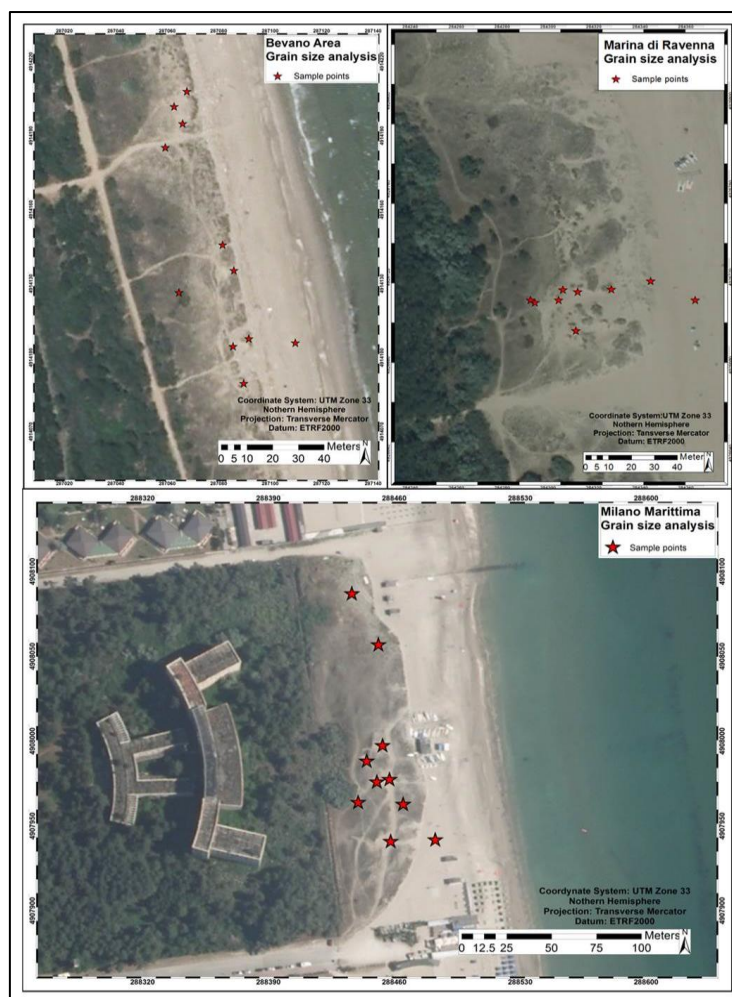


Figure 5.1: Grain size analysis sampling point, for the three sites.

5.2 Aeolian Data Analysis.

In this study, the evaluation of wind climate has been based on two different lines of research. Both started from National Network data, but while the first approach considered a direct evaluation of those data, the second one implicated the Fryberger's methods elaboration.

For what concerns the first, more general, evaluation, both years analyzed were split in two seasons, "summer" and "winter", to highlight wind climate characteristics and to synchronize this evaluation to the volumetric seasonal monitoring applied to dunes.

Yearly data, already shown in previous chapter, indicated in general which winds are to be considered "regnant", more frequent, and which are "dominant", stronger. In this case offshore winds, resulted to be the yearly regnant winds: both in 2012 and 2013 these winds came from W and WNW quadrants, with a respective frequency of 14,9 % and 11.0 %, in 2012, 14.4 % and 13.1 % in 2013. The less represented winds were those blowing from N and NNW (both 2.1 % in 2012, 2.6 % in 2013).

Examining dominant winds, the study revealed that the highest velocities were recorded in correspondence of those winds which blew from NE/NNE and SE, but with much more less frequency. In 2012 the maximum was 21.7 m/s (from NE), while in 2013 it was 22.1 m/s (NE). To examine wind climate with more accuracy, the two summer periods, as well as the two winter periods have been isolated (figures 5.2 and 5.3).

During the summer, even if it is the period when dominant onshore winds are more frequent, the maximum wind velocity recorded was lower than winter: 20.2 m/s for 2012, 20.1 for 2013. Most frequent winds blew from West (12.1 % in 2012; 12.8 % in 2013), but it was also recorded a considerable percentage of onshore wind, coming from E (7.1% in 2012; 7.0 % in 2013), ESE (9.4 % in 2012; 10.0 % in 2013), SE (8.2 % in 2012; 9.1 % in 2013) and SSE (7.1 % in 2012; 7.7 % in 2013).

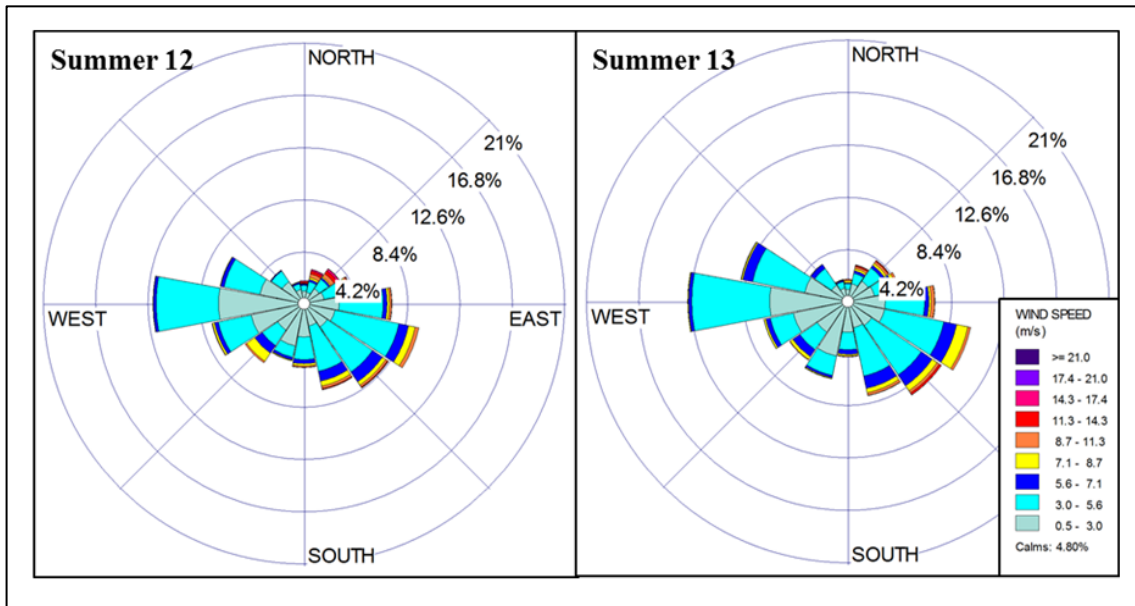


Figure 5.2: wind rose summer diagram for 2012 and 2013.

During winters (figure 5.3) most frequent winds were, as before, coming from West, but in this case the slice of provenience (and the frequencies) was wider. In both 2012 and 2013 regnant winds blew from W (respectively 18.7 % and 14.1 %), WNW (17.5 % and 19.9 %) and NW (7.16 % and 8.3 %). All other directions recorded low frequency, from a minimum of 1.9 to a maximum of 6.45. In spite of this, highest wind velocities were recorded in these seasons and blew from North-East.

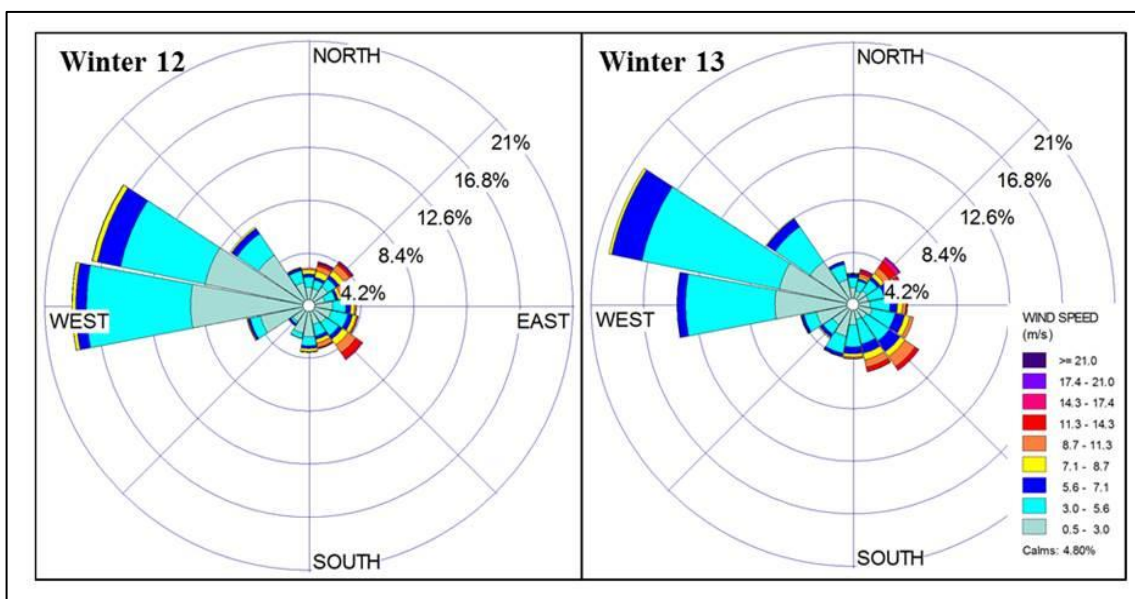


Figure 5.3: wind rose winter diagram for 2012 and 2013.

The Fryberger's model application to these wind data was very useful to understand some other characteristics about aeolian local climate. In this meaning Fryberger's method helps in two ways: giving a reference to have an idea of the real quantity of sand transported, on a yearly time scale; on the other hand, the interpolation of numeric indexes and relative sand roses gives several information about the real influence of winds in modifying sand distribution (drift potential transport local climate).

Remembering what wrote in the paragraph 4.3 about the Lettau and Lettau (1978) equation, it is important to specify something about annual rate of potential sediment drift: in effect Q is not technically a true measure of sediment flux, because it is measured in terms of Volume/Area/Time, while it should be used a mass dimension (i.e. Kg). In this form it is a relative measure of sediment transport potential (in VU) defined solely by available wind energy. This can be converted readily to a flux value if wind speed units are converted to m/s and an appropriate value for bulk density of the sand in transport is applied (Bullard, 1997).

To convert the volume (m^3) to kg is sufficient to use the bulk density of the sand in question. Arens (2004) studied this complication and found a value of $1600 \text{ kg}/m^3$. It is assumed that the period taken in consideration is one year long (to be as much as possible representative) and that sediment surfaces consist of dry, loose quartz sand (0.25–0.30 mm diameter) with sparse vegetation cover and no bed form roughness greater than ripples.

In figure 5.3 yearly Sand Roses and relative values are reported. Following what just written, the annual rate of potential sand drift is $32.25 \text{ m}^3/m^2/\text{year}$ for 2012, and $35.22 \text{ m}^3/m^2/\text{year}$, for 2013. To have these results in term of mass sediment flux, the author converted them multiplying the values for the quartz sand density:

- 2012 → $32.25 * 1.6 = 51.6 \text{ Kg}/m^2/\text{yr}$
- 2013 → $35.22 * 1.6 = 56.3 \text{ Kg}/m^2/\text{yr}$

The annual Sand Rose graphs can be consulted in figure 5.4. As reported in "Materials and Methods" chapter, it is assumed that, in a yearly time scale, they describe the wind environment (Fryberger, 1979) and basing on relative results, the author had the opportunity to classify the local transport climate.

Looking at the diagrams two preferential directions were individuated, from which the most effective winds blow. These, which are called “peak directions”, correspond to NE/NNE and SE. Thus the wind environment is “Bimodal”, because of these two peak directions. The angle measure between these two directions is about 106° , so wider than a right angle. That defines the second feature of the local climate: Wide Bimodal.

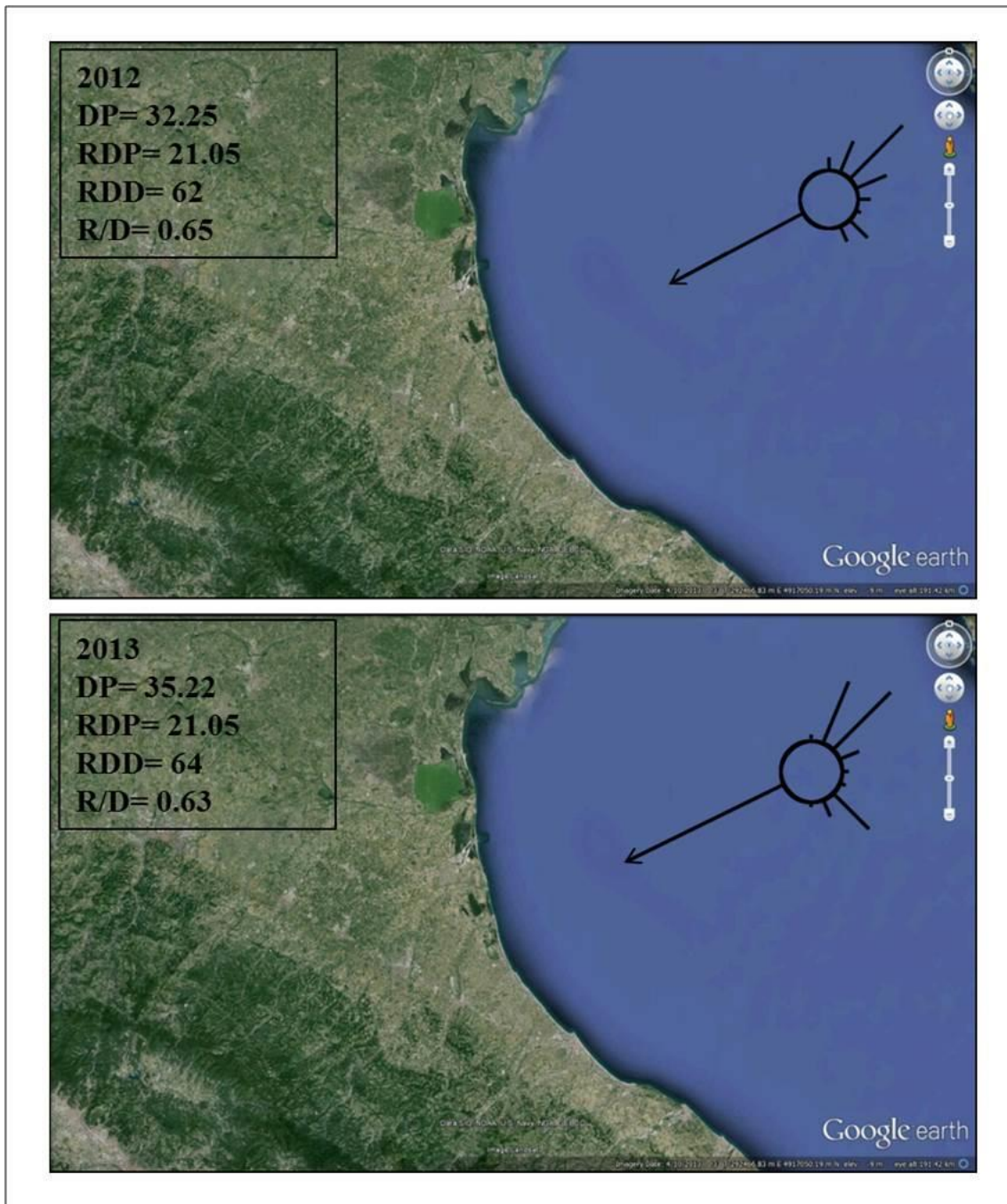


Figure 5.4: 2012 and 2013 sand roses. Segments represents the principal wind (blowing from) components of the total DP; values lower than 0.5 were not drawn. The arrow represent the Resultant Drift Potential and its direction is determined by the Resultant Drift Direction.

For a better comprehension of the environment, seasonal sand roses were plotted too (figure 5.5). These data are much more variables and don't indicate any trend. It is clear that winter diagrams are more similar to the yearly ones, and very similar to each other. The summer, instead, seems to be much more variable and the roses are very different one from each other and both from the yearly ones.

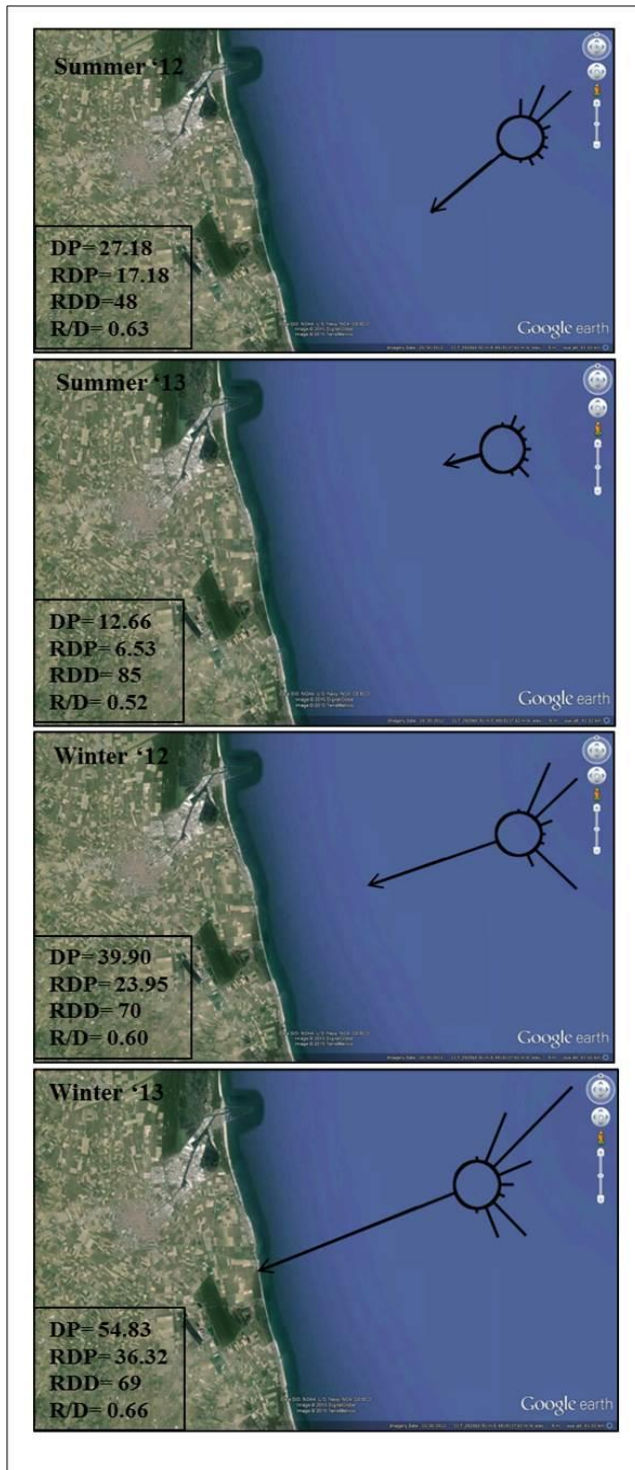


Figure 5.5: seasonal Sand Roses.

During summer 2013 the climate seemed to be particularly mild, but data presented at the beginning of this paragraph deny that happening. The reason is probably to be researched in wind frequency distribution subdivided by quadrant: the frequency distribution was so that the different components compensate, at least in part, each other. This is decisively confirmed by the low Directional Variability Index value (0.52).

5.3 Terrestrial Laser Scanner Discussion.

5.3.1 Validation tests.

Validation tests executed in this study gave results very satisfying in several meanings. First of all, both the UAV and GNSS tests confirmed the substantial reliability of Terrestrial Laser Scanner data. Probably in this sense, GNSS test gave best results, especially in terms of linear regression.

The numbers of points is more than trustable, above all for Milano Marittima (906), and the standard error in both cases proves the integrity of this validation test. Moreover it is interesting to notice that the better results are given by the test with more points (Milano Marittima).

LINEAR REGRESSION STATISTIC			
<u>Marina di Ravenna</u>		<u>Milano Marittima</u>	
R multiple	0.987343121	R multiple	0.99668
R ²	0.97479292	R ²	0.99337
R ² correct	0.97479292	R ² correct	0.993363
Standard error	0.154293513	Standard error	0.069621
Samples	472	Samples	906

Table 5.1: Linear regression statistic of GNSS/TLS comparison.

For what concerns UAV and TLS comparison, this experiment, which has already become a published article (Mancini et al., 2013), gave more articulated results. First of all both methodologies exhibited a very good degree of agreement with GNSS ground truths. Comparisons show average differences at centimeters levels with related root mean square of 22 cm in the worst case. Anyway a systematic positive difference between TLS and UAV elevations has been noticed.

Examining the spatial error distribution map (figure 5.6), resulted from the TLS/UAV DEMs comparison, it can be seen how the surfaces have an almost perfect fitting everywhere, but a few central spots which affect the whole dataset and explain the little deviation. This map was obtained by using a particular ArcGIS tool, called

“Spatial Join”, with “Closest” option checked. This option is for searching a radius set to 10 cm to compare closest points.

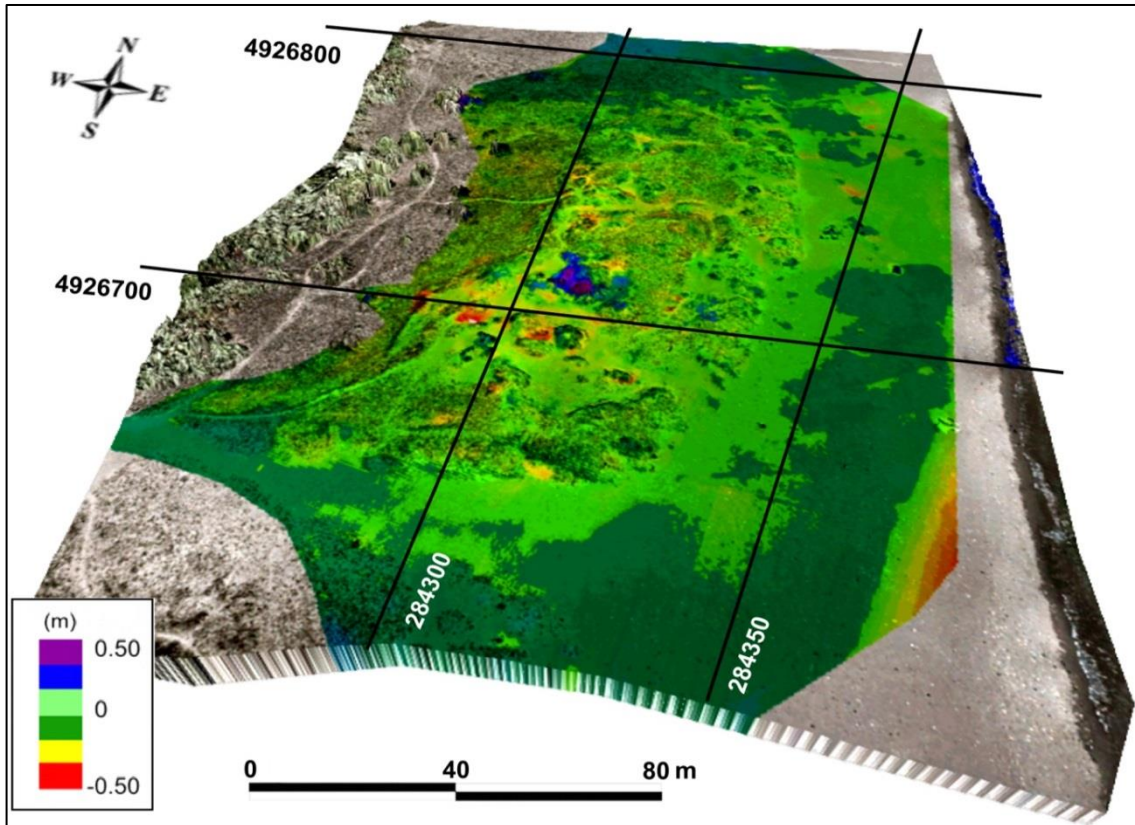


Figure 5.6: Spatial Error Distribution Map. Elevation differences are shown in different colors.

The source of these errors, for example the one colored in purple at the center of the DEM is not so clear because of its sporadic nature. The elevation differences are almost neutral all over the investigated area (green tones), but not in those spots where sudden changes on topographic features are encountered and the vertical differences exhibit higher values. This is probably due to the smooth morphology of the dune which not always allows the right angle of incidence for laser beam and for its collection by the device. Probably this could be avoided making some other scans from different positions.

For what concern the systematic error revealed by the GNSS test can be invoke as cause the oblique data capture geometry of the laser sensing more sensitive towards the sporadic presence of vegetation or surface roughness. More generally comparison shows a very small average distance between surfaces (0.015m) and a root mean square of 0.220 m

5.3.2 Volumetric seasonal monitoring.

The seasonal volumetric monitoring started in May 2012 and ended in May 2014, for a total of 15 surveys and relative digital models. Volumetric calculations were played in GIS environment (Arcmap), referred to the ETRF2000 System (UTM projection), all measurements are in meters, meters square or meters cube.

Site – Period	Sum (m ³)	Tot. (m ³)
Bevano I	126	304
Bevano II	496	
Bevano III	-35	
Bevano IV	-276	
Minali Marittima I	258	-444
Milano Marittima II	-1164	
Milano Marittima III	564	
Milano Marittima IV	-102	
Marina di Ravenna I	458	-299
Marina di Ravenna II	-348	
Marina di Ravenna III	-60	
Marina di Ravenna IV	-349	

Table 5.2: volume seasonal changes (m³).

It has been already explained how to read cut and fill results: a positive value mean erosion and it is indicated by red cells in maps, while a negative value means deposition/accretion and it is indicated by blue cells. They grey tone indicates no changes, but almost every cell of the digital model have changed its volume in every survey (for every sites).

In figure 5.7 Bevano's analysis can be consulted; it is pretty clear to see that nor in numeric data, neither in spatial changes maps, any trend is detectable. Only a) and b) maps could indicate an inversion of patterns: while in the first map, which describes what happened during the summer 2012, a widespread erosion seems to be happened, in the second, thus during the following winter a widespread deposition happened. Other data seem to indicate no biannual pattern nor in numeric, neither in spatial results. Uncommonly the dune foot resulted completely eroded during winter 2012/2013, completely accreted the summer after.

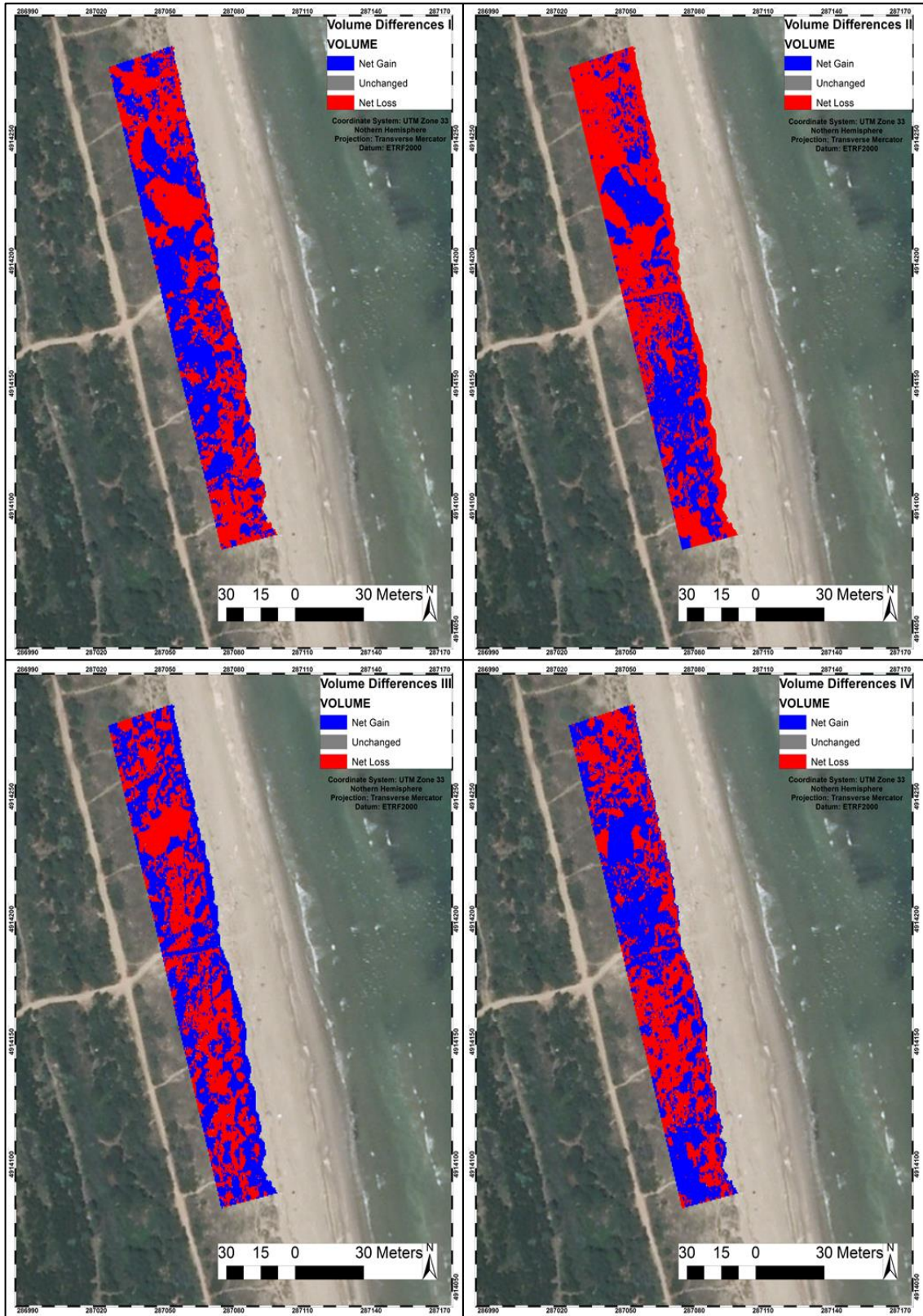


Figure 5.7: Bevano seasonal volumetric differences; I) May 2012 Vs October 2012; II) October 2012 Vs May 2013; III) May 2013 Vs October 2013; IV) October 2013 Vs May 2014.

For what concern Marina di Ravenna surveys, situation is a bit different. Volumetric data do not highlight any trend, even though, in relation to the previous analysis, they are more in line each other.

The spatial analysis, shown in figure 5.8, clearly indicates a trend which contemplates erosion overtaking deposition during summer periods, while the opposite situation happens during winter months. This pattern is not so clear, as it can be easily noticed reading the 5.2 table, especially for the “Volume Differences III” period, when the map seems to indicate erosion, while numeric data highlight a slight accretion.

This is due probably to the north area where a strong deposition happened. This area, in effect results to be subjected to accretion for each period surveyed. It is hard to not connect this pattern to the human impact and the strong modification of the beach dynamic. In next paragraph it will be explained more in detail.

The same situation can be observed in the 2012 summer DEM, even if involved different quantities of sand. On the other hand, is interesting to notice how data relative to the II and the IV period are perfectly in line, indicating both a deposition of almost 350 m³ of sand.

Milano Marittima table shows a clean pattern for what concern signs, positives (erosion) for summer periods and negatives (deposition) for winter periods. However this is only slightly confirmed by the quantities in game, because data numeric values are very different one from each other, and volumetric changes they indicates are not in line at all. Anyway it is undeniable that there is a diametrically opposite erosion behavior for this dune field, which during summer is for most part eroded, while during the winter it increases its total volume.

At last, total volume data, summarized for the entire two years monitoring period, identify a cumulative erosive trend only for the Bevano area dune field, while for other two, an accretion pattern is determined, even though with pretty strong differences in quantity of sand moved. No spatial connection resulted with morphological features or zones.

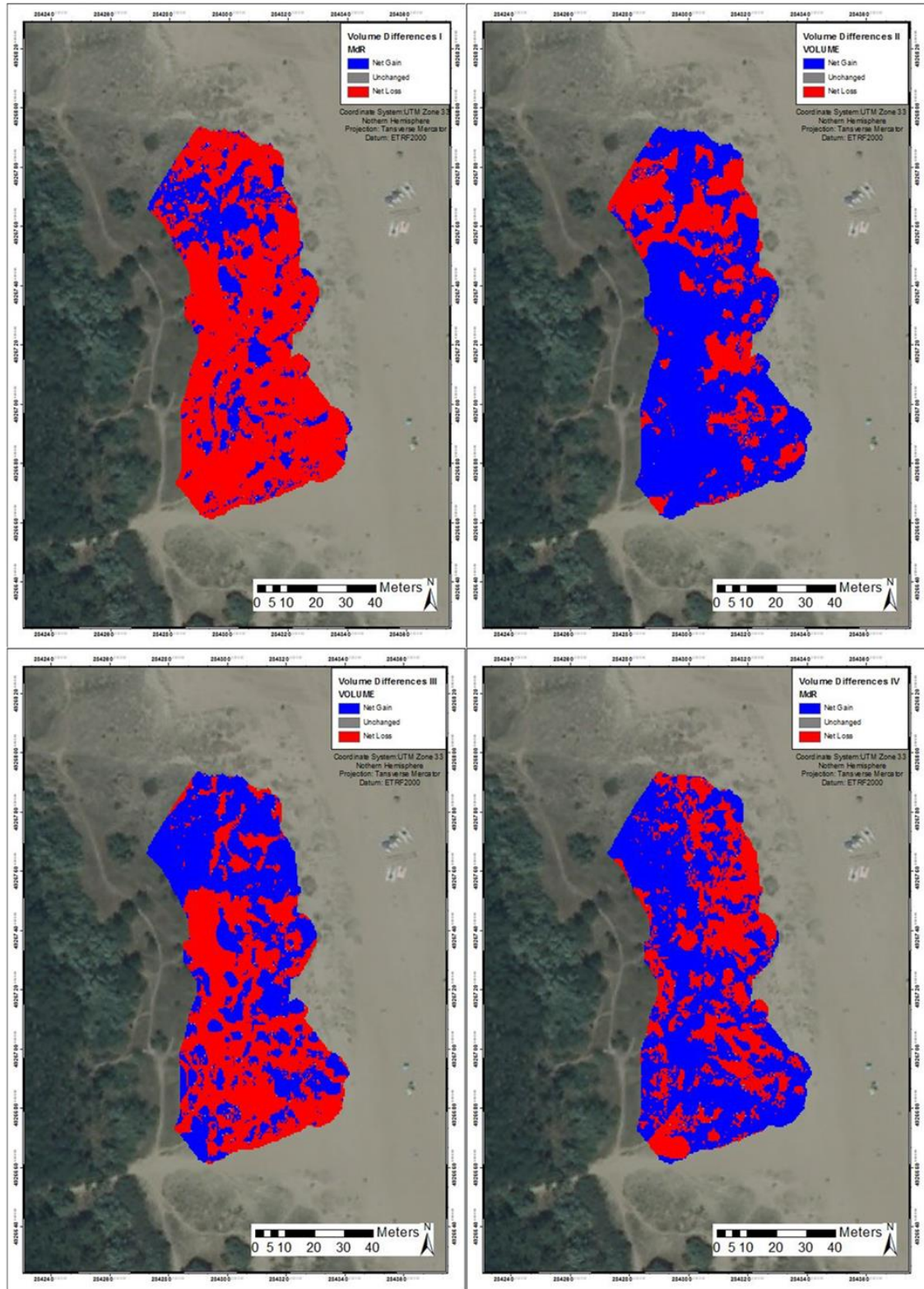


Figure 5.8: Marina di Ravenna seasonal volumetric differences; I) May 2012 Vs October 2012; II) October 2012 Vs May 2013; III) May 2013 Vs October 2013; IV) October 2013 Vs May 2014.

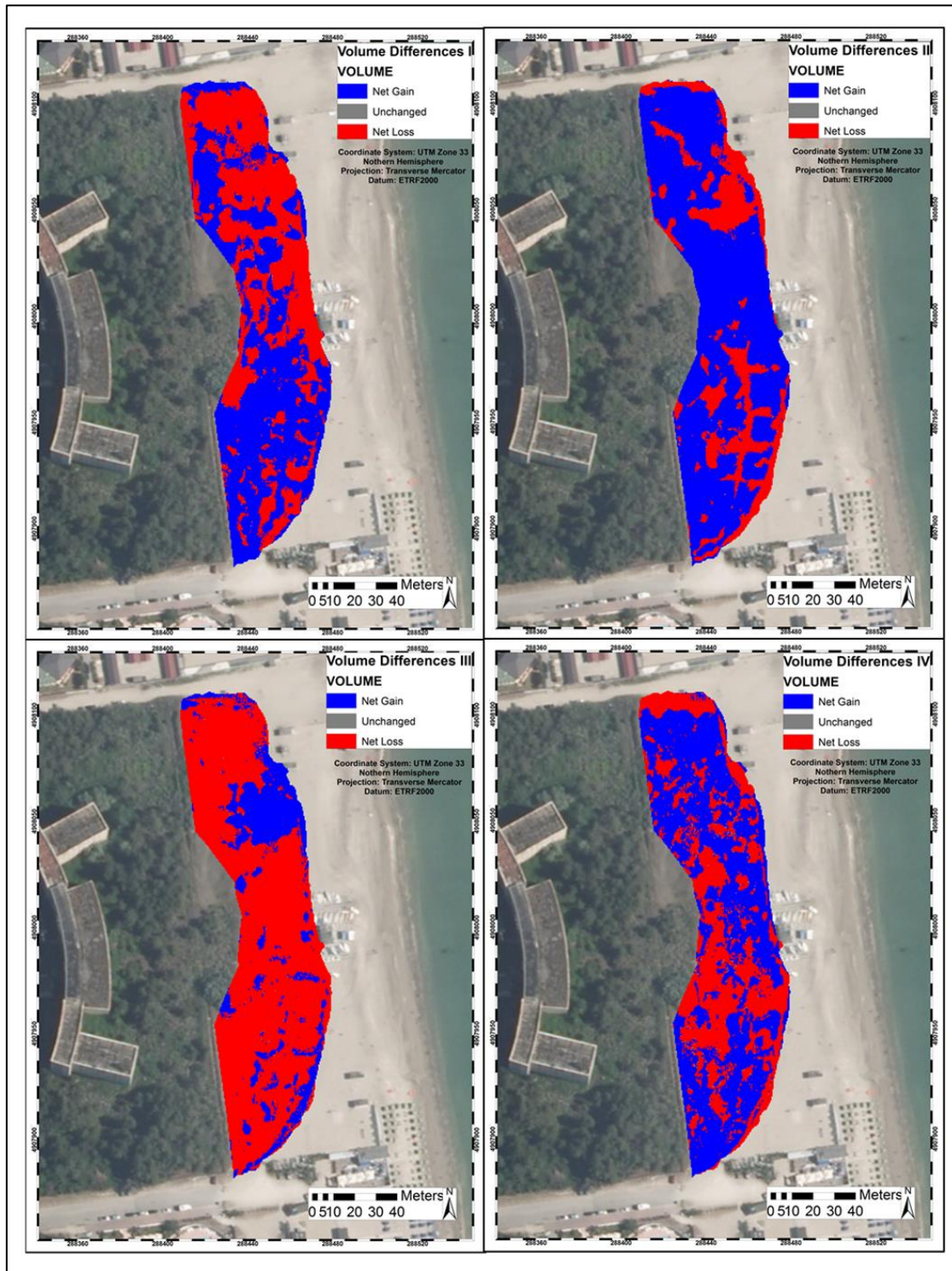


Figure 5.9: Milano Marittima seasonal volumetric differences; I) May 2012 Vs October 2012; II) October 2012 Vs May 2013; III) May 2013 Vs October 2013; IV) October 2013 Vs May 2014.

5.3.3 Morphological Analysis: two examples of investigation.

The morphological analysis begins from the topographic area data analysis, presented in tables 4.5, 4.6 and 4.7, in Results chapter. In this chapter the spatial variation will be discussed for each area of study. Bevano dune field data are reported in table 5.3.

Period	3D Area WD (m²)	3D Area GD (m²)	3D Area BD (m²)
May 2012	2955.31	801.64	1446.15
Oct. 2012	2708.37	706.48	1385.64
May 2013	2564.32	761.13	1332.76
Oct. 2013	2679.78	608.50	1974.45
May 2014	2363.59	611.55	2163.11

Table 5.3: Bevano Sub-Zones extension for each period of surveying.

Bevano's White Dune has reported a linear behavior, which in table is highlighted by the continuous decreasing of the 3D area. This is aligned with DSAS data, which confirmed for this area a low, but progressive and continuous moving landward of the dune foot line. This could be probably linked to the storm waves actions, amplified in this area by the beach width, which is about the half of other two areas of study.

The Black Dune area, instead reports a normal behavior only until October 2013 when its extension increased considerably (about 600 m² more respect May), and it keeps growing in the further period (May 2014); contemporary the Grey Dune decreased its area more than in any other period. To understand what could influence in such a way the dune morphology, the author isolated this area and divided it in two parts (north and south, relative to the central path) in table 5.4 split area data since May 2013 to May 2014 are shown.

Period	South Black Dune (m²)	North Black Dune (m²)
May 2013	440	980
October 2013	940	1186
May 2014	1025	1259

Table 5.4: Bevano sub-areas extension in m².

It is clear that the South part is the one which has been subjected to the strongest morphological modification and, during summer 2013, its area increase of about 500 m², of the 600 total. This datum indicated where to search: in the extreme south zone, there is a morphological feature, clearly originated by the sea. It is probably the remaining of an old over-wash which left a lower and smoother part of the dune (figure 5.7), probably more easily erodible by the sea than other cordon parts.



Figure 5.10: picture of the over-wash, taken in October 2013; the smooth morphology is still visible, even though the dune is in a re-building phase.

To understand what happened to this spot, in GIS environment laser scanner DEM data on this particular area were analyzed at a microscopic detail (1:100). The author found that starting from May 2013 this spot was affected by a strong modification, especially in terms of elevation: the average elevation, in fact, changes from 3.01 m (o.s.l.) in May 2013, to 2.80 in October, and back to 3.22 in May 2014.

Basically during summer 2013 the sea had the opportunity to over wash this spot, probably causing a strong change of this area, and of the inner land, which is the Black Dune: salt water, sand, woody debris are just some of the noxious elements the sea could carries.

In figure 5.11, the planimetric and the orthogonal 3D vision of the spot can be examined. Thanks to the April extra survey, the author was allowed to reduce the period when the real modification on elevations happened. Comparing the April DEM to the May one, it is clear how a spatial portion of this feature, which was a barrier residual, completely disappeared, making easier for the sea to overtake this point. At the end of

the summer, a part of the barrier seems to be repaired; in further surveys the subzones spatial changes returned in the norm.

As last step of this “investigation” the author checked meteorological sea data, to find confirms. During the analyzed period two were the high energy events identified: one in August the 20th lasted 7 hours with an average waves’ height of 1.68 m and a maximum of 1.95 m; the other in October the 7th, stronger, lasted 14.5 hours with an average waves’ height of 1.74 and a maximum of 2.38.

Considering that this last event was stronger and happened not many days before the survey, it could be ascribed at least of the last part this modification.

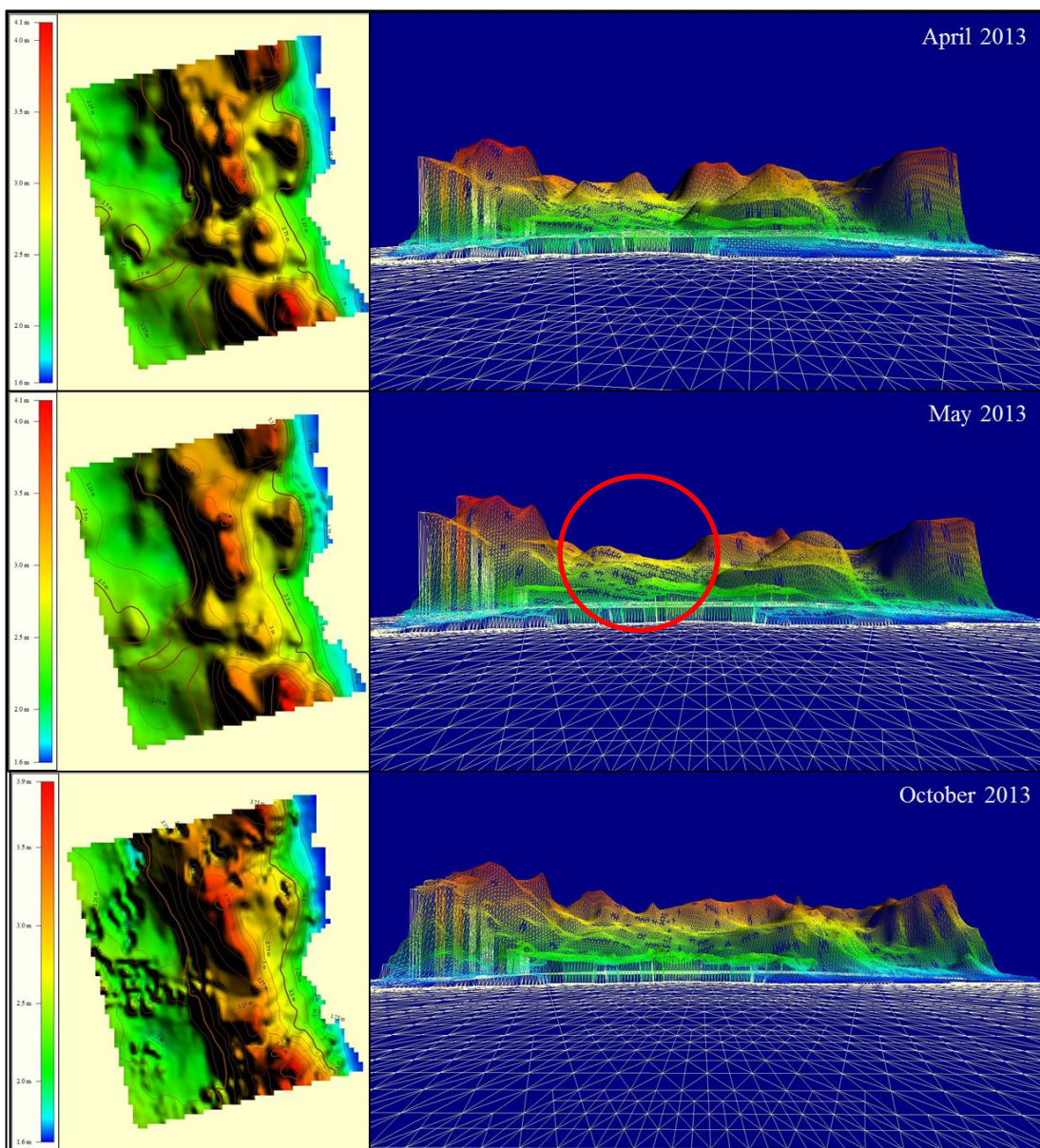


Figure 5.11: Over-wash area DEMs, planimetric and 3D views. In the 3D view elevations are exasperated for a better view.

Marina di Ravenna Sub-Zones data are not less interesting. Starting from White Dune, data indicate an intriguing behavior: during every summer this zone tends to increase its area, while during the winter it tends to decrease.

This is not a natural behavior in this part of Adriatic coast, especially assuming that the beach width is double respect to Bevano area. The summer, which is the onshore winds season, should be (in a pure theoretical line) the aeolian erosion period, while the winter, due to offshore winds and sand moisture, should be a neutral/low deposition period.

Period	3D Area WD	3D Area GD	3D Area BD
May 2012	2927.85	701.21	913.51
Oct. 2012	3046.85	646.21	872.90
May 2013	2927.60	875.75	880.64
Oct. 2013	2966.61	763.11	835.57
May 2014	3044.04	684.41	815.44

Table5.5: Marina di Ravenna Sub-Zones extension for each period of surveying.

This complicated situation requires a more accurate investigation, especially with a different temporal scale survey campaign. Anyway even analyzing seasonal data some interesting deductions turned up.

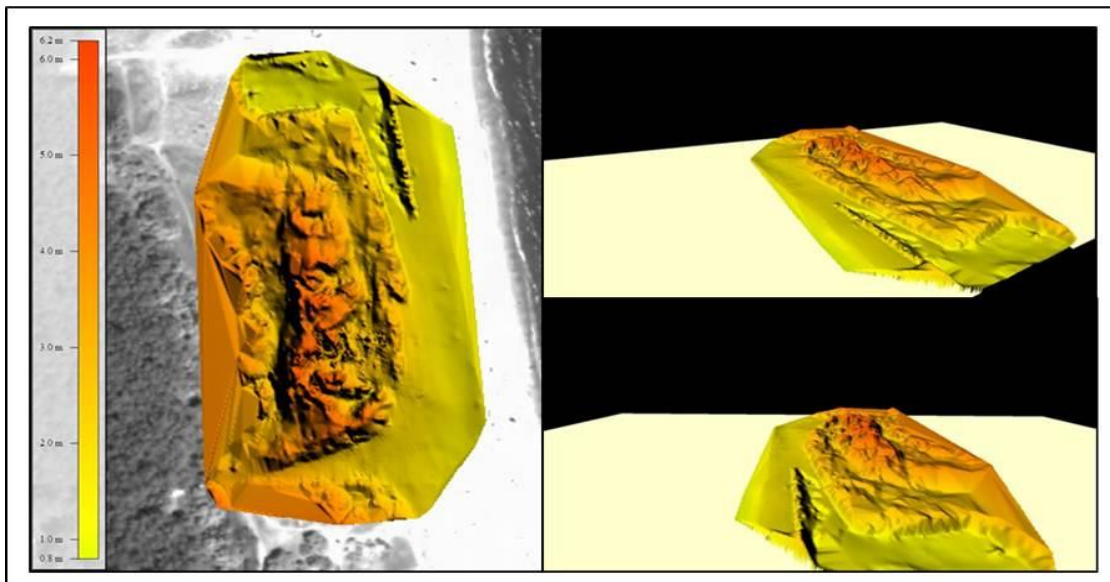


Figure 5.12: Winter wall ("dune") erected by bulldozers before winter.

The deviation from a natural behavior is probably linked to the human management of the beach: during winter a sand wall (called “winter dune”) is built up by caterpillars, in order to defend touristic buildings from storms (figure 5.12).

This has a strong effect on the dune morphology: in the North part of the foredune a sort of huge false foot developed in correspondence to the wall. It is plausible that this modification has effect on the morphological behavior of the whole dune body.

At the beginning of the summer this “false foot”, which is already strongly stabilized by several years of this practice, is dense vegetated (figure 5.13), thus the onshore winds blow on a vegetated surface before to come to the real dune foot.

This dynamic causes a strong deviation from the erosion/deposition natural behavior, which can explain, at least in part, this anomaly.



Figure 5.13: the “false dune foot” in its summer habitus: the surface is dense vegetated by *Cyperus Captatus*.

Another interesting feature appeared from this data is related to the huge blowout in the most South part of the field: at the end of every summer the depositional lobe is broken by the onshore winds (figure 5.11) this action has several effects, above all gravity falls, sand remobilization and its negative consequences (vegetation killing). This could explain, once again at least in part, the Gray Dune area oscillations.

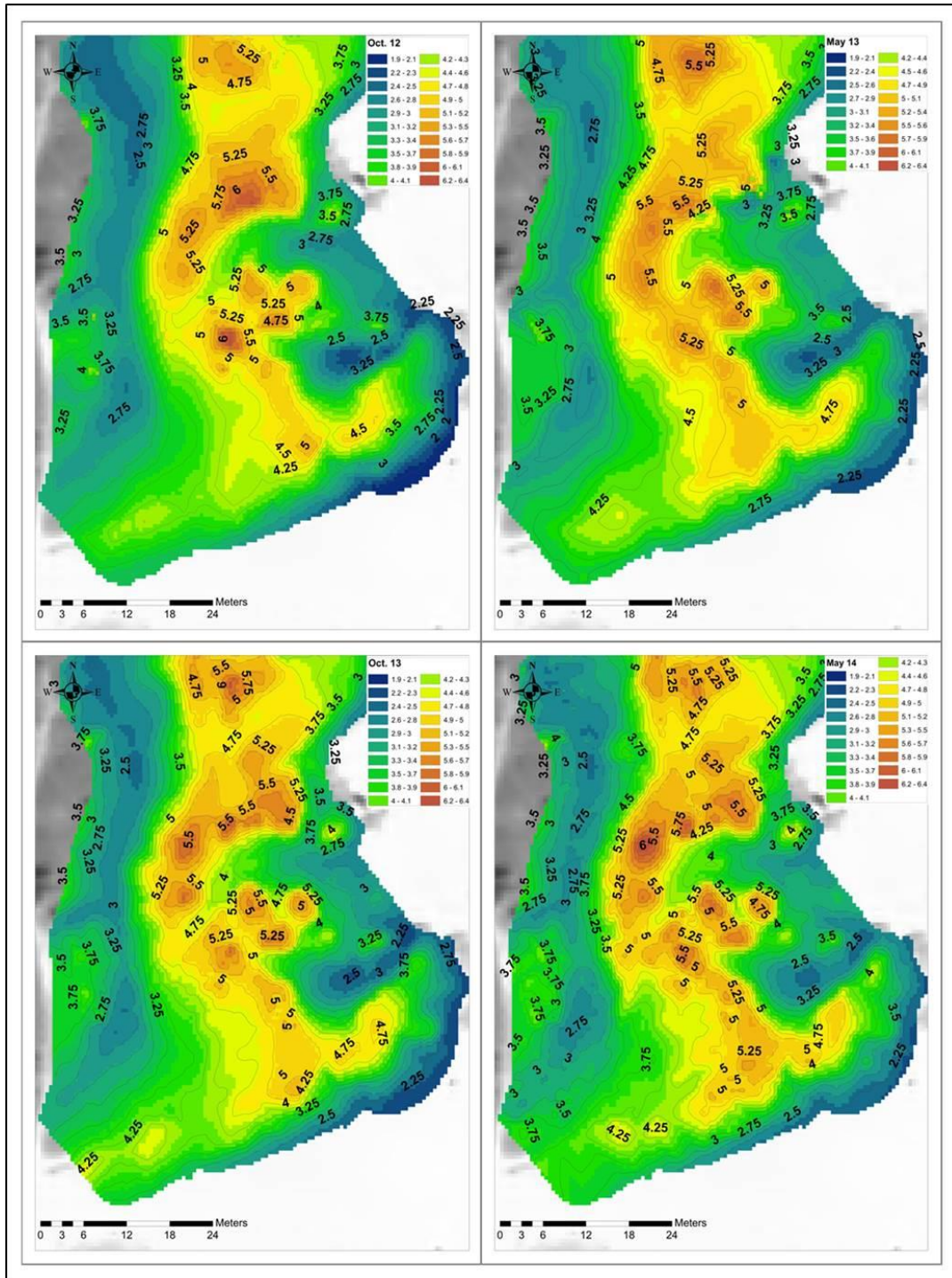


Figure 5.14: Marina di Ravenna Blowout evolution, starting from October 2012 to May 2014.

Milano Marittima data gave less food for toughs: due to the strong beach management the White Dune Area seems to be almost stable (which is just by itself a deviation by a natural behavior). Probably the 2013 decreasing is just due to the organization of the touristic building on the beach (very next to the dune foot line).

For what concern Grey Dune extension it intensely decreases starting from May 2013, but this is related to the vegetation growing from the landward abandoned building area.

Period	3D Area WD	3D Area GD
May 2012	7463.82	786.03
Oct. 2012	7465.24	857.94
May 2013	7370.81	563.40
Oct. 2013	7321.07	556.09
May 2014	7448.76	452.42

Table 5.6: Milano Marittima Sub-Zones extension for each period of surveying.

Blowouts morphological data didn't highlight any particular situation or change. An interesting characteristic appeared from the DEMs analysis is related to their orientation, which is in the very most cases North-East/South-West, exactly the direction of "Bora", the strongest local onshore wind (Appendix I).

5.3.4 The DSAS analysis.

Looking at the table 4.12 in Chapter 4, it is clear how from a general point of view all the three dune foot line analysis resulted in negative values, while the two crests lines exhibited opposite behaviors.

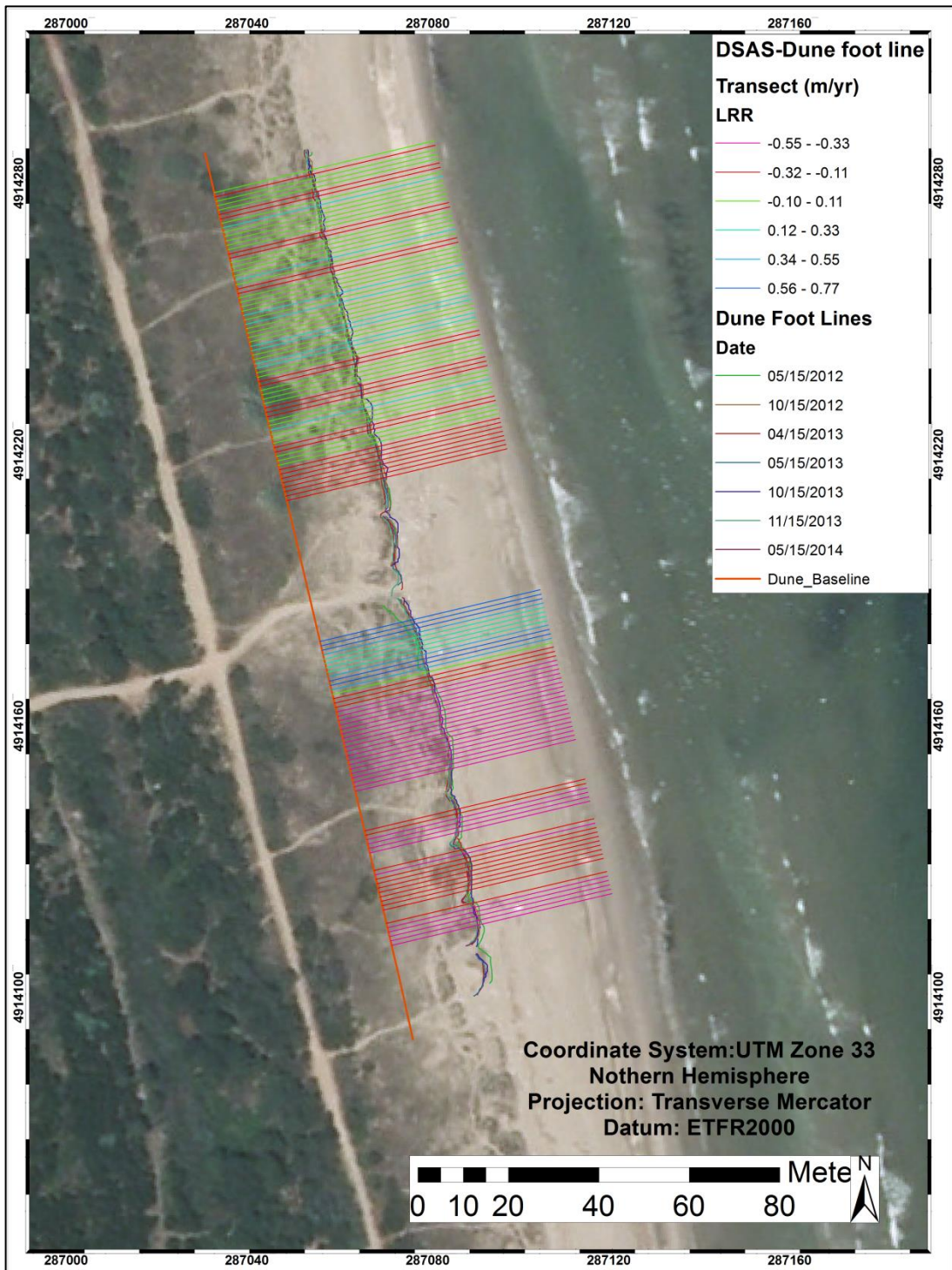


Figure 5.15: Bevano area dune foot line examination.

Seven dune foot lines and seven dune crest lines were examined with the DSAS tool in GIS environment, for the Bevano area (figure 5.15). Every dune foot lines was drawn in a range from about 22 to 38 degrees of slope. The dune crest lines remain in a range of height from 3.9 m to the maximum height of each DEM. The statistical result relative to the both features movement can be consulted in Appendix IV too. The end point rate value indicates a general moving back for the foot line, which seems to move with a rate of about -0.16 meters per year; the linear regression value, instead, is lower (-0.11 m/yr) but always on the same order. Some authors (Shangam S. et al., 2013; Temitope D., 2014) consider this a more realistic value because of the algorithm which is applied: the LRR in effect is a much more articulated measure than EPR, which substantially gives a result based on the first and the last movement; this is because LRR considers every movement in relation with the moment (the “x” and the “y” of the linear equation).

The net shoreline movement shows a value of about 0.3 meters of total movement, almost the EPR double, which is not surprising as result (the double of EPR), considering that the analysis last about 2 years (from May 2012 to May 2014). Belonging to these data the dune foot line is fundamentally moving back with a rate of the order of about 10 cm per year.

The graphical analysis is shown in figure 5.15. The color choice was focused on red and purple for back movements, blue and azure for forward movements and green tones for lines showing an almost stable trend. The movement range was subdivided in six equal classes of about 20 cm, depending on the movement range.

It is clear to see how the diagram is split in two and the South part is the one where the back movements are dominant, while in the North segment the foot line is much more stable. This is probably linked to the morphology of the south part much more carved by erosional features created by both sea and wind action. In any cases there is a clear inversion of trend in a particular spot next to the tourists path, north of which the foot line tends to progradates or to stand stable, while turning South the back moving pattern is net and undeniable.

The dune crest line analysis gave interesting results too. The EPR averaged value indicated a very short movement on the order of one centimeter. This is confirmed by the LRR result which is -0.1 cm (basically stable). NSM once again resulted the double of EPR, about 0.2 meter of net total movement.

The crest shows first of all a very different behavior compared to the foot line. It is clearly much more stable for the whole dune ridge extension (that examined) and in some segments demonstrate an accretion pattern (blue transects) recalling what hypothesized by Psuty in 2009. A few spots are moving back at a first approach without rule, but the author thinks it could be linked to the vegetation cover and its density. In any cases it would be really interesting combining this purposed methodology with a vegetation survey and overall with a vegetation map.

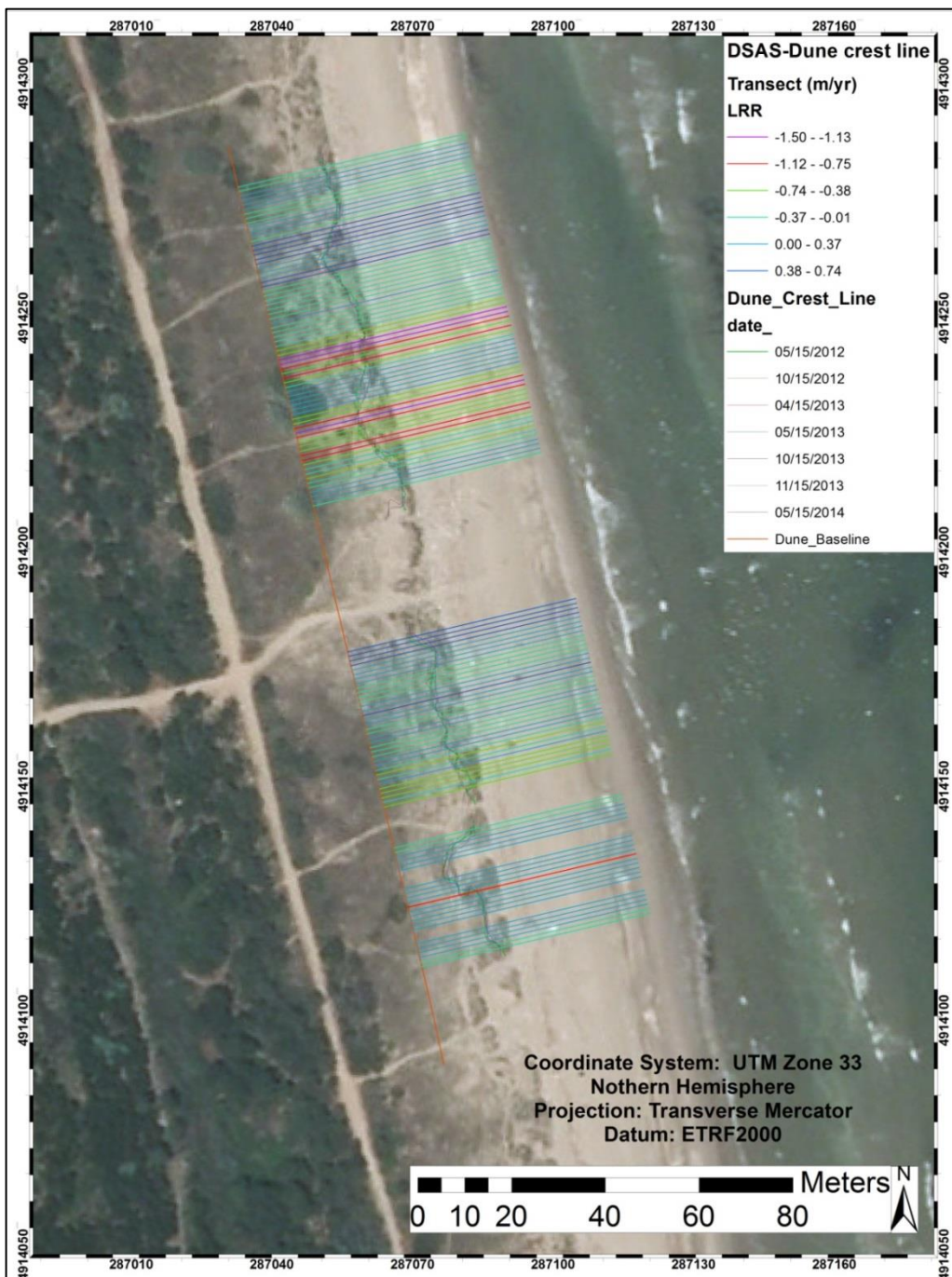


Figure 5.16: Bevano area dune crest line examination.

Marina di Ravenna analysis indicates a general moving back of the foot line (17-30°) (shown in figure 4.8, Chapter 4), as well as Bevano dune foot, but in this case the general movement was shorter. The LRR value indicates a movement of less than 10 cm; watching transects map it can be seen how almost the whole line is stable or slightly accreting.

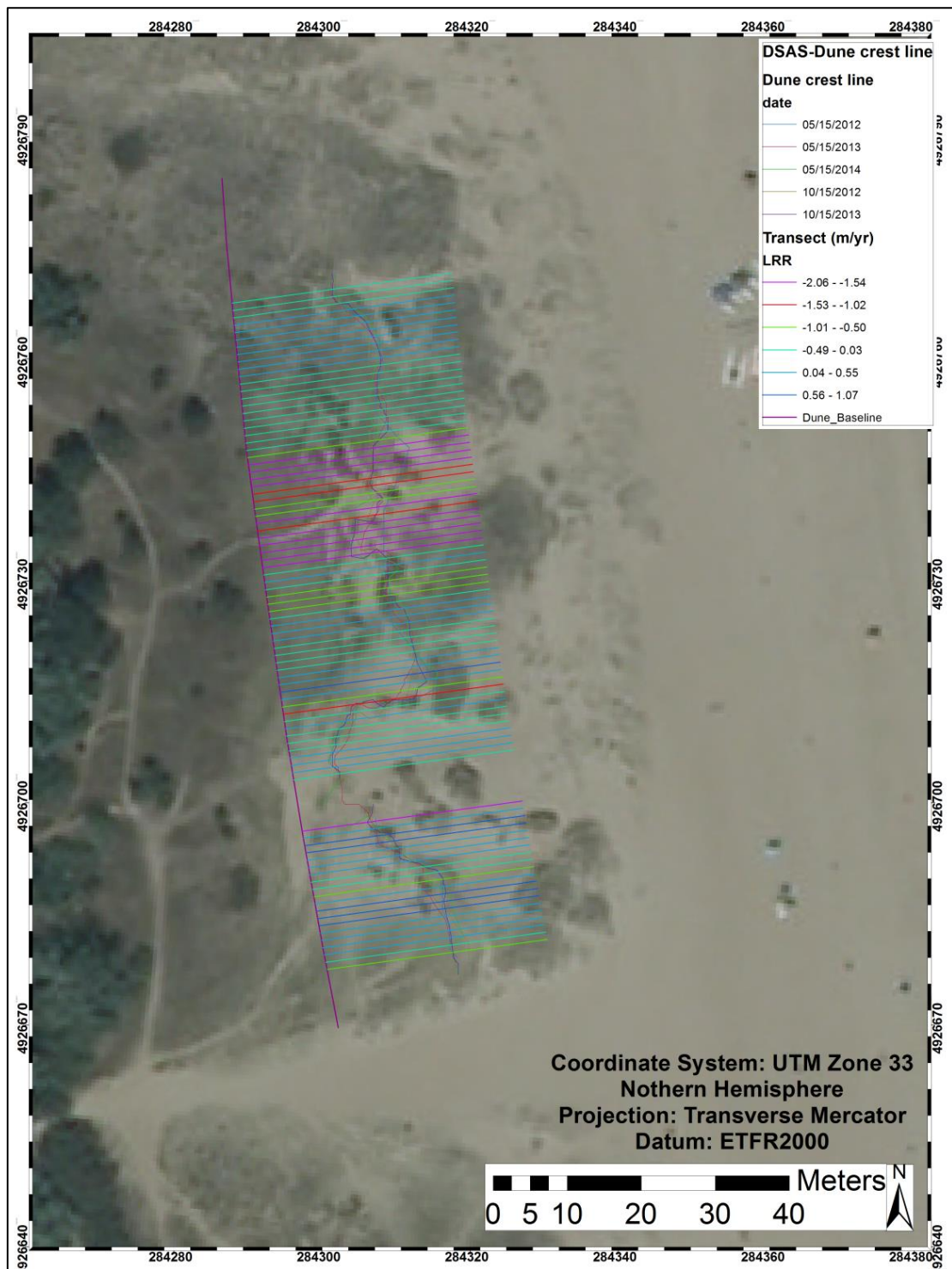


Figure 5.17: Marina di Ravenna dune crest line examination.

Only the most North part of the dune foot line results strongly move back. This is probably due to the beach management and the erosion/deposition pattern explained in previous paragraph.

The dune crest line (4.9 m – 6.1 m) examination gave more interesting results: the Bevano situation is completely reversed and the crest has moved during the surveyed period in a much more intense way (about 30 cm, while the foot line LRR value was -0.09).

The cause of this huge movement, which was not expected, is a strong modification which affects the crest line in correspondence of the central blowout.

Maybe the blowout ramp can operate as tunnel for wind acceleration, which could dump its force on the dune crest, without being decelerated by vegetation or dune stoss before. Obviously the crest fragmentation already in action would facilitate this process.

Milano Marittima results are aligned but probably corrupted. The much more evident movement of the foot line is probably (more than probably) connected to the human activities and foot reprofiling. The dune foot line range goes from about 19 to 30 degrees.

Looking at transects map it is easy to individuate a spot of particular moving back by the foot line. This is probably linked to the management of the beach at the beginning of the touristic period of every year, which includes the beach set up by bulldozers. Beyond this it can be helpful to understand this behavior to notice that exactly in front of this spot there are two abandoned concrete structures, which shelter this spot deviating its natural condition.

Another interesting pattern has been found in a central position, in which the foot line moved forward starting from October 2012. Also this trend is imputable to human activities: during the first surveyed summer the author noticed that in this position a touristic operator was allowed to parks his boats for rent. In figure 5.15 can be seen the DSAS analysis plot with the “boats park” and buildings for tourists (North).

It is plausible that those obstacles operate as retention structures for sand and cause a shadow effect which induces deposition by wind. The rest of the analyzed area seems to be substantially stable.

All DAS analysis results can be consulted in Appendix VI.

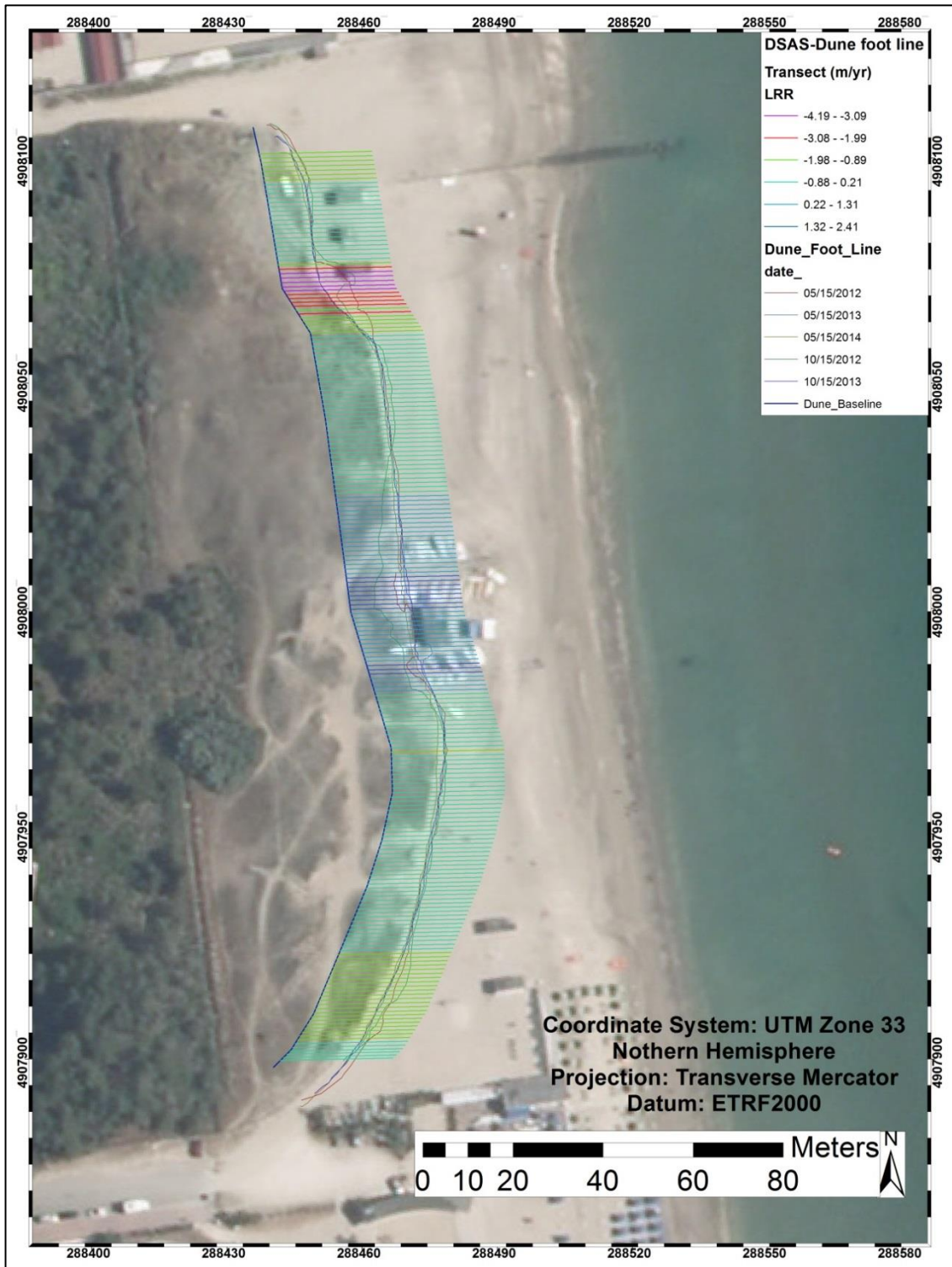


Figure 5.18: Milano Marittima dune crest line examination.

5.4 Principal Component Analysis Discussion.

Principal Component Analysis was elaborated and plotted by RStudio. Three were the tests elaborated: the first analyzed volume and 3D area differences, in relation to Forcing Factors. In figure 5.19 the original graph, plotted by R, can be consulted. It is important to remember that every spatial data was statistically analyzed as absolute value.

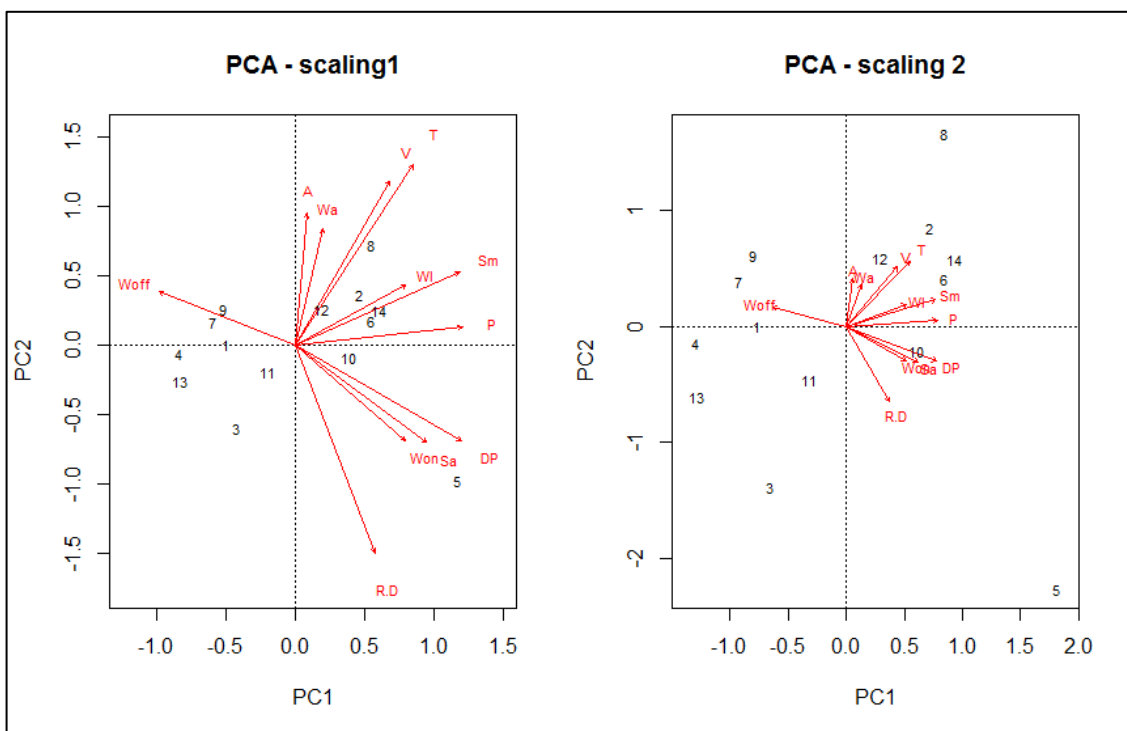


Figure 5.19: PCA diagram based on volume (V) and topographical area changes (A).

Volume differences (V) result to be positive correlated especially with storms last (number of hours wave have exceeded 1.5 m height), because the two vectors are almost coinciding; moreover this index resulted positive correlated, even if in a lower way, to alongshore winds percentage (Wa), maximum water level of the period (Wl) and storm waves' maximum height (Sm). A little positive correlation to rain data appeared too. The Directional Variability Index (R.D.) and, in a smaller manner, onshore winds percentage (Won), resulted to be in negative correlation to volume

changes. Drift Potential values (DP) and offshore winds percentage (Woff), instead, revealed no correlation, just as the storm waves' average height.

Areal differences (A) shows a strong positive correlation first of all to the alongshore winds percentage and, secondly, to the T factor. A decreasing positive correlation was founded with WI, Sm and P. As before there was no correlation with DP, Woff and Sa, while R.D. is linked to area differences by a negative correlation.

It is interesting how A and V vectors are almost aligned, datum which confirmed the reliability of the TLS datasets.

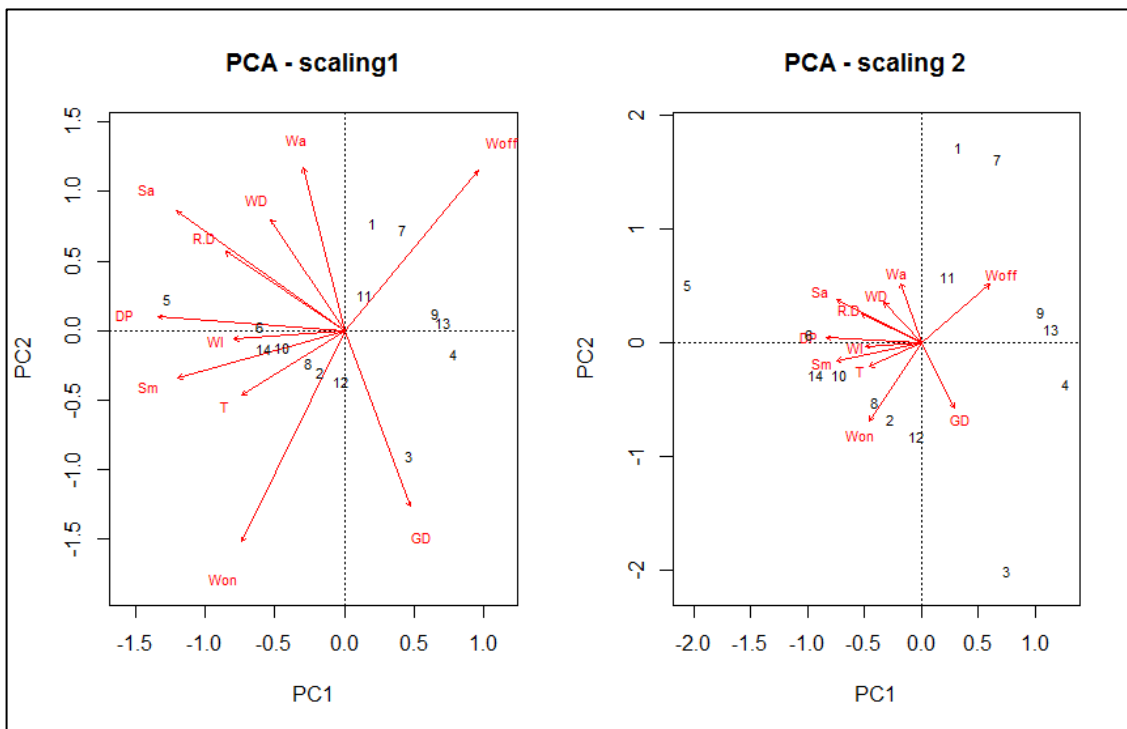


Figure 5.20: PCA diagram based on White Dune (WD) and Grey Dune (GD) spatial changes.

The second PCA test was computed using morphological sub-zones spatial changes, in term of 3D area. The first element highlighted by the graph in figure 5.20, is the absolute negative correlation between the changes of the two zones. This, at least, proves the fact that white and grey dune, are really two different zones of the foredune from a morphological and a dynamical point of view.

White dune (WD) oscillations are strictly positive related to alongshore winds (Wa) overall, and then to Sa and R.D.; still positive, but much less strong is the relation to water level and drif potential. Eventually, Woff, T and Sm can be considered in negative relation.

Grey Dune spatial variations showed no positive correlation to any of the forcing factors, but onshore winds percentage. As WD opposite vector it is obviously related in a negative way to those indexes positive linked to WD: a strong negative correlation to alongshore wind can be invoked. Woff and T have no relation with Grey Dune spatial variations.

Last PCA calculated involved blowouts spatial changes. Once again alongshore winds percentage seems to have a key role and showed an almost perfect coincidence with blowout vector (BO). Some other factors like T, Wl, Sm and P are in a decreasing plus relation. Moreover, analyzing the 5.21 graph, the author recognized other fetures, also presented in the two graphs before: drift potential and offshore winds have again no correlation to blowout data; eventually directional variability index is negative related.

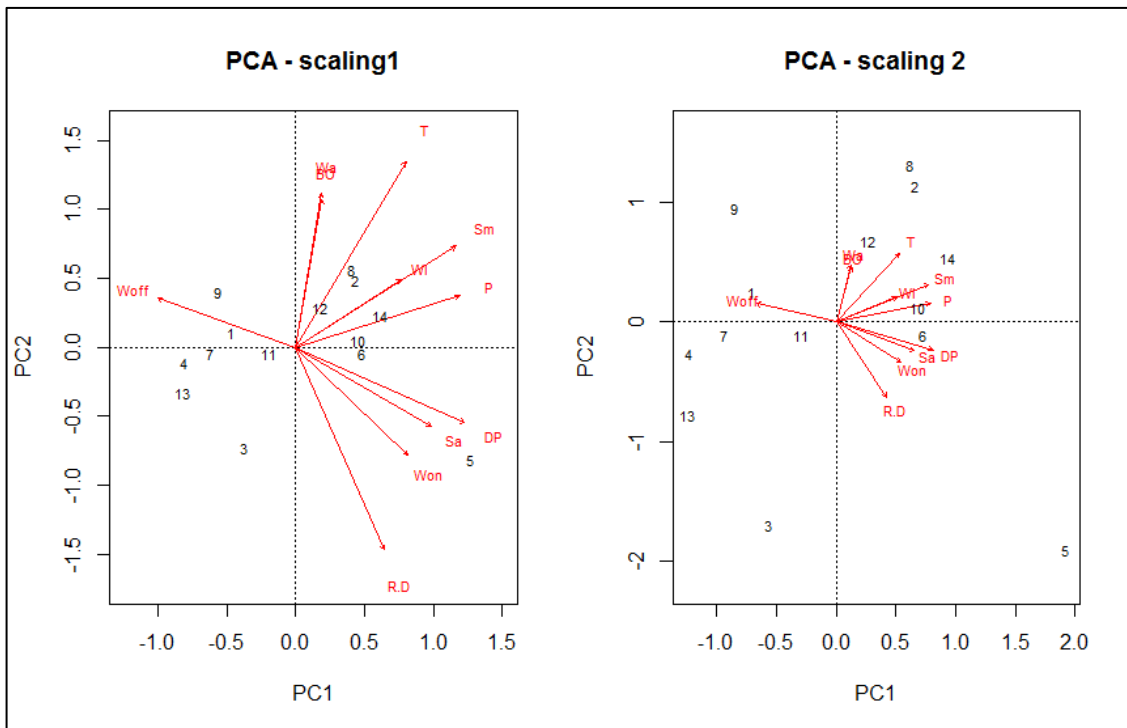


Figure 5.21: PCA diagram based on Blowouts spatial changes.

5.5 Computational Fluid Dynamic Discussion.

From the Computational Fluid Dynamic analysis some very interesting results appeared: some spots onto the dune ridge revealed to have an almost perfect correlation between wind speed values projection and height differences.

Assuming that only wind values which exceeded the threshold velocity were taken in consideration, the three different components of wind with their correlation to height differences is plotted in figure 5.22. Even though in the whole data set the regression did not approach the positive correlation value, it can be seen how data are anyway aligned.

It is interesting also to notice how across wind and along wind data set distribution relative to topographical changes are very similar one to each other. The vertical wind component data set is instead more diverged both for expected values and the data distribution (much more narrow). Probably the best correlation is the one between the vertical wind speed component and the height differences: this could be due to the lower influence of the vegetation in the real-world measures of this component.

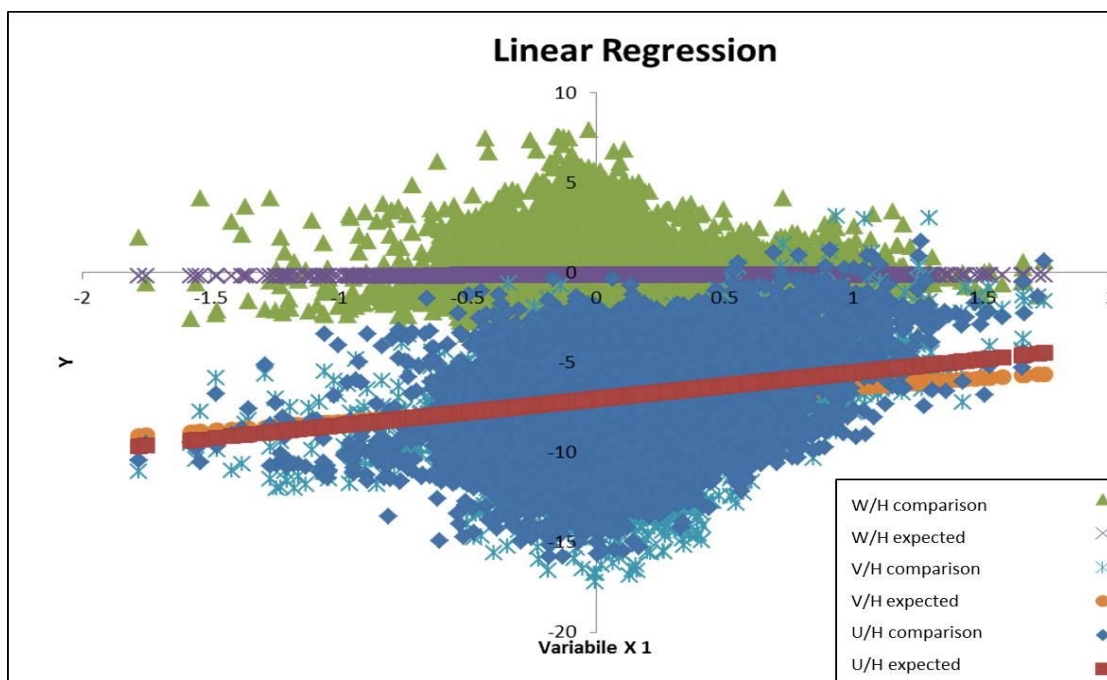


Figure 5.22: Linear regression graph. Green/violet: vertical wind speed Vs Height differences; azure/orange: across wind speed Vs height differences; blue/red: along wind speed Vs Height differences.

Figure 5.23 shows these results, plotting only some interesting spots of the comparison DEM.

Looking at the plot a) and e) spots are the best well-fitting zones of the DEM resulting a R^2 value of about 0.91, for a), and 0.82 for e). b) and c) points show a medium value of, respectively, 0.79 and 0.52, involving a not so strong correlation. The two spots which shown the lowest degree of correlation, d) and f), are the two where the highest speed were modeled, both located on the seaward crest area.

The author didn't recognize a spatial trend in the R^2 values distribution for the whole area of interest, even though the best fitting nodes seem to be spotted in lowest wind speed areas and are usually correlated with deposition. Figure 5.23 is really clear showing this. It is plausible that this is due on one hand always to the vegetation distribution, on the other to the more simple conditions to calculate in a lower wind speed dynamics.

Unfortunately a strong limit of this test was represented by the fact that there was no opportunity to insert or correlate data relative to vegetation cover. This is probably the factor which influenced the results presented above. It is plausible that the best fitting spots are those where the vegetation was less dense or absents, while spots with low or no correlation could be occupied by plants with a stronger density and in some cases affecting the measurements because of the type of species (wooden or brush).

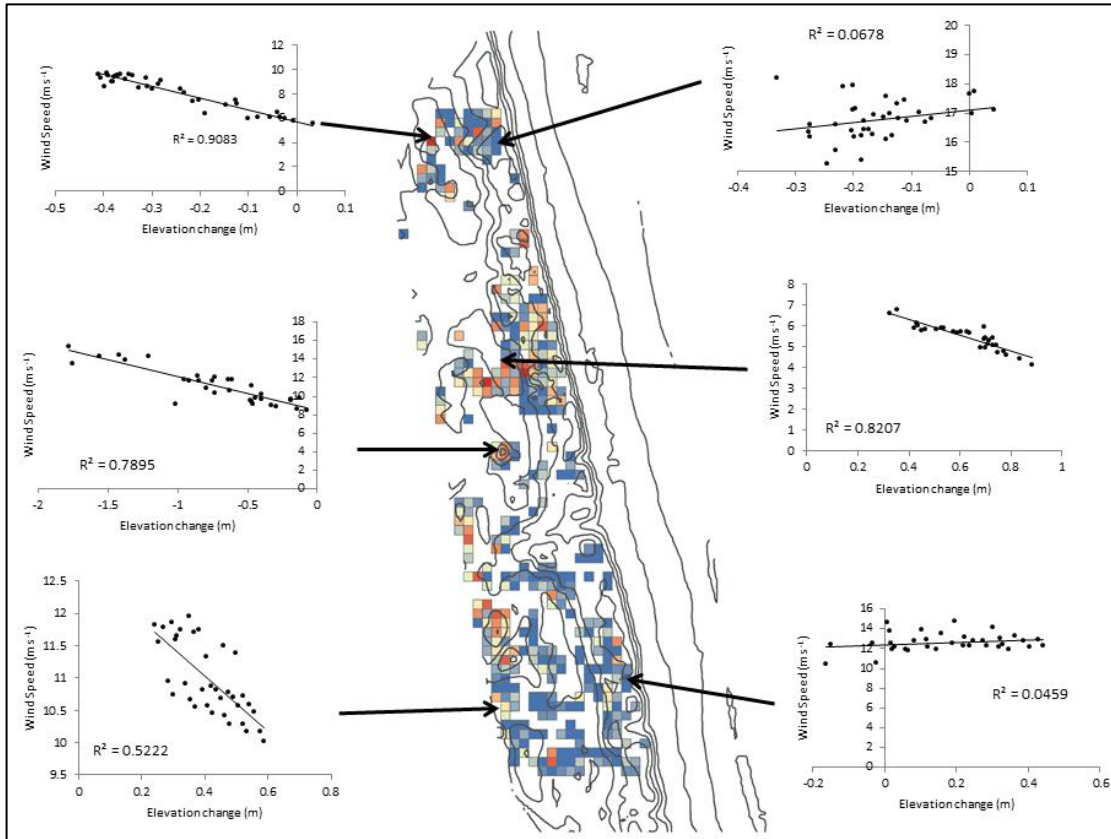


Figure 5.23: Linear regression results plotted on topographical map.

6 CONCLUSIONS

6.1 Terrestrial Laser Scanner.

6.1.1 Validation tests conclusions.

Validation tests executed in this study had both returned positive feedback and proved TLS reliability. Their importance was not limited to the confirmation of terrestrial laser scanner data, but the two test methodology purposed have a general merit to be applicable to several diverse remote sensing “situations” (especially those related to 3D technology).

About first case, the TLS versus GPS-GNSS comparison, it is opinion of the author that this kind of proves should be the first step of every terrestrial laser scanning survey campaign, in order to calibrate the methodology.

This should be made not only to prove the reliability of data: it is a fundamental part of the TLS method, especially when planning a monitoring survey program, a sort of calibration between the range of scans and their “quality”, in term of resolution. Clearly the higher is the quality and the range of scans, the higher is the size of data and the density of the point cloud, but also the noise error and the surveying time.

Moreover there is another feature to consider: the higher is the general quality of scans, the harder the laser device works, the longer are times of operation; this, that could be considered a secondary factor, instead it is crucial in an outside field monitoring.

However this compromise should be specific for each determined environment, depending on its morphological characteristics too: an environment formed most of all by straight planes and inclined surfaces with strong slopes (for example a cave) would require very different settings from an environment with smooth surfaces and weak slopes, like a dune field.

This is very important for three principal purposes: first, to minimize systematic errors, especially those linked to objects features and environmental conditions.

Secondly the TLS is a very powerful tool and according to the author its power should be used at the right scale of high detail, to have its best performances and to define its proper use in the remote sensing panorama.

The third reason is connected to the role of TLS in environmental monitoring, which should consider the field applicability of the whole methodology. In this meaning the temporal dimension is very important, because of its applicability and to be comparable with other monitoring devices.

In last analysis a calibration test TLS/GNSS based should be done to be sure of TLS data and to have the opportunity to work on them without doubts. Moreover the certainty of recorded data helps to reduce processing time in post processing procedures.

The second case, the comparison to drone data, had a different planning in the background. First of all it was made to test the UAV methodology more than the TLS one, and to compare them. In this meaning there are several important considerations to explain: the alignment of the data coming from the two devices was more than satisfying, but more proves like this one, maybe in different environments, have to be done. In any cases, what appeared from this particular test is that both devices are trustable in environmental monitoring based on remote sensing.

In relation to the environment, there are some features that promote the UAV application, some others the TLS: the field work is much more shorter for drone, but the post processing is much longer and consider a stronger manipulation of data; more over it do need of a powerful computer to process the huge number of pictured needed to build up a digital model. TLS post-processing instead is pretty short and does not require strong manipulations. Weather conditions can limit both devices, but in different ways: sun, rain, fog and snow are the TLS enemies, while wind and rain could stop drone.

At last, there are two important differences to considerer, which probably make all the difference: first of all the cost of these two devices is very different and TLS is usually much more expensive than UAV. The second difference has a legislative nature: while the TLS employment has no legal limitation, the young UAV practice is, at the moment, under evaluation by the National Agency of Flying Assistance (E.N.A.V.) which is thinking to limit the use of drones only to those operator who will get a specific license; moreover restrictions on the automatic pilot and on the urban-suburban

area to fly, are about to come out. These could limited the nature of these devices which would not be “Unmanned” any more.

Finally results obtained from the validation procedure of digital models from both methodologies deserve an additional consideration, because this could be a starting point whenever an accuracy assessment of 3D products is required.

6.1.2 Seasonal volume survey and morphological Sub-Zone analysis.

The seasonal volume survey gave different feedbacks for each area of study. The Bevano area survey, which is also the only completely natural area, was for some aspects disappointing: no trend has been found nor in numeric data, neither in spatial erosion/accumulation maps.

Remembering what written about the beach width in this site, the absence of particular patterns is probably connected to the strong effect that the sea could have here, on the morphology of the foredune. In this mean, the volume value revealed by TLS could be intensely influenced by the moment of survey relative to the last storm time. To confirm this hypothesis the author compared two periods both from 2013 pretty similar for last, but really different for results.

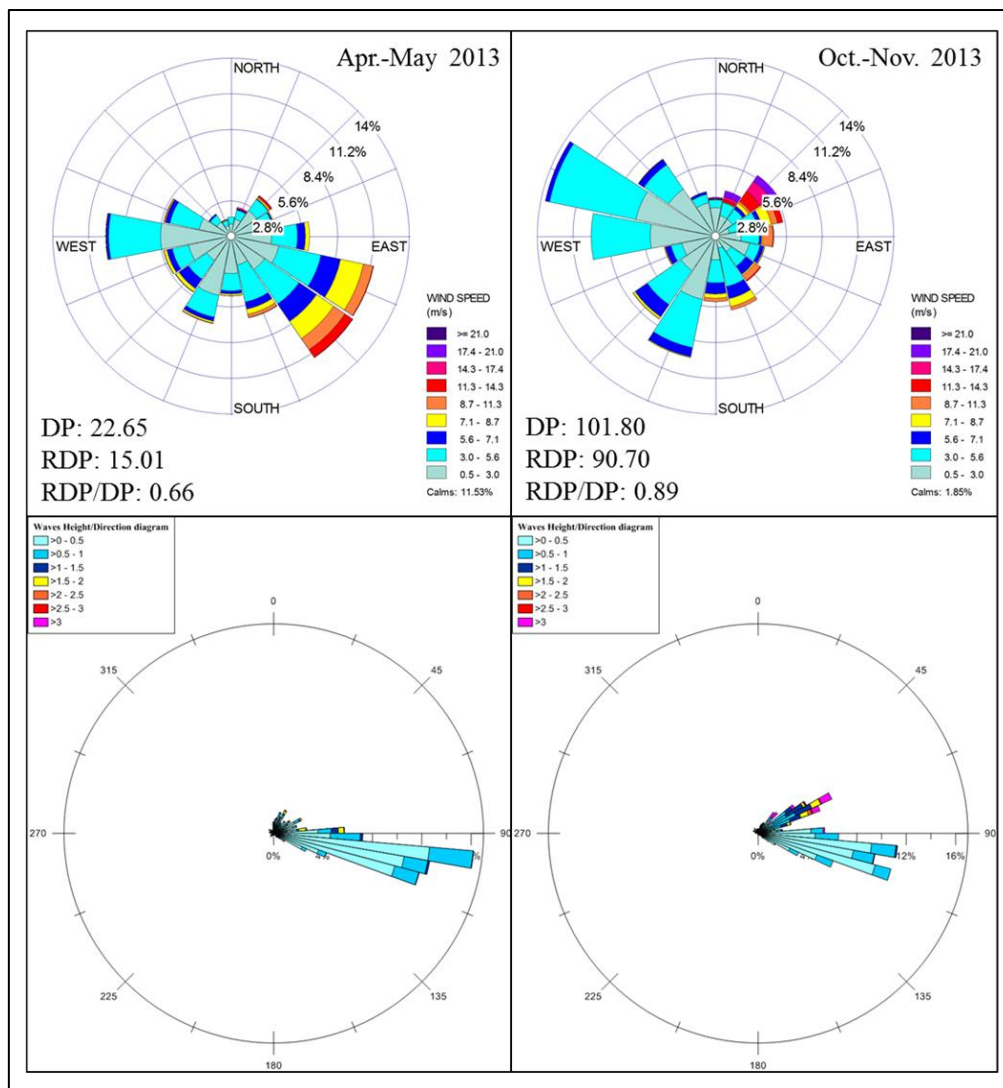


Figure 6.1: wind and sea rose diagrams for the two compared periods.

The first period examined started in April the 9th and ended the successive May the 29th; this period was rather calm for what concerns both wind and sea condition: data showing this are plotted in figure 6.1, including drift potential calculations, which reported a 22.65 uv value.

The total amount of sand movement, after 50 days, indicates deposition, with the value of about 80 m³. The second period studied went from October the 17th 2013 to November the 18th, same year, for a last of 32 days and recorded a DP value of 101.80 uv due to the strength of winds. This particular survey was specifically done to record changes, 2 days after an intensive storm and reported a volume difference (in terms of erosion) of about -370 m³ (figure 6.2).

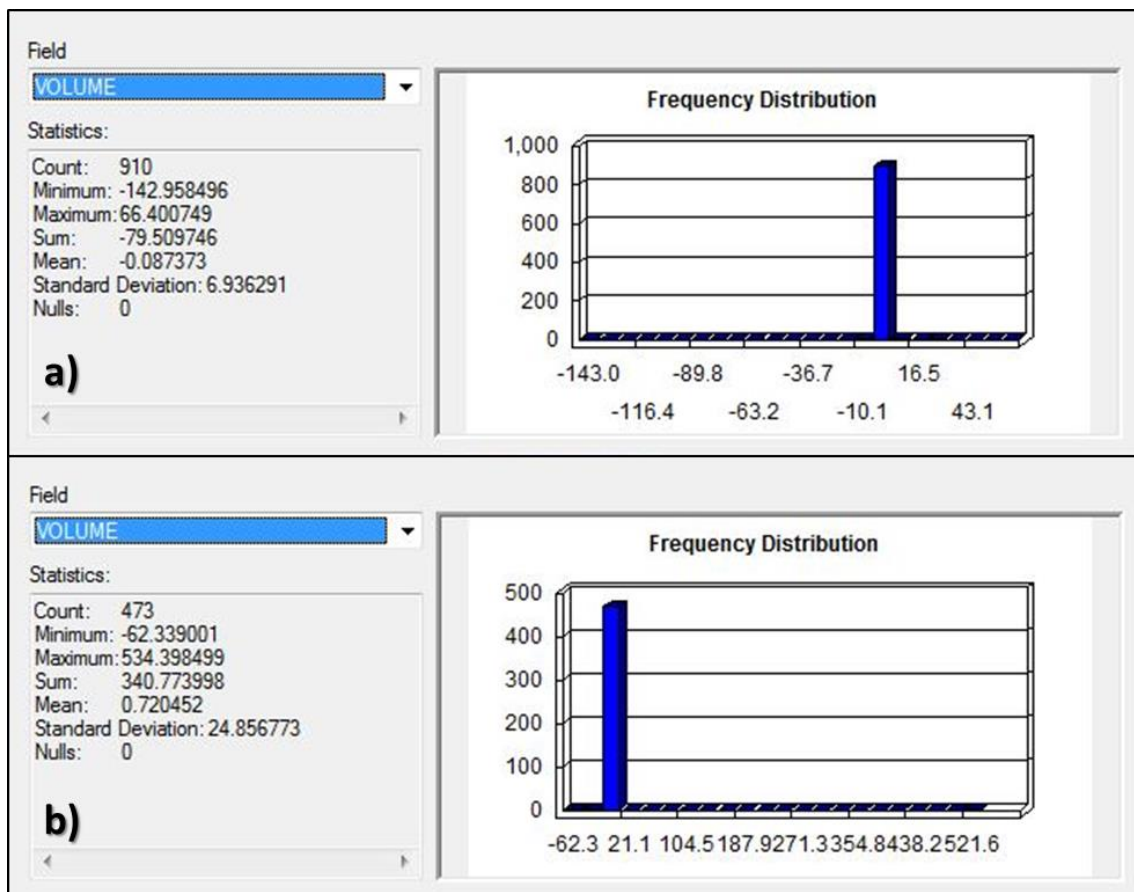


Figure 6.2. "Cut and fill" statistics relative to the two compared periods: a) April to May; b) October to November.

This value is not even comparable to the previous one, in spite of the shorter last of the surveyed period, prove that the volume value is probably strictly influenced by short high energy events, while, in other periods, changes more the foredune morphology than the real mass of sand.

Marina di Ravenna volume seasonal oscillations resulted to be slightly more aligned, even if they don't indicate any pattern. The two winter periods indicated an almost identical behavior, with the same deposition amount, while the two summer periods were much more variable. This is probably in part connected to the weather conditions (the 2013 summer was much milder than the 2012), in part to the human impact and management of the beach (the "false foot" vegetation inducing deposition).

In the previous chapter it was explained how during summers probably the dune behavior deviates from its natural status, due to the vegetated "false foot" in front of the north part of real foredune. Summers maps in figure 5.5 clearly show a preferential area of sand deposition in north part, while the rest dune field is most of all affected by erosion.

Moreover this is in a marked opposition to the south blowout behavior, which at the end of each summer (even the 2013 mild one) results broken in its depositional lobe, confirming the erosion pattern. Individuating this dynamic highlighted a specific critical situation for this site: this erosional trend, in fact, has not only the consequence on that spot but onto the whole neighborhood which is affected by the typical sand remobilization from blowout depositional lobe (figure 6.3).



Figure 6.3: Marina di Ravenna sand remobilization. Pictures taken in October 2013, at the same time of the TLS survey.

It is known (Hesp P., 1991) that this process can have strong effects on a wider area because the remobilized sand typically bury and kill other vegetation in the landward area (plots resistant to sand bury are on the seaward side).

In next years some management actions to stop this dynamic will must be taken to avoid the situation become irreparable. Building fences and seeding plants probably are the first and more realistic actions to do as soon as possible.

The Milano Marittima survey shows alignment of sign but not of data. Unfortunately this is the site where the human impact is the highest. Beyond the few buildings located on the beach in front of the dune, there the problem of the management which often implicates the use of caterpillar even on the dune to rectify the dune foot line.

During the last survey, in May 2014, the author discovered that this treatment is not limited to the dune foot line, but sometimes caterpillars “manage” the sand even on the dune body. Figure 6.4 is a perfect example of this on the north corner of the dune appeared a brand new ramp of sand, clearly made by humans.

In any case the dune shown to be still active and demonstrated erosion during both summers and deposition during winters

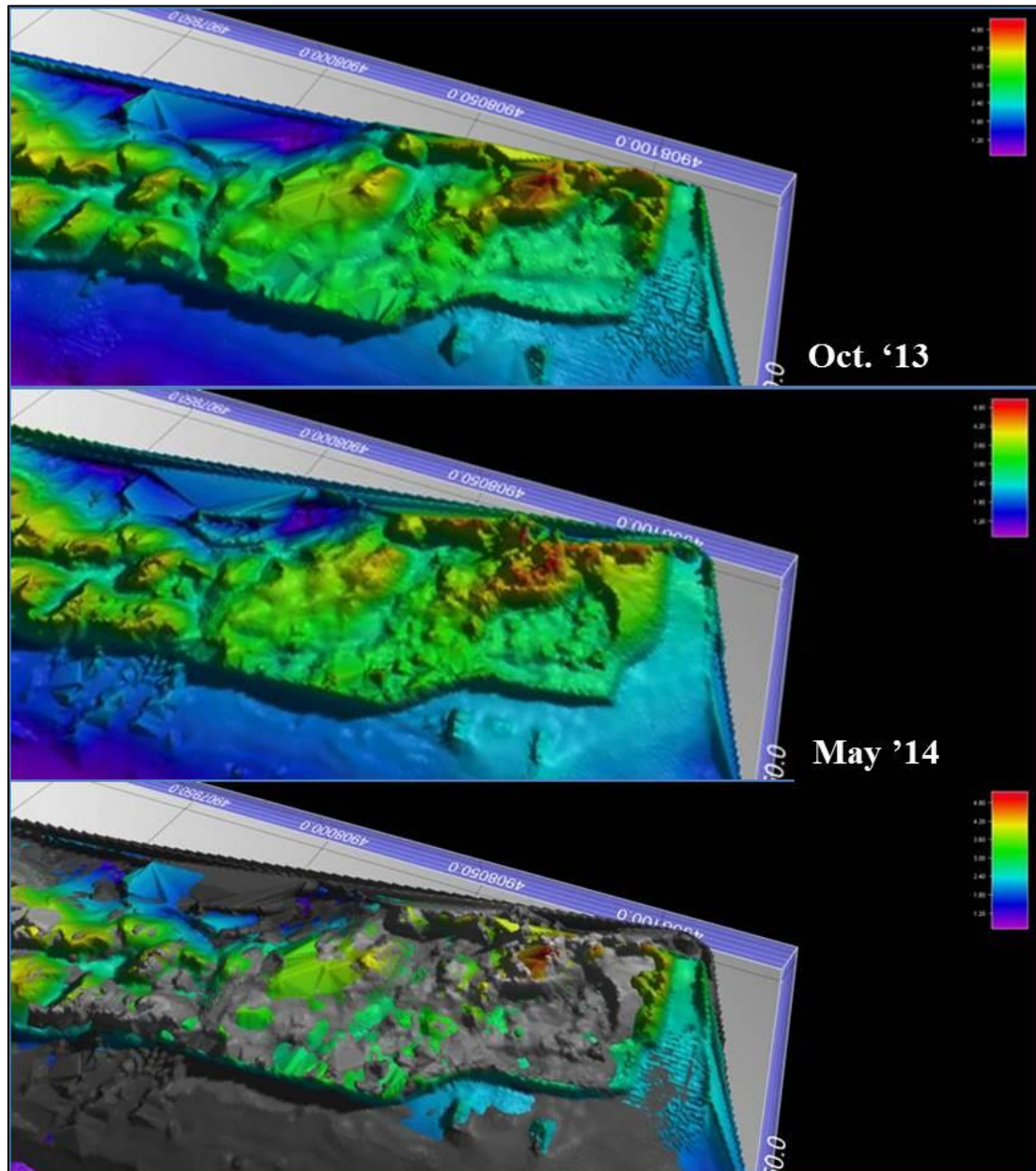


Figure 6.4: morphological differences between last two surveys, Milano Marittima

6.2 Meteorological Data and Multivariate Analysis.

6.2.1 Aeolian data conclusions.

Wind data analysis was one of the fundamental parts of this study. Relative results were for a large part expected, but not for all. The analytic method applied, carrying parallel studies on coarse wind data and drift potential calculation, unfortunately was limited by the lack of comparable data before 2012.

Checking data from the National Network Tide Gauge, it was possible going back up to 1998, but the time scale changed starting from 2011, when the sensor caught one datum every 30 minutes, and so on before that year. This made impossible comparisons at drift potential level, which for this research was based on every 10 minutes data. Thus it was a choice of the author to limit the analysis to 2012 and on, with the hope that this work won't end with this thesis and that it will be helpful for some other future work.

Anyway yearly reconstruction of wind climate for both 2012 and 2013 were so fitting to let the author consider that they are anyway representative of the local conditions. This is true not only for the coarse data examination, but for the drift potential too. Thus in conclusion, the local wind climate of this area, foresees a regency of offshore winds, especially those which come from West on West-North-West quadrant, "Ponente" or "Maestrale" while the dominance is taken by onshore winds, most of all those coming from North-East, "Bora", and "South-East", "Scirocco". These results find confirmations in literature (Deserti M. et al, 2011; Perini L. et al 2010).

More interesting and unexpected was the seasonal distribution of these winds: the winter season appears to be the monopoly of offshore winds, but this is only in part true, because the frequency of onshore wind is pretty low, even if the maximum speeds reached are the highest of the whole year. During summers data highlighted a much more variable condition.

Offshore wind are still most frequent than any other, but strictly followed by onshore ones (North-East and South-East at 2nd and 3rd place in 2012), so these are much more frequent than during winter, but with a lower peak velocity.

What was unexpected is the frequency of along shore winds which revealed an important presence in the yearly frequency tables. Moreover checking carefully table

presented in table 4.10, it is clear how alongshore winds, in terms of percentage of effective speeds, are comparable to the offshore winds percentages and in several cases they are higher.

Sand roses diagrams achieved thanks to the Fryberger's method helped to better determinate this climate "profile". Yearly graph are very similar one to each other and indicate a "Wide Bimodal" drift potential climate, based on the fundamental contribution of Scirocco wind and Bora wind. The resultant hypothetical transport would be directed to South-West, indicating that the Bora's effect is stronger than Scirocco's one.

Seasonal sand roses were not so interesting, and much more variable. The summer 2013 sand rose was the one less aligned with the others of all data set; in spite of this it was the one interesting: checking frequencies tables relative to the two summers and considering only effective winds what missed in 2013 was the contribution of alongshore winds, especially those coming from North and North-East ("Tramontana") (table 6.1).

6. Conclusions

	7.1 - 8.7	8.7 - 11.3	11.3 - 14.3	14.3 - 17.4	17.4 - 21.0	DP's
N	0.03	0.04	0.13	0.08	0.00	3.13
NNE	0.17	0.30	0.23	0.13	0.02	6.66
NE	0.10	0.31	0.30	0.17	0.02	8.38
ENE	0.19	0.17	0.06	0.02	0.00	1.69
E	0.19	0.17	0.02	0.00	0.00	0.81
ESE	0.55	0.30	0.00	0.00	0.00	1.12
SE	0.33	0.17	0.07	0.02	0.00	1.63
SSE	0.42	0.21	0.06	0.02	0.00	1.70
S	0.17	0.11	0.02	0.00	0.00	0.60
SWS	0.07	0.01	0.00	0.00	0.00	0.10
SW	0.79	0.14	0.00	0.00	0.00	0.79
WSW	0.16	0.05	0.00	0.00	0.00	0.22
W	0.02	0.01	0.00	0.00	0.00	0.04
WNW	0.05	0.00	0.00	0.00	0.00	0.02
NW	0.02	0.00	0.00	0.00	0.00	0.14
NNW	0.05	0.00	0.00	0.00	0.00	0.15
TOTAL	3.29	2.00	0.90	0.42	0.05	27.18

	7.1 - 8.7	8.7 - 11.3	11.3 - 14.3	14.3 - 17.4	17.4 - 21.0	DP's
N	0.15	0.12	0.01	0.00	0.00	0.52
NNE	0.16	0.18	0.10	0.03	0.00	2.25
NE	0.20	0.19	0.07	0.02	0.00	1.80
ENE	0.26	0.18	0.01	0.00	0.00	0.76
E	0.18	0.29	0.02	0.00	0.00	1.11
ESE	0.93	0.21	0.00	0.00	0.00	1.05
SE	0.48	0.21	0.18	0.01	0.00	2.81
SSE	0.36	0.21	0.02	0.00	0.00	0.98
S	0.12	0.06	0.01	0.00	0.00	0.30
SWS	0.07	0.02	0.00	0.00	0.00	0.10
SW	0.26	0.05	0.00	0.00	0.00	0.31
WSW	0.14	0.01	0.00	0.00	0.00	0.10
W	0.06	0.01	0.00	0.00	0.00	0.10
WNW	0.11	0.04	0.00	0.00	0.00	0.21
NW	0.02	0.00	0.01	0.00	0.00	0.00
NNW	0.04	0.04	0.00	0.00	0.00	0.00
TOTAL	3.54	1.84	0.45	0.07	0.00	0.00

Table 6.1: summer 2013 frequency table. In red alongshore quadrants and frequencies.

6.2.2 *Principal Component Analysis (PCA).*

PCA confirmed its valor as powerful and robust technique to identify dominant patterns of change in meteorology and coastal sciences (Houser et al., 2008). Vectors graphs resulted from the three PCA conducted have already been shown and discussed in the previous chapter. In this paragraph the author will just highlight most important results.

First of all meteorological data themselves gave some interesting results: effective offshore winds didn't show any positive correlation to any factor in all three tests, while it always shown a strong negative connection to the Drift Potential.

The Directional Variability Index instead had just one connection with White dune area. It could be intriguing even to know why the maximum storm waves height could be connected to the maximum water level, while the average waves height is more correlated to wind factors (DP or R.D.).

The intense positive correlation between volume variations and storms cumulative last was credible, meaning that volume changes are more linked to sea conditions than to winds; this is what resulted from the morphological analysis too, thus it could be considered more than plausible.

Every morphological feature analyzed for this study (Volume and Area differences, Sub-Zone spatial changes and blowouts cover) resulted to be linked somehow to effective alongshore winds, and this is very interesting, especially thinking that this particular winds have a slice of provenience lower than others (70° instead if 145°). Effective alongshore winds percentage thus is the factor most attracted interest: the vector representing its variability, in fact, resulted strongly correlated in a positive way especially with white dune surface variations, as well as to the blowouts. In graph 5.14 it can be seen how the letters labelling relative vectors are not even noticeable (BO and Wa), because of the superimposition of the two vectors. Obviously this forcing factor is negative correlated to the grey dune.

This was not expected; on one hand because of the lack of studies about alongshore winds, especially in this particular part of the world, on the other hand because of the narrowness of the slice of provenience. This is one of the most intriguing result that emerged by this study and it is opinion of the author that a branch of research on these particular meteorological topic should be opened.

Another really interesting feature appeared from PCA graph is the diametrically opposite behavior of the White and the Grey dunes.

Beyond the dynamic that drive this datum, the very important fact is that this two zone shown a linked but completely different behavior, sign that they are really two different areas, in term of morphology and dynamic, but belonging to the same “body”. This fact confirms the validity of the morphological Sub-Zones proposition, and of the methodology applied.

Unfortunately Black dune data were able to be used in PCA, but it would be very interesting test it too. In any cases it was very helpful in individuating particular events, and, at least, confirmed the double worth of this method.

6.2 Digital Shoreline Analysis System (DSAS) and computational Fluid Dynamic (CFD) conclusions.

In this study the Terrestrial Laser Scanner (TLS) has confirmed itself as a powerful tool to applicate both in practical environmental monitoring and in pure theoretical research. In this meaning the application of TLS data to DSAS or CFD analysis wanted to explore some new potentialities of this tool in order to purpose fundamentally a new level of use.

The application of DSAS tool on the dune foot line and the dune crest line revealed by TLS data was made to purpose not only a new detail of analysis which seems to be really fitting with TLS features, but also in order to answer a claimed need of new features to monitor in coastal sand dunes environments.

Having said that, the research have given positive feedbacks in both senses: according to the author both the foot line and the crest line movements’ analysis was satisfying and it could be the first step in a new path of monitoring features.

Several works can be found in literature which already applied this tool to the dune foot line (Crespo Jones H., 2013; Pallottini G. et al, 2008), usually basing the analysis on airborne LIDAR or photographicical data, but this was never done (in the knowledge of the author) on TLS data with that possibility of detail (a resolution grid of 0.25 m²).

The dune foot line instead was never tested with this technique and gave, especially for what concerns the Bevano natural area interesting results strongly aligned with what was expected. This work shows that this feature's behavior should be better investigate, monitoring its movements, beyond its fragmentation; this could be also an interesting and brand new method to evaluate the dune stability, especially comparing to the foot line behavior.

The DSAS analysis, moreover, could be used to identify particular situations, for example critics conditions in damaged spot of the dune body, being in this meaning a new tool for dune management, which would allow intervening on a punctual spatial and temporal scale.

The Computational Fluid Dynamics test was applied to test the TLS suitable for this kind of brand new studies (CFD). In the perspective of substitute wind flow tunnel by this new branch of research, laser scanner data could be the best fitting and "natural" integration. It could supply the proper base for computational dynamics modeling, reproducing every kind of general or specific environment.

In these years several project acknowledge this idea, and many authors produced results in this sense using both airborne or terrestrial laser data, but applying CFD above all to urbanized territories (Mandlbürger, G. et al., 2008; Maragkogiannis K. et al, 2013).

In this study the particular test gave some very positives results, but beyond this it gave positive feedback and ideas. According to the author further develops of CFD application to sand dunes environment should be directed to find a way to introduce the vegetation component and its interaction with wind. This could allow also to better investigate the TLS possibilities of interaction with CFD.

References

- AA.VV., CALABRESE L., PERINI L., 2009. *Foce Bevano: l'area naturale protetta e l'intervento di salvaguardia* Assessorato alla sicurezza territoriale difesa del suolo e della costa protezione civile. Centro Stampa della Regione Emilia-Romagna. 1-10.
- AA.VV., PERINI L., E CALABRESE L., 2010: *Il sistema mare-costa dell'Emilia-Romagna*; Bologna: Pendragon. Monografie ISBN 978-888342847. 87-98
- AA.VV., PERINI L., E CALABRESE L., 2011. *Le mareggiate e gli impatti sulla costa in Emilia-Romagna 1946-2010*. I quaderni di Arpa. Arpa Emilia-Romagna, 33-41.
- ANGELOPOULOU, ELLI and WRIGHT, JOHN R. JR., 1999. *Laser Scanner Technology*. Technical Reports (CIS). Paper 74.
- ARENS S.M., Q. SLINGS AND C.N. DE VRIES, 2004. *Mobility of a remobilised parabolic dune in Kennemerland, the Netherlands*. *Geomorphology* 59: 175-188.
- ARMAROLI C., CIAVOLA P., PERINI L. & LUCIANI P., 2007. *Morfologia delle spiagge ravennati e vulnerabilità per fenomeni di inondazione*. In: Terzo Forum Nazionale, Pianificazione e tutela del territorio costiero; questioni, metodi, esperienze a confronto, vol. 127, pp. 363-389.
- BAGNOLD, R.A., 1941. *The physics of blown sand and desert dunes*. Methuen, London. 265
- BAGNOLD, R.A. 1960. *Sediment discharge and stream power; a preliminary announcement*. U.S. geol. Surv. Circular. 421
- BARRÈRE P., 1994. *Dynamics and management of the coastal dunes of the Landes, Gascony, France*. Coastal Dunes, Carter, Curtis & Sheehy-Skeffington (eds) Balkema, Rotterdam. ISBN 90 5410 058 3. 25-32.
- BERTONI W., BRIGHENTI G., GAMBOLATI G., GATTO P., RICCERI G., VUILLERMIN E., 1988, *Risultati degli Studi e delle Ricerche sulla Subsidenza di Ravenna*. Comune di Ravenna.
- BEZZI A, FONTOLAN G., NORDSTROM K.F., CARRER D., JACKSON N.L., 2009. *Beach nourishment and foredune restoration: practices and constraints along the venetian sholine, Italy*. *Journal of coastal research*. Special Issue 56.
- BONDESAN M., FAVERO V., VIGNALS M.J. 1995. *New evidence on the evolution of the Po-delta coastal plain during the Holocene*. *Quaternary International*, 29/30, pp. 105-110, 5.
- BORCARD D., GILLET F., LEGENDRE P., 2011. *Numerical Ecology with R*, Use R, DOI 10.1007/978-1-4419-7976-6_5, © Springer Science+Business Media, LLC 281-297.
- BULLARD, J. E. 1997. *A Note on the Use of the 'Fryberger Method' for Evaluating Potential Sand Transport by Wind*. *J. Sediment. Res.* 67(3A): 499-501.

- CANESTRELLI P., MANDICH M., PIRAZZOLI P.A. AND TOMASIN A., 2001. Wind, depression and seiches: tidal perturbation in Venice (1951, 2000). Venice, Italy: Comune di Venezia, Centro Previsioni e Segnalazioni Maree, pp. 105.
- CARTER R.W.G., WILSON P. 1990. *The geomorphological, ecological and pedological development of coastal foredunes at Magilligan Point, Northern Ireland*. In K Nordstrom, N Psuty and B Carter, eds., Coastal dunes: form and process. Wiley, Chichester. 129-157
- CREMONINI S., 2007. *Some remarks on the evolution of the Po River plain (Italy) over the last four millennia*. In Marabini F., Galvani A., Ciabatti M. (Eds.) China-Italy bilateral symposium on the coastal zone: evolution and safeguard, 4-8 November 2007. Lo Scarabeo, Bologna, 17-24.
- DAVENPORT, A.G., 1960. *Rationale for determining design wind velocities*. Journal of the Structural Division, American Society of Civil Engineers, 86, pp. 39–68.
- DEACON E.L., 1949. *Vertical diffusion in lowest layers of the Atmosphere*. Royal Meteorological society. Quaternary Journal, vol. 75, n. 323, 89-103.
- DESERTI M., PERINI L., LORITO S., 2011. *Il clima meteo-marino del bacino adriatico nel settore emiliano romagnolo*. Regione Emilia-Romagna. Servizio Geologico Sismico e dei Suoli. 1-8.
- FABBRI P., 2001. *Studio sul sistema costiero del Comune di Ravenna*. Comune di Ravenna, Rapporto interno. 146.
- HAILS J.R., BENNET J.M., 1981. *Wind and sediment movement in coastal dune areas*. Proc. 17th Internet. Coastal Engineering Conf. ASCE, New York. 1565-1575.
- HESP, P.A., 1991. *Ecological processes and plant adaptations on coastal dunes*. J. Arid Environments 21: 165-191
- HESP P.A., 1999. The beach backshore and beyond. In: Short, A.D. (Ed.), Handbook of Beach and Shoreface Morphodynamics. Wiley, London. 145-170.
- HESP P.A., 1996. *Flow dynamic in a trough blowout*. Boundary-layer Meteorology 77: Kluwer academic publisher. 305-330
- HESP P.A., 2000. *Coastal Sand Dunes form and function*. Forest Research (coastal dune vegetation network). CDVN technical bulletin No. 4.1-24
- HESP P.A., 2002 *Foredune and blowouts: initiation, geomorphology and dynamics*. Geomorphology 48 245-248.
- HESP P.A., DAVIDSON-ARNOFF, R., WALKER, I.J., OLLERHEAD, J., 2005. *Flow dynamics over a foredune at Prince Edward Island, Canada*. Geomorphology 65 (1–2), 71–84
- HESP P.A., Walker I.J., 2012. *Coastal Dunes*. In: Treatise on Estuarine and Coastal Science. Volume 3, Estuarine and Coastal Geology and Geomorphology. Elsevier. ISBN: 978-0-12- 374711-2.
- HESP P.A., 2012. *Surfzone-beach-dune interactions*. Jubilee Conference Proceedings, NCK-Days. 35-40.
- HIMMELSTOSS, E.A., 2009. *DSAS 4.0—Installation Instructions and User Guide*. In: Thieler, E.R., Himmelstoss, E.A., Zichichi, J.L. and Ergul, A., Eds., The Digital Shoreline Analysis System (DSAS) Version 4.0—An ArcGIS Extension for

Calculating Shoreline Change: US Geological Survey Open-File Report 2008-1278, ver. 4.2. 81 p. <http://pubs.usgs.gov/of/2008/1278/>

HOTTA S., KUBOTA S., HORIKAWA K., 1984. *Sand transport by wind on a wet sand surface*. Proceeding of the 19th Coastal engineering conference.

HOUSER, C., HAPKE, C. AND HAMILTON, S., 2008. *Controls on coastal dune morphology, shoreline erosion and barrier island response to extreme storms*. *Geomorphology*, 100, 223-240

HSU, S.A., 1977. *Boundary-layer meteorological research in the coastal zone*. In: Walker, H.J. (Ed.), *Geoscience and Man*, V. of XVIII. *Research Techniques in Coastal Environments*. 99 – 111.

HSU, S.A., 1987. *Structure of air flow over sand dunes and its effect on eolian sand transport in coastal regions*. In: Kraus, C. (Ed.), *Coastal Sediments '87*. American Society of Civil Engineers, New York. 188 – 201.

INGENSAND, H., RYF, A. AND SCHULZ, T., 2003. *Performances and experiences in terrestrial laser scanning*. In *Optical 3-D Measurement Techniques VI*, A. Grün / H. Kahmen (Eds.). 1-67.

ISPRA 2010. *Rilievo di dettaglio della batimetria costiera laziale con tecnologie LIDAR e valutazione delle caratteristiche fisiche e biologiche in aree marine della costa laziale di specifico interesse ambientale. Fase 2 – Caratterizzazione morfologica*. Regione Lazio. 28-67.

JACKSON, D.W.T., BEYERS, J.H.M., COOPER, J.A.G., BAAS, A.C.W., DELGADO-FERNANDEZ, I., 2011. *Investigation of three-dimensional wind flow behaviour over a coastal dune morphology under offshore winds using computational fluid dynamics (CFD) and ultrasonic anemometry*. *Earth Surface Processes and Landforms* 36, 1113–1124.

JUNCIERUS P.D., VAN DRE MEULEN F., 1989. *The development of dune blowouts, as measured with erosion pins and sequential air photos*. *Catena* 16, 369-376.

KEIJSERS J., POORTINGA A., RIKSEN M., MARAULIS J., 2014. *Spatio-Temporal variability in accretion and erosion of coastal foredunes in the Netherlands: regional climate and local topography*. *PLoS ONE* 9(3): e91115. doi: 10.1371/journal.pone.0091115. 1-11

GABBIANELLI G., 2009. *L'area protetta di foce bevano*. In: *Foce Bevano: l'area naturale protetta e l'intervento di salvaguardia* Assessorato alla sicurezza territoriale difesa del suolo e della costa protezione civile. Centro Stampa della Regione Emilia-Romagna. 8

INGENSAND, H., 2006. *Methodological aspects in terrestrial laser-scanning technology*. In *Proceedings of the 3rd IAG Symposium of Geodesy for Geotechnical and Structural Engineering and 12th FIG Symposium on Deformation Measurements*. May 22 – 24, Baden, Austria. On a CD.

LACASTER N., 2012. *Aeolian Processes*. In: *Treatise on Estuarine and Coastal Science*. Volume 3, *Estuarine and Coastal Geology and Geomorphology*. Elsevier. ISBN: 978-0-12- 374711-2.

LETTAU, K., LETTAU, H.H., 1978. *Experimental and micrometeorological field studies on dune migration*. In: Lettau, K., Lettau, H.H. (Eds.), *Exploring the World's*

Driest Climate. University of Wisconsin-Madison, Institute for Environmental Studies. 110– 147.

LINDSAY I., SMITH A., 2002. *A tutorial on Principal Components Analysis*, February 26, 2-11.

MANCINI F., DUBBINI M, GATTELLI M, STECCHI F., FABBRI S., GABBIANELLI G., 2013. *Using Unmanned Aerial Vehicles (UAV) for high resolution reconstruction of topography: the Structure from Motion approach on coastal environments*. Remote Sensing. ISSN 2072-4292. 6880-6898.

MARTÍNEZ M.L., PSUTY N.P. and LUBKE R.A., 2004. *A Perspective on Coastal Dunes*. Ecological Studies, Vol. 171 M.L. Martínez, N.P. Psuty (Eds.) Coastal Dunes, Ecology and Conservation © Springer-Verlag Berlin Heidelberg 2004. 3-7.

MAUN A., 2009. *The Biology of Coastal Sand Dunes*. Oxford UK: Oxford University Press.1-22

MCKEE, E.D. 1979. *A Study of Global Sand Seas*. Geological Survey Professional Paper 1052. United States Department of Interior, Washington, DC. 137-169

MIOT DA SILVA G., HESP, P. (2010). *Coastline orientation, aeolian sediment transport and foredune and dunefield dynamics of Moçambique Beach, Southern Brazil*. Geomorphology, 120(3-4). 258-278.

MITASOVA, H., OVERTON, M., HARMON, R.S., 2005, *Geospatial analysis of a coastal sand dune field evolution: Jockey's Ridge, North Carolina*. Geomorphology 72. 204-221.

MOLLEMA P.N., ANTONELLINI M, MINCHIO A, GIABBIANELLI G., 2008. *The influence of three-dimensional Dune topography on salt water intrusion in Marina Romea. Italy: a numerical modeling study using Lidar data*. Proceedings of salt water intrusion meeting Naples, Florida, 23-27.

MONTREUIL, A-L., BULLARD, J.E., CHANDLER, J.H., 2013. *Detecting seasonal variations in embryo dune morphology using a terrestrial laser scanner*. Journal of Coastal Research, Special Issue No. 65, 1313-1318.

OLSON J.S., 1958. *Wind-velocity profiles*, Pt. 1 of Lake Michigan dune development. Journal of Geology, vol. 66, n. 3, 254-263.

OYEDOTUN T.D.T., 2014. *Shoreline Geometry: DSAS as a Tool for Historical Trend*. Geomorphological Techniques, Chap. 3, Sec. 2.2. British Society for Geomorphology. 1-12

PRANDTL, L. 1935. *The Mechanics of Viscous Fluids*. In: W.F, D. (ed.) Aerodynamic Theory III. Berlin: Springer.

PRANZINI E., (2004). *La forma delle coste*. Geomorfologia costiera impatto antropico e difesa dei litorali. Zanichelli. 2004. 108-125.

PASCHOTTA R., 2007 *Encyclopedia of Laser Physics and Technology*. Available from: <http://www.rp-photonics.com/encyclopedia.html>.

PSUTY, N.P., 1988. Sediment budget and beach/dune interaction, in: N.P. Psuty (Ed), Dune/Beach Interaction. J. Coastal

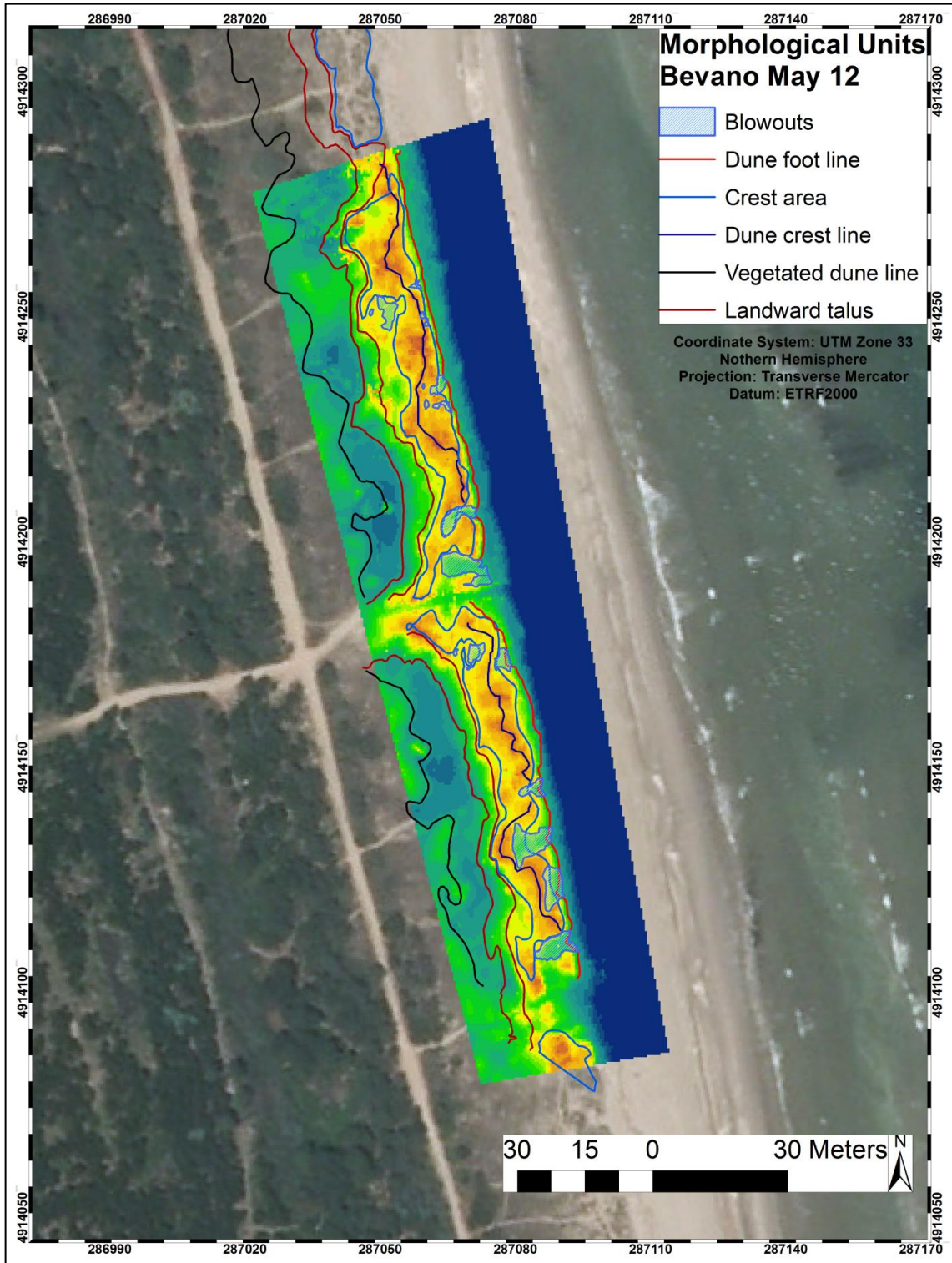
- Research Special Issue No. 3: 1-4. PSUTY N.P., 2004. *The Coastal Fore-dune: A Morphological Basis for Regional Coastal Dune Development*. Ecological studies, Vol 171. M.L. Martinez, N.P. Psuty (Eds.). Coastal Dunes, Ecology and Conservation. Springer-Verlag Berlin Heidelberg. 11-18
- PSUTY, N. P. and SILVEIRA, T. M., 2009. *Trend in fore-dune crestline displacement, Fire Island National Seashore, New York, USA, 1976-2005*. Journal of Coastal Research, SI 56 (Proceedings of the 10th International Coastal Symposium). Lisbon, Portugal, ISSN 0749-0258. 15-19.
- RUSSELL, P.E. AND O'HARE, T.J. (eds.), Proceedings 12^o International Coastal Symposium (Plymouth, England), Journal of Coastal Research, Special Issue No. 65, pp. 1313-1318, ISSN 0749-0208.
- SHANMUGAM S., NAYAK J., 2013. *Remote sensing and field studies to evaluate the performance of groynes in protecting an eroding stretch of the coastal city of Chennai*. GIS Ostrava 2013 - Geoinformatics for City Transformation. 1-10.
- SEYMOUR R.J., 2005. Cross-shore sediment transport. In: Encyclopedia of coastal science. Schwartz M. Spinger ed.. 352.
- SHORT A.D., WOODROFFE C.D., 2009. *The Coast of Australia*. Cambridge University Press, UK, 288.
- SMYTH T.A.G., JACKSON D.W.T., COOPER A.G., 2012. *High resolution measured and modelled three-dimensional airflow over a coastal bowl blowout*. Geomorphology., 177-178, 62-73.
- STAIGER, R., 2005. *The Geometrical Quality of Laser Scanner (TLS)*. In Proceedings of FIG Working Week 2005 and GSDI-8. Cairo, Egypt, April.URL: <http://www.fig.net/pub/cairo/index.htm>. 16 – 21
- STEFANI M., VINCENZI S., 2005. *The interplay of eustasy, climate and human activity in the late Quaternary depositional evolution and sedimentary architecture of the Po Delta system*. Marine Geology 222–223, 19–48
- THIEL, K.-H. AND WEHR, A., 2004. *Performance capabilities of laser scanners – an overview and measurement principle analysis*. Proceedings of the ISPRS working group VIII/2 “Laser Scanners for Forest and Landscape Assessment”. Freiburg, Germany, October 3. 14-18.
- THIELER, E.R., HIMMELSTOSS, E.A., ZICHICHI, J.L., AND ERGUL, AYHAN, 2009. *Digital Shoreline Analysis System (DSAS) version 4.0 — An ArcGIS*
- TOMASI, C., KANADE, T., 1992. Shape and Motion from Image Streams Under Orthography: A Factorization Method. Int. J. Comput. Vision, 9, 2, 137-154.
- VERSTEEG H.K., MALALASEKERA W., 1995. *An introduction to computational fluid dynamic*. The finite volume method. Longman Scientific & Technical. ISBN 0-582-21844-5. 1-31.
- YAKHOT, V., ORSZAG, S.A., THANGAM, S., GATSKI, T.B., SPEZIALE, C.G., 1992. *Development of turbulence models for shear flows by a double expansion technique*. Physics of Fluids A 4 (7), 1510–1520.
- WALKER I.J., PEARCE K.I., 2005. *Frequency and magnitude biases in the Fryberger model, with implications for characterizing geomorphically effective winds*. Geomorphology 68, 39 – 55.

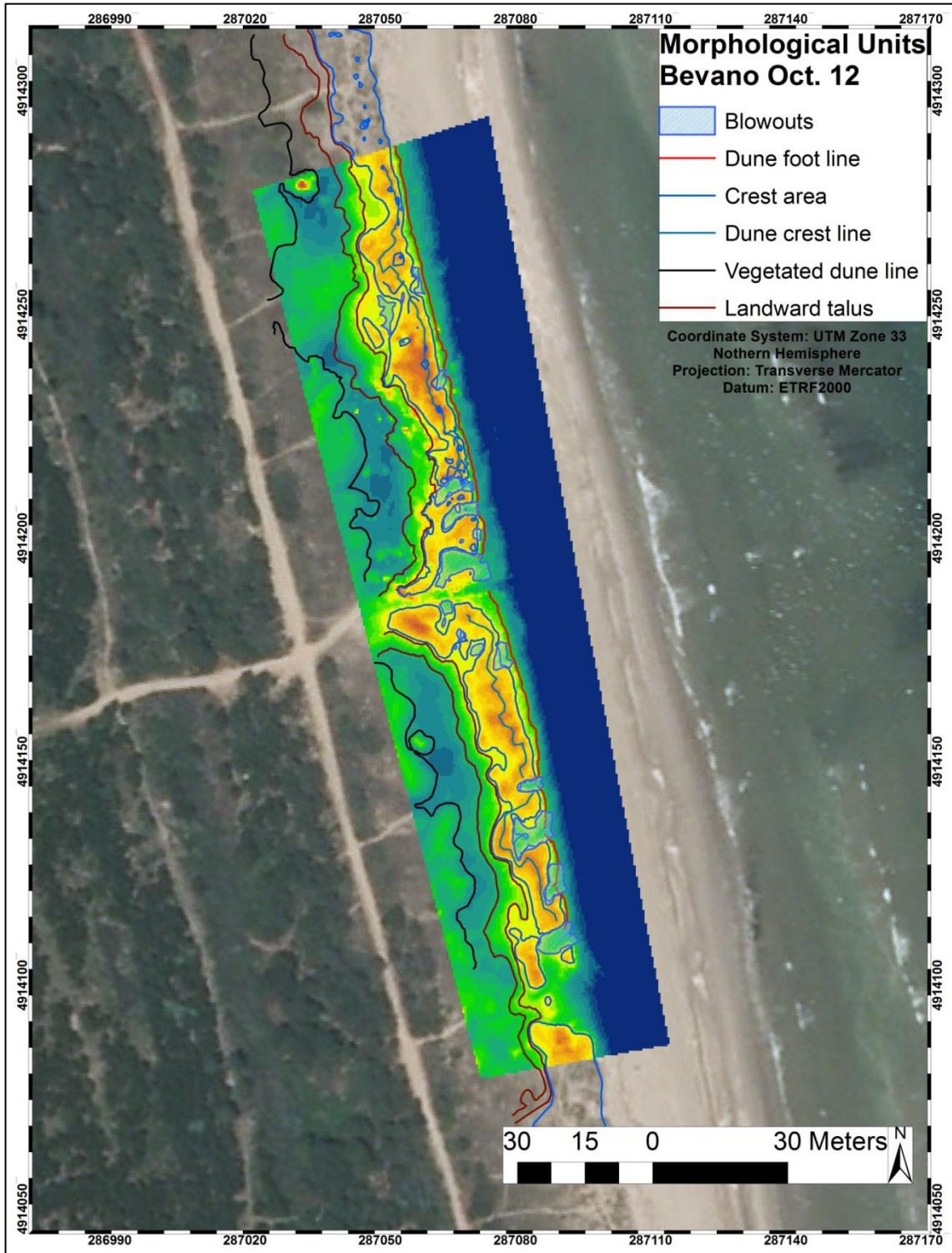
WALKER I.J., HESP P.A., 2012. *Fundamental of Aeolian sediment transport: airflow over dunes*. In: *Treatise on Estuarine and Coastal Science*. Volume 3, Estuarine and Coastal Geology and Geomorphology. Elsevier. ISBN: 978-0-12-3747.1278-1291.

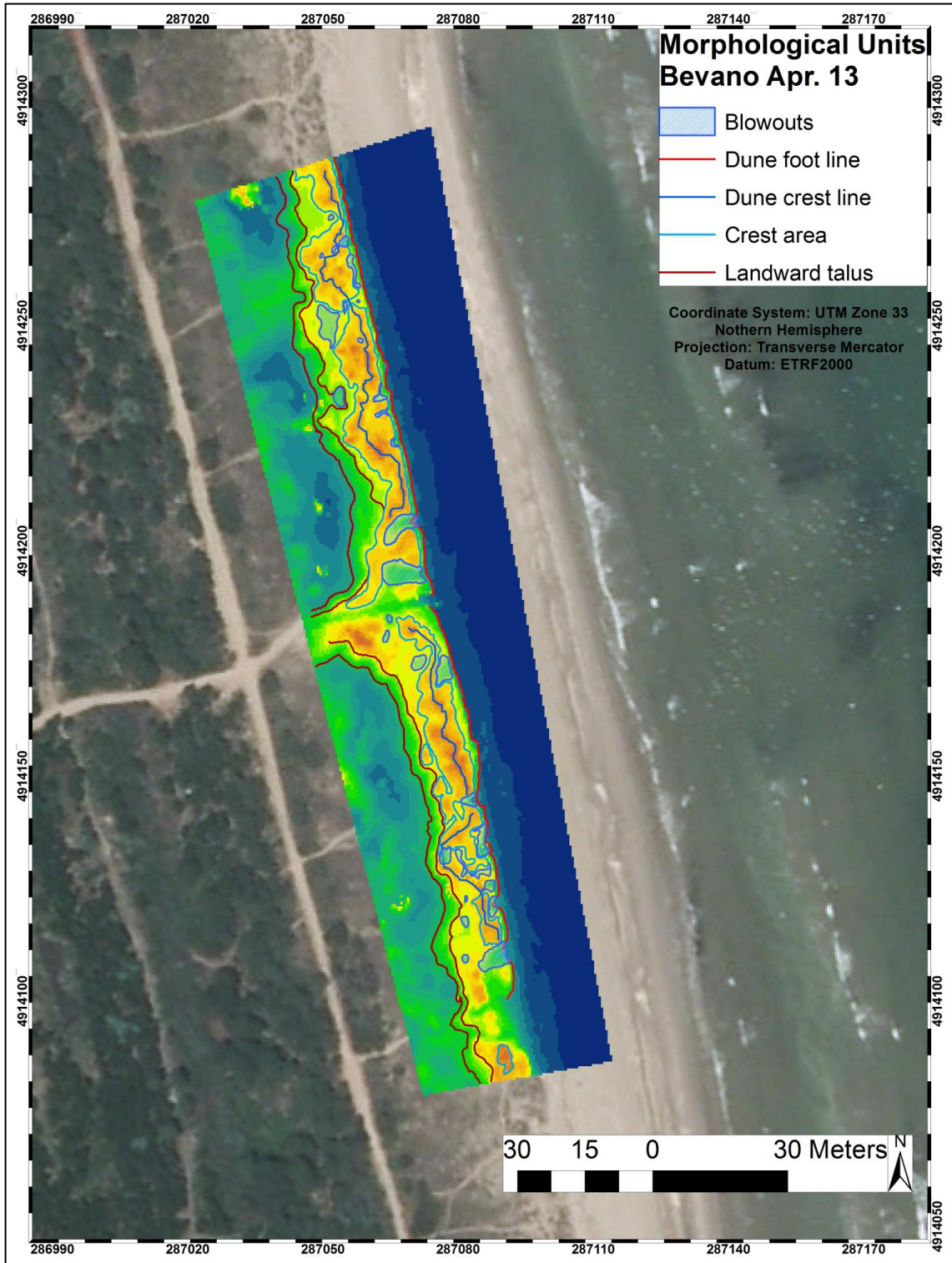
WIERINGA, J., 1980b: *Representativeness of wind observations at airports*. *Bulletin of the American Meteorological Society*, 61. 962–971.

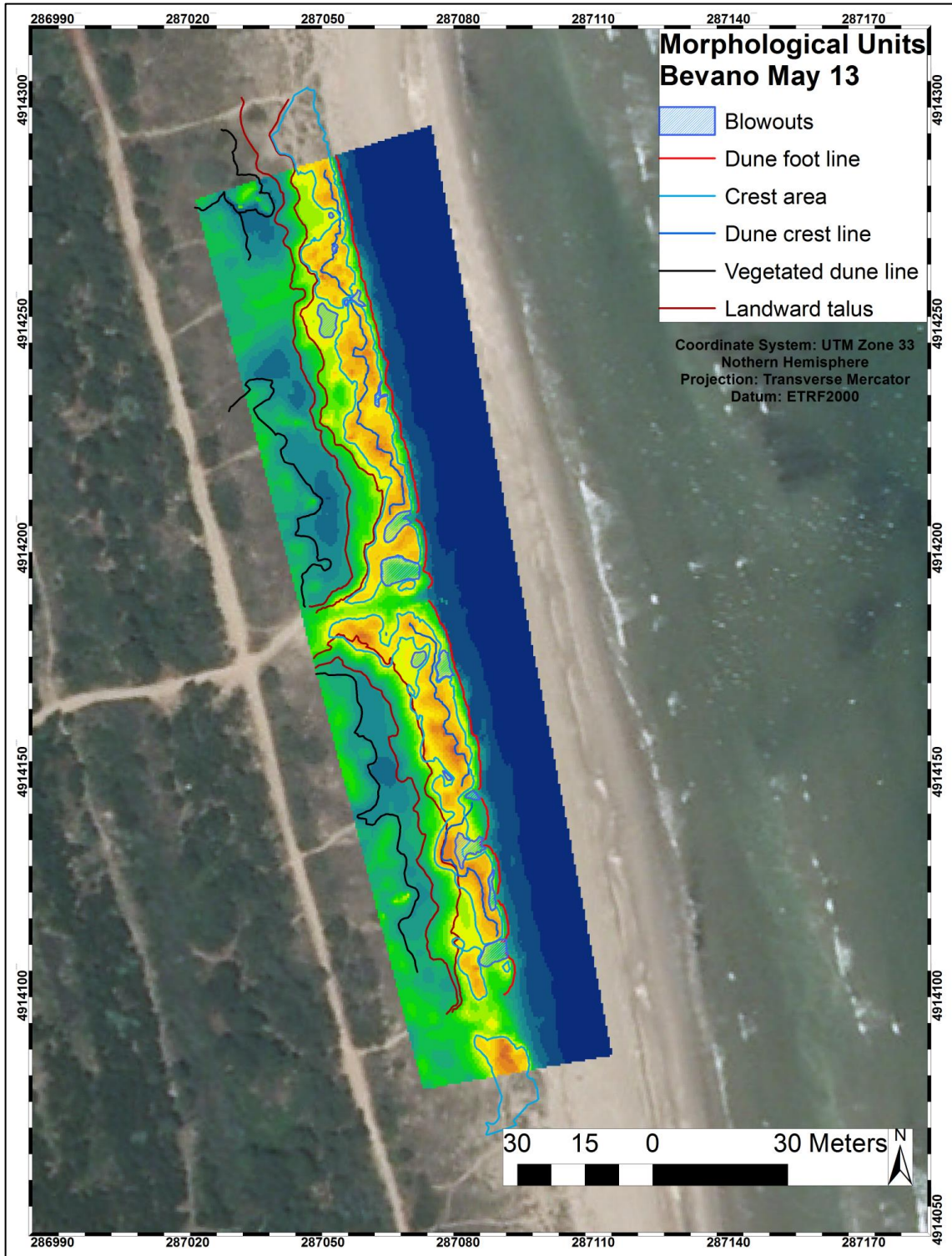
WORLD METEOROLOGICAL ORGANIZATION, 2008. *Guide to Meteorological Instruments and Methods of Observation*, WMO-No. 8 Seventh edition.

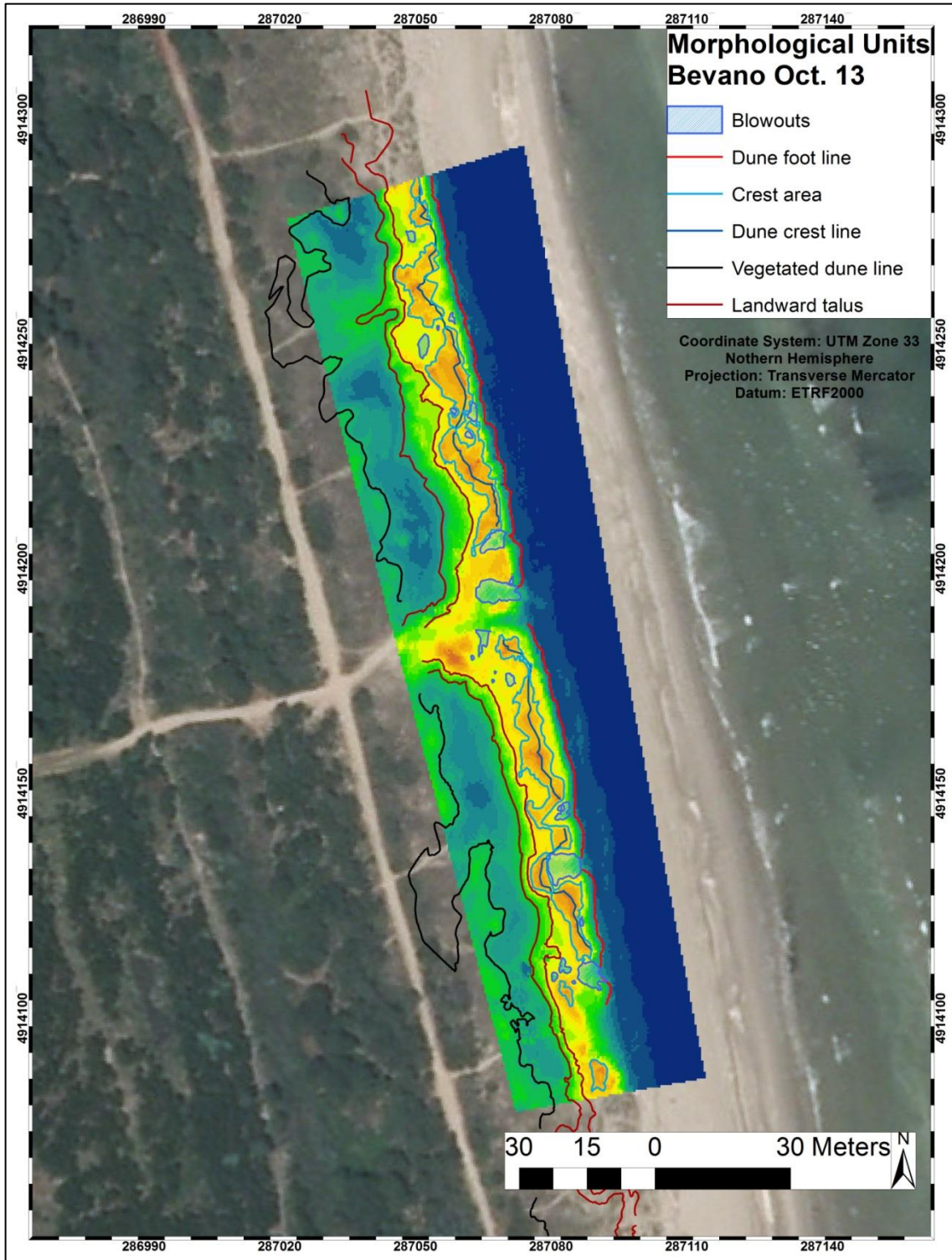
APPENDIX I (Morphological Units maps)

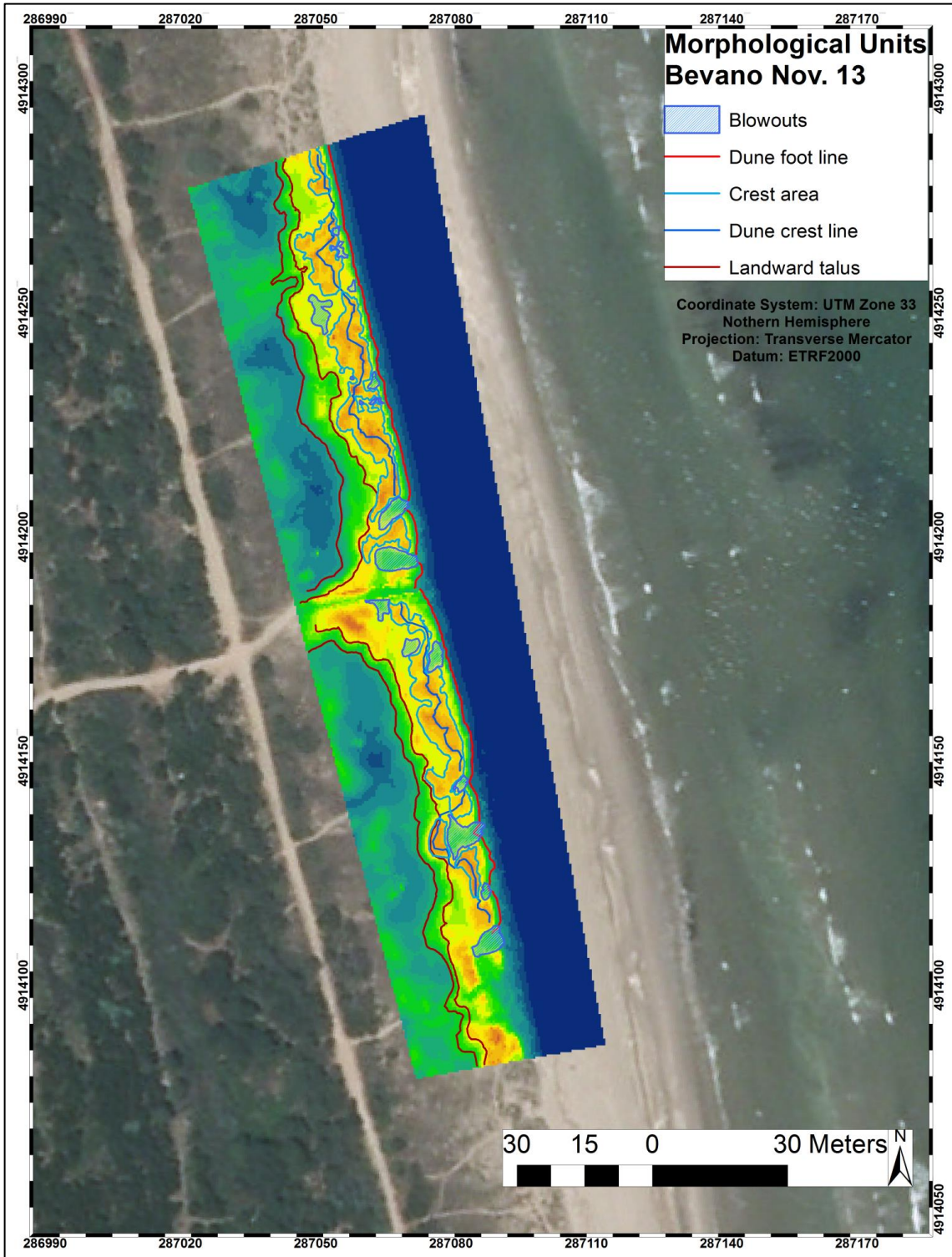


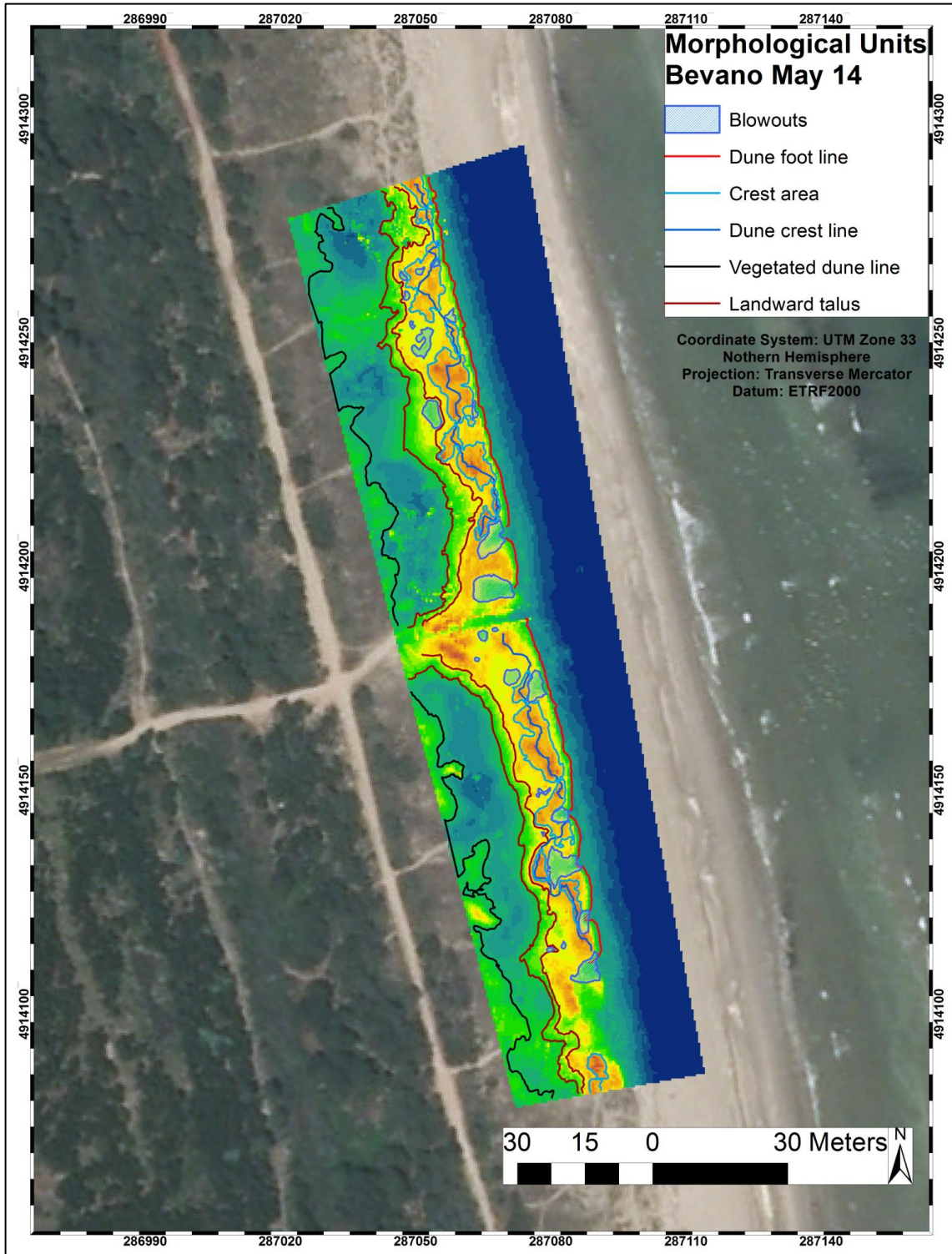


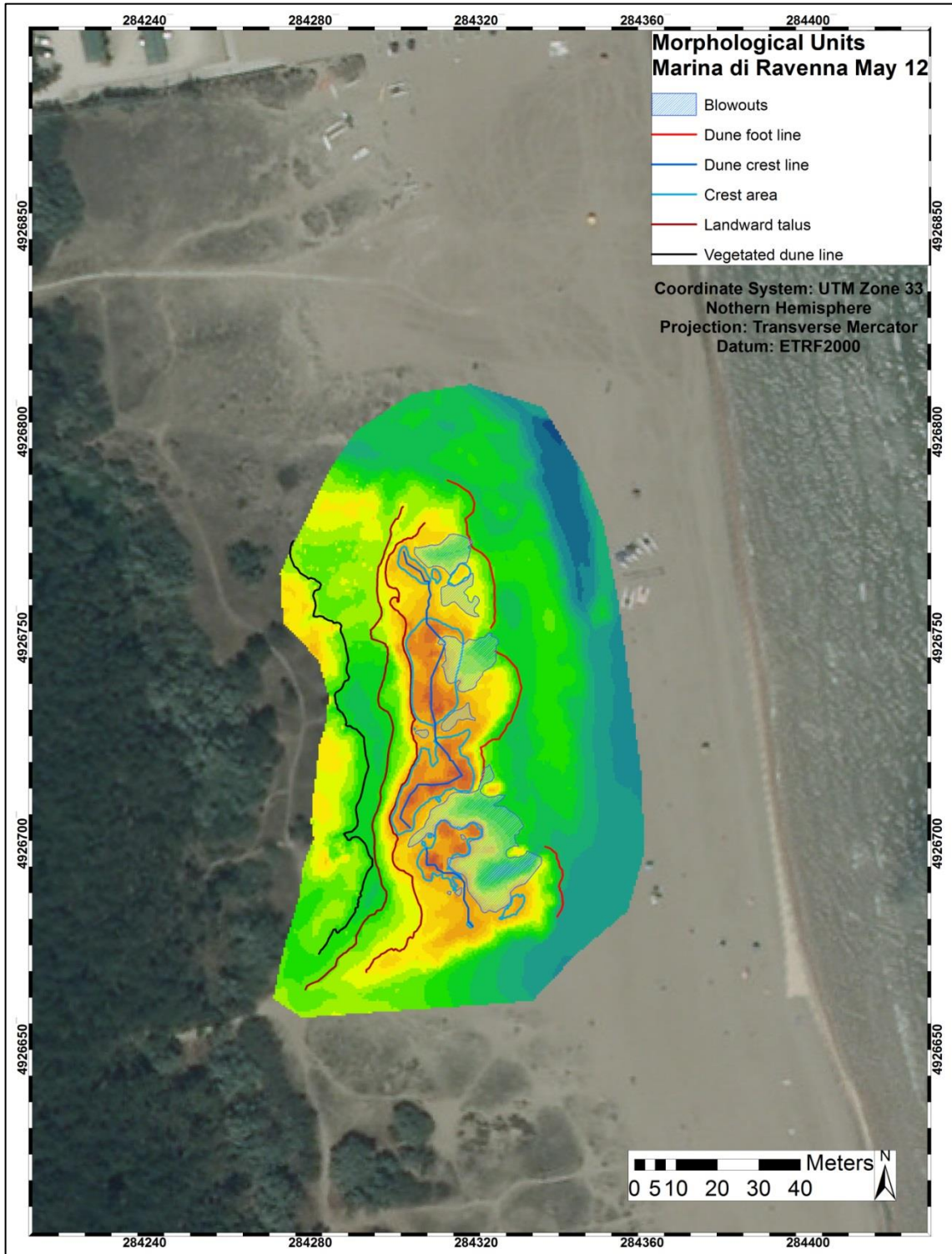


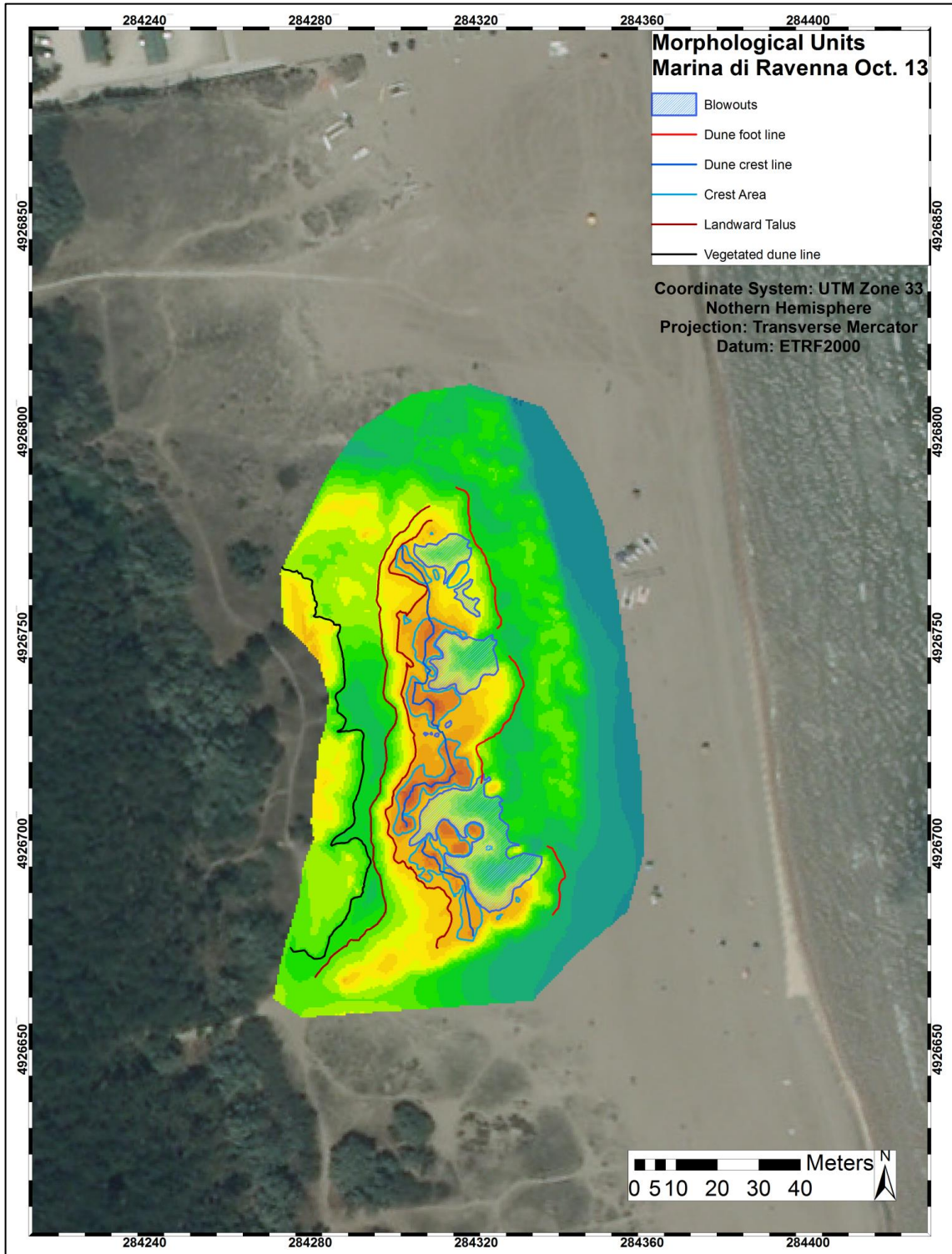


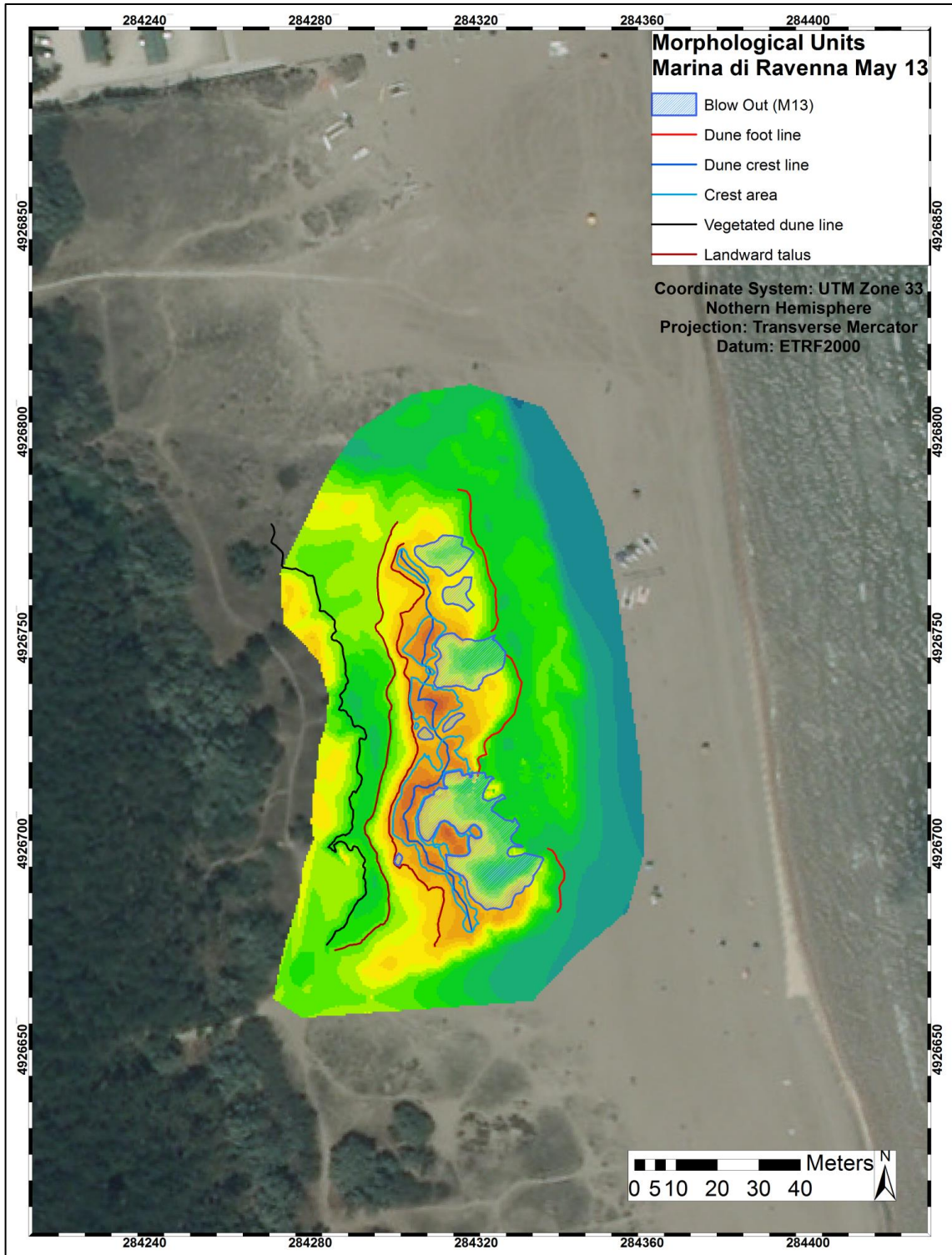


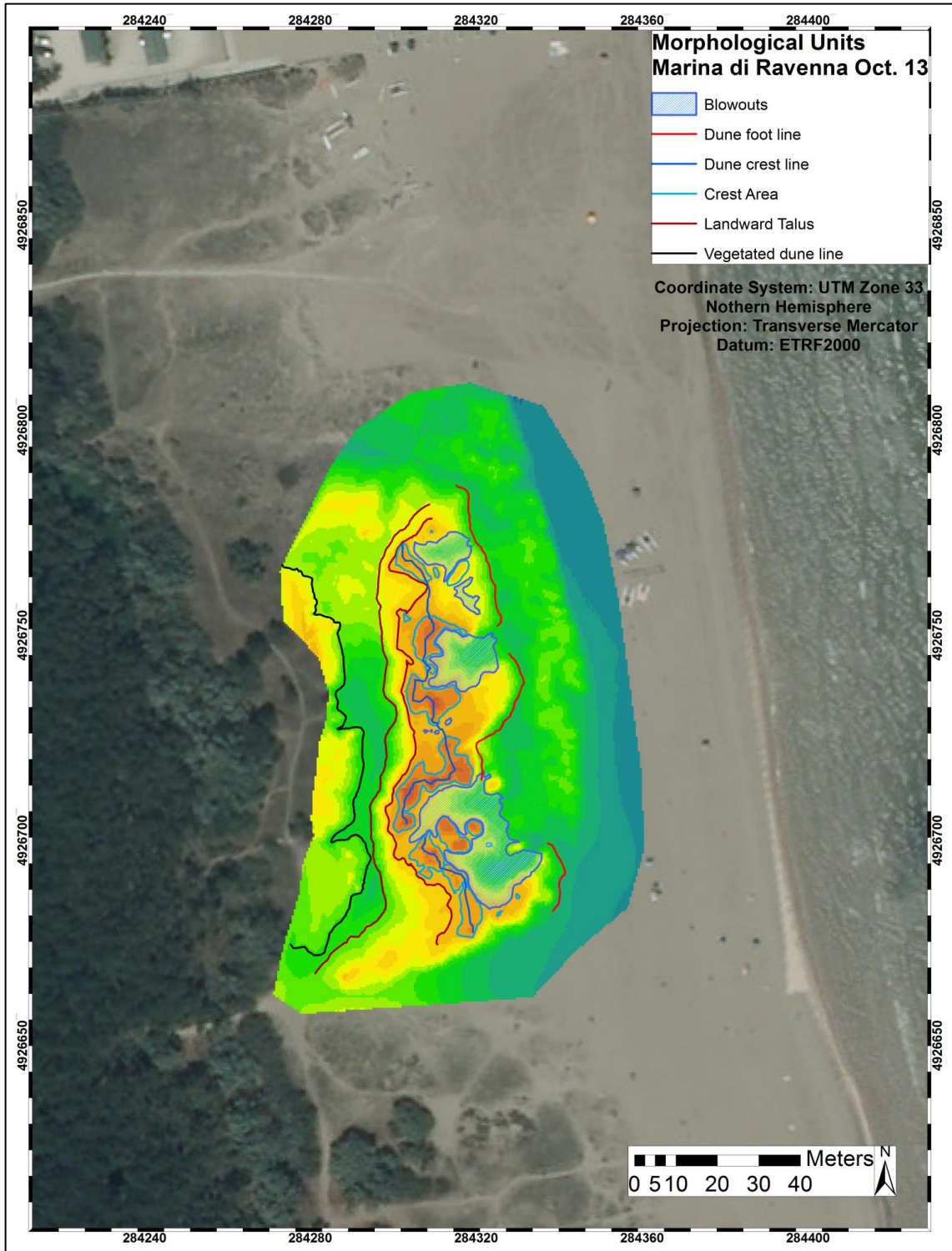


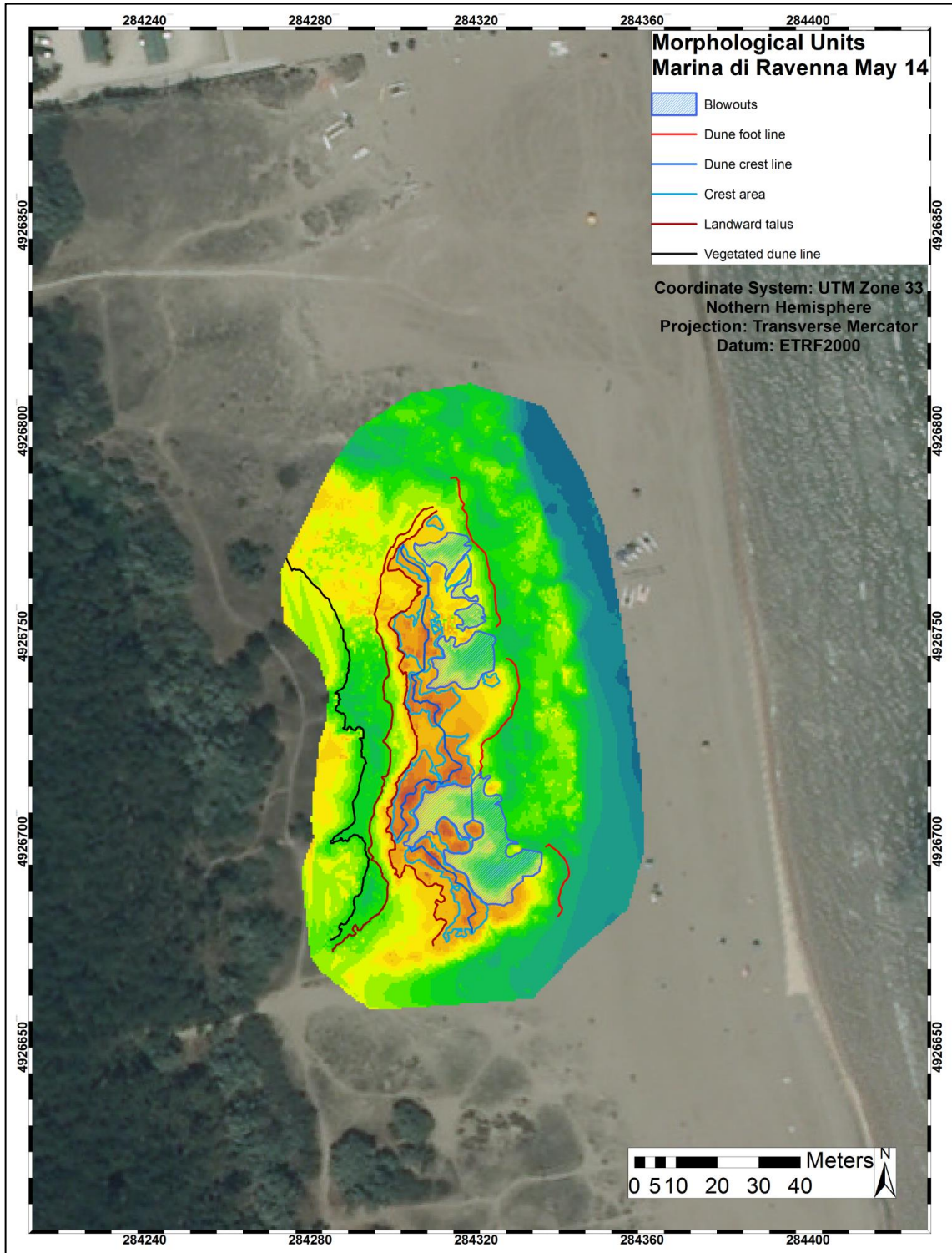


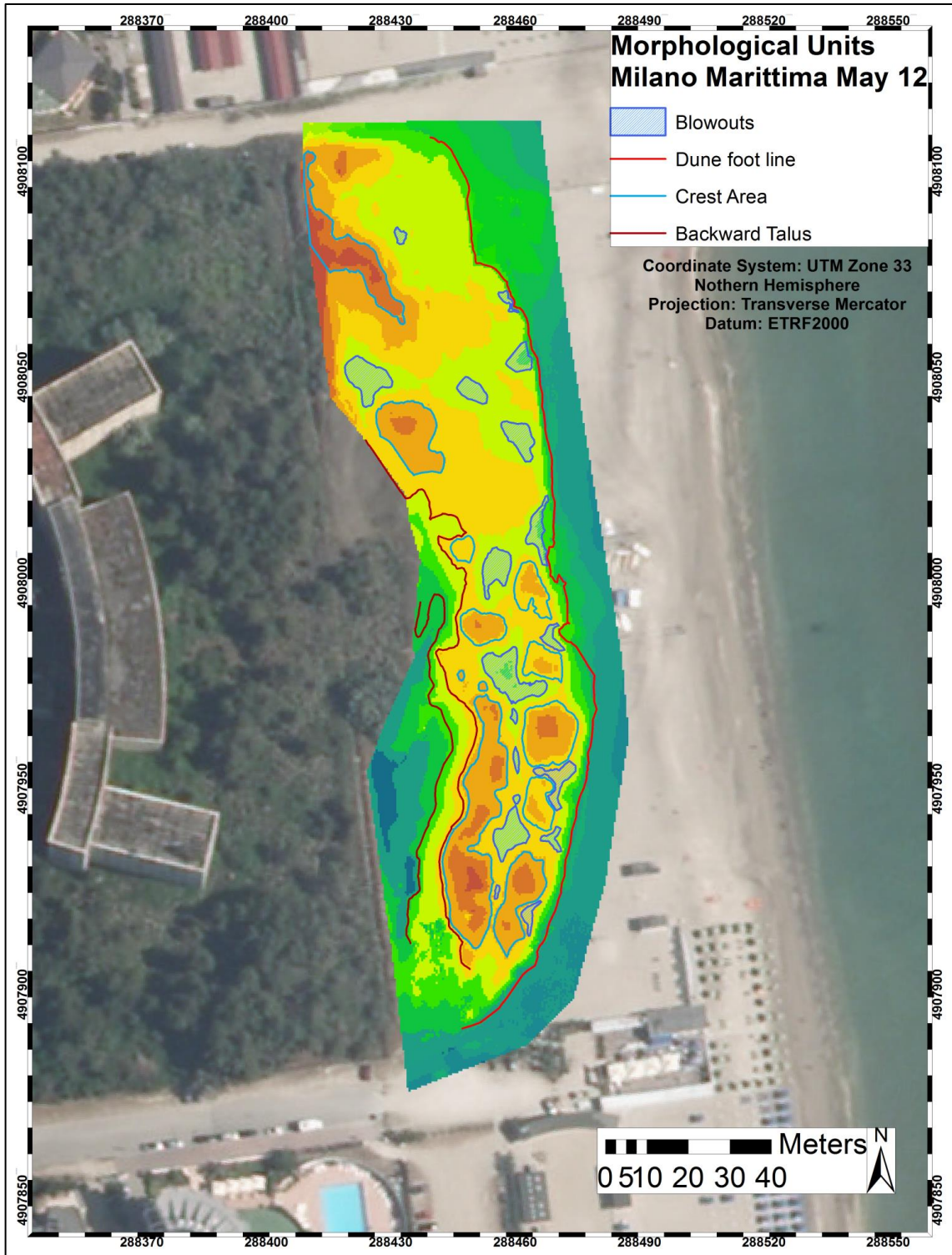


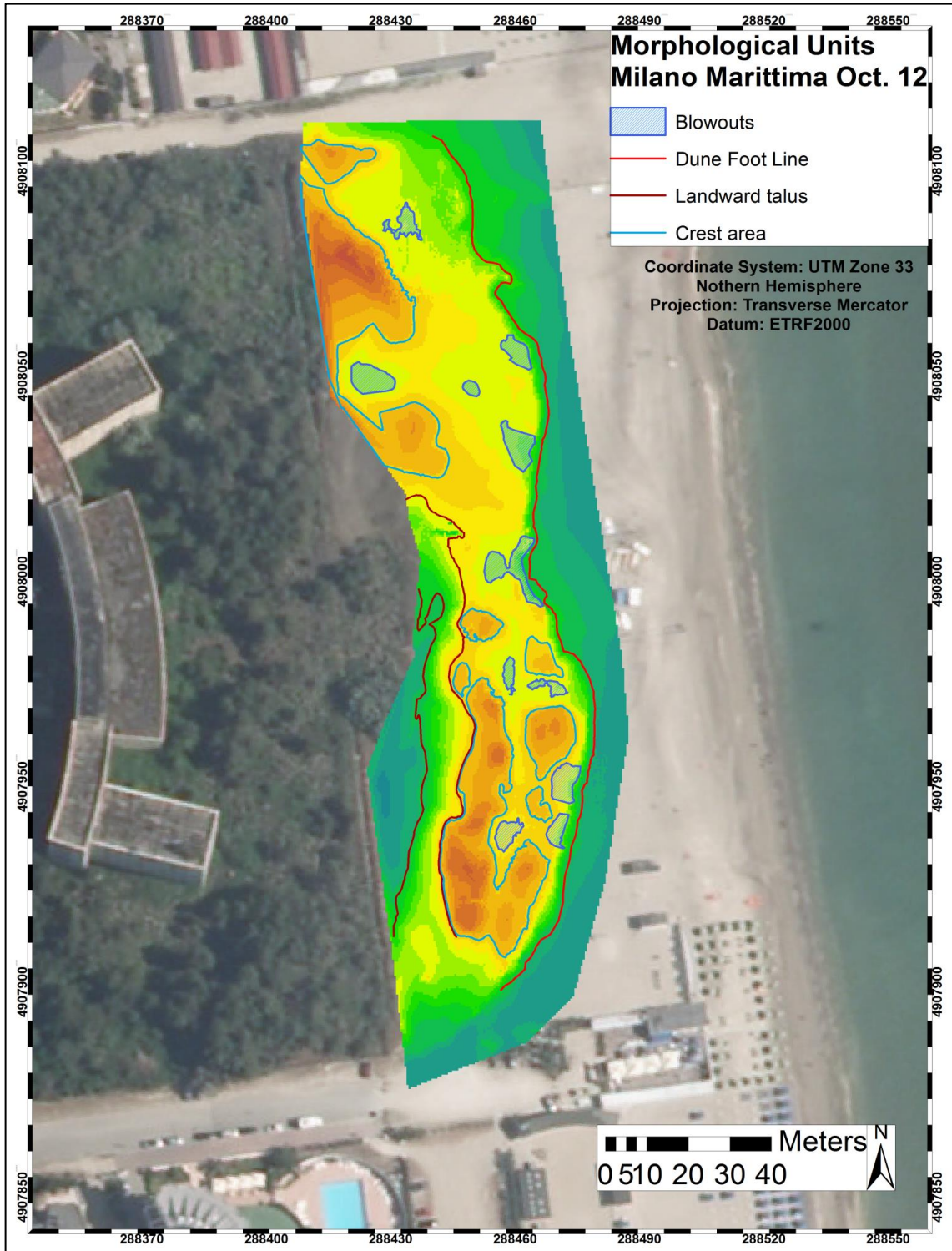


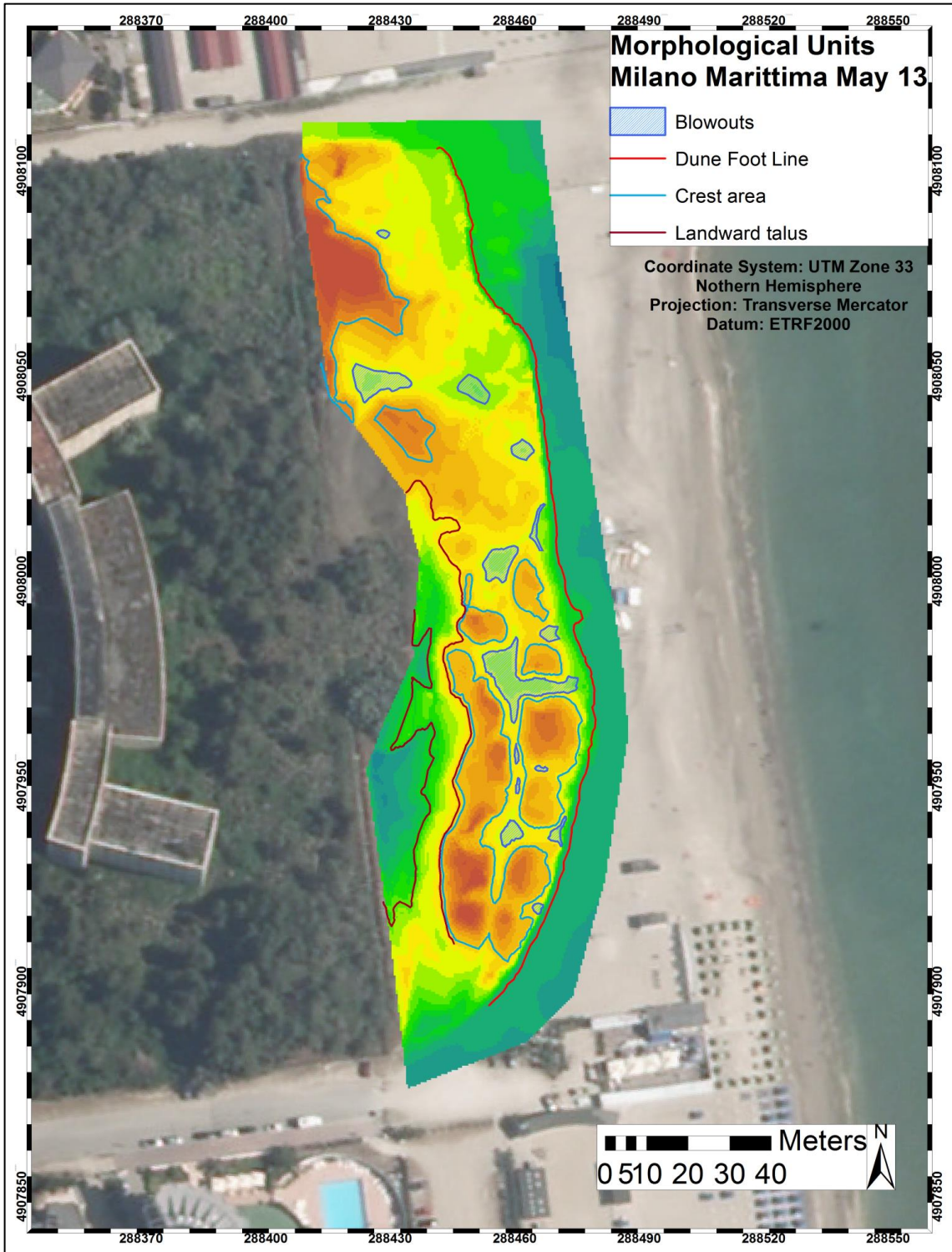


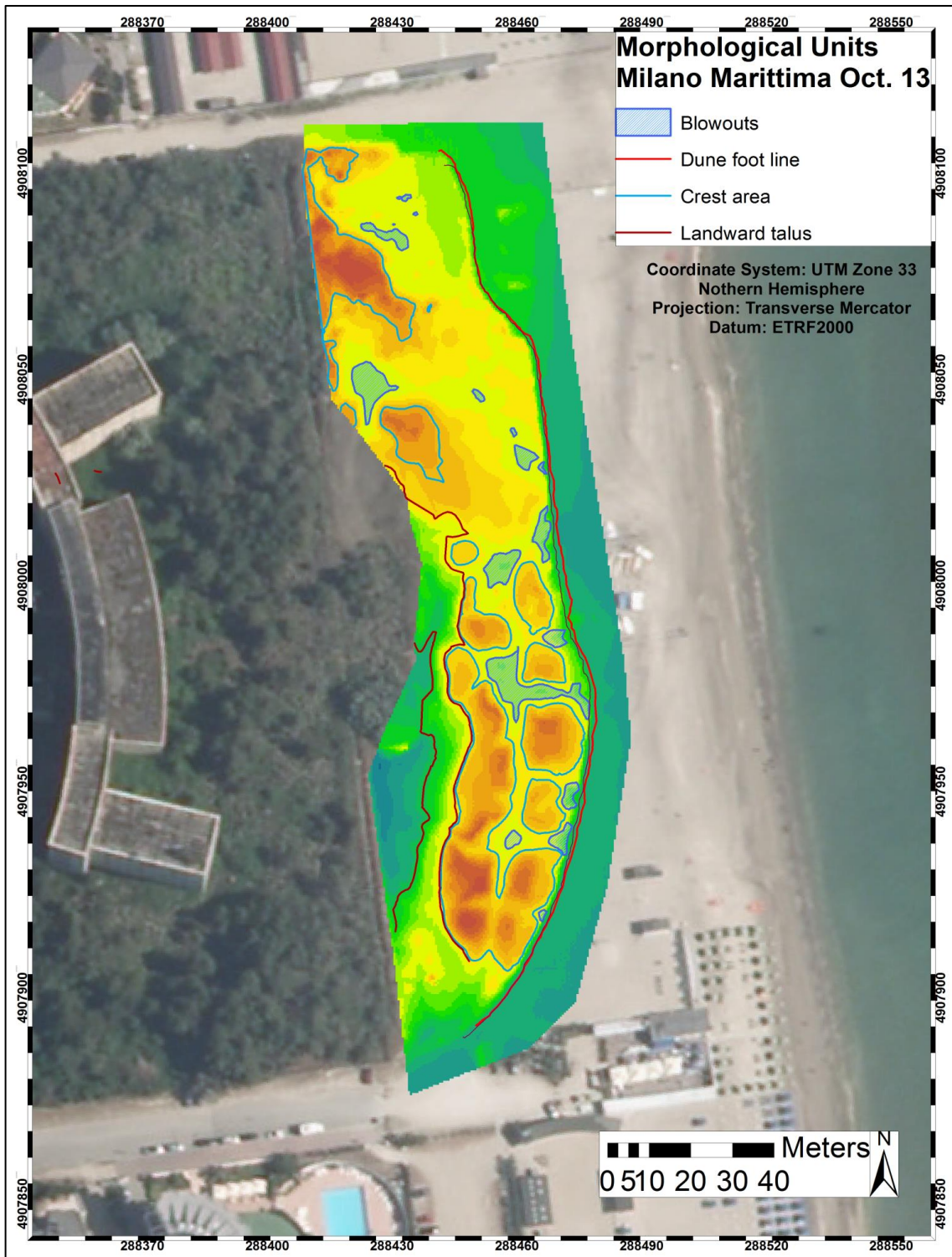


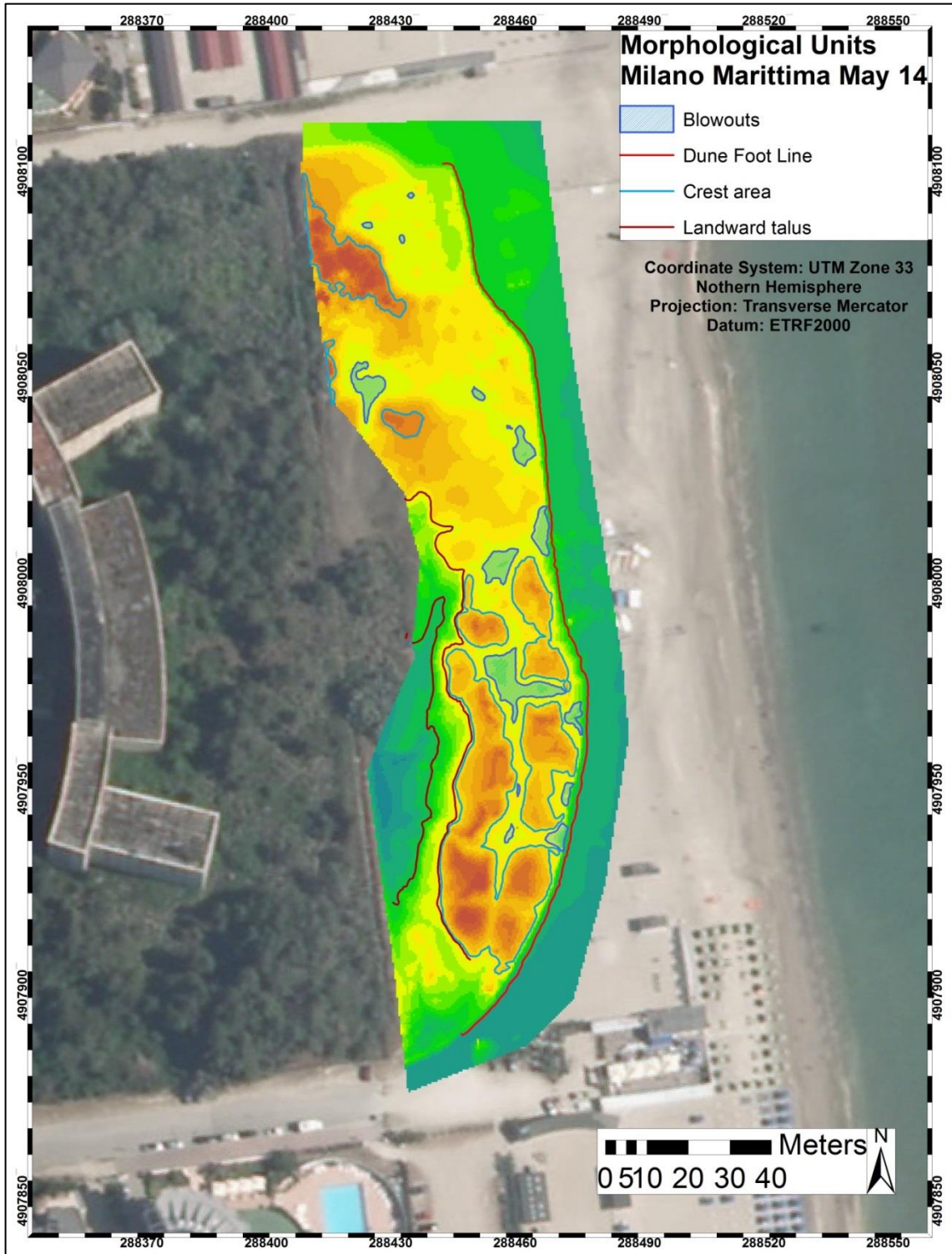










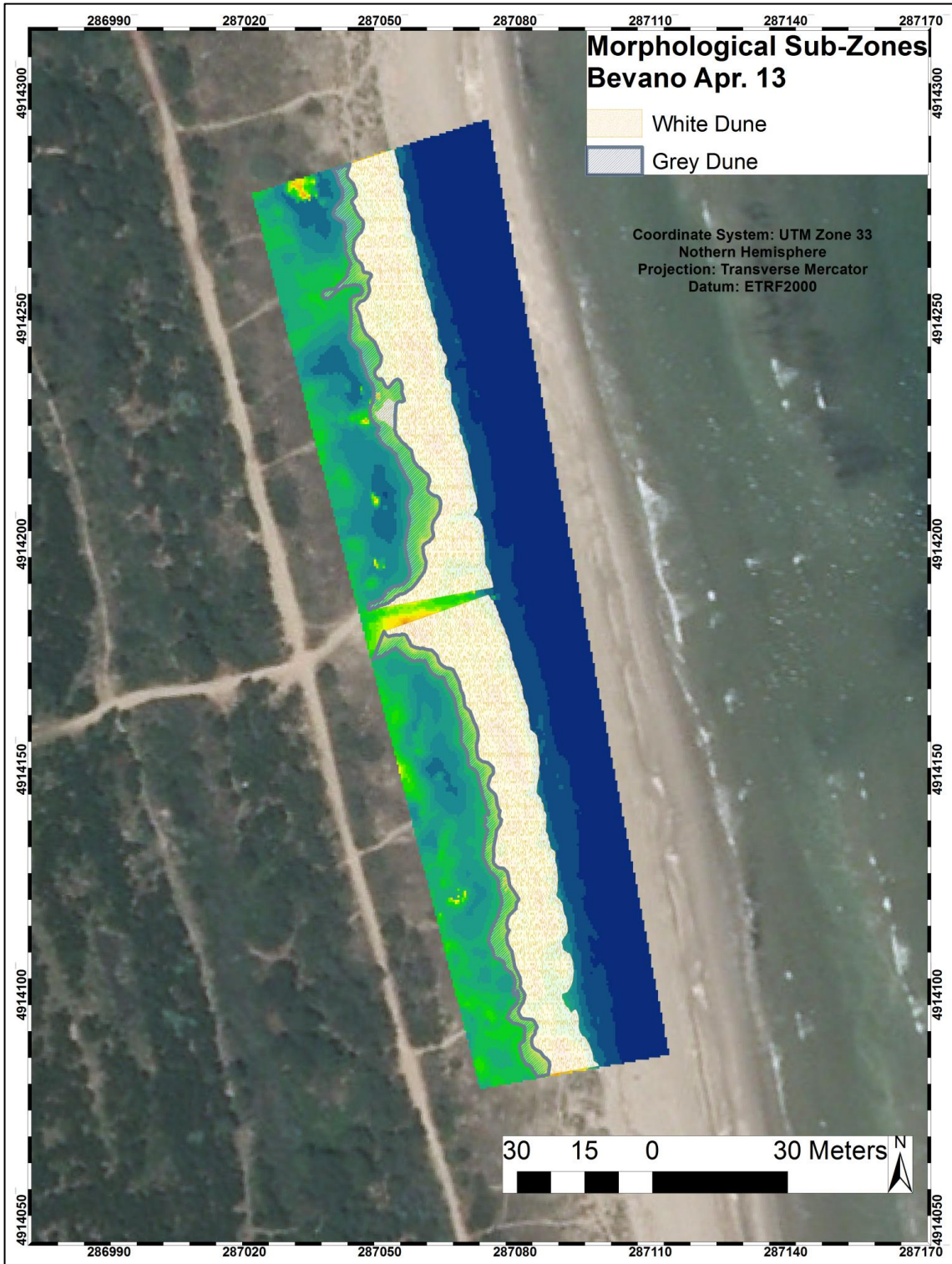


APPENDIX II (Morphological Sub-Zones)

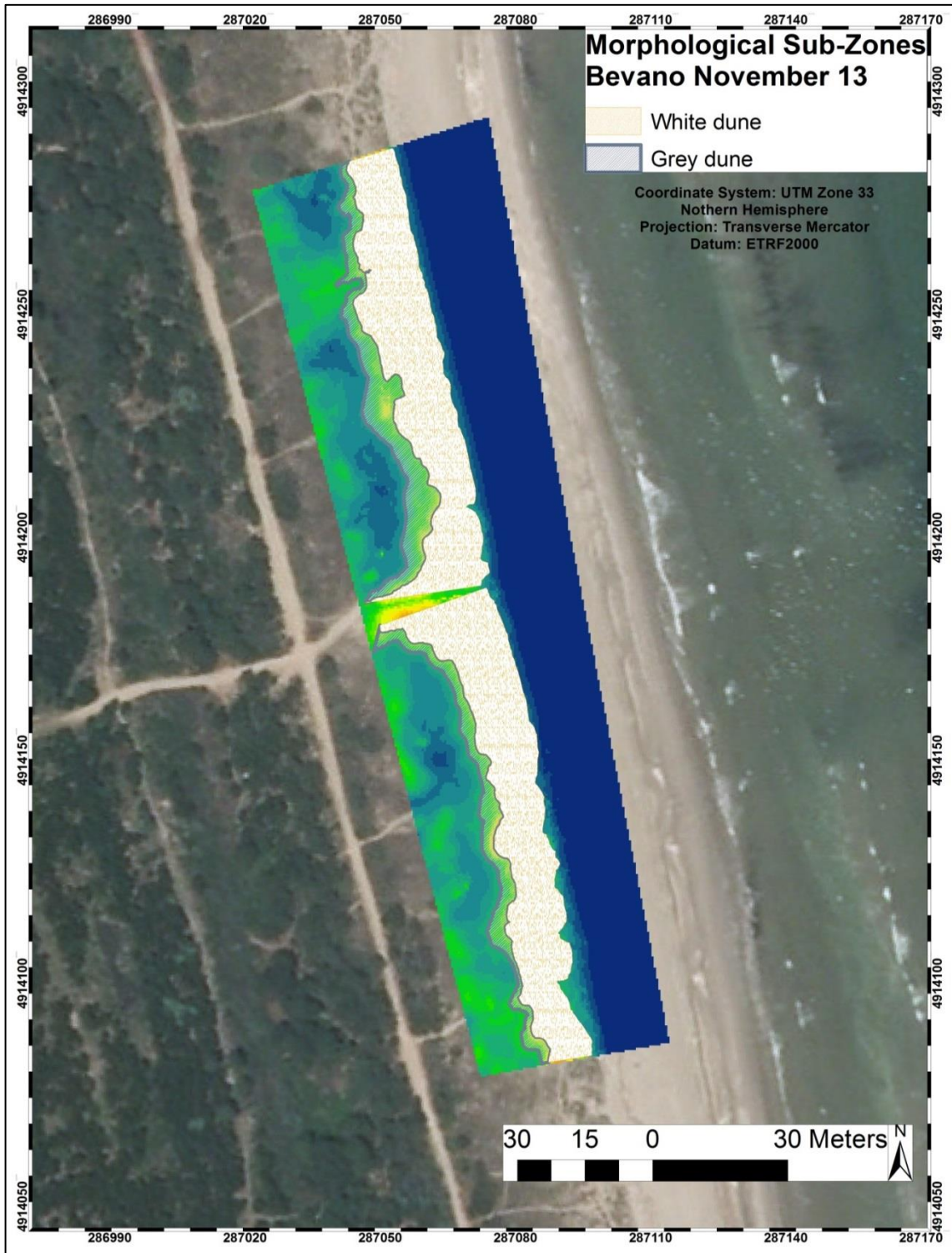




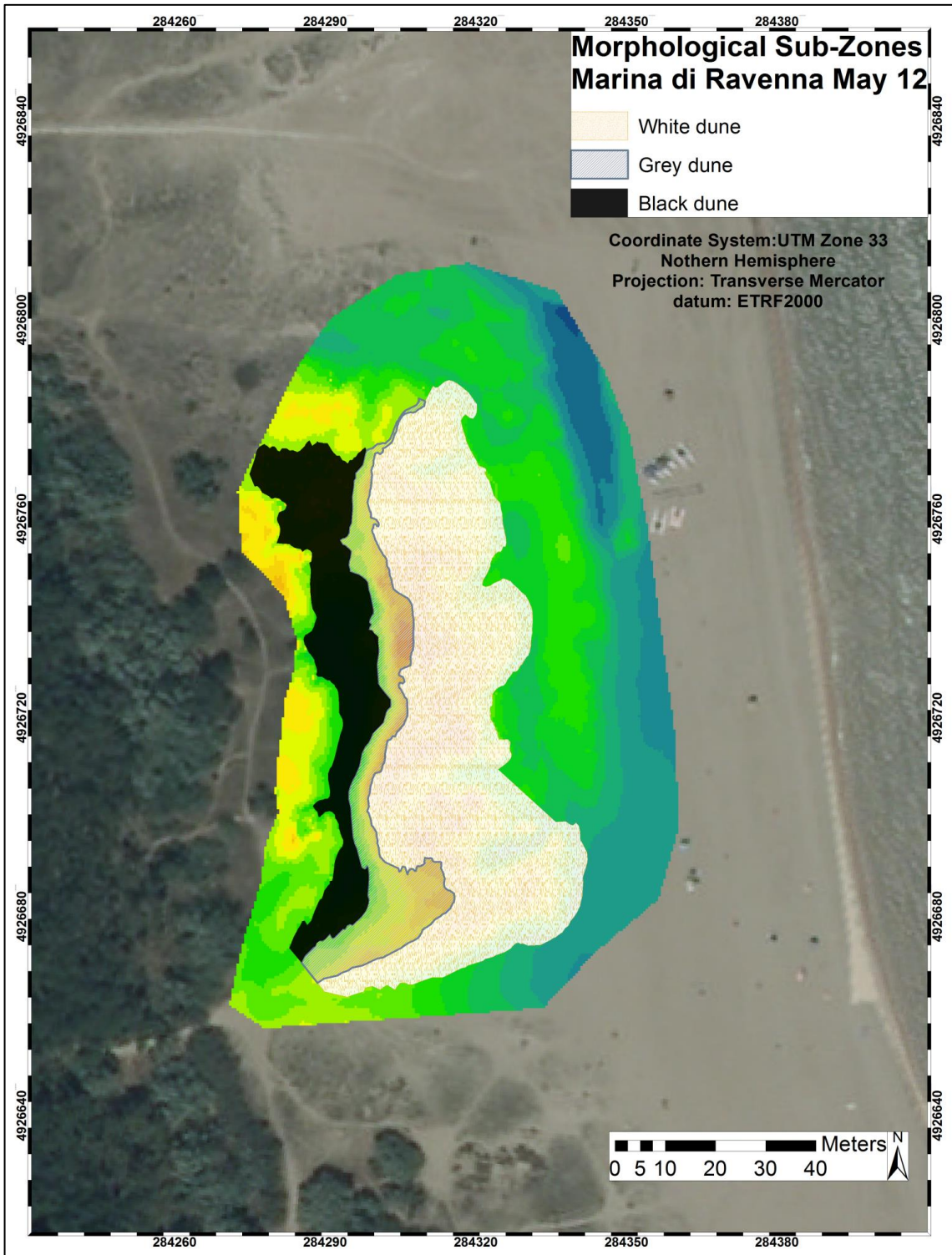




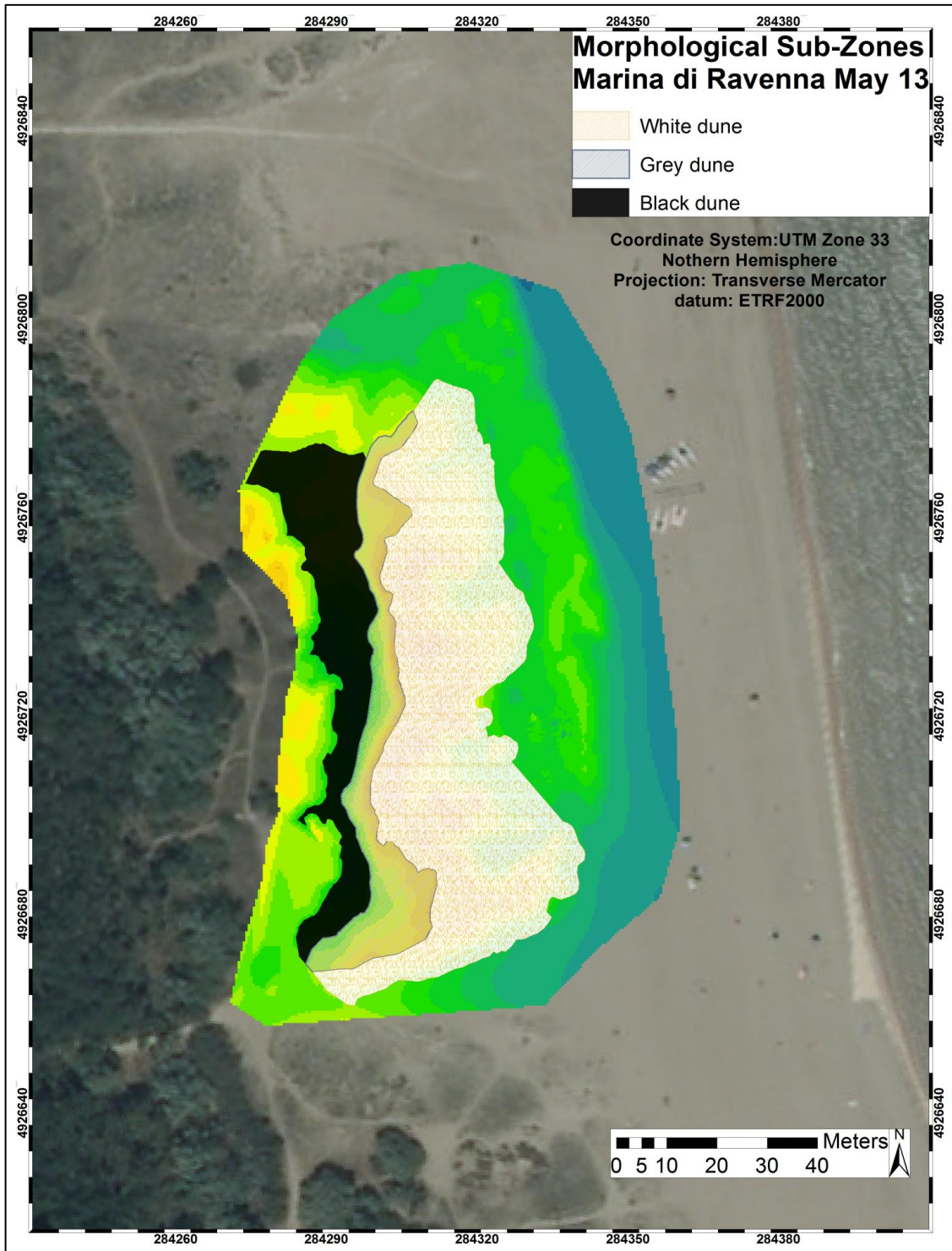


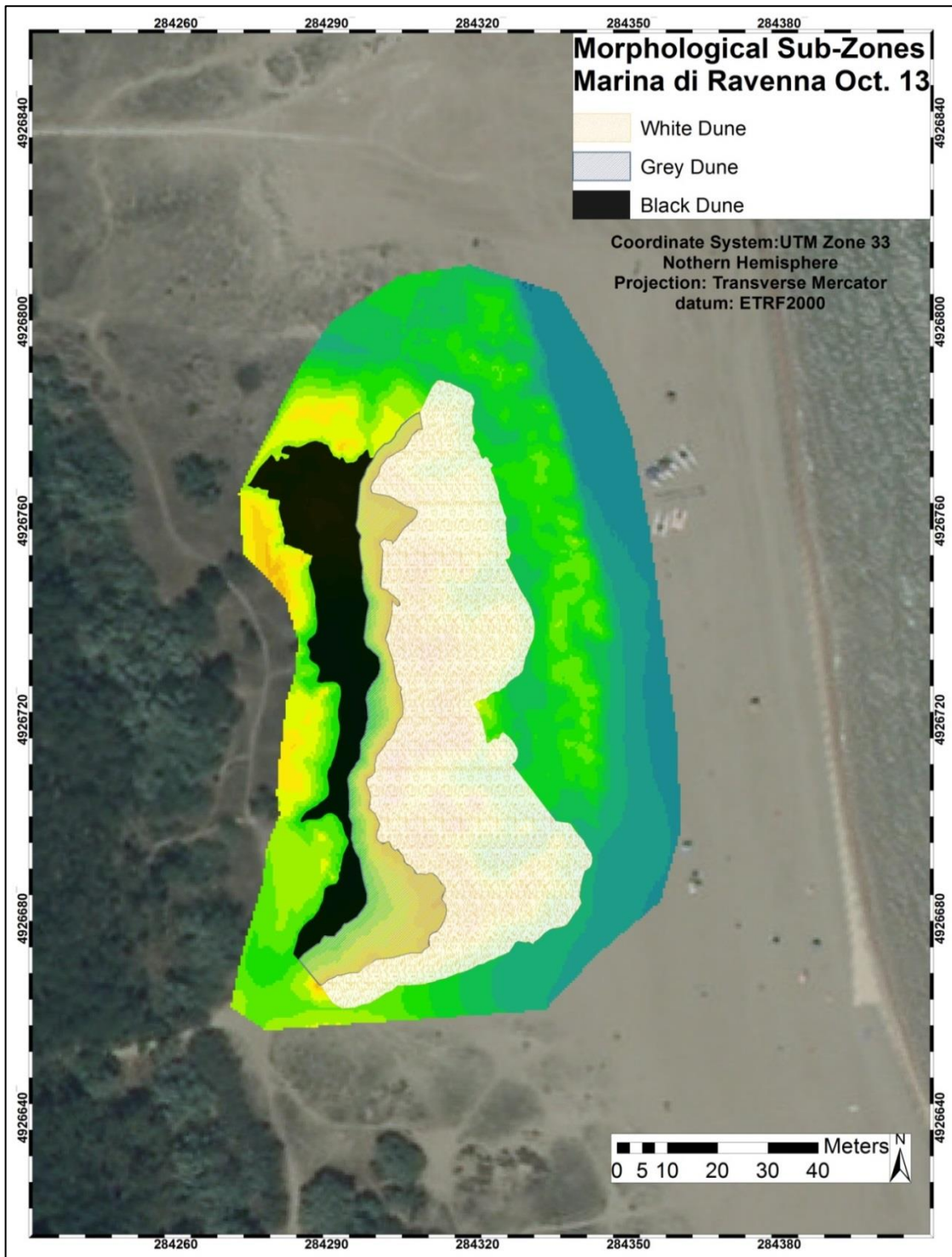


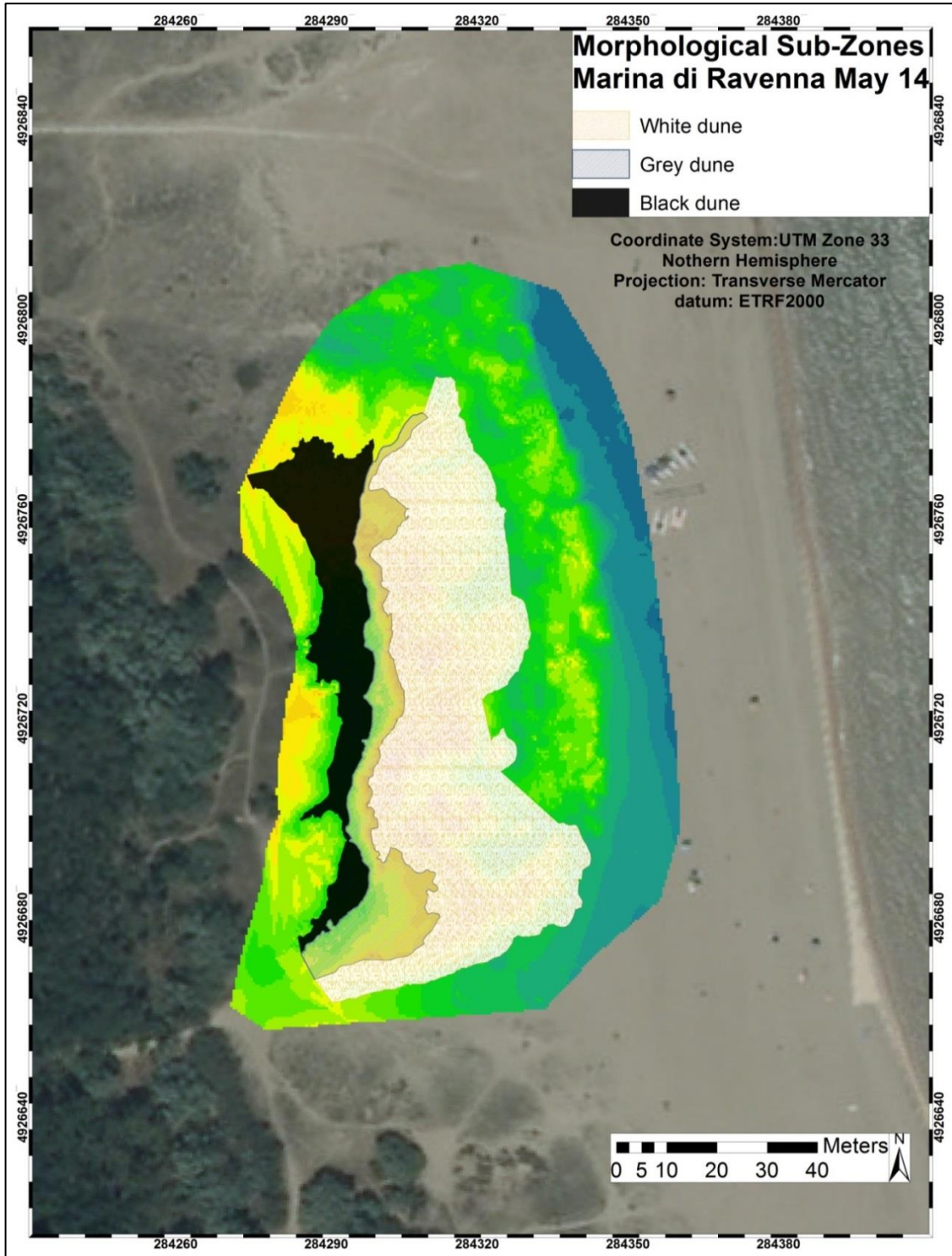






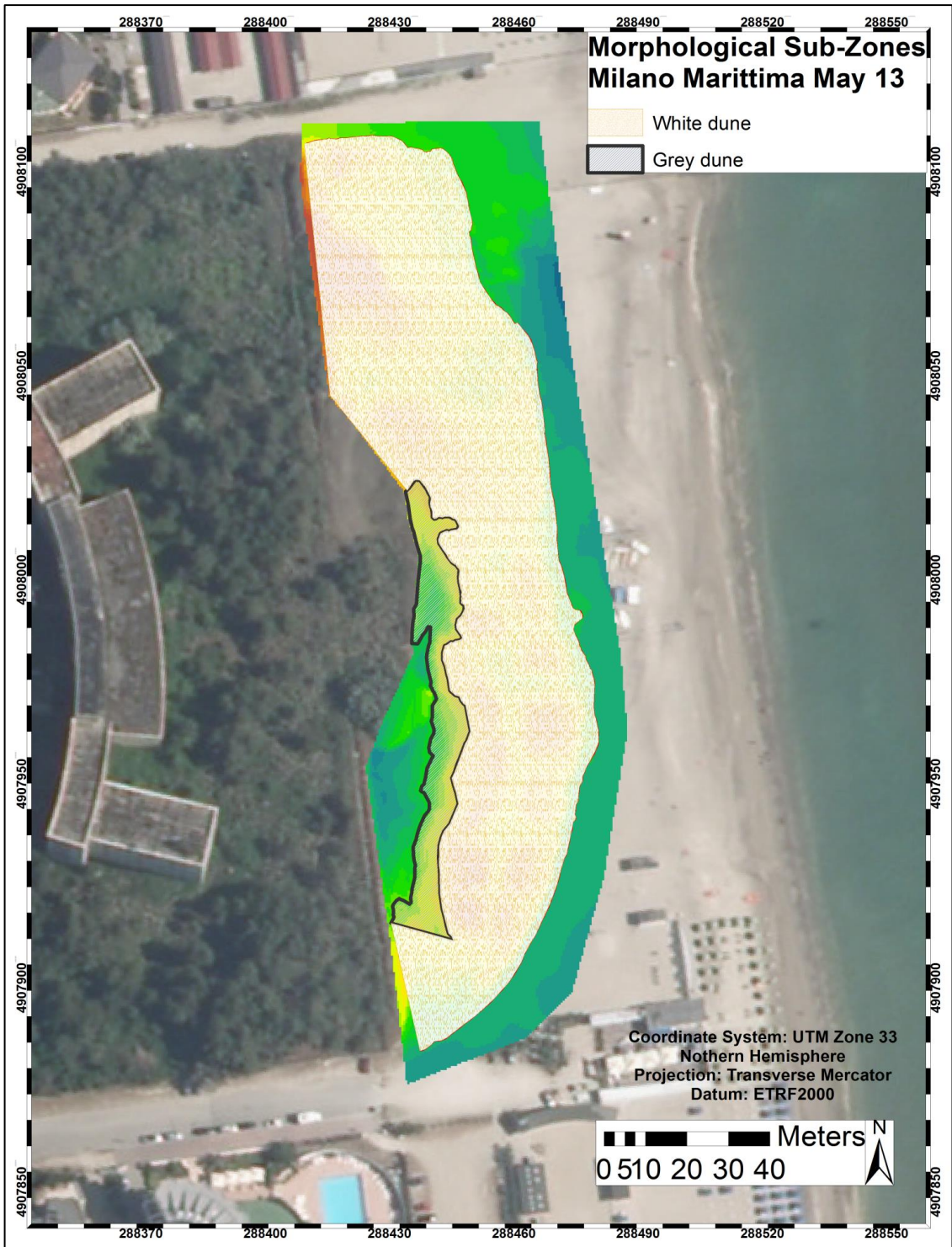
















APPENDIX III (PCA R script)

```
library (ade4)
library (gclus)
library (ape)

pcatrix<-read.table("C:\\Directory path\\File-Table.txt")
summary(pcatrix)
pcatrix.pca<-rda(pcatrix,scale=TRUE)
pcatrix.pca
summary (pcatrix.pca, scaling=1)
ev<-pcatrix.pca$CA$eig
ev [ev > mean(ev)]
n<-length (ev)
bsm<-data.frame(j=seq(1:n), p=0)
bsm$p[1]<-1/n
for (i in 2:n)
+ {bsm$p[i]=bsm$p[i-1]+(1/n-1-i)}
bsm$p<-100*bsm$p/n
bsm
par(mfrow=c(2,1))
barplot(ev, main="Eigenvalue", col="bisque", las=2)
abline (h=mean (ev), col="red")
legend("topright", "Average eigenvalue", lwd=1, col=2, bty="n")
barplot(t(cbind(100*ev/sum(ev), bsm$p[n:1])), beside=TRUE, main="% variance",
col=c("bisque",2),las=2)
legend("topright",c("% eigenvalue", "Broker stick model"),pch=15, col=c("bisque",2),
bty="n")
par(mfrow=c(1,2))
biplot.rda(pcatrix.PCA, scaling=1, main="PCA - scaling1")
biplot.rda(pcatrix.PCA, main="PCA - scaling 2")
```

APPENDIX IV (DSAS tables)

1-Bevano dune foot line table.

OBJECTID	TransectId	StartX	StartY	EndX	EndY	EPR	ECI	NSM	LRR	LR2
5	5	287032	4914277	287080.7	4914289	0.10	0.354	0.2	-0.08	0.03
6	6	287032.2	4914276	287080.9	4914288	-0.18	0.354	-0.36	-0.17	0.15
7	7	287032.5	4914275	287081.1	4914287	0.05	0.354	0.1	0.03	0
8	8	287032.7	4914274	287081.4	4914286	-0.04	0.354	-0.08	-0.11	0.12
9	9	287032.9	4914273	287081.6	4914285	0.03	0.354	0.06	-0.03	0.01
10	10	287033.2	4914272	287081.8	4914284	-0.21	0.354	-0.41	-0.18	0.11
11	11	287033.4	4914271	287082.1	4914283	-0.36	0.354	-0.72	-0.27	0.2
12	12	287033.6	4914270	287082.3	4914282	-0.07	0.354	-0.14	-0.02	0
13	13	287033.8	4914269	287082.5	4914281	0.15	0.354	0.3	0.16	0.13
14	14	287034.1	4914268	287082.8	4914280	-0.03	0.354	-0.05	0.02	0
15	15	287034.3	4914268	287083	4914279	-0.13	0.354	-0.26	-0.03	0
16	16	287034.5	4914267	287083.2	4914278	-0.01	0.354	-0.01	0.09	0.02
17	17	287034.8	4914266	287083.4	4914277	-0.10	0.354	-0.19	-0.01	0
18	18	287035	4914265	287083.7	4914276	-0.12	0.354	-0.23	-0.07	0.02
19	19	287035.2	4914264	287083.9	4914275	-0.29	0.354	-0.57	-0.29	0.43
20	20	287035.5	4914263	287084.1	4914274	-0.32	0.354	-0.63	-0.19	0.16
21	21	287035.7	4914262	287084.4	4914273	-0.03	0.354	-0.05	-0.03	0.01
22	22	287035.9	4914261	287084.6	4914272	-0.05	0.354	-0.09	-0.07	0.08
23	23	287036.1	4914260	287084.8	4914271	-0.13	0.354	-0.26	-0.09	0.08
24	24	287036.4	4914259	287085.1	4914270	-0.12	0.354	-0.24	-0.09	0.06
25	25	287036.6	4914258	287085.3	4914269	0.17	0.354	0.33	0.14	0.11
26	26	287036.8	4914257	287085.5	4914268	-0.02	0.354	-0.04	-0.03	0.01
27	27	287037.1	4914256	287085.7	4914267	-0.25	0.354	-0.5	-0.29	0.4
28	28	287037.3	4914255	287086	4914266	-0.24	0.354	-0.48	-0.27	0.22
29	29	287037.5	4914254	287086.2	4914265	-0.06	0.354	-0.11	-0.07	0.07
30	30	287037.8	4914253	287086.4	4914264	-0.05	0.354	-0.09	-0.01	0
31	31	287038	4914252	287086.7	4914263	-0.09	0.354	-0.18	-0.05	0.01
32	32	287038.2	4914251	287086.9	4914262	0.04	0.354	0.07	0.09	0.02
33	33	287038.4	4914250	287087.1	4914261	0.12	0.354	0.23	0.2	0.09
34	34	287038.7	4914249	287087.3	4914260	0.16	0.354	0.32	0.09	0.11
35	35	287038.9	4914248	287087.6	4914259	0.23	0.354	0.45	0.16	0.2
36	36	287039.1	4914247	287087.8	4914258	-0.06	0.354	-0.12	0	0
37	37	287039.4	4914246	287088	4914258	-0.05	0.354	-0.09	-0.02	0
38	38	287039.6	4914245	287088.3	4914257	0.03	0.354	0.05	0.05	0.01
39	39	287039.8	4914244	287088.5	4914256	-0.06	0.354	-0.12	0.01	0
40	40	287040	4914243	287088.7	4914255	0.04	0.354	0.07	0.12	0.04
41	41	287040.3	4914242	287089	4914254	0.10	0.354	0.2	0.15	0.06
42	42	287040.5	4914241	287089.2	4914253	-0.04	0.354	-0.07	0.06	0.01
43	43	287040.7	4914240	287089.4	4914252	0.04	0.354	0.08	0.04	0.01
44	44	287041	4914239	287089.6	4914251	0.17	0.354	0.33	0.11	0.06
45	45	287041.2	4914238	287089.9	4914250	0.22	0.354	0.44	0.11	0.12
46	46	287041.4	4914237	287090.1	4914249	0.13	0.354	0.26	0.03	0.01
47	47	287041.7	4914236	287090.3	4914248	0.03	0.354	0.06	0.03	0.01
48	48	287041.9	4914235	287090.6	4914247	-0.08	0.354	-0.16	-0.12	0.03
49	49	287042.1	4914234	287090.8	4914246	-0.03	0.354	-0.06	-0.2	0.16
50	50	287042.3	4914233	287091	4914245	-0.01	0.354	-0.02	-0.09	0.04
51	51	287042.6	4914232	287091.3	4914244	0.05	0.354	0.1	-0.01	0
52	52	287042.8	4914231	287091.5	4914243	0.00	0.354	0	0.03	0
53	53	287043	4914231	287091.7	4914242	-0.22	0.354	-0.43	-0.1	0.03
54	54	287043.3	4914230	287091.9	4914241	-0.05	0.354	-0.1	-0.17	0.23
55	55	287043.5	4914229	287092.2	4914240	-0.08	0.354	-0.16	-0.16	0.33

Appendix IV

56	56	287043.7	4914228	287092.4	4914239	-0.07	0.354	-0.14	-0.18	0.39
57	57	287044	4914227	287092.6	4914238	0.02	0.354	0.03	0	0
58	58	287044.2	4914226	287092.9	4914237	-0.17	0.354	-0.34	0.07	0.01
59	59	287044.4	4914225	287093.1	4914236	-0.04	0.354	-0.08	0.15	0.02
60	60	287044.6	4914224	287093.3	4914235	-0.06	0.354	-0.11	0.04	0
61	61	287044.9	4914223	287093.5	4914234	-0.18	0.354	-0.36	-0.02	0
62	62	287045.1	4914222	287093.8	4914233	-0.13	0.354	-0.25	-0.1	0.03
63	63	287045.3	4914221	287094	4914232	-0.23	0.354	-0.46	-0.14	0.04
64	64	287045.6	4914220	287094.2	4914231	-0.35	0.354	-0.7	-0.23	0.11
65	65	287045.8	4914219	287094.5	4914230	-0.15	0.354	-0.29	-0.08	0.02
66	66	287046	4914218	287094.7	4914229	-0.14	0.354	-0.28	-0.06	0.01
67	67	287046.2	4914217	287094.9	4914228	-0.23	0.354	-0.45	-0.08	0.01
68	68	287046.5	4914216	287095.2	4914227	-0.27	0.354	-0.54	-0.15	0.04
69	69	287046.7	4914215	287095.4	4914226	-0.24	0.354	-0.48	-0.19	0.09
70	70	287046.9	4914214	287095.6	4914225	-0.13	0.354	-0.26	-0.14	0.08
71	71	287047.2	4914213	287095.8	4914224	-0.30	0.354	-0.59	-0.28	0.31
72	72	287047.4	4914212	287096.1	4914223	-0.22	0.354	-0.44	-0.2	0.15
73	73	287047.6	4914211	287096.3	4914222	-0.26	0.354	-0.51	-0.15	0.03
74	74	287047.9	4914210	287096.5	4914222	-0.36	0.354	-0.71	-0.26	0.13
75	75	287048.1	4914209	287096.8	4914221	-0.27	0.354	-0.54	-0.26	0.15
107	107	287055.4	4914178	287104.1	4914189	0.97	0.354	1.93	0.77	0.46
108	108	287055.7	4914177	287104.3	4914188	0.72	0.354	1.44	0.62	0.34
109	109	287055.9	4914176	287104.6	4914187	0.79	0.354	1.58	0.73	0.35
110	110	287056.1	4914175	287104.8	4914186	0.43	0.354	0.85	0.44	0.39
111	111	287056.4	4914174	287105	4914185	0.19	0.354	0.38	0.18	0.14
112	112	287056.6	4914173	287105.3	4914185	0.27	0.354	0.54	0.22	0.16
113	113	287056.8	4914172	287105.5	4914184	0.26	0.354	0.52	0.21	0.15
114	114	287057	4914171	287105.7	4914183	0.33	0.354	0.65	0.31	0.33
115	115	287057.3	4914170	287105.9	4914182	0.49	0.354	0.98	0.43	0.27
116	116	287057.5	4914169	287106.2	4914181	0.62	0.354	1.23	0.57	0.45
117	117	287057.7	4914168	287106.4	4914180	0.72	0.354	1.43	0.57	0.46
118	118	287058	4914167	287106.6	4914179	0.61	0.354	1.21	0.47	0.31
119	119	287058.2	4914166	287106.9	4914178	-0.13	0.354	-0.26	-0.11	0.18
120	120	287058.4	4914165	287107.1	4914177	-0.23	0.354	-0.46	-0.21	0.41
121	121	287058.6	4914164	287107.3	4914176	-0.27	0.354	-0.53	-0.17	0.11
122	122	287058.9	4914163	287107.6	4914175	-0.23	0.354	-0.46	-0.16	0.07
123	123	287059.1	4914162	287107.8	4914174	-0.48	0.354	-0.95	-0.38	0.49
124	124	287059.3	4914161	287108	4914173	-0.52	0.354	-1.03	-0.37	0.35
125	125	287059.6	4914160	287108.2	4914172	-0.63	0.354	-1.25	-0.42	0.31
126	126	287059.8	4914159	287108.5	4914171	-0.67	0.354	-1.33	-0.51	0.41
127	127	287060	4914158	287108.7	4914170	-0.58	0.354	-1.16	-0.44	0.42
128	128	287060.3	4914158	287108.9	4914169	-0.69	0.354	-1.38	-0.52	0.48
129	129	287060.5	4914157	287109.2	4914168	-0.64	0.354	-1.28	-0.51	0.44
130	130	287060.7	4914156	287109.4	4914167	-0.60	0.354	-1.19	-0.45	0.36
131	131	287060.9	4914155	287109.6	4914166	-0.62	0.354	-1.23	-0.46	0.43
132	132	287061.2	4914154	287109.9	4914165	-0.61	0.354	-1.22	-0.41	0.37
133	133	287061.4	4914153	287110.1	4914164	-0.56	0.354	-1.12	-0.38	0.33
134	134	287061.6	4914152	287110.3	4914163	-0.55	0.354	-1.09	-0.48	0.6

2-Bevano dune crest line table.

OBJECTID	TransectId	StartX	StartY	EndX	EndY	EPR	ECI	NSM	LRR	LR2
1	5	287032	4914277	287080.7	4914289	0.06	0.354	0.11	-0.04	0.01
2	6	287032.2	4914276	287080.9	4914288	0.07	0.354	0.13	-0.02	0.01
3	7	287032.5	4914275	287081.1	4914287	0.37	0.354	0.74	0.24	0.46
4	8	287032.7	4914274	287081.4	4914286	0.32	0.354	0.64	0.12	0.1
5	9	287032.9	4914273	287081.6	4914285	0.27	0.354	0.53	0.03	0
6	10	287033.2	4914272	287081.8	4914284	0.14	0.354	0.27	0.1	0.13
7	11	287033.4	4914271	287082.1	4914283	-0.02	0.354	-0.03	-0.07	0.06
8	12	287033.6	4914270	287082.3	4914282	-0.16	0.354	-0.31	-0.17	0.25
9	13	287033.8	4914269	287082.5	4914281	-0.05	0.354	-0.09	-0.04	0.03
10	14	287034.1	4914268	287082.8	4914280	0	0.354	0	0.06	0.03
11	15	287034.3	4914268	287083	4914279	0.14	0.354	0.28	0.08	0.02
12	16	287034.5	4914267	287083.2	4914278	0.5	0.354	0.99	0.35	0.25
13	17	287034.8	4914266	287083.4	4914277	-0.47	0.354	-0.94	-0.24	0.15
14	18	287035	4914265	287083.7	4914276	0.66	0.354	1.31	0.38	0.21
15	19	287035.2	4914264	287083.9	4914275	0.84	0.354	1.67	0.74	0.73
16	20	287035.5	4914263	287084.1	4914274	0.69	0.354	1.38	0.66	0.62
17	21	287035.7	4914262	287084.4	4914273	0.77	0.354	1.53	0.68	0.54
18	22	287035.9	4914261	287084.6	4914272	0.51	0.354	1.02	0.4	0.11
19	23	287036.1	4914260	287084.8	4914271	0.09	0.354	0.18	0.14	0.02
20	24	287036.4	4914259	287085.1	4914270	-0.13	0.354	-0.25	0.11	0.02
21	25	287036.6	4914258	287085.3	4914269	-0.34	0.354	-0.67	0.2	0.03
22	26	287036.8	4914257	287085.5	4914268	0.15	0.354	0.3	0.58	0.22
23	27	287037.1	4914256	287085.7	4914267	0.08	0.354	0.16	0.67	0.21
24	28	287037.3	4914255	287086	4914266	-0.18	0.354	-0.36	-0.12	0.02
25	29	287037.5	4914254	287086.2	4914265	-0.2	0.354	-0.4	-0.06	0.01
26	30	287037.8	4914253	287086.4	4914264	-0.06	0.354	-0.12	-0.11	0.05
27	31	287038	4914252	287086.7	4914263	0.06	0.354	0.12	-0.09	0.02
28	32	287038.2	4914251	287086.9	4914262	-0.14	0.354	-0.27	-0.21	0.15
29	33	287038.4	4914250	287087.1	4914261	-0.29	0.354	-0.58	-0.26	0.24
30	34	287038.7	4914249	287087.3	4914260	-0.31	0.354	-0.61	-0.25	0.16
31	35	287038.9	4914248	287087.6	4914259	-0.06	0.354	-0.11	0.04	0
32	36	287039.1	4914247	287087.8	4914258	-0.25	0.354	-0.5	-0.17	0.23
33	37	287039.4	4914246	287088	4914258	-0.12	0.354	-0.24	-0.06	0.08
34	38	287039.6	4914245	287088.3	4914257	-0.25	0.354	-0.49	-0.21	0.31
35	39	287039.8	4914244	287088.5	4914256	-0.11	0.354	-0.21	-0.16	0.07
36	40	287040	4914243	287088.7	4914255	-0.11	0.354	-0.22	-0.33	0.12
37	41	287040.3	4914242	287089	4914254	-0.06	0.354	-0.11	-0.47	0.12
38	42	287040.5	4914241	287089.2	4914253	0.03	0.354	0.06	-0.47	0.08
39	43	287040.7	4914240	287089.4	4914252	-1.3	0.354	-2.6	-1.5	0.55
40	44	287041	4914239	287089.6	4914251	-1.28	0.354	-2.55	-1.33	0.49
41	45	287041.2	4914238	287089.9	4914250	-1.16	0.354	-2.31	-1	0.4
42	46	287041.4	4914237	287090.1	4914249	-1.04	0.354	-2.07	-0.7	0.24
43	47	287041.7	4914236	287090.3	4914248	-1.39	0.354	-2.77	-0.82	0.22
44	48	287041.9	4914235	287090.6	4914247	-1.12	0.354	-2.24	-0.65	0.23
45	49	287042.1	4914234	287090.8	4914246	-0.45	0.354	-0.89	-0.11	0.01
46	50	287042.3	4914233	287091	4914245	0.12	0.354	0.24	0.22	0.06
47	51	287042.6	4914232	287091.3	4914244	0.19	0.354	0.38	0.26	0.04
48	52	287042.8	4914231	287091.5	4914243	-0.01	0.354	-0.01	0.1	0.01
49	53	287043	4914231	287091.7	4914242	0.35	0.354	0.7	0.31	0.07
50	54	287043.3	4914230	287091.9	4914241	0.65	0.354	1.3	0.29	0.05
51	55	287043.5	4914229	287092.2	4914240	0.79	0.354	1.58	0.21	0.02
52	56	287043.7	4914228	287092.4	4914239	0.26	0.354	0.52	-0.41	0.06
53	57	287044	4914227	287092.6	4914238	0.17	0.354	0.33	-0.53	0.09
54	58	287044.2	4914226	287092.9	4914237	-0.04	0.354	-0.08	-0.84	0.19
55	59	287044.4	4914225	287093.1	4914236	-0.26	0.354	-0.51	-1.21	0.22
56	60	287044.6	4914224	287093.3	4914235	0.14	0.354	0.28	-1.08	0.14
57	61	287044.9	4914223	287093.5	4914234	0.75	0.354	1.5	-0.52	0.04
58	62	287045.1	4914222	287093.8	4914233	0.54	0.354	1.08	-0.63	0.06

Appendix IV

59	63	287045.3	4914221	287094	4914232	0.4	0.354	0.79	-0.71	0.08
60	64	287045.6	4914220	287094.2	4914231	-0.03	0.354	-0.05	-0.97	0.17
61	65	287045.8	4914219	287094.5	4914230	-0.19	0.354	-0.38	-0.87	0.25
62	66	287046	4914218	287094.7	4914229	0.21	0.354	0.42	-0.6	0.1
63	67	287046.2	4914217	287094.9	4914228	0.47	0.354	0.94	-0.35	0.03
64	68	287046.5	4914216	287095.2	4914227	0.56	0.354	1.11	-0.33	0.03
65	69	287046.7	4914215	287095.4	4914226	-0.11	0.354	-0.22	-0.59	0.16
66	70	287046.9	4914214	287095.6	4914225	0.09	0.354	0.17	-0.26	0.04
67	71	287047.2	4914213	287095.8	4914224	0.04	0.354	0.08	-0.2	0.04
68	72	287047.4	4914212	287096.1	4914223	0.26	0.354	0.51	0.16	0.12
69	73	287047.6	4914211	287096.3	4914222	0.14	0.354	0.28	0.17	0.56
70	74	287047.9	4914210	287096.5	4914222	0.17	0.354	0.33	0.17	0.3
71	75	287048.1	4914209	287096.8	4914221	0.01	0.354	0.01	-0.05	0.02
72	107	287055.4	4914178	287104.1	4914189	0.64	0.354	1.27	0.44	0.22
73	108	287055.7	4914177	287104.3	4914188	0.74	0.354	1.48	0.65	0.23
74	109	287055.9	4914176	287104.6	4914187	0.45	0.354	0.89	0.53	0.29
75	110	287056.1	4914175	287104.8	4914186	0.5	0.354	0.99	0.48	0.9
76	111	287056.4	4914174	287105	4914185	0.14	0.354	0.27	0.12	0.24
77	112	287056.6	4914173	287105.3	4914185	0.26	0.354	0.52	0.21	0.33
78	113	287056.8	4914172	287105.5	4914184	0.04	0.354	0.07	0.08	0.09
79	114	287057	4914171	287105.7	4914183	0.03	0.354	0.05	0.06	0.09
80	115	287057.3	4914170	287105.9	4914182	0.02	0.354	0.03	-0.01	0
81	116	287057.5	4914169	287106.2	4914181	-0.17	0.354	-0.34	-0.02	0
82	117	287057.7	4914168	287106.4	4914180	-0.61	0.354	-1.21	-0.28	0.1
83	118	287058	4914167	287106.6	4914179	-0.32	0.354	-0.64	-0.04	0
84	119	287058.2	4914166	287106.9	4914178	0.11	0.354	0.22	0.22	0.13
85	120	287058.4	4914165	287107.1	4914177	0.27	0.354	0.54	0.26	0.16
86	121	287058.6	4914164	287107.3	4914176	0.57	0.354	1.13	0.4	0.23
87	122	287058.9	4914163	287107.6	4914175	0.44	0.354	0.87	0.29	0.28
88	123	287059.1	4914162	287107.8	4914174	0.13	0.354	0.26	0.07	0.1
89	124	287059.3	4914161	287108	4914173	-0.15	0.354	-0.29	-0.28	0.35
90	125	287059.6	4914160	287108.2	4914172	-0.26	0.354	-0.52	-0.3	0.39
91	126	287059.8	4914159	287108.5	4914171	0.54	0.354	1.08	0.33	0.21
92	127	287060	4914158	287108.7	4914170	0.53	0.354	1.05	0.33	0.21
93	128	287060.3	4914158	287108.9	4914169	0.1	0.354	0.19	-0.09	0.03
94	129	287060.5	4914157	287109.2	4914168	-0.18	0.354	-0.36	-0.23	0.22
95	130	287060.7	4914156	287109.4	4914167	-0.13	0.354	-0.25	-0.04	0
96	131	287060.9	4914155	287109.6	4914166	0.07	0.354	0.13	0.02	0
97	132	287061.2	4914154	287109.9	4914165	0.09	0.354	0.17	0.02	0
98	133	287061.4	4914153	287110.1	4914164	-0.19	0.354	-0.37	-0.27	0.14
99	134	287061.6	4914152	287110.3	4914163	-0.17	0.354	-0.33	-0.46	0.21
100	135	287061.9	4914151	287110.5	4914162	0.06	0.354	0.12	-0.23	0.1
101	136	287062.1	4914150	287110.8	4914161	0.21	0.354	0.42	0.02	0
102	137	287062.3	4914149	287111	4914160	-0.15	0.354	-0.29	-0.58	0.18
103	138	287062.6	4914148	287111.2	4914159	-0.15	0.354	-0.3	-0.56	0.18
104	139	287062.8	4914147	287111.5	4914158	-0.2	0.354	-0.39	-0.4	0.09
105	140	287063	4914146	287111.7	4914157	-0.23	0.354	-0.46	-0.37	0.07
106	141	287063.2	4914145	287111.9	4914156	-0.46	0.354	-0.91	-0.51	0.37
107	150	287065.3	4914136	287114	4914148	-0.24	0.354	-0.48	-0.12	0.05
108	151	287065.5	4914135	287114.2	4914147	-1.01	0.354	-2.01	-0.07	0
109	152	287065.8	4914134	287114.4	4914146	-0.29	0.354	-0.57	0.18	0
110	153	287066	4914133	287114.7	4914145	-0.21	0.354	-0.41	0.23	0.02
111	154	287066.2	4914132	287114.9	4914144	0.04	0.354	0.08	0.17	0.03
112	155	287066.5	4914131	287115.1	4914143	-0.03	0.354	-0.06	0.04	0
116	159	287067.4	4914127	287116.1	4914139	0.36	0.354	0.71	0.24	0.16
117	160	287067.6	4914126	287116.3	4914138	0.09	0.354	0.18	0	0
118	161	287067.8	4914125	287116.5	4914137	0.12	0.354	0.24	0.15	0.09
119	162	287068.1	4914124	287116.7	4914136	0	0.354	0	0.03	0
120	163	287068.3	4914123	287117	4914135	-1.82	0.354	-3.64	-0.97	0.15

Appendix IV

121	164	287068.5	4914122	287117.2	4914134	0.11	0.354	0.21	0.18	0.03
122	165	287068.8	4914122	287117.4	4914133	0.22	0.354	0.44	0.2	0.09
123	166	287069	4914121	287117.7	4914132	0.1	0.354	0.2	0.11	0.08
124	167	287069.2	4914120	287117.9	4914131	0.18	0.354	0.35	0.1	0.19
125	168	287069.4	4914119	287118.1	4914130	0.21	0.354	0.42	0.08	0.05
128	171	287070.1	4914116	287118.8	4914127	0.2	0.354	0.39	0.13	0.21
129	172	287070.4	4914115	287119	4914126	0.26	0.354	0.51	0.27	0.45
130	173	287070.6	4914114	287119.3	4914125	0.2	0.354	0.4	0.21	0.21
131	174	287070.8	4914113	287119.5	4914124	0.15	0.354	0.29	0.15	0.12
132	175	287071	4914112	287119.7	4914123	-0.03	0.354	-0.06	-0.09	0.14

3-Marina di Ravenna dune foot line table.

OBJECTID	TransectId	StartX	StartY	EndX	EndY	EPR	ECI	NSM	LRR	LR2
9	9	284300.7	4926677	284345.3	4926684	0.21	0.354	0.41	-0.1	0.01
10	10	284300.5	4926678	284345.1	4926685	-0.31	0.354	-0.61	-0.38	0.75
11	11	284300.3	4926679	284344.9	4926686	-0.49	0.354	-0.97	-0.49	0.96
12	12	284300.1	4926680	284344.7	4926687	-0.43	0.354	-0.86	-0.43	1
13	13	284299.9	4926681	284344.5	4926688	-0.2	0.354	-0.4	-0.24	0.73
14	14	284299.8	4926682	284344.3	4926689	0.1	0.354	0.2	-0.04	0.02
15	15	284299.6	4926683	284344.2	4926690	0.5	0.354	1	0.3	0.33
16	16	284299.4	4926684	284344	4926690	0.8	0.354	1.6	0.54	0.46
17	17	284299.2	4926685	284343.8	4926691	0.8	0.354	1.59	0.75	0.89
18	18	284299.1	4926686	284343.6	4926692	0.75	0.354	1.5	0.75	0.84
19	19	284298.9	4926687	284343.5	4926693	0.73	0.354	1.46	0.73	0.77
20	20	284298.7	4926688	284343.3	4926694	0.85	0.354	1.7	0.78	0.78
21	21	284298.5	4926689	284343.1	4926695	0.7	0.354	1.39	0.6	0.62
22	22	284298.3	4926690	284342.9	4926696	0.49	0.354	0.97	0.37	0.47
23	23	284298.2	4926691	284342.7	4926697	0.22	0.354	0.44	0.25	0.26
24	24	284298	4926692	284342.6	4926698	0.15	0.354	0.29	0.16	0.52
45	45	284294.6	4926713	284339.2	4926719	-0.44	0.354	-0.88	-0.39	0.35
46	46	284294.5	4926714	284339.1	4926720	-0.2	0.354	-0.39	-0.29	0.26
47	47	284294.3	4926715	284338.9	4926721	-0.41	0.354	-0.82	-0.56	0.41
48	48	284294.2	4926716	284338.8	4926722	-0.23	0.354	-0.45	-0.51	0.22
49	49	284294.1	4926717	284338.6	4926723	0.01	0.354	0.02	-0.42	0.19
50	50	284293.9	4926718	284338.5	4926724	0.06	0.354	0.12	-0.44	0.13
51	51	284293.8	4926719	284338.4	4926725	0.11	0.354	0.22	-0.44	0.12
52	52	284293.6	4926720	284338.2	4926726	-0.48	0.354	-0.96	-0.92	0.5
53	53	284293.5	4926721	284338.1	4926727	-0.75	0.354	-1.49	-0.93	0.39
54	54	284293.4	4926722	284337.9	4926728	-0.56	0.354	-1.12	-0.54	0.63
55	55	284293.2	4926723	284337.8	4926729	-0.53	0.354	-1.06	-0.48	0.8
56	56	284293.1	4926724	284337.7	4926730	-0.44	0.354	-0.87	-0.48	0.65
57	57	284292.9	4926725	284337.5	4926731	-0.09	0.354	-0.18	-0.1	0.14
58	58	284292.8	4926726	284337.4	4926732	-0.16	0.354	-0.31	-0.18	0.39
59	59	284292.7	4926727	284337.2	4926733	-0.27	0.354	-0.53	-0.2	0.39
60	60	284292.5	4926728	284337.1	4926734	-0.32	0.354	-0.64	-0.28	0.54
61	61	284292.4	4926729	284337	4926735	-0.16	0.354	-0.31	-0.08	0.19
62	62	284292.2	4926730	284336.8	4926736	-0.25	0.354	-0.49	-0.36	0.41
63	63	284292.1	4926731	284336.7	4926737	-0.22	0.354	-0.44	-0.33	0.36
64	64	284292	4926732	284336.6	4926738	-0.26	0.354	-0.52	-0.28	0.3
65	65	284291.8	4926733	284336.4	4926739	-0.22	0.354	-0.43	-0.18	0.09
66	66	284291.7	4926734	284336.3	4926740	-0.18	0.354	-0.35	-0.13	0.06
67	67	284291.6	4926735	284336.1	4926741	-0.17	0.354	-0.34	-0.14	0.14
68	68	284291.4	4926736	284336	4926742	-0.12	0.354	-0.23	0.42	0.12
69	69	284291.3	4926737	284335.9	4926743	-0.04	0.354	-0.08	0.38	0.16
70	70	284291.1	4926738	284335.7	4926744	0.03	0.354	0.05	0.55	0.2
80	80	284289.8	4926748	284334.4	4926754	0.91	0.354	1.82	0.87	0.68
81	81	284289.7	4926749	284334.3	4926755	0.67	0.354	1.34	0.63	0.66
82	82	284289.6	4926750	284334.2	4926756	0.49	0.354	0.98	0.47	0.66
83	83	284289.5	4926751	284334.1	4926757	0.15	0.354	0.3	0.21	0.48
84	84	284289.4	4926752	284334	4926758	0.14	0.354	0.28	0.21	0.61
85	85	284289.3	4926753	284333.9	4926759	0.13	0.354	0.25	0.16	0.5
86	86	284289.2	4926754	284333.8	4926760	0.06	0.354	0.11	0.15	0.23

Appendix IV

87	87	284289.1	4926755	284333.7	4926761	0.06	0.354	0.12	0.2	0.28
88	88	284289	4926756	284333.6	4926762	0.09	0.354	0.17	0.22	0.3
89	89	284288.9	4926757	284333.5	4926763	-0.06	0.354	-0.11	0.12	0.09
90	90	284288.8	4926758	284333.4	4926764	-0.23	0.354	-0.46	-0.14	0.3
91	91	284288.7	4926759	284333.3	4926765	-0.42	0.354	-0.84	-0.41	0.91
92	92	284288.6	4926760	284333.2	4926766	-0.39	0.354	-0.78	-0.43	0.71
93	93	284288.5	4926761	284333.1	4926767	-0.28	0.354	-0.56	-0.38	0.43
94	94	284288.4	4926762	284333	4926768	-0.29	0.354	-0.57	-0.38	0.45
95	95	284288.3	4926763	284332.9	4926769	-0.28	0.354	-0.56	-0.33	0.61
96	96	284288.2	4926764	284332.8	4926770	-0.12	0.354	-0.23	-0.1	0.26
97	97	284288.1	4926765	284332.7	4926771	0.15	0.354	0.29	0.13	0.77
98	98	284288	4926766	284332.6	4926772	0.34	0.354	0.67	0.3	0.64
99	99	284287.9	4926767	284332.5	4926773	0.58	0.354	1.16	0.69	0.58
100	100	284287.8	4926768	284332.4	4926774	0.51	0.354	1.02	0.6	0.59
101	101	284287.8	4926769	284332.3	4926775	0.24	0.354	0.47	0.37	0.26
102	102	284287.7	4926770	284332.2	4926776	0.17	0.354	0.34	0.28	0.21
103	103	284287.6	4926771	284332.1	4926777	0.23	0.354	0.45	0.21	0.14
104	104	284287.5	4926772	284332.1	4926778	0.07	0.354	0.13	-0.04	0
105	105	284287.4	4926773	284332	4926779	-0.02	0.354	-0.03	-0.22	0.06
106	106	284287.3	4926774	284331.9	4926780	0.12	0.354	0.23	-0.19	0.03
107	107	284287.2	4926775	284331.8	4926781	-0.15	0.354	-0.3	-0.39	0.22
108	108	284287.1	4926776	284331.7	4926782	-0.97	0.354	-1.93	-1.01	0.95
109	109	284287	4926777	284331.6	4926783	-1.43	0.354	-2.86	-1.32	0.9
110	110	284287	4926778	284331.5	4926784	-1.32	0.354	-2.63	-1.16	0.91
111	111	284286.9	4926779	284331.5	4926785	-1.46	0.354	-2.91	-1.19	0.76

4-Marina di Ravenna dune crest line table.

OBJECTID	TransectId	StartX	StartY	EndX	EndY	EPR	ECI	NSM	LRR	LR2
9	9	284300.7	4926677	284330.4	4926682	-0.08	0.354	-0.16	-0.55	0.18
10	10	284300.5	4926678	284330.2	4926683	0.08	0.354	0.16	-0.43	0.1
11	11	284300.3	4926679	284330	4926684	0.94	0.354	1.87	0.38	0.09
12	12	284300.1	4926680	284329.8	4926685	0.74	0.354	1.47	0.33	0.11
13	13	284299.9	4926681	284329.7	4926685	0.61	0.354	1.21	0.34	0.18
14	14	284299.8	4926682	284329.5	4926686	0.66	0.354	1.31	0.42	0.28
15	15	284299.6	4926683	284329.3	4926687	0.72	0.354	1.43	0.6	0.44
16	16	284299.4	4926684	284329.1	4926688	0.62	0.354	1.24	0.68	0.34
17	17	284299.2	4926685	284329	4926689	0.25	0.354	0.5	0.57	0.18
18	18	284299.1	4926686	284328.8	4926690	-0.23	0.354	-0.46	0.15	0.01
19	19	284298.9	4926687	284328.6	4926691	-1.1	0.354	-2.2	-0.53	0.11
20	20	284298.7	4926688	284328.4	4926692	-0.62	0.354	-1.24	-0.16	0.02
21	21	284298.5	4926689	284328.2	4926693	-0.44	0.354	-0.87	-0.25	0.14
22	22	284298.3	4926690	284328.1	4926694	0.49	0.354	0.98	0.46	0.69
23	23	284298.2	4926691	284327.9	4926695	0.56	0.354	1.12	0.37	0.4
24	24	284298	4926692	284327.7	4926696	0.36	0.354	0.71	0.4	0.42
25	25	284297.8	4926693	284327.5	4926697	1.16	0.354	2.32	1.07	0.55
26	26	284297.6	4926694	284327.4	4926698	0.58	0.354	1.15	0.64	0.48
27	27	284297.5	4926695	284327.2	4926699	0.07	0.354	0.13	0.06	0.05
28	28	284297.3	4926696	284327	4926700	-1.9	0.354	-3.8	-1.68	0.78
35	35	284296.1	4926703	284325.9	4926707	-0.06	0.354	-0.11	-0.04	0.18
36	36	284296	4926704	284325.7	4926708	0.03	0.354	0.05	0.05	0.03
37	37	284295.8	4926705	284325.5	4926709	0.09	0.354	0.17	0.17	0.18
38	38	284295.7	4926706	284325.4	4926710	0.11	0.354	0.22	0.12	0.05
39	39	284295.5	4926707	284325.2	4926711	-0.31	0.354	-0.62	-0.28	0.09
40	40	284295.3	4926708	284325.1	4926712	-0.09	0.354	-0.18	-0.18	0.04
41	41	284295.2	4926709	284324.9	4926713	-0.29	0.354	-0.57	-0.38	0.17
42	42	284295	4926710	284324.8	4926714	0.59	0.354	1.17	0.41	0.32
43	43	284294.9	4926711	284324.6	4926715	0.08	0.354	0.15	-0.16	0.09
44	44	284294.8	4926712	284324.5	4926716	-0.01	0.354	-0.01	-1.47	0.13
45	45	284294.6	4926713	284324.3	4926717	-1.47	0.354	-2.93	-0.89	0.14
46	46	284294.5	4926714	284324.2	4926718	-0.25	0.354	-0.49	0.27	0.01
47	47	284294.3	4926715	284324.1	4926719	0.54	0.354	1.07	0.77	0.13
48	48	284294.2	4926716	284323.9	4926720	0.17	0.354	0.34	0.31	0.07
49	49	284294.1	4926717	284323.8	4926721	0.17	0.354	0.33	0.2	0.38
50	50	284293.9	4926718	284323.6	4926722	0.06	0.354	0.12	-0.01	0
51	51	284293.8	4926719	284323.5	4926723	0.1	0.354	0.2	-0.15	0.05
52	52	284293.6	4926720	284323.4	4926724	0.28	0.354	0.55	-0.19	0.02
53	53	284293.5	4926721	284323.2	4926725	0.67	0.354	1.33	-0.03	0
54	54	284293.4	4926722	284323.1	4926726	1.03	0.354	2.06	0.25	0.01
55	55	284293.2	4926723	284322.9	4926727	1.12	0.354	2.23	0.29	0.02
56	56	284293.1	4926724	284322.8	4926728	0.98	0.354	1.95	0.15	0
57	57	284292.9	4926725	284322.7	4926729	0.54	0.354	1.07	-0.35	0.02
58	58	284292.8	4926726	284322.5	4926730	0.08	0.354	0.15	-0.92	0.14
59	59	284292.7	4926727	284322.4	4926731	0.02	0.354	0.04	-0.84	0.15
60	60	284292.5	4926728	284322.2	4926732	0.15	0.354	0.3	-0.63	0.1
61	61	284292.4	4926729	284322.1	4926733	0.73	0.354	1.46	-0.02	0
62	62	284292.2	4926730	284322	4926734	0.84	0.354	1.68	0.41	0.18
63	63	284292.1	4926731	284321.8	4926735	-0.04	0.354	-0.08	0	0
64	64	284292	4926732	284321.7	4926736	-2.05	0.354	-4.09	-1.98	0.52
65	65	284291.8	4926733	284321.6	4926737	-2.22	0.354	-4.44	-1.99	0.76
66	66	284291.7	4926734	284321.4	4926738	-2.11	0.354	-4.21	-1.75	0.62
67	67	284291.6	4926735	284321.3	4926739	-2.08	0.354	-4.15	-1.6	0.53
68	68	284291.4	4926736	284321.1	4926740	-1.92	0.354	-3.84	-1.57	0.55

Appendix IV

69	69	284291.3	4926737	284321	4926741	-2.12	0.354	-4.23	-1.5	0.56
70	70	284291.1	4926738	284320.9	4926742	-2.53	0.354	-5.06	-1.9	0.61
71	71	284291	4926739	284320.7	4926743	-1.53	0.354	-3.05	-0.97	0.42
72	72	284290.9	4926740	284320.6	4926744	-1.49	0.354	-2.98	-0.96	0.35
73	73	284290.7	4926741	284320.5	4926745	-1.73	0.354	-3.45	-1.29	0.38
74	74	284290.6	4926742	284320.3	4926746	-1.96	0.354	-3.91	-1.49	0.42
75	75	284290.5	4926743	284320.2	4926747	-2.16	0.354	-4.31	-1.64	0.47
76	76	284290.3	4926744	284320	4926748	-2.33	0.354	-4.65	-1.94	0.6
77	77	284290.2	4926745	284319.9	4926749	-2.48	0.354	-4.96	-2.06	0.59
78	78	284290	4926746	284319.8	4926750	-2.06	0.354	-4.11	-1.59	0.44
79	79	284289.9	4926747	284319.6	4926751	-1.3	0.354	-2.59	-0.75	0.19
80	80	284289.8	4926748	284319.5	4926752	-0.89	0.354	-1.77	-0.18	0.01
81	81	284289.7	4926749	284319.4	4926753	-0.75	0.354	-1.5	-0.36	0.14
82	82	284289.6	4926750	284319.3	4926754	-0.64	0.354	-1.27	-0.35	0.1
83	83	284289.5	4926751	284319.2	4926755	-0.57	0.354	-1.14	-0.41	0.11
84	84	284289.4	4926752	284319.1	4926756	-0.54	0.354	-1.08	-0.46	0.17
85	85	284289.3	4926753	284319	4926757	-0.44	0.354	-0.88	-0.45	0.32
86	86	284289.2	4926754	284318.9	4926758	-0.38	0.354	-0.76	-0.38	0.51
87	87	284289.1	4926755	284318.8	4926759	-0.49	0.354	-0.98	-0.38	0.68
88	88	284289	4926756	284318.7	4926760	-0.34	0.354	-0.67	-0.24	0.49
89	89	284288.9	4926757	284318.6	4926761	-0.24	0.354	-0.47	-0.05	0.01
90	90	284288.8	4926758	284318.5	4926762	-0.19	0.354	-0.38	0.18	0.04
91	91	284288.7	4926759	284318.4	4926763	-0.07	0.354	-0.13	0.23	0.09
92	92	284288.6	4926760	284318.3	4926764	-0.07	0.354	-0.14	0.17	0.06
93	93	284288.5	4926761	284318.2	4926765	0.38	0.354	0.76	0.43	0.61
94	94	284288.4	4926762	284318.1	4926766	0.34	0.354	0.67	0.35	0.57
95	95	284288.3	4926763	284318	4926767	0.24	0.354	0.47	0.27	0.25
96	96	284288.2	4926764	284318	4926768	0.37	0.354	0.73	0.46	0.39
97	97	284288.1	4926765	284317.9	4926769	0.34	0.354	0.68	0.53	0.47
98	98	284288	4926766	284317.8	4926770	0.11	0.354	0.21	0.02	0.01
99	99	284287.9	4926767	284317.7	4926771	-0.2	0.354	-0.39	-0.32	0.44
100	100	284287.8	4926768	284317.6	4926772	-0.31	0.354	-0.62	-0.39	0.57

5-Milano Marittima dune foot line table.

OBJECTID	TransectId	StartX	StartY	EndX	EndY	EPR	ECI	NSM	LRR	LR2
7	7	288437.1	4908101	288462.1	4908101	-1.04	0.354	-2.07	-1.05	0.92
8	8	288437.3	4908100	288462.3	4908101	-0.78	0.354	-1.55	-0.92	0.77
9	9	288437.5	4908099	288462.5	4908100	-0.81	0.354	-1.62	-0.95	0.73
10	10	288437.7	4908098	288462.7	4908099	-0.92	0.354	-1.83	-1.08	0.71
11	11	288437.8	4908097	288462.8	4908098	-1	0.354	-2	-1.11	0.87
12	12	288438	4908096	288463	4908097	-1.01	0.354	-2.01	-1.05	0.89
13	13	288438.2	4908095	288463.2	4908096	-0.95	0.354	-1.89	-1.06	0.85
14	14	288438.3	4908094	288463.3	4908095	-0.72	0.354	-1.43	-0.79	0.79
15	15	288438.5	4908093	288463.5	4908094	-0.57	0.354	-1.13	-0.65	0.65
16	16	288438.7	4908092	288463.7	4908093	-0.34	0.354	-0.68	-0.49	0.38
17	17	288438.8	4908091	288463.8	4908092	-0.39	0.354	-0.77	-0.53	0.38
18	18	288439	4908090	288464	4908091	-0.3	0.354	-0.6	-0.42	0.33
19	19	288439.2	4908089	288464.2	4908090	-0.22	0.354	-0.43	-0.33	0.28
20	20	288439.3	4908088	288464.3	4908089	-0.13	0.354	-0.26	-0.23	0.23
21	21	288439.5	4908087	288464.5	4908088	-0.12	0.354	-0.24	-0.18	0.19
22	22	288439.7	4908086	288464.7	4908087	-0.11	0.354	-0.22	-0.14	0.13
23	23	288439.8	4908085	288464.8	4908086	-0.09	0.354	-0.17	-0.13	0.21
24	24	288440	4908084	288465	4908085	-0.03	0.354	-0.06	-0.07	0.12
25	25	288440.2	4908083	288465.2	4908084	0.05	0.354	0.09	0.04	0.06
26	26	288440.3	4908082	288465.3	4908083	0.1	0.354	0.19	0.07	0.6
27	27	288440.5	4908081	288465.5	4908082	0.07	0.354	0.14	0.06	0.22
28	28	288440.7	4908080	288465.6	4908081	0	0.354	0	-0.06	0.06
29	29	288440.8	4908079	288465.8	4908080	-0.17	0.354	-0.33	-0.31	0.45
30	30	288441	4908078	288466	4908079	-0.2	0.354	-0.4	-0.48	0.36
31	31	288441.2	4908077	288466.1	4908078	-0.11	0.354	-0.22	-0.59	0.23
32	32	288441.3	4908076	288466.3	4908077	-1.02	0.354	-2.04	-1.93	0.45
33	33	288441.5	4908075	288466.5	4908076	-2.26	0.354	-4.52	-3.07	0.68
34	34	288441.7	4908074	288466.6	4908075	-2.64	0.354	-5.28	-3.51	0.7
35	35	288441.8	4908073	288466.8	4908074	-2.79	0.354	-5.57	-3.89	0.66
36	36	288442	4908072	288467	4908073	-3.18	0.354	-6.35	-4.19	0.7
37	37	288442.1	4908071	288467.1	4908072	-3.11	0.354	-6.22	-3.46	0.79
38	38	288442.6	4908070	288467.6	4908071	-3.04	0.354	-6.07	-3.11	0.8
39	39	288443.1	4908070	288468.1	4908070	-2.87	0.354	-5.74	-2.68	0.72
40	40	288443.6	4908069	288468.6	4908069	-2.61	0.354	-5.22	-2.38	0.67
41	41	288444.2	4908068	288469.2	4908068	-2.65	0.354	-5.29	-2.44	0.69
42	42	288444.7	4908067	288469.7	4908068	-2.48	0.354	-4.96	-2.34	0.71
43	43	288445.2	4908066	288470.2	4908067	-2.14	0.354	-4.27	-1.99	0.7
44	44	288445.8	4908065	288470.8	4908066	-2.52	0.354	-5.03	-2.14	0.69
45	45	288446.3	4908065	288471.3	4908065	-2.3	0.354	-4.6	-1.91	0.59
46	46	288446.9	4908064	288471.8	4908064	-2.24	0.354	-4.48	-1.83	0.65
47	47	288447.4	4908063	288472.4	4908063	-2.11	0.354	-4.21	-1.68	0.63
48	48	288447.9	4908062	288472.9	4908063	-1.7	0.354	-3.4	-1.34	0.54
49	49	288448.5	4908061	288473.5	4908062	-1.39	0.354	-2.78	-1.02	0.51
50	50	288448.6	4908060	288473.6	4908061	-0.9	0.354	-1.79	-0.62	0.43
51	51	288448.8	4908059	288473.8	4908060	-0.58	0.354	-1.16	-0.35	0.35
52	52	288449	4908058	288474	4908059	-0.46	0.354	-0.91	-0.47	0.49
53	53	288449.2	4908057	288474.2	4908058	-0.26	0.354	-0.52	-0.45	0.3
54	54	288449.3	4908056	288474.3	4908057	0.01	0.354	0.01	-0.28	0.11
55	55	288449.5	4908055	288474.5	4908056	-0.03	0.354	-0.05	-0.28	0.13
56	56	288449.7	4908054	288474.7	4908055	-0.22	0.354	-0.43	-0.39	0.35
57	57	288449.9	4908053	288474.9	4908054	-0.37	0.354	-0.74	-0.56	0.5
58	58	288450	4908052	288475	4908053	-0.35	0.354	-0.69	-0.54	0.47
59	59	288450.2	4908051	288475.2	4908052	-0.42	0.354	-0.84	-0.6	0.54
60	60	288450.4	4908050	288475.4	4908051	-0.46	0.354	-0.92	-0.67	0.47

Appendix IV

61	61	288450.5	4908049	288475.5	4908050	-0.5	0.354	-0.99	-0.75	0.46
62	62	288450.7	4908048	288475.7	4908049	-0.34	0.354	-0.68	-0.67	0.38
63	63	288450.9	4908047	288475.9	4908048	-0.3	0.354	-0.59	-0.59	0.38
64	64	288451.1	4908046	288476.1	4908047	-0.33	0.354	-0.66	-0.57	0.47
65	65	288451.2	4908045	288476.2	4908046	-0.39	0.354	-0.77	-0.64	0.54
66	66	288451.4	4908044	288476.4	4908045	-0.41	0.354	-0.81	-0.66	0.51
67	67	288451.6	4908043	288476.6	4908044	-0.36	0.354	-0.71	-0.63	0.45
68	68	288451.8	4908042	288476.8	4908043	-0.34	0.354	-0.68	-0.61	0.41
69	69	288451.9	4908042	288476.9	4908042	-0.31	0.354	-0.62	-0.55	0.36
70	70	288452	4908041	288477	4908041	-0.39	0.354	-0.78	-0.6	0.38
71	71	288452.2	4908040	288477.2	4908040	-0.36	0.354	-0.72	-0.58	0.45
72	72	288452.3	4908039	288477.3	4908039	-0.37	0.354	-0.74	-0.55	0.54
73	73	288452.4	4908038	288477.4	4908038	-0.36	0.354	-0.71	-0.46	0.62
74	74	288452.6	4908037	288477.5	4908037	-0.31	0.354	-0.62	-0.37	0.67
75	75	288452.7	4908036	288477.7	4908036	-0.28	0.354	-0.55	-0.29	0.87
76	76	288452.8	4908035	288477.8	4908035	-0.24	0.354	-0.47	-0.18	0.68
77	77	288452.9	4908034	288477.9	4908034	-0.31	0.354	-0.62	-0.08	0.03
78	78	288453.1	4908033	288478.1	4908033	-0.41	0.354	-0.81	-0.1	0.02
79	79	288453.2	4908032	288478.2	4908032	-0.44	0.354	-0.88	-0.06	0
80	80	288453.3	4908031	288478.3	4908031	-0.55	0.354	-1.1	-0.08	0.01
81	81	288453.5	4908030	288478.5	4908030	-0.67	0.354	-1.34	-0.12	0.01
82	82	288453.6	4908029	288478.6	4908029	-0.74	0.354	-1.47	-0.14	0.01
83	83	288453.7	4908028	288478.7	4908028	-0.69	0.354	-1.37	-0.05	0
84	84	288453.9	4908027	288478.9	4908027	-0.67	0.354	-1.34	0.02	0
85	85	288454	4908026	288479	4908026	-0.57	0.354	-1.14	0.2	0.01
86	86	288454.1	4908025	288479.1	4908025	-0.53	0.354	-1.06	0.35	0.03
87	87	288454.3	4908024	288479.3	4908024	-0.54	0.354	-1.08	0.34	0.03
88	88	288454.4	4908023	288479.4	4908023	-0.56	0.354	-1.11	0.37	0.03
89	89	288454.5	4908022	288479.5	4908022	-0.5	0.354	-1	0.42	0.04
90	90	288454.7	4908021	288479.6	4908021	-0.47	0.354	-0.93	0.42	0.04
91	91	288454.8	4908020	288479.8	4908020	-0.48	0.354	-0.96	0.42	0.04
92	92	288454.9	4908019	288479.9	4908019	-0.6	0.354	-1.2	0.37	0.03
93	93	288455	4908018	288480	4908018	-0.64	0.354	-1.28	0.46	0.03
94	94	288455.2	4908017	288480.2	4908017	-0.58	0.354	-1.15	0.61	0.05
95	95	288455.3	4908016	288480.3	4908016	-0.37	0.354	-0.73	0.84	0.09
96	96	288455.4	4908015	288480.4	4908015	-0.31	0.354	-0.61	0.88	0.09
97	97	288455.6	4908014	288480.5	4908014	-0.25	0.354	-0.5	0.88	0.1
98	98	288455.7	4908013	288480.7	4908013	-0.22	0.354	-0.44	0.92	0.11
99	99	288455.8	4908012	288480.8	4908012	-0.26	0.354	-0.52	0.86	0.1
100	100	288455.9	4908011	288480.9	4908011	-0.32	0.354	-0.64	0.78	0.09
101	101	288456.1	4908010	288481.1	4908010	-0.19	0.354	-0.38	0.86	0.12
102	102	288456.2	4908009	288481.2	4908009	-0.34	0.354	-0.68	0.78	0.09
103	103	288456.3	4908008	288481.3	4908008	0.04	0.354	0.08	1.21	0.19
104	104	288456.4	4908007	288481.4	4908007	0.66	0.354	1.32	1.86	0.34
105	105	288456.6	4908006	288481.6	4908006	0.76	0.354	1.52	2.1	0.34
106	106	288456.7	4908005	288481.7	4908005	0.86	0.354	1.71	2.28	0.35
107	107	288456.8	4908004	288481.8	4908004	0.66	0.354	1.31	2.13	0.3
108	108	288457	4908003	288482	4908003	0.7	0.354	1.39	2.18	0.3
109	109	288457.1	4908002	288482.1	4908002	0.76	0.354	1.52	2.3	0.31
110	110	288457.2	4908001	288482.2	4908001	0.83	0.354	1.65	2.41	0.31
111	111	288457.3	4908000	288482.3	4908000	0.53	0.354	1.06	2.2	0.25
112	112	288457.5	4907999	288482.5	4907999	-0.9	0.354	-1.8	0.73	0.04
113	113	288457.8	4907998	288482.8	4907998	-0.62	0.354	-1.24	0.86	0.07
114	114	288458.1	4907997	288483.1	4907998	-0.67	0.354	-1.34	0.69	0.05
115	115	288458.4	4907996	288483.4	4907997	-0.75	0.354	-1.5	0.52	0.04
116	116	288458.7	4907995	288483.7	4907996	-0.77	0.354	-1.53	0.64	0.04
117	117	288459	4907994	288484	4907995	-0.65	0.354	-1.29	0.76	0.06
118	118	288459.3	4907993	288484.3	4907994	-0.57	0.354	-1.14	0.61	0.05
119	119	288459.6	4907992	288484.5	4907993	-0.55	0.354	-1.1	0.38	0.02
120	120	288459.8	4907991	288484.8	4907992	-0.43	0.354	-0.85	0.31	0.01

Appendix IV

121	121	288460.1	4907990	288485.1	4907991	-0.37	0.354	-0.74	0.38	0.02
122	122	288460.4	4907989	288485.4	4907990	-0.45	0.354	-0.9	0.34	0.02
123	123	288460.7	4907988	288485.7	4907989	0.54	0.354	1.08	1.14	0.28
124	124	288461	4907987	288486	4907988	1.1	0.354	2.2	1.65	0.49
125	125	288461.3	4907986	288486.3	4907987	1.05	0.354	2.09	1.62	0.47
126	126	288461.6	4907985	288486.6	4907986	0.91	0.354	1.81	1.48	0.46
127	127	288461.9	4907985	288486.8	4907985	0.36	0.354	0.71	1.07	0.28
128	128	288462.1	4907984	288487.1	4907984	0	0.354	0	0.85	0.16
129	129	288462.4	4907983	288487.4	4907983	-0.23	0.354	-0.45	0.72	0.1
130	130	288462.7	4907982	288487.7	4907982	-0.36	0.354	-0.72	0.4	0.06
131	131	288463	4907981	288488	4907981	-0.29	0.354	-0.57	0.2	0.03
132	132	288463.3	4907980	288488.3	4907980	-0.59	0.354	-1.18	-0.16	0.03
133	133	288463.6	4907979	288488.5	4907979	-0.87	0.354	-1.74	-0.43	0.18
134	134	288463.8	4907978	288488.8	4907978	-1.07	0.354	-2.13	-0.64	0.29
135	135	288464.1	4907977	288489.1	4907977	-0.96	0.354	-1.92	-0.59	0.33
136	136	288464.4	4907976	288489.4	4907976	-0.95	0.354	-1.89	-0.63	0.48
137	137	288464.7	4907975	288489.7	4907975	-0.79	0.354	-1.58	-0.55	0.52
138	138	288465	4907974	288489.9	4907974	-0.71	0.354	-1.42	-0.49	0.47
139	139	288465.2	4907973	288490.2	4907974	-0.73	0.354	-1.45	-0.54	0.46
140	140	288465.5	4907972	288490.5	4907973	-0.74	0.354	-1.47	-0.61	0.56
141	141	288465.8	4907971	288490.8	4907972	-0.82	0.354	-1.64	-0.69	0.58
142	142	288466.1	4907970	288491.1	4907971	-0.79	0.354	-1.57	-0.69	0.64
143	143	288466.3	4907969	288491.3	4907970	-0.96	0.354	-1.92	-0.84	0.75
144	144	288466.4	4907968	288491.4	4907969	-1.13	0.354	-2.25	-0.99	0.83
145	145	288466.4	4907967	288491.4	4907968	-0.98	0.354	-1.96	-0.85	0.67
146	146	288466.4	4907966	288491.4	4907967	-0.8	0.354	-1.59	-0.68	0.44
147	147	288466.5	4907965	288491.5	4907966	-0.71	0.354	-1.42	-0.64	0.38
148	148	288466.5	4907964	288491.5	4907965	-0.74	0.354	-1.48	-0.72	0.44
149	149	288466.5	4907963	288491.5	4907964	-0.7	0.354	-1.4	-0.74	0.5
150	150	288466.6	4907962	288491.6	4907963	-0.64	0.354	-1.28	-0.73	0.64
151	151	288466.6	4907961	288491.6	4907962	-0.58	0.354	-1.15	-0.67	0.64
152	152	288466.6	4907960	288491.6	4907961	-0.49	0.354	-0.98	-0.6	0.55
153	153	288466.6	4907959	288491.6	4907960	-0.42	0.354	-0.83	-0.55	0.44
154	154	288466.4	4907958	288491.4	4907959	-0.25	0.354	-0.5	-0.45	0.33
155	155	288466.2	4907957	288491.2	4907958	-0.24	0.354	-0.47	-0.48	0.33
156	156	288466	4907956	288491	4907957	-0.33	0.354	-0.66	-0.5	0.46
157	157	288465.8	4907955	288490.8	4907956	-0.49	0.354	-0.97	-0.54	0.67
158	158	288465.6	4907954	288490.6	4907955	-0.45	0.354	-0.89	-0.52	0.59
159	159	288465.4	4907953	288490.4	4907954	-0.54	0.354	-1.07	-0.59	0.71
160	160	288465.1	4907952	288490.1	4907953	-0.62	0.354	-1.24	-0.67	0.8
161	161	288464.9	4907951	288489.9	4907952	-0.62	0.354	-1.24	-0.71	0.87
162	162	288464.7	4907950	288489.7	4907951	-0.46	0.354	-0.92	-0.59	0.71
163	163	288464.5	4907949	288489.5	4907950	-0.38	0.354	-0.75	-0.41	0.66
164	164	288464.3	4907948	288489.3	4907949	-0.34	0.354	-0.67	-0.31	0.49
165	165	288464	4907947	288489	4907948	-0.31	0.354	-0.61	-0.25	0.22
166	166	288463.7	4907947	288488.6	4907947	-0.24	0.354	-0.48	-0.21	0.1
167	167	288463.3	4907946	288488.3	4907946	-0.13	0.354	-0.26	-0.17	0.06
168	168	288463	4907945	288488	4907945	0.01	0.354	0.01	-0.12	0.03
169	169	288462.7	4907944	288487.7	4907944	-0.02	0.354	-0.03	-0.17	0.06
170	170	288462.4	4907943	288487.4	4907943	-0.09	0.354	-0.18	-0.24	0.12
171	171	288462.1	4907942	288487.1	4907942	-0.13	0.354	-0.25	-0.23	0.12
172	172	288461.8	4907941	288486.8	4907941	-0.22	0.354	-0.43	-0.26	0.2
173	173	288461.5	4907940	288486.5	4907940	-0.22	0.354	-0.43	-0.32	0.24
174	174	288461.2	4907939	288486.2	4907939	-0.12	0.354	-0.24	-0.23	0.09
175	175	288460.8	4907938	288485.8	4907939	-0.08	0.354	-0.15	-0.17	0.06
176	176	288460.5	4907937	288485.5	4907938	-0.06	0.354	-0.12	-0.17	0.07
177	177	288460.1	4907936	288485.1	4907937	-0.1	0.354	-0.19	-0.17	0.1
178	178	288459.7	4907935	288484.7	4907936	-0.19	0.354	-0.37	-0.22	0.18
179	179	288459.3	4907934	288484.3	4907935	-0.11	0.354	-0.22	-0.14	0.13

Appendix IV

179	179	288459.3	4907934	288484.3	4907935	-0.11	0.354	-0.22	-0.14	0.13
180	180	288458.9	4907933	288483.9	4907934	-0.13	0.354	-0.26	-0.19	0.18
181	181	288458.5	4907932	288483.5	4907933	-0.13	0.354	-0.25	-0.22	0.18
182	182	288458.2	4907932	288483.2	4907932	-0.11	0.354	-0.21	-0.25	0.17
183	183	288457.8	4907931	288482.8	4907931	-0.17	0.354	-0.34	-0.33	0.27
184	184	288457.4	4907930	288482.4	4907930	-0.27	0.354	-0.53	-0.41	0.49
185	185	288457	4907929	288482	4907929	-0.33	0.354	-0.66	-0.46	0.69
186	186	288456.6	4907928	288481.6	4907928	-0.38	0.354	-0.76	-0.48	0.8
187	187	288456.3	4907927	288481.2	4907927	-0.43	0.354	-0.85	-0.52	0.73
188	188	288455.9	4907926	288480.9	4907927	-0.3	0.354	-0.59	-0.43	0.48
189	189	288455.5	4907925	288480.5	4907926	-0.43	0.354	-0.86	-0.6	0.61
190	190	288455.1	4907924	288480.1	4907925	-0.65	0.354	-1.29	-0.84	0.74
191	191	288454.7	4907923	288479.7	4907924	-0.7	0.354	-1.4	-0.93	0.73
192	192	288454.3	4907922	288479.3	4907923	-0.75	0.354	-1.5	-1.03	0.67
193	193	288453.9	4907921	288478.9	4907922	-0.87	0.354	-1.73	-1.19	0.65
194	194	288453.5	4907920	288478.5	4907921	-0.92	0.354	-1.83	-1.29	0.62
195	195	288453.2	4907920	288478.1	4907920	-0.84	0.354	-1.67	-1.25	0.57
196	196	288452.8	4907919	288477.8	4907919	-0.79	0.354	-1.57	-1.27	0.54
197	197	288452.4	4907918	288477.4	4907918	-0.76	0.354	-1.52	-1.31	0.51
198	198	288452	4907917	288477	4907917	-0.75	0.354	-1.49	-1.33	0.49
199	199	288451.6	4907916	288476.6	4907916	-0.85	0.354	-1.7	-1.43	0.53
200	200	288451.2	4907915	288476.2	4907915	-0.93	0.354	-1.86	-1.5	0.57
201	201	288450.8	4907914	288475.8	4907915	-1.08	0.354	-2.15	-1.57	0.63
202	202	288450.4	4907913	288475.4	4907914	-1.21	0.354	-2.42	-1.68	0.71
203	203	288450	4907912	288475	4907913	-1.21	0.354	-2.41	-1.51	0.84
204	204	288449.7	4907911	288474.6	4907912	-1.11	0.354	-2.21	-1.26	0.86
205	205	288449.3	4907910	288474.3	4907911	-0.96	0.354	-1.92	-1.08	0.81
206	206	288448.8	4907909	288473.8	4907910	-1	0.354	-1.99	-1.06	0.83
207	207	288448.2	4907909	288473.2	4907909	-1.24	0.354	-2.47	-1.26	0.85
208	208	288447.7	4907908	288472.7	4907908	-1.55	0.354	-3.1	-1.51	0.88
209	209	288447.2	4907907	288472.2	4907907	-1.67	0.354	-3.34	-1.59	0.87
210	210	288446.7	4907906	288471.6	4907907	-1.59	0.354	-3.18	-1.41	0.72
211	211	288446.1	4907905	288471.1	4907906	-1.32	0.354	-2.64	-1.25	0.87
212	212	288445.6	4907904	288470.6	4907905	-0.92	0.354	-1.83	-1.03	0.91
213	213	288445.1	4907903	288470.1	4907904	-0.7	0.354	-1.39	-0.8	0.91
214	214	288444.5	4907903	288469.5	4907903	-0.78	0.354	-1.55	-0.79	0.91
215	215	288443.9	4907902	288468.9	4907902	-0.85	0.354	-1.7	-0.79	0.82
216	216	288443.2	4907901	288468.2	4907902	-0.86	0.354	-1.71	-0.73	0.7
217	217	288442.5	4907900	288467.5	4907901	-0.78	0.354	-1.55	-0.51	0.27
218	218	288441.8	4907900	288466.8	4907900	-0.69	0.354	-1.38	-0.37	0.12